Microplastic-Contaminant Interactions: From Experimental Data to Environmental Implications

Dissertation

der Mathematisch-Naturwissenschaftlichen Fakultät
der Eberhard Karls Universität Tübingen
zur Erlangung des Grades
eines Doktors der Naturwissenschaften
(Dr. rer. nat.)

vorgelegt von
Sven Seidensticker
aus Höxter

Tübingen
2019

Gedruckt mit Genehmigung der Mathematisch-Naturwissenschaftlichen Fakultät der Eberhard Karls Universität Tübingen.

Tag der mündlichen Qualifikation:	25.06.2019
Dekan:	Prof. Dr. Wolfgang Rosenstiel
1. Berichterstatter:	Prof. Dr. Peter Grathwohl
2. Berichterstatter:	Jun. Prof. Christiane Zarfl

Abstract

Microplastic particles are ubiquitously detected in the environment. Despite intensive public and scientific discussions, an assessment of their potential to transport hydrophobic organic contaminants in rivers and oceans under environmental conditions is still needed. To consider such particle facilitated transport, this thesis aims to quantify the underlying sorption mechanisms and to develop a comprehensive mechanistic model with parameter values derived from experimental data. Within batch experiments various types of microplastic particles and common wastewater contaminants were applied to investigate both sorption isotherms and kinetics. The subsequently developed models consider material characteristics, physico-chemical properties of chemical compounds as well as different types of sorption isotherms were considered. In order to determine the dominant mass transfer mechanisms they account for both diffusion within the particles and through an external aqueous boundary layer. Which of these two fluxes controls the kinetics depends on the sorption strength, particle size, diffusion coefficients, and time. For the case of linear sorption patterns, as observed for polyethylene, a semi-analytical model was developed. Experiments performed with polystyrene and polyamide, however, revealed non-linear sorption isotherms which required a numerical model to simulate the coupled mass transfer. Both model types were successfully validated, allowing to describe the measured kinetics and to obtain reasonable parameter values.

To broaden the scope and environmental relevance of this thesis, further experiments were performed. Applying changing pH conditions, data and model implied that the partitioning is strongly dependent on the compound's hydrophobicity and that neutral species contribute largely to sorption. Furthermore, the presence of additional natural sorbents significantly influenced both equilibrium partitioning and desorption kinetics.

Due to the combination of experimental work with modelling tools, it was possible to elucidate that material properties have the largest impact on the kinetics whereas the shape of the sorption isotherms has only a minor influence. Contrary to common believe, it was demonstrated that for high partition coefficients, desorption kinetics is fast in batch experiments and controlled by an external mass transfer while for low partition coefficients caused e.g. by high organic carbon loads kinetics was slow and limited by intraparticle diffusion. Conversely, under environmental conditions an increasing sorption slows down kinetics which is the fundamental difference between laboratory and field conditions. Consequently, time scales observed under experimental conditions may not be transferred to field conditions without an appropriate mechanistic model accounting for coupled mass transfer and the specific boundary conditions. Eventually, appropriate hydrodynamic relationships coupled to a thorough mass transfer analysis can serve to assess the vector function of pollutant loaded particles and to evaluate whether microplastics rather act as a passive sampler or show potential to facilitate long-range contaminant transport. Moreover, as the theoretical mass transfer considerations also apply to other suspended particles, well-defined microplastic particles are ideally suited to perform in-depth mass transfer studies and to act as surrogates for particles occurring in the environment, including microplastics in urban runoff and contaminated sediment.

Zusammenfassung

Mikroplastikpartikel sind allgegenwärtig in der Umwelt und, obwohl in der Öffentlichkeit und in der Wissenschaft intensive Diskussionen dazu geführt werden, steht eine Bewertung ihres Potenzials, hydrophobe organische Schadstoffe in Flüssen und Ozeanen zu transportieren, weiterhin aus. Ein Ziel dieser Arbeit ist daher, auf Grundlage experimenteller Daten, ein detailliertes mechanistisches Modell zur angemessenen Beschreibung dieses partikel-gebundenen Schadstofftransorts zu entwickeln. Die notwendigen Daten lieferten Experimente zu Sorptions-Interaktionen zwischen verschiedenen Typen von Mikroplastikpartikeln und weit verbreiteten Abwasser-Schadstoffen. Basierend auf den experimentellen Ergebnissen wurde ein mechanistisches Modell entwickelt, das neben Materialcharakteristika und physikalisch-chemischen Eigenschaften der Schadstoffe auch verschiedene Arten der Sorption berücksichtigt. Die Aufnahme von Substanzen und Partikeln beruht dabei parallel auf der Diffusion in einer wässrigen Grenzschicht und auf der Diffusion in der partikulären Phase selbst. Welcher dieser beiden Prozesse die Aufnahme dominiert, hängt von der Stärke der Sorption, der Partikelgröße, den Diffusionskoeffizienten und der Zeit ab. Für den Fall der linearen Sorption, wie bei Polyethylen beobachtet, wurde ein semi-analytisches Modell entwickelt. Für Polystyrol und Polyamid wurde hingegen eine nicht-lineare Sorption festgestellt, die ein numerisches Modell zur Beschreibung des gekoppelten Stoffübergangs erfordert. Beide Modellvarianten wurden erfolgreich validiert und resultierten in sinnvollen Abschätzungen der relevanten Parameter.

Zur Erhöhung der Umweltrelevanz wurden weitere Experimente durchgeführt. Zum einen wurde bei variablen pH-Bedingungen gezeigt, dass die Aufnahme der Schadstoffe im Wesentlichen durch ihre Hydrophobie bestimmt wird und dass ungeladene Spezies dabei am stärksten zur Sorption beitragen. Außerdem konnte verdeutlicht werden, dass die Verteilung und die Abgabe der Schadstoffe durch Mikroplastik signifikant durch die Anwesenheit gelösten organischen Materials beeinflusst wird.

Durch die Kombination aus Laborarbeit und Modellierung wurde bewiesen, dass die Materialeigenschaften des Plastiks die größte Bedeutung für die Kinetik haben. Weiterhin und im Gegensatz zur allgemeinen Annahme, hat sich erwiesen, dass im geschlossenen System bei starker Sorption eine schnelle Abgabe und bei geringen Verteilungskoeffizienten, eine langsame Desorption stattfindet. Dadurch offenbart sich ein fundamentaler Unterschied zu Feldverhältnissen, da dort die Kinetik bei starker Sorption verlangsamt wird. Damit wurde deutlich, dass nur durch ein geeignetes Modell, das gekoppelte Stoffübertragung und die jeweils spezifischen Randbedingungen berücksichtigt, eine Übertragung experimentell beobachteter Zeitskalen auf Umweltbedingungen möglich ist. Die Verwendung hydrodynamischer Beziehungen in Verbindung mit einer detaillierten Analyse der Sorptions-Wechselwirkungen machte es weiterhin möglich, das Vektorpotenzial des Mikroplastiks zu bewerten und abzuschätzen, welche Parameter dafür bedeutend sind. Da die theoretischen Erwägungen und Modelle auch auf andere Arten suspendierter Partikel zutreffen, sind wohl-definierte Plastikteilchen letztlich ein probates Mittel zur ausführlichen Untersuchung von Sorption und geeignet, natürlich vorkommende Partikel in Experimenten zu repräsentieren.

Acknowledgements

All the work and efforts that were necessary to successfully complete my PhD would not have been possible without the encouragement, help, and support of many different people. All of you are responsible that this thesis finally turned out the way it is.

First and foremost, I am very grateful to Peter Grathwohl. As my supervisor, Peter provided great support and inspiration. You gave me freedom to follow my own ideas and offered guidance whenever necessary. I really enjoyed our scientific discussions and there is so much I learned from you. Moreover, you are not only an outstanding scientist but as a well a wonderful person.

The time would have not been the same without Christiane Zarfl my second supervisor. You have always been there for me whenever I needed help. Beyond that, I really enjoyed the time together and the friendly reception in the whole research group.

I want to thank a few people from the Center for Applied Geoscience (ZAG). I really appreciated to have worked with you:

Jana who shared an office with me for more than three years and even though she did almost completely the same as me, she always got quite different results.

Anjela for valuable discussions and providing me some insights in a scientific area I was completely unfamiliar with. Thanks also for your support with Latex.

Renate Seelig and Thomas Wendel and the other great people in the Lab. I am very thankful regarding your help with the experimental work and for listening always carefully even if I had to complain about Swabians once again.

Greta Fellenberg, Dominik Ranker, and Jonas Lamprecht. You were great students and I was very pleased to supervise you. Keep your curiosity and your enthusiasm.

The entire Hydrogeochemisrty Group for a great time. Our Christmas parties and in particular our wine tasting are moments I will never forget.

Olaf Cirpka for your invaluable support regarding the modelling.

Beate Escher for highly appreciated discussions throughout the whole time. Your indication was responsible for my application for this PhD.

Indeed, this thesis would be literally different if Berit and Jakob would not have proofread it. Thank you for your valuable remarks and useful comments.

The whole PhD would have failed if there had not been a rowing club! Particularly I want to express thankfulness to Joana and Julia. You were always there to go on the water together and I really enjoyed our rows. Over time you have become real friends.

Also the *Maultaschen* ultimate frisbee team was a large backing and even a greater distraction.

Aurelia, you have been a great support! You enrich my life and I am looking forward to creating many more memories.

Finally, I wanted to thank my family which always encouraged me in going my own way.

So many people have supported me during this project and thus I might have forgotten to mention some of you, but all of you are greatly appreciated!

DANKESCHÖN!

Table of Contents

List of Figures

List of Tables

List of Abbreviations

ABL	aqueous boundary layer
AIC	*Akaike* Information criterion
BET	*Brunauer-Emmett-Teller* surface area analysis
BIC	*Bayesian* Information criterion
BJH	*Barrett-Joyner-Halenda* pore analysis
DOC	dissolved organic carbon
DOM	dissolved organic matter
FD	film diffusion
HOC	hydrophobic organic contaminants
IPD	intraparticle diffusion
OC	organic carbon
PA	polyamide
PAH	polycyclic aromatic hydrocarbons
PBS	phosphate buffered saline
PCB	polychlorinated biphenyls
PE	polyethylene
POC	particulate organic carbon
PS	polystyrene
SEM	scanning electron microscope
TOC	total organic carbon

List of Symbols

b	[-]	*Polanyi* exponent
C_P	[M M^{-1}]	concentration in particulate phase
C_{PE}	[M M^{-1}]	concentration in polyethylene
C_W	[M L^{-3}]	concentration in aqueous phase
C_W^*	[M L^{-3}]	concentration in aqueous bulk phase
$C_{W/P}$	[M L^{-3}]	C_W at particle surface
C_{surf}	[M L^{-2}]	sorbate mass per surface area
D_{aq}	[L^2 T^{-1}]	aqueous diffusion coefficient
D_P	[L^2 T^{-1}]	intraparticle diffusion coefficient
d_P	[L]	particle diameter
E	[M L^2 T^{-2}]	characteristic free energy of absorption
f_i	[-]	fraction of ionic species
f_n	[-]	fraction of neutral species
K_d	[L^3 M^{-1}]	linear partition coefficient
K_{Fr}	[M^{1-n} L^{3n} M^{-1}]	*Freundlich* coefficient
K_{DOM}	[L^3 M^{-1}]	DOM-water partition coefficient
K_{OW}	[L^3 M^{-1}]	octanol-water partition coefficient
K_P	[L^3 M^{-1}]	plastic-water partition coefficient
$K_{P,i}$	[L^3 M^{-1}]	K_P of ionic species
$K_{P,n}$	[L^3 M^{-1}]	K_P of neutral species
$K_{P,app}$	[L^3 M^{-1}]	apparent plastic-water partition coefficient
K_{PE}	[L^3 M^{-1}]	polyethylene-water partition coefficient
K_{PE}^*	[L^3 M^{-1}]	polyethylene-bulk solute partition coefficient
K_{surf}	[L]	virtual plastic layer thickness
k_w	[L T^{-1}]	mass transfer coefficient
m_p	[M]	mass of particles
n_{Fr}	[-]	*Freundlich* exponent
P_{pH}	[L^3 M^{-1}]	pH-dependent partition coefficient

pK_a	[-]	Acid dissociation constant
R	[M L^2 T^{-2} N^{-1} $temp^{-1}$]	ideal gas constant
r	[L]	radial coordinate
r_P	[L]	particle radius
Re	[-]	*Reynolds* number
Sc	[-]	*Schmidt* number
Sh	[-]	*Sherwood* number
T	[temp]	temperature
T_g	[temp]	glass transistion temperature
t	[T]	time
V_o	[L^3 M^{-1}]	maximum volume of sorbate per unit of sorbent
V_W	[M^3]	volume of water
WS_{sub}	[M L^{-3}]	subcooled liquid solubility
δ_W	[L]	aqueous boundary layer thickness
ε	[L^2 T^{-3}]	turbulent energy dissipation rate
ρ_o	[M L^{-3}]	sorbate density
ρ_P	[M L^{-3}]	particle density
σ	[-]	standard deviation
τ_{ch}	[T]	characteristic time of mass transfer
$\tau_{ch}^{external}$	[T]	characteristic time of external mass transfer
$\tau_{ch}^{internal}$	[T]	characteristic time of internal mass transfer

Part I

Thesis

1 Introduction & Background

Freshwater and marine ecosystems are increasingly threatened by anthropogenic pollution, mainly chemical contamination which has even been considered to be a planetary boundary threat, i.e. it irreversibly imperils vital Earth system processes (MacLeod et al., 2014; Rockström et al., 2009). The growing number of chemicals present in the aquatic environments cause harmful effects on organisms and even human health (Schwarzenbach et al., 2006). A major fraction of such contaminants comprises organic chemicals which are known to be persistent, bioaccumulative, and toxic and some of which are targeted by the Stockholm Convention on persistent organic pollutants (Lallas, 2001). As these pollutants are persistent and bioaccumulative, one intrinsic property is usually their low water solubility and thus their hydrophobicity (Mackay & Fraser, 2000; Mackay et al., 2001). Such hydrophobic organic contaminants (HOC) are often associated with organic carbon-rich particles rather than being freely dissolved in the water column (Karickhoff et al., 1979). Since transport of particles and sorbed contaminants is different compared to that of purely dissolved substances, particle properties such as material, density, size, and shape are decisive parameters controlling sorption/desorption kinetics of associated contaminants (Ghosh et al., 2001; Pignatello & Xing, 1996). Sorbed contaminants are less available for biodegradation and may, therefore, be transported further than freely dissolved chemicals that are prone to transformation processes (Alexander, 2000; Forbes et al., 1998). Consequently, particles or sediments act as long-term sinks and subsequently become secondary sources of HOCs (Allan et al., 2012; Jones & De Voogt, 1999). Thus, to understand the environmental fate of HOCs and to assess their impact, the investigation of particle-facilitated transport is important (Barber et al., 2006; Ko & Baker, 2004). The relevant particle types include colloids, such as natural organic substances, suspended sediments and different types of black carbon. Quite recently, plastic litter was added to that list as it is ubiquitously detected in all environmental compartments (Barnes et al., 2009; Horton et al., 2017; Law & Thompson, 2014). First almost exclusively recognized as marine litter, it is now known that plastic debris contaminates aquatic ecosystems on a global scale from rivers and lakes to the coast, the open ocean and even to remote areas as the polar regions (Browne et al., 2011; Horton et al., 2017; Law, 2017; Peeken et al., 2018; Ryan & Moloney, 1993). Besides attracting scientific attention, it has been tremendously discussed in the media and raised concern worldwide.

1.1 Microplastics

In terms of the number of detected plastic particles, microplastics has the largest share (Eriksen et al., 2014; Poulain et al., 2019; Worm et al., 2017). Such particles are defined as any synthetic polymer with a size smaller than 5 mm (Thompson et al., 2004). They can be introduced directly (primary microplastics) or originate from the progressive fragmentation of larger items (secondary microplastics) due to physical and mechanical stress (Browne et al., 2007). Whereas the effects of macroplastics are commonly described, the ecological consequences of microplastic particles remain largely speculative and a variety of scientific articles report partially contradictory results (Burns & Boxall, 2018; Gregory & Andrady, 2003; Katsnelson, 2015). It has been observed, that microplastic particles can be ingested and accumulated by organisms and transferred within the food web (Syberg et al., 2015; Wright et al., 2013). On the individual and population level, the uptake of such particles can alter the feeding behavior and the metabolic demand and can thus cause reduced growth and reproductive output and may finally lead to a population decline (Galloway & Lewis, 2016; Worm et al., 2017). For smaller particles, it is also hypothesized that they may pass membranes and can thus cause adverse effects on the (sub-)cellular level (Galloway & Lewis, 2016).

An additional and maybe even larger hazard is not caused by the mere presence of microplastics particles but by their ability to contain and interact with HOCs (Teuten et al., 2009). However, most published studies focus on the detection and quantification of plastic particles in various environmental matrices as well as on their fate or ecotoxicological effects on organisms. Even though there is an ongoing discussion how microplastics contribute to the transport of contaminants in aquatic systems (Burns & Boxall, 2018; Koelmans et al., 2016), only a limited number of studies addresses the subject of sorption and desorption kinetics, the underlying mechanisms and the corresponding role of microplastics as a probable pollutant vector (Hartmann et al., 2017; Zarfl & Matthies, 2010). It has been shown that microplastic particles sampled in the field contain for instance polycyclic aromatic hydrocarbons (PAHs) or polychlorinated biphenyls (PCBs) in concentrations orders of magnitude above those in the surrounding water phase (Alimi et al., 2018; Wang et al., 2018). Consequently, plastic may act as a pollutant transporter, increasing the exposure of organisms towards contaminants due to particle ingestion.

Recent modelling studies could show that under certain conditions and time scales, plastic particles may contribute to the accumulation of PAHs in aquatic food webs (Diepens & Koelmans, 2018). On the other hand, ingested particles may also act as a sink, resulting in a decreased bioaccumulation potential (Koelmans et al., 2013; Teuten et al., 2009). An increasing number of studies concluded that plastic ingestion do not significantly influence the exposure of organisms towards plastic associated contaminants on different trophic levels (Gouin et al., 2011; Koelmans et al., 2016). These findings however, cannot pass over the fact that microplastics interact with contaminants and their ability to take up and transport chemicals cannot be neglected. Accordingly, a growing number of studies reported sampling of plastic particles from various environmental compartments and the extraction of associated pollutants (Chen

et al., 2017; Karapanagioti et al., 2011; Mendoza & Jones, 2015). Whether such sorbed pollutants represent ambient concentrations, in which microplastics act as passive sampler, or traveled long distance with the plastic, i.e. it act as transport vector, is unclear. Therefore, the role of microplastics as a pollutant vector is actively debated and in order to address this question, the development and validation of mechanistic models is necessary as they can be utilized to extrapolate the knowledge obtained from experimental data to environmentally relevant time scales and settings.

1.2 Microplastic-Pollutant Interactions

Generally, approaches regarding the interactions between plastic particles and contaminants can be classified in two groups. Both the equilibrium sorption as well as the sorption and desorption kinetics can be analyzed. Equilibrium sorption of organic contaminants into plastic particles has been described by different types of isotherms such as the linear, *Freundlich*, and *Langmuir* models (Hüffer & Hofmann, 2016). Quite recently more subtle approaches such as the poly-parameter linear free energy relationship were applied to describe and predict equilibrium sorption (Hüffer et al., 2018). However, as the sorption process involves the incorporation of the chemicals into the polymeric matrix of the solid plastic items, assuming local equilibrium between the water and the particulate phase may be misleading.

Still a minority, there is an increasing number of publications dealing with kinetics. Within these, a variety of different models have been applied to describe the kinetics of sorption onto/into the plastic particles (Endo et al., 2013; Teuten et al., 2009). The most applied approaches are reaction-based models such as the *first-order kinetics* or the *pseudo second-order model* (Alimi et al., 2018; Ho & McKay, 1999). Within these model types, all relevant physical, chemical, and thermodynamic processes are condensed in fitted bulk rate constants which cannot provide details on the underlying mechanisms (Tan & Hameed, 2017). Additionally, these models are usually derived from experimental data obtained under laboratory conditions and thus simplified assumptions are necessary once the findings should be transferred to environmental settings. Nevertheless, reaction-based models are most frequently applied if evaluation of contaminant sorption to microplastics is concerned, e.g. in Llorca et al. (2018) , Rochman et al. (2013), Teuten et al. (2007), Wang & Wang (2018a), and Zhang et al. (2018).

On the other hand, mechanistic models based on Fick's laws of diffusion (Fick, 1855). can be applied. Typically, diffusion parametrized by these laws allows to identify the rate limiting step. Diffusion between a particulate and a liquid phase is usually subdivided into two mass transfer processes (Pignatello & Xing, 1996; Seidensticker et al., 2017; Tcaciuc et al., 2015): (i) transport from the bulk water phase to the particle surface, i.e. external mass transfer, and (ii) subsequent diffusion within the particles, i.e. internal mass transfer. Within this framework, external mass transfer can be described as the diffusion through an aqueous boundary layer (ABL) surrounding the particle, following a first-order approach (Grathwohl, 2012). Thus, within external mass transfer the mass flux is proportional to the concentration difference across the ABL. The internal mass transfer, i.e. intraparticle diffusion, however, requires a description accounting

for the temporal change of the concentration profile within the particle (Grathwohl & Reinhard, 1993). Commonly, external and internal mass transfer are studied using separate models. For instance Weber & Morris (1963) proposed a modelling approach to describe kinetics which are limited by intraparticle diffusion. Regarding microplastics, this model was e.g. used by Wang & Wang (2018a). As an extension to this approach more complex models are applied. These are usually based on the analytical solution for Fick's 2nd law derived by Crank (1979) but again account for either pure film or intraparticle diffusion. The same holds for the corresponding short-term and long-term approximations which are applied as well to describe sorption to microplastics (Endo et al., 2013; Karapanagioti & Klontza, 2008; Lee et al., 2018). However, to accurately transfer experimental data to environmental conditions, a coupled models considering both mass transfer processes in series is necessary (Seidensticker et al., 2017).

Thesis Aims & Objectives 2

Almost half a century passed since the first detection of plastic particles in the environment reported by Carpenter et al. (1972) and the increasingly recognized pollution of aquatic environments (Ryan & Moloney, 1993). Within this time period plastic debris attracted growing attention and until today it is highly controversial whether such debris may release pollutants to the environment (Burns & Boxall, 2018).

The overall objective of the present thesis was to elucidate mass transfer mechanisms of urban organic pollutants on different types of microplastic particles and to clarify their role as sink and/or source of contaminants in aquatic ecosystems. Even though many studies detected plastic in the both the world's marine and limnic environments (Horton et al., 2017; Law, 2017) it is an ongoing debate if such particles contribute to contaminant transport (Alimi et al., 2018; Koelmans et al., 2016; Zarfl & Matthies, 2010; Ziccardi et al., 2016). Nevertheless, one has to keep in mind that a vast majority of such estimations are limited to the current amount of plastics in the environment and even though it is not necessarily easy to predict future quantities, most studies dealing with that issue prognosticate increasing amounts of plastic debris (Geyer et al., 2017; Jambeck et al., 2015). Taking the plastic production data since 1950 published by Geyer et al. (2017), assuming that every year approximately 3% of the total production enters the ocean as estimated by Jambeck et al. (2015), and extrapolating this information results in an increase of the cumulative plastic waste in the ocean from about 260 Mt in 2017 to ~ 910 Mt in 2050 (for details see SI 1). From this particular aspect it is worthwhile to investigate and characterize sorption interactions between anthropogenic contaminants and polymer particles.

Within this thesis I focused on rivers as they are one major path for microplastics to enter freshwater ecosystems, particularly via the effluent of wastewater treatment plants and via sewage overflows (Mintenig et al., 2017; Murphy et al., 2016). In such effluents, however, also increased concentrations of micropollutants such as pharmaceuticals and pesticides occur (Gasperi et al., 2008; Gavrilescu et al., 2015; Li et al., 2016). Thus, plastic particles might especially act as a sorbent and potential vector for frequently occurring wastewater contaminants. Consequently, I studied the interactions between microplastic and common wastewater pollutants. Furthermore, the experimental data obtained from the sorption experiments served as a base to develop and parametrize mechanistic kinetic models. Subsequently, I used those models to extrapolate from laboratory conditions to environmentally relevant settings and to draw conclusions regarding the role of microplastic particles in contaminant transport. Figure 2.1 gives an overview of the main hypotheses and objectives of this thesis and illustrates the gradually increasing environmental relevance of the performed experiments.

Polyethylene is one of the most produced and environmentally abundant polymers (Auta et al., 2017; Mintenig et al., 2017; Peeken et al., 2018). It is well known for its ability to take up hydrophobic contaminants and is thus widely applied as passive sampler (Allan et al., 2009; Lohmann, 2011; Thompson et al., 2015). If sorption is studied, however, the investigations usually concentrate on equilibrium partitioning and only a minor percentage pay particular attention to the sorption kinetics. Thus, in **paper I** an in-depth investigation of sorption kinetics to polyethylene is presented and a coupled mass transfer model was developed to mechanistically describe these kinetics. This way, the role of the different mass transfer processes was revealed. Subsequently, we compared this model with other commonly applied models and deliberated its advantages.

Although polyethylene makes up the largest part of plastics in the environment, also other polymers such as polystyrene and polyamide are frequently detected (Mintenig et al., 2017). In **paper II** we describe our experiments to investigate sorption isotherms and kinetics of phenanthrene to these three polymers. Conversely to polyethylene, polystyrene and polyamide showed non-linear sorption isotherms. Therefore, we set up and validate a numerical model to simulate coupled mass transfer for both linear and non-linear sorption and to assess the influence of particle and substance characteristics on the sorption process.

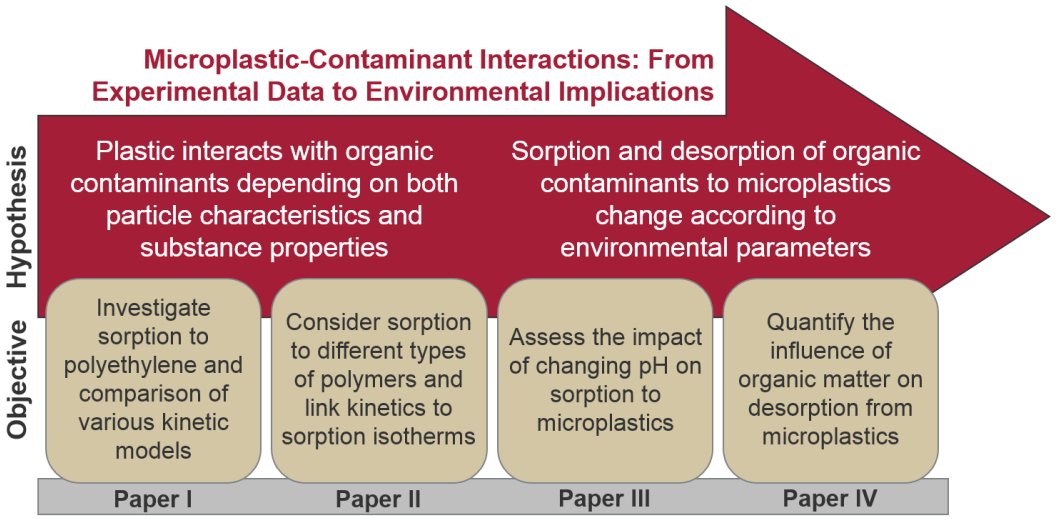

Figure 2.1: **Overview of the main hypotheses and objectives of this thesis and the corresponding papers.**

From studies with natural particles and sediments, it is known that sorption interactions mostly occur between sorbents and neutral species whereas charged compound species sorb only little or not at all (Karlsson et al., 2017). However, unlike many natural particles, microplastics can be charged electrostatically (Wang et al., 2015; Yokota et al., 2017) and thus ionic bonds may evolve between plastic particles and charged species. Therefore, in **paper III** (Seidensticker et al., 2018) we present our investigations on equilibrium partitioning between polyethylene and polystyrene microplastic particles and a set of frequently occurring contaminants (e.g. pesticides, pharmaceuticals, and industrial chemicals) some of which were ionizable. The aim of

that study was, to elucidate the sorption interactions between plastic particles and the selected contaminants under varying pH conditions.

Since microplastic particles are not the only occurring sorbent in natural environments, the aim of our study presented in **paper IV** (Seidensticker et al., 2017) was to analyze and quantify the sorption kinetics of wastewater pollutants to polyethylene microplastic particles and how they are influenced by the presence of natural dissolved organic matter. More specifically, we examined the shift of mass transfer from external film diffusion to intraparticle diffusion as a function of partition coefficients which change according to the concentration of dissolved organic matter.

Theory & State of the Art 3

3.1 Equilibrium Sorption

For the evaluation of equilibrium sorption and partitioning, I applied three different sorption isotherms. The outcomes of the isotherm experiments are mainly described in **paper II**. The simplest is linear sorption with a constant distribution coefficient K_d [L^3 M^{-1}] (Schwarzenbach et al., 2005). I also considered the *Freundlich* and the *Polanyi-Dubinin-Manes* non-linear sorption isotherms in which the sorption coefficient depends on the amount of sorbed contaminant (Allen-King et al., 2002; Kleineidam et al., 2002). The *Freundlich* model is an empirical relationship with non-linearity represented by the *Freundlich* exponent n_{Fr} which usually takes values between 0 and 1 (Xia & Ball, 1999). The *Polanyi-Dubinin-Manes* model on the other hand is derived from Polanyi's potential theory for a vapor phase system and is commonly applied to describe pore-filling mechanisms (Kleineidam et al., 2002; Xia & Ball, 1999). The three different isotherm models are given as:

$$\textit{linear} \qquad C_{P,eq} = K_d C_{W,eq} \tag{3.1}$$

$$\textit{Freundlich} \qquad C_{P,eq} = K_{Fr} C_{W,eq}^{n_{Fr}} \tag{3.2}$$

$$\textit{Polanyi} \qquad C_{P,eq} = V_o \rho_o \exp\left[\left(\frac{-RT\left(ln\frac{WS_{sub}}{C_{W,eq}}\right)}{E}\right)^b\right] \tag{3.3}$$

with K_{Fr} [M^{1-n} L^{3n} M^{-1}] and n_{Fr} being the *Freundlich* partition coefficient and the *Freundlich* exponent, V_o denoting the maximum volume of sorbate per unit of sorbent [L^3 M^{-1}], ρ_o [ML^{-3}] sorbate's density, $R = 8.314$ J mol^{-1} K^{-1} the ideal gas constant, T [temp] absolute temperature, and WS_{sub} the subcooled liquid solubility of the compound in water [ML^{-3}]. E [ML^2T^{-2}] is the characteristic free energy of absorption (Allen-King et al., 2002). The exponent b [-] is usually an integer with $1 > b > 5$. $C_{P,eq}$ and $C_{W,eq}$ represent the equilibrium concentrations in the particle and the water phase, respectively.

In **paper III** I extended the aforementioned approach. The sorption of ionizable compounds needs to be computed differently if the contribution of neutral and charged species should be quantified. Thus, the pH-dependent partition coefficient P_{pH} is:

$$P_{pH} = K_{P,n} f_n + K_{P,i} f_i \tag{3.4}$$

where f_n and f_i are the fractions of the neutral and ionized species and $K_{P,n}$ and $K_{P,i}$ are the species-specific partition coefficients for the neutral and the ionized species, respectively. I calculated f_n and f_i from the known pK_a and pH values according to the rearranged *Henderson-Hasselbalch* equation.

According to previous findings within **paper IV** only linear equilibrium partitioning was considered as I only used polyethylene as sorbent (Lohmann, 2011). By introducing a second dissolved phase, here humic acids, the chemical has to equilibrate between the three phases in the system and the partition coefficient K^*_{PE-W} between the overall aqueous solution and the solids decreases with increasing concentration of dissolved organic matter (DOM) is (Schwarzenbach et al., 2005):

$$K^*_{PE-W} = \frac{K_{PE-W}}{1 + K_{DOM} DOM} = \frac{C_{PE}}{C^*_{W,eq}} \tag{3.5}$$

K_{DOM} and K_{PE-W} are the partition coefficients [L^3 M^{-1}] between pure water and dissolved organic matter or polyethylene, respectively. Only if the product $K_{DOM} \times DOM$ becomes larger than unity, a significant change in partitioning of a compound between aqueous solution and solids may be expected. Since DOM contents typically are below 0.001 kg L^{-1}, only compounds with K_{DOM} larger than 1000 are significantly affected. C^*_W represents the concentration in the bulk solution, i.e. the freely dissolved concentration plus the concentration in the DOM phase. Based on the mass balance in the three-phase system, the equilibrium concentration $C^*_{W,eq}$ [M L^{-3}] in the DOM-inclusive aqueous phase for given initial concentration C_{PE} (0) [M M^{-1}] in the polyethylene and C^*_W (0) [M L^{-3}] in the aqueous phase (in our experiments always zero) can be computed as a function of the liquid-to-solid ratio V_W/m_P [M^3 M^{-1}] and the overall partition coefficient by:

$$C^*_{W,eq} = \frac{C_{PE}(0) + C^*_W(0)\frac{V_W}{m_P}}{\frac{V_W}{m_P} + K^*_{PE-W}} \tag{3.6}$$

3.2 Mass Transfer Model and Mass Conservation Laws

The mass transfer of organic pollutants between a particulate phase and a surrounding bulk solution of finite volume involves transfer from the bulk solution to the particle surface through an aqueous boundary layer (external mass transfer) and subsequent diffusion within the solids (internal mass transfer) if the sorption case is concerned (Thompson et al., 2015). The slower process controls the overall kinetics. A coupled model which can describe both mass transfer mechanisms separately but as well in combination is necessary to fully analyze and understand the kinetics. The underlying assumptions for the analysis of my finite-volume batch experiments were: (i) the bulk solution is homogeneously mixed, (ii) the external mass transfer between the particles and the bulk solution is proportional to the difference of the aqueous concentrations between the bulk solution and the particle surface, (iii) at the particle surface, local equilibrium between the two phases exists, and (iv) the mass flux within the plastic particles is by diffusion in the polymer. To consider both internal and external mass transfer in series, I formulated a coupled transport model. Within the microplastic particles, the diffusion equation in spherical coordinates, i.e. Fick's 2nd law, applies:

$$\frac{\partial C_P}{\partial t} - D_P \left[\frac{\partial^2 C_P}{\partial r^2} + \frac{2}{r} \frac{\partial C_P}{\partial r} \right] = 0 \tag{3.7}$$

$$\left. \frac{\partial C_P}{\partial r} \right|_{r=0} = 0 \ \forall t \tag{3.8}$$

The initial concentration in the particle phase is considered to be uniform:

$$C_P(r, t = 0) = C_P(0) \ \forall r \tag{3.9}$$

with C_P [M M^{-1}] denoting the mass-related concentration of the organic compound in the plastic, t [T] is time, and D_P [L^2 T^{-1}] and r [L] are the material-dependent intraparticle diffusion coefficient and the radial coordinate, respectively. A concentration gradient of zero in the spheres' center and sorption equilibrium between the plastic and water at the surface of the plastic particles are assumed as boundary conditions. The particle exchanges mass with a surrounding bulk solution of a defined volume V_W [L^3] via the aqueous boundary layer. Mass transfer through the boundary layer is driven by the concentration gradient between the bulk solution and the aqueous concentration at the interface between the particles and the water. Then, the mass balance at the surface requires:

$$K_P \frac{dC_{W/P}}{dt} = \left(C_W(t) - C_{W/P}(t) \right) k_W - D_P \rho_P \left. \frac{\partial C_P}{\partial r} \right|_{r_P} \tag{3.10}$$

in which C_W [M L^{-3}] denotes the bulk-phase concentration, $C_{W/P}$ (t) [M L^{-3}] the aqueous concentration at the particle surface, K_P [L^3 M^{-1}] the partition coefficient, r_P

[L] the particle radius, and k_W [L T^{-1}] the mass-transfer velocity. Multiplication by the mass density ρ_P [M L^{-3}] of the particles in the intraparticle-diffusion term of the equation is needed because the concentration in the particles is expressed as mass of the compound per mass of the particle material, whereas the concentration in the aqueous phase is volumetric.

Under finite bath boundary conditions, the concentration in the bulk water changes according to the total mass flux across the area of all particles, leading to the following mass balance equation:

$$\frac{dC_W}{dt} = \left(C_{W/P}(r_P,t) - C_W(t)\right) k_W \frac{3}{r_P} \frac{m_P}{V_W \rho_P} \tag{3.11}$$

in which m_P [M] is the mass of all particles, the factor $3/r_P$ is the area-to-volume ratio of a single particle, and m_P/ρ_P is the total volume of all particles. Equations 3.10 & 3.11 must be amended by initial conditions of C_W and $C_{W/P}$. In addition to absorption within the particles, in some cases instantaneous adsorption onto the surface was assumed, obeying the same sorption isotherm of the plastic material:

$$C_{surf}(t) = K_{surf} \rho_P C_{P,eq}\left(C_{W/P}(t)\right) \tag{3.12}$$

with C_{surf} [M L^{-2}] denoting the mass of the sorbate per surface area, $C_{P,eq}\left(C_{W/P}(t)\right)$ [MM^{-1}] as the equilibrium concentration in the plastic material for a given aqueous concentration $C_{W/P}(t)$ at the plastic-water interface, and K_{surf} [L] as the thickness of a virtual plastic layer instantaneously sorbing the contaminant. The latter parameterizes the effects of surface roughness. As I show in Appendix II 5 (SEM images of the particles) and in Table 1, many particles have rough surfaces and the true surface areas are different from those calculated for perfect spheres. I accounted for these effects by considering effective surface adsorption.

The analytical solution of Equations 3.7-3.11 was derived after Laplace transformation in time (see Appendix IV 4.3), and consider three cases of mass-transfer controls: (i) by external mass-transfer only, i.e. in the limit of $D_P \to \infty$, (ii) by intraparticle diffusion only, i.e. in the limit $k_W \to \infty$, and (iii) by both processes. The analytical Laplace-transform solution of the bulk-phase concentration is back-transformed into the time domain by the numerical method of de Hoog et al. (1982), implemented in Matlab. The specific case of linear sorption without instantaneous adsorption (i.e. $K_{surf} = 0$) was applied within **papers I & IV** but for the case of a non-linear sorption isotherm with $C_{P,eq}(C_w)$ as determined in **paper II**, a closed-form solution in the Laplace-domain cannot be derived, requiring thus a numerical scheme. For this purpose Equation 3.7 was spatially discretized by the Finite Volume method, i.e. the particles were subdivided into n [-] shells of identical thickness. The resulting non-linear system of ordinary differential equations was integrated by the Gear solver `ode15s` implemented in Matlab (see Appendix II 5 for details).

3.3 Analysis of Characteristic Times

According to the explanations above, the overall mass transfer in my experiments is controlled by an external and an internal process in series. The relative importance of these two processes can be evaluated by using the characteristic time τ_{ch} [T] which were derived from the Laplace-transform analytical solution and synopsizes the equilibration times between the particles and the bulk solution. It is defined as:

$$\tau_{ch} = \frac{\int_0^\infty \left(C_W(t) - C_{W,eq}\right) dt}{C_W(0) - C_{W,eq}} \tag{3.13}$$

It can be split into a characteristic time for the case of internal mass transfer:

$$\tau_{ch}^{internal} = \frac{r_P^2}{\left(1 + K_P \frac{m_P}{V_W}\right) 15 D_P} \tag{3.14}$$

and congruently to a characteristic time for the case of external mass transfer:

$$\tau_{ch}^{external} = \frac{K_P \rho_P r_P}{\left(1 + K_P \frac{m_P}{V_W}\right) 3 k_W} \tag{3.15}$$

As the coupled mass transfer is the sum of film and intraparticle diffusion, likewise the two characteristic times are additive, i.e. the overall mass transfer is slower than either of the single processes. Note, that for increasing K_P, the characteristic time in the case of external control (Equation 3.15) becomes independent of K_P whereas the characteristic time of the internally limited mass transfer (Equation 3.14) decreases with increasing K_P. Under environmental settings, V_W tends to infinity and for both cases the term in the parentheses becomes 1. While in Equation 3.15 the characteristic time refers to 63.2% of the equilibrium concentration, in Equation 3.14 the degree of equilibration depends on the solid-to-liquid ratio and K_P (see Appendix II 5).

The relative importance of the respective mass-transfer process for the overall mass transfer can be expressed as the ratio of their characteristic times:

$$\frac{\tau_{ch}^{external}}{\tau_{ch}^{internal}} = \frac{5 K_P \rho_P D_P}{k_W r_P} \tag{3.16}$$

For values >1, external mass transfer limits the kinetics and internal mass transfer controls for values <1. Equation 3.16 exemplifies that the relative importance of the two processes does not depend on the liquid-to-solid ratio. Consequently, for internal mass transfer an increasing partition coefficient accelerates the kinetics in batch systems despite decreasing aqueous equilibrium concentrations. Mass transfer of hydrophobic compounds, however, is externally controlled due to high partition coefficients.

Materials & Methods 4

4.1 Microplastic Particles

Across **papers I-IV**, I performed experiments with four different types of particles made of three different polymers. Their relevant properties are listed in Table 4.1. For all particles except the large polyethylene, scanning electron microscope (SEM) images are provided in the Appendix II 5.

Table 4.1: **Sources and properties of the microplastic particles used in this thesis.** *a*: nominal diameters, normally distributed with σ^2=0.05, *b*: literature values from Hüffer & Hofmann (2016).

Parameter	Small Polyethylene (PE)	Large Polyethylene (PE)	Polystyrene (PS)	Polyamide (PA)
Supplier	Azelis, Gotalene 120	German Federal Institute for Materials Research and Testing	Goodfellow	Goodfellow
Mean diameter [μm][a]	260	4.2×10^3	250	25
Density [kg L^{-1}]	0.92	0.92	1.05	1.14
Calculated surface area [m^2 g^{-1}]	0.03	0.002	0.023	0.30
BET surface area [m^2 g^{-1}]	0.23	0.18	0.65	0.86
BJH pore volume [cm^3 g^{-1}]	*no pores*	*no pores*	0.003	0.000013
Porosity [%]			0.32	0.01
Average pore width [Å]	*no pores*	*no pores*	195.3	18.8
Glass transition temperature[b] [°C]	-120	-120	100	50
Applied in	**Papers I-IV**	**Paper I**	**Papers II & III**	**Paper II**

4.2 Chemicals

In total, 21 different chemicals were tested for their sorption interactions with different types of microplastic. These chemicals include seven bases with dissociation constants (pK_a) ranging from 1.09 to 8.37, seven acids covering pK_a values of 3.13 to 7.90 and seven neutral substances. Details on the physico-chemical properties of these compounds and their experimental application are listed in Table 2. All chemicals were purchased from LGC standards (Wesel, Germany), except phenanthrene and tonalide which were purchased from Sigma-Aldrich Supelco (Bellefonte, PA, USA).

4.3 Batch Experiments

To study both equilibrium distribution and sorption kinetics, I performed batch experiments. The experimental setups differ slightly from **paper I** to **paper IV**. The details are described in the different papers in the Appendices II 5-IV 4.3. Here, I will give a brief overview and explain the most important details. The common across all setups was the solid-to-liquid ratio which was always 10^{-3} kg L^{-1}. All experiments were performed either in amber glass bottles (**papers I-III**) or in glass bottles wrapped with aluminum foil (**paper IV**) and contained certain amounts of NaN_3 to avoid photo-oxidation and biodegradation, respectively. In the case of sorption experiments (**papers I-III**), I spiked the batches from aqueous contaminant solutions, either containing a single substance or a substance mix. To avoid co-solvent effects of organic solvents, their fraction was always below 0.1%. Only in **paper IV** the initial solution contained humic acids, and the plastic particles were previously spiked with contaminants as the desorption case was examined. I prepared all these solutions in ultrapure water and in the sorption case, the initial concentration of every substance was below 1% of its water solubility to avoid competitive sorption or crystallization effects. As additional constituents, the batches either contained pH adjusting substances (**paper III**) to maintain constant pH values of 4 (formic acid), 7 (0.02 M Na_2PO_4), or 10 (7N NH_3). For experiments reported in **paper IV**, humic acids in six different concentrations (0, 0.15, 0.25, 0.50, 0.75, and 1.00 g L^{-1}) and the corresponding phosphate-buffered saline (PBS) buffer were constituents. PBS was necessary to keep slightly alkaline conditions with a pH of 7.7 to ensure the complete dissolution of the humic acids. All further details regarding the exact experimental procedure, the sampling techniques, and the subsequent chemical analysis and parameter estimations are carefully described in the particular paper and the corresponding supporting information.

Table 4.2: **Physico-chemical properties of the investigated substances.** Either taken from ChemSpider (molecular weight MW, molecular volume MV and log K_{OW} of neutral species), the PubChem database (pK_a), or EU regulatory and evaluation data. Subcooled liquid solubilities (WS_{sub}) of neutral species were estimated based on melting points (Kan & Tomson, 1996; Liu et al., 2013). For substances with melting points <0° C, WS_{sub} is written in italics. Aqueous and polyethylene-intraparticle diffusion coefficients D_{aq} and D_{PE} were calculated based on the MW according to Worch (1993) and Rusina et al. (2010), respectively. TCPP = Tris(2-chloroisopropyl)-phosphate; DEET = N,N-Diethyl-3-methylbenzamide; MCPA: 2-methyl-4-chlorophenoxyacetic acid.

Compound	CAS#	MW [g mol^{-1}]	MV [cm^3 mol^{-1}]	WS_{sub} [mol L^{-1}]	log K_{OW}	$D_{aq} \times 10^{10}$ [m^2 s^{-1}]	$D_{PE} \times 10^{14}$ [m^2 s^{-1}]	pK_a	Acid-base reaction	Analysis method	Used in paper
Atrazine	1912-24-9	215.69	169.9	5.43×10^{-3}	2.6	6.86	10.84	1.60	base	LC-MS/MS	III
Benzophenone	119-61-9	188.2	167.5	1.38×10^{-3}	3.2	7.38	25.80		neutral	GC-MS	IV
Benzotriazole	95-14-7	119.13	88.3	1.05	1.4	9.40	227.99	8.37	base	LC-MS/MS	III
Caffeine	58-08-2	194.19	133.4	1.65×10^{1}	0.1	7.26	21.36		neutral	LC-MS/MS	III
Carbamazepine	298-46-4	236.28	186.6	3.10×10^{-3}	2.5	6.54	5.66	13.9	acid	LC-MS/MS	III
Carbendazim	10605-21-7	191.19	134.5	9.27×10^{-2}	1.5	7.32	23.48	4.29	base	LC-MS/MS	III
DEET	134-62-3	191.28	194.0	2.03×10^{-4}	2.2	7.31	23.41		neutral	LC-MS/MS	III
Diazinon	333-41-5	304.35	260.5	$.31 \times 10^{-3}$	3.8	5.72	0.66	2.60	base	LC-MS/MS	III
Diclofenac	15307-86-5	296.15	206.8	1.87×10^{-4}	4.5	5.80	0.86	3.99	acid	LC-MS/MS	III
Ibuprofen	15687-27-1	206.29	200.3	3.69×10^{-4}	4.0	7.03	14.58	4.45	acid	LC-MS/MS	III
MCPA	94-74-6	200.62	152.8	3.13×10^{-2}	3.3	7.13	17.44	3.13	acid	LC-MS/MS	III
Mecoprop	7085-19-0	214.65	169.7	1.62×10^{-2}	3.2	6.88	11.20	3.78	acid	LC-MS/MS	III
4-Nonylphenol	104-40-5	220.36	236.2	4.78×10^{-5}	5.8	6.78	9.36	10.7	acid	GC-MS	III
Phenanthrene	85-01-8	178.24	157.7	3.95×10^{-5}	4.5	7.59	35.33		neutral	GC-MS	I-IV
Propiconazole	60207-90-1	342.22	244.9	1.20×10^{-4}	3.7	5.37	0.20	1.09	base	LC-MS/MS	III
TCPP	13674-84-5	327.57	255.6	8.80×10^{-4}	2.6	5.50	0.32		neutral	LC-MS/MS	III
Tebuconazole	107534-96-3	307.83	268.1	3.69×10^{-4}	3.7	5.68	0.59	1.76	base	LC-MS/MS	III
Terbutryn	886-50-0	241.36	212.7	7.15×10^{-4}	3.7	6.47	4.82	4.30	base	LC-MS/MS	III
Tonalide	21145-77-7	258.2	280.9	1.13×10^{-5}	5.7	6.24	2.84		neutral	GC-MS	IV
Torasemide	56211-40-6	348.42	271.4	2.10×10^{-2}	3.4	5.32	0.16	6.68	acid	LC-MS/MS	III
Triclosan	3380-34-5	289.55	194.3	7.55×10^{-5}	4.8	5.87	1.05	7.90	acid	LC-MS/MS	III

Results & Discussion 5

5.1 Equilibrium Sorption Isotherms

The measured sorption isotherms discussed in **paper II** revealed, that polyamide and polystyrene follow non-linear sorption patterns whereas polyethylene shows linear partitioning. While for polyamide, the *Freundlich* model scored best, the *Polanyi-Dubinin-Manes* isotherm described the sorption of phenanthrene onto polystyrene the best. These results were confirmed by the calculation of model selection criteria which are outlined in the Appendix II 5. They are moreover in agreement with other findings Hüffer & Hofmann (2016) as well as with the measured pore volumes of polyamide and polystyrene (Table 4.1) as an increasing presence of pores shifts the isotherm towards a non-linear shape Kleineidam et al. (2002). The experimental results are shown in Figure 5.1.

5.2 Sorption to Polyethylene Microplastics and Model Comparison

Within **paper I**, the sorption of phenanthrene to various sized polyethylene particles were thoroughly investigated. The measured kinetics were evaluated with different models which were subsequently compared. The results of the kinetic experiments are shown in Figure 5.2. It is clearly visible, that mass transfer to small polyethylene particles is largely limited by film diffusion (left panel), i.e. the mass transfer resistance in the water phase limits the uptake of phenanthrene. Sorption to the large particles is in contrast limited by internal mass transfer, thus the diffusion within the particles controls the kinetics (right panel). This is in accordance with our model assumptions, in which an increasing size is accompanied by a relatively thinner aqueous boundary layer. Accordingly, the growing mass transfer resistance in the particle phase leads to longer equilibration times. Thus, the larger the particles the more kinetics is limited by intraparticle diffusion. Consequently, the fitted coefficients for film diffusion are not sensitive for large polyethylene and hence I used the film diffusion parameters fitted for small polyethylene to estimate the mass transfer coefficient k_W for large polyethylene adapted to both the particle size and the hydrodynamic conditions. For that purpose, a *Sherwood* relationship scaled by the particle diameter was utilized to characterize the well-known mass transfer in the aqueous boundary layer.

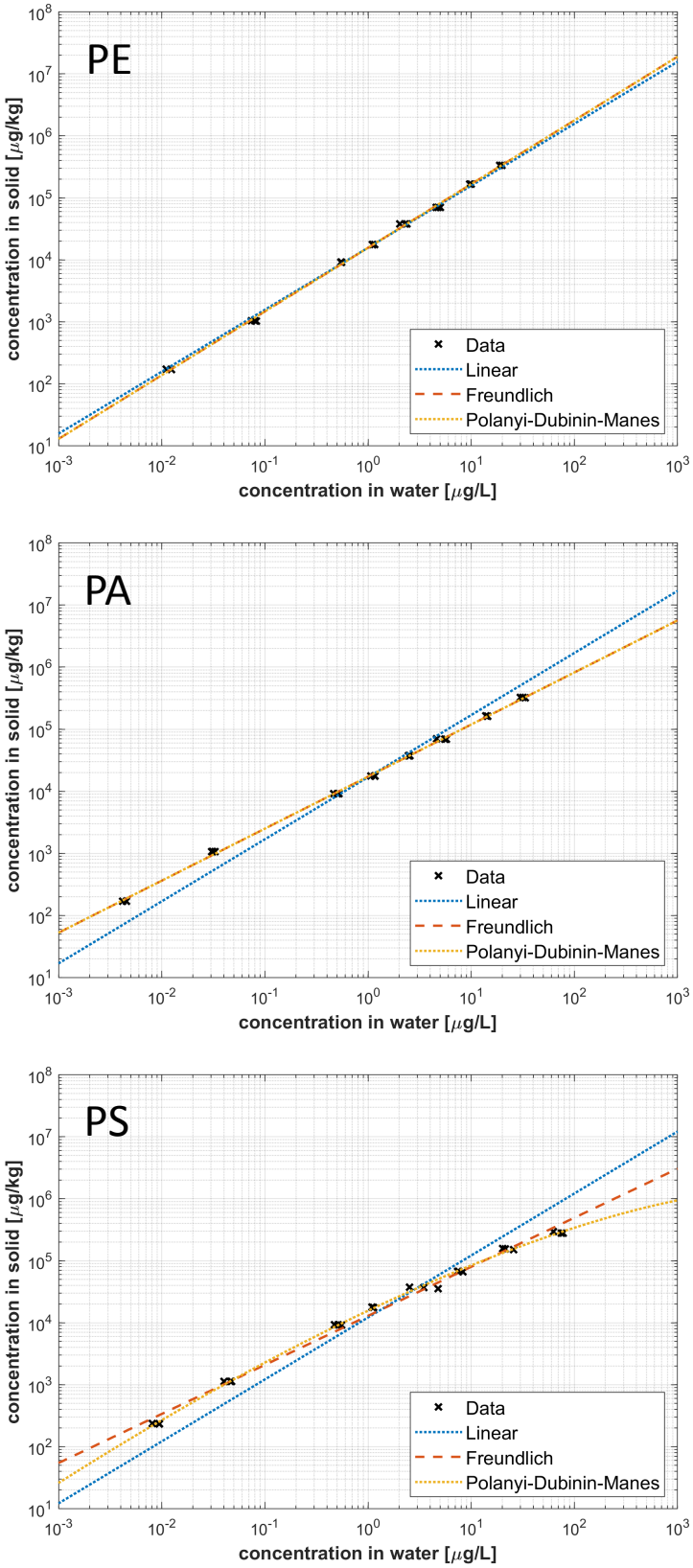

Figure 5.1: **Double logarithmic plot of data and models (linear, *Freundlich*, and *PDM*) for sorption isotherms of phenanthrene to PE, PA, and PS.** The different applied isotherms are indicated in the legends.

This is transferable to different experimental setups according to hydrodynamics represented by the *Reynolds* and the *Schmidt* number, Re and Sc, respectively. The *Sherwood* number Sh here was calculated as (Ohashi et al., 1981):

$$Sh = 2 + cRe^{1/2}\, Sc^{1/3} = 2 + 0.59 \left(\frac{d_P^{4/3} \varepsilon^{1/3}}{\nu} \right)^{0.57} \left(\frac{\nu}{D_{aq}} \right)^{1/3} \tag{5.1}$$

with the particle diameter d_P [L], the kinematic viscosity of water ν [L^2 T^{-1}], the substance specific aqueous diffusion coefficient D_{aq} [L^2 T^{-1}], and the unknown energy dissipation rate ε [L^2 T^{-3}]. If mass transfer is limited by film diffusion, k_W may be sensitively fitted and Sh ($Sh = k_W d_P D_{aq}^{-1}$) can be calculated from the experimental results. Eventually, Sh for small polyethylene was computed as 7.1 and based on Equation 5.1, ε for our experimental setup could now be estimated as $10^{4.2}$m^2 s^{-3} which is reasonable for stirred systems and can be used to calculate a theoretical k_W for the large particles (Kawase & Moo-Young, 1987). Within the parameter estimation, however, I did not set k_W to a fixed value but allowed fitting results with the range of ±10%. Subsequently, I performed another fitting without any restrictions and it appeared that the theoretically expected and the fitted *Sherwood* number differed slightly and the thickness of the boundary layer was larger than estimated. Thus, film diffusion seemed to be still relevant for larger particles in particular at early times. A possible explanation may be the shape of the larger particles which was rather cylindrical than spherical and hence influenced the film diffusion whereas internal mass transfer was hardly affected. Accordingly, the fitted intraparticle diffusion were similar for the two polyethylene types as it would be expected for the same material and were moreover in good agreement with literature values (Hale et al., 2010; Lohmann, 2011). Additionally, the partition coefficients compared very well to earlier measurements (Lohmann, 2011; Rusina et al., 2010). As I expected from the model predictions, the larger particles took considerably longer to reach equilibrium, namely around $10^{3.9}$ h compared to $10^{1.5}$ h for the small particles. This is different by a factor of ~ 250 and reflects the difference between the particle diameters squared which is a factor of ~ 260. Figure 5.2 (second row) additionally shows the measured and modeled time-dependent apparent distribution coefficients $K_{P,app}(t)$ for the different kinetic models as function of time. Such $K_{P,app}$ are more sensitive than aqueous concentrations because the latter get very small at late times. Within Figure 5.2 I do not only display the results of the new coupled mass transfer model, but show as well the results of a *first-order* and a *pseudo second-order* model, which are most frequently used if microplastic-contaminant interactions are examined (Llorca et al., 2018; Rochman et al., 2013; Teuten et al., 2007; Wang & Wang, 2018a).

To evaluate the model performance, I calculated two different model selection criteria, the *Akaike Information Criterion* (*AIC*, Akaike (1974)) and the *Bayesian Information Criterion* (*BIC*, Schwarz et al. (1978)). Both do not just appraise the *goodness-of-fit* but as well consider the complexity by contemplating the number of fitted parameters. For both approaches, a smaller value indicates a better suitability of the model and thus I

confirmed that the coupled model performed best for both particle sizes (Figure 5.2, third row). However, the difference between these selection criteria was greater for the large particles. This is attributed to the fact, that mass transfer to the small particles was mostly limited by film diffusion which can be estimated with an exponential function. On the other hand, the shift from film to intraparticle diffusion was much more pronounced for the large particles and thus the coupled model has a greater advantage as both processes need to be considered.

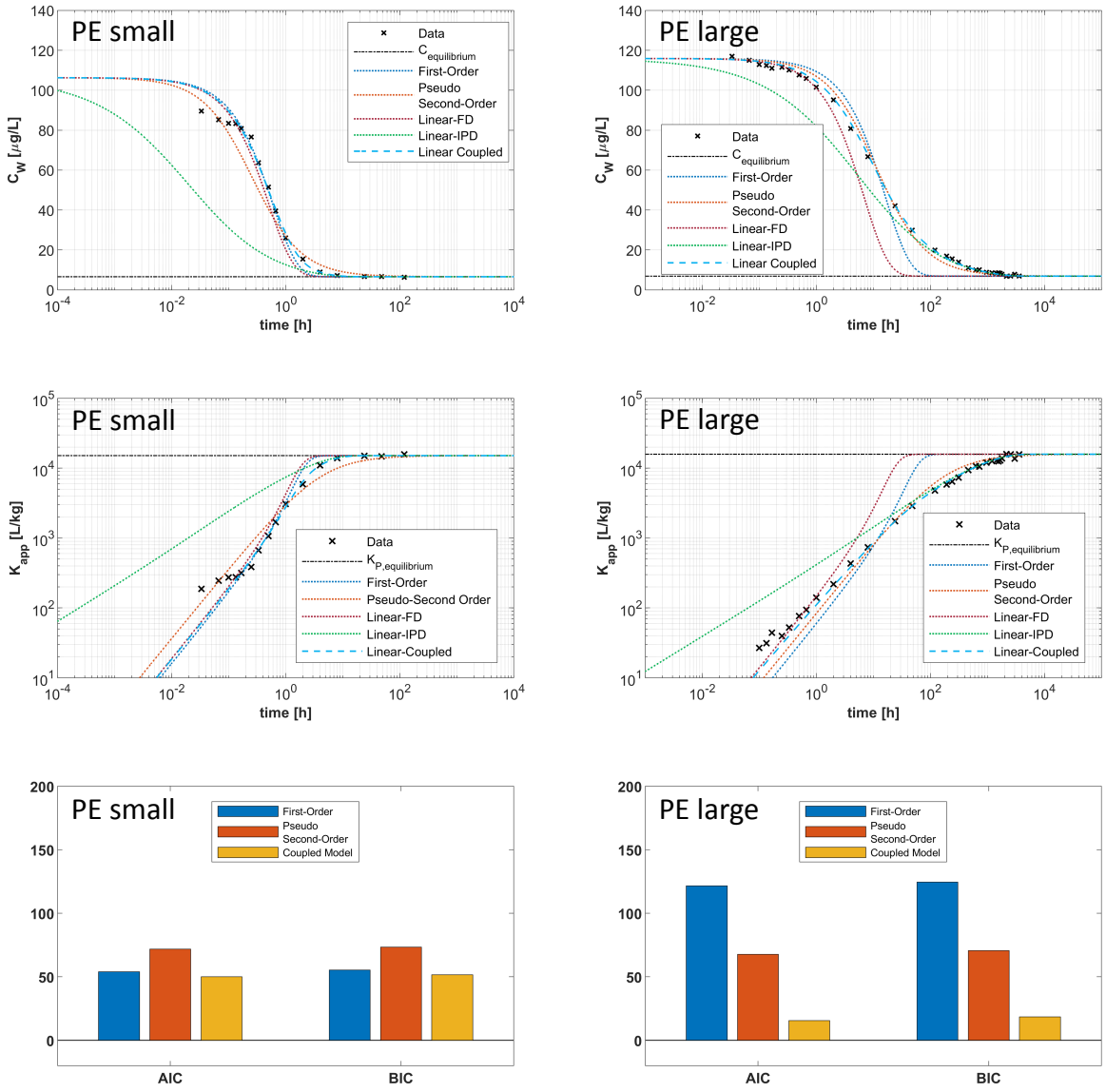

Figure 5.2: **Experimental and modelling results of phenanthrene sorption to small PE (left panel) and to large PE (right panel).** First and second row show semi-logarithmic plots of the measured aqueous concentrations and double-logarithmic plots of apparent partition coefficients over time, respectively. The respective denotations are indicated in the legends. FD=film diffusion, IPD=intraparticle diffusion. In the third row the results of the calculated model information criteria *AIC* and *BIC* are illustrated. Note, that smaller values for the *ICs* indicate a better model performance.

5.3 Influence of Non-Linearity and Surface Structure

In addition to polyethylene, I performed sorption experiments with polyamide and polystyrene in **paper II**. As the semi-analytical coupled model requires sorption to be linear, for the case of non-linear sorption with $C_{P,eq}(C_W)$, a numerical scheme is required. As explained above, I discretized Equation 3.7 for this purpose applying a Finite Volume approach. To model the kinetics for polyethylene, I considered only linear sorption whereas for polyamide and polystyrene, I followed *Freundlich* and *Polanyi-Dubinin-Manes* sorption, respectively, in the non-linear fits. In contrast to polyethylene, the kinetics of polystyrene (Figure 5.3, left panel) and polyamide (Figure 5.3, right panel) were controlled by internal mass transfer almost all the time because intraparticle diffusion coefficients within these materials are several orders of magnitude lower than those in polyethylene (Pascall et al., 2005). Thus, as for the aforementioned large polyethylene particles, the fitted mass transfer coefficients for external mass transfer were not sensitive. Since all kinetic experiments were performed with the same experimental procedure, empirical relationships can be applied to consistently estimate the respective mass transfer parameters. As explained above, I again utilized Equation 5.1 and the k_W-value determined for the small polyethylene particles to estimate *Sherwood* numbers for polystyrene and polyamide adapted to hydrodynamic conditions and particle size. I applied these approximated *Sherwood* numbers and subsequently scaling factors to compute the value of k_W in the polystyrene and polyamide experiments and used these scaling factors (±10%) as initial guess in the fitting of the models. Finally, Sh of 7.0 and 2.7 were obtained for polystyrene and polyamide, respectively.

Within the kinetic experiments, I revealed that at early times, the measured aqueous concentrations were always lower than those predicted by the model. Consequently, not only the well-known swift external mass transfer may have influenced the kinetics but as well an unknown strong sorption process is indicated. A potential mechanism for such a process could be the additional sorption of phenanthrene onto the heterogeneous external surface of the microplastics. As reported in Table 4.1, considerable errors are expectable if the surface areas are just calculated rather than measured which implies that the surface roughness of the particles has to be taken into account. This was confirmed by SEM images which are shown in the Appendix II 5. Such rough surfaces may lead to fast sorption processes and hence I consistently included apparent instantaneous sorption in the non-linear model. This was adapted by a fit of the surface absorption coefficient K_{surf}, which gives the virtual thickness of the outermost plastic shell and corresponds to the influence of instantaneous sorption. The estimated K_{surf} values were in the order of 0.1, 0.58, and 0.62 μm for polyethylene, polyamide, and polystyrene, respectively. This indicated that this process although being observable in laboratory experiments is most likely negligible under environmental conditions where time scales of interest are much larger than observed here. Nevertheless, implementing K_{surf} resulted in a better description of the data in comparison to the linear semi-analytical model where instantaneous sorption was not considered, with root mean square errors for polyamide and polystyrene of 1.5 *vs.* 4.2 μg L^{-1} and 7.9 *vs.* 10.7 μg L^{-1} for the non-linear *vs.* the linear model, respectively. Intraparticle diffusion coefficients

estimated for polystyrene and polyamide based on non-linear sorption were slightly different compared to the estimations of the linear model. To my knowledge, so far only two studies determined intraparticle diffusion coefficients for phenanthrene in polystyrene. Li et al. (2017) and Fischer et al. (2018) determined D_P to be 1.4×10^{-17} m^2 s^{-1} and 3.5×10^{-16} m^2 s^{-1} which is a factor of five smaller and a factor of five greater, respectively, in comparison to 7.3×10^{-17} m^2 s^{-1} calculated from my experimental results. For polyamide, I am not aware of any study which measured intraparticle diffusion coefficients. However, ranges of one order of magnitude are expected for diffusion coefficients in such diverse materials.

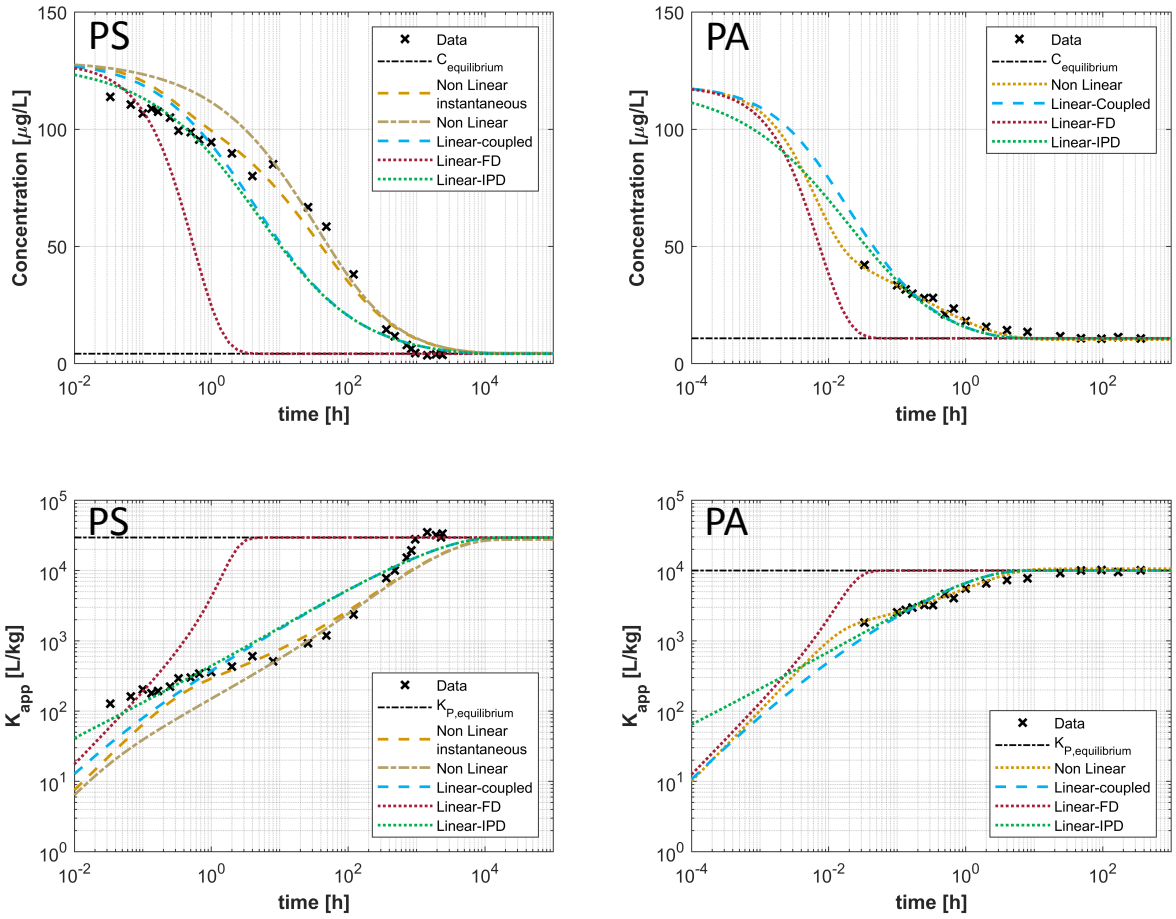

Figure 5.3: **Results of the sorption of phenanthrene to PS (left panel) and PA (right panel).** The top row shows semi-logarithmic plots of aqueous concentrations over time and the bottom row shows double-logarithmic plots of apparent partition coefficients over time. The respective denotations are indicated in the legends. FD=film diffusion, IPD=intraparticle diffusion.

Figure 5.3 additionally shows the time dependent apparent distribution coefficients $K_{P,app}(t)$ for the two cases of instantaneous and normal kinetics as function of time in comparison to the data. The curve of the data points confirms that both polyamide and polystyrene were controlled by intraparticle diffusion already at early times as $K_{P,app}$ increases with the square root of time. For polystyrene, however, the plot indicates that pure external mass transfer matches the data best at early times whereas the

non-linear model with pure consideration of diffusion takes over when approximately 30% equilibration is reached. As illustrated in Figures 5.2 & 5.3, I needed a combination of film and intraparticle diffusion to explain the sorption to polyethylene, while the sorption to polystyrene and polyamide could only be explained when considering non-linear sorption, film and intraparticle diffusion, and swift surface sorption. Among all contributions to the kinetics, the slow intraparticle diffusion depends the strongest on the particle material.

5.4 Effects of Particle Characteristics

Microplastic particles found in the environment have a broad spectrum of numerous characteristics. They are for instance highly variable in size, shape, color, age, and origin and moreover consist of different polymers (Hartmann et al., 2019). Some of those properties have a particular influence on the microplastic-contaminant interactions (Wang et al., 2018). The outstanding advantage of the developed mechanistic coupled mass transfer model is, that the influence of these characteristics can be evaluated and quantified. Regarding sorption and desorption the properties of particular importance are the size, the material, and the sorption capacity. The effects of the particle diameter, the intraparticle diffusion coefficient, and the partition coefficient on the experimental characteristic times are illustrated in Figure 5.4. In the two cases in the top row, the effect of the sorption capacity either in combination with a changing particle size (left) or a changing intraparticle diffusion coefficient (right) are shown. Additionally, in the bottom row the combined effects of the three parameters on the times needed for 20% (left) and 90% (right) equilibration, respectively, are illustrated. The time scales presented within Figure 5.4 are valid for our experimental conditions, scaled according to Equation 5.1, and calculated based on the previous estimated energy dissipation rate ε.

The characteristic times increase with increasing particle diameter squared and with decreasing intraparticle diffusion coefficient. This is caused by lengthened intraparticle diffusion distances in larger particles. Thus, the kinetics are slower and more affected by internal mass transfer in particular at larger time scales. Additionally, lower intraparticle diffusion coefficients, slow down the internal mass transfer and hence the whole kinetics. D_P is strongly related to the glass transition temperature T_g of the plastic material (Pascall et al., 2005). Is the ambient temperature $>T_g$, the segmental mobility of the polymer chains and thus the free intraparticle volume is increased which results in higher diffusion. Additionally, characteristic times may increase with increasing partition coefficient due to an increase importance of the aqueous boundary layer diffusion and thus a slowed external mass transfer. Depending on contaminants and not so much on plastic types, the partition coefficient can spread over several orders of magnitude as well. However, the changes in the material-dependent parameters, i.e. size and intraparticle diffusion, affect the time scales much more than variations in the partition coefficient (Figure 5.4). Note, that the calculation results illustrated in Figure 5.4 are strictly speaking only valid for microplastic types which show linear sorption patterns. Nevertheless, as for most polymers an existing non-linearity is not

very pronounced (Hüffer & Hofmann, 2016; Wang & Wang, 2018b), the conclusions drawn from Figure 5.4 apply in general.

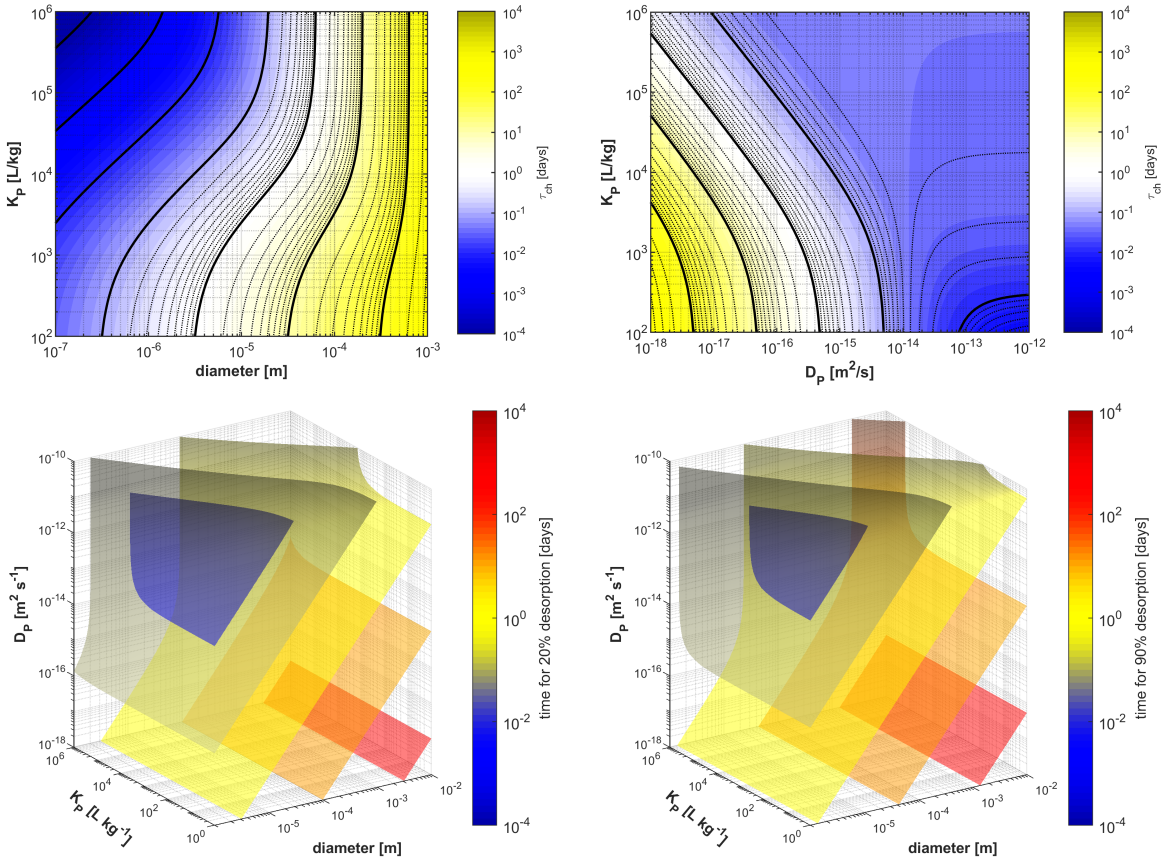

Figure 5.4: **Effects of particle and material properties on total characteristic times (top row) and on time scales for 20% (bottom, left) and 90% (bottom right) equilibration, respectively, in batch experiments.** Total characteristic times τ_{ch} (external + internal mass transfer) were calculated with either $D_P = 10^{-13}$ m^2 s^{-1} (top left) or $d_P = 260\mu$m (top right). The solid-to-liquid ratio in both cases was set to 10^{-3} kg L^{-1} as in my experimental conditions. External mass transfer was calculated based on a water film thickness δ_W of d_P/Sh with $Sh = 7.1$ as determined for polyethylene in my experimental conditions. The characteristic equilibration time scales (bottom) are illustrated through coloring and plotted in iso-surfaces, i.e. identical times are connected by colored areas. The external mass transfer is scaled according to Equation 5.1. Equilibration is fast for small particles and high intraparticle diffusion coefficients and slow for large particles and small intraparticle diffusion coefficients. The surfaces show the sum of characteristic times for film diffusion and intraparticle diffusion.

5.5 Effects of Experimental Parameters and Environmental Conditions

5.5.1 Influence of Proton Activity

In freshwater systems, a major pathway for microplastic particles to enter the aquatic environments is the introduction of wastewater treatment plant effluents or the discharge of stormwater overflows (Mintenig et al., 2017; Murphy et al., 2016). Such effluents, however, show also high concentrations of organic micropollutants (Gavrilescu et al., 2015; König et al., 2017; Li et al., 2016) and can thus be considered to be a pollutant hotspot and plastic particles might particularly come into contact with frequently occurring wastewater contaminants. However, a large share of such pollutants can be charged under certain pH conditions (Karlsson et al., 2017) and unlike most natural sorbents, under certain conditions microplastics can be charged electrostatically as well (Yokota et al., 2017). Thus, my objective in **paper III** was to elucidate whether interactions between ionizable compounds and microplastic particles go beyond mere partitioning. The selected contaminants (seven acids, seven bases, and five non-ionizables) and their corresponding pK_a-values are listed in Table 4.2. I used pristine polyethylene and polystyrene particles since in the wastewater canalization system "young" particles occur and enter the wastewater treatment plant and both of them are among the most abundant in wastewater treatment plants and their effluents (Mintenig et al., 2017). The equilibrium partitioning between particles and contaminants were studied at three different pH levels (4, 7, and 10). To quantify the concentrations and ensure that the equilibrium was reached, I took samples at the beginning and after two, four, seven, and eleven (only for polystyrene) days of experimental duration.

Sorption to polyethylene is in general mostly driven by partitioning and strongly dependent on both the substance properties and the polymer characteristics such as density, branching, and crystallinity (Endo et al., 2005; O'Connor et al., 2016). In my experiments with polyethylene, sorption of neutral species was stronger than sorption of charged species and uptake of polar compounds was less compared to uptake of non-polar compounds (Figure 5.5).

Polystyrene showed in general higher sorption capacities than polyethylene (Figure 5.6) which was likely driven by both partitioning and adsorption mechanisms as e.g. pore-filling which can be deduced from the non-linear sorption isotherms (Figure 5.1 and Appendix III 3.5). The higher distribution coefficients for polystyrene are in agreement with other published findings (Hüffer & Hofmann, 2016; Wang & Wang, 2018a).

Nevertheless, the sorption coefficients for both polymers were within the same order of magnitude and in both cases the sorption was driven by hydrophobicity. Substances that have been absorbed strongly by one polymer showed also high affinities to the other. In both cases the model (Equation 3.4) could be fitted well to the measured overall pH-dependent partition coefficient P_{pH} and for both cases those fits were better for stronger sorbing compounds. Based on the deduced $K_{P,n}$ and $K_{P,i}$ sorption of neutral species to polystyrene was stronger than to polyethylene whereas sorption of the ionic species was weaker for most of the substances (see tables in **paper III**).

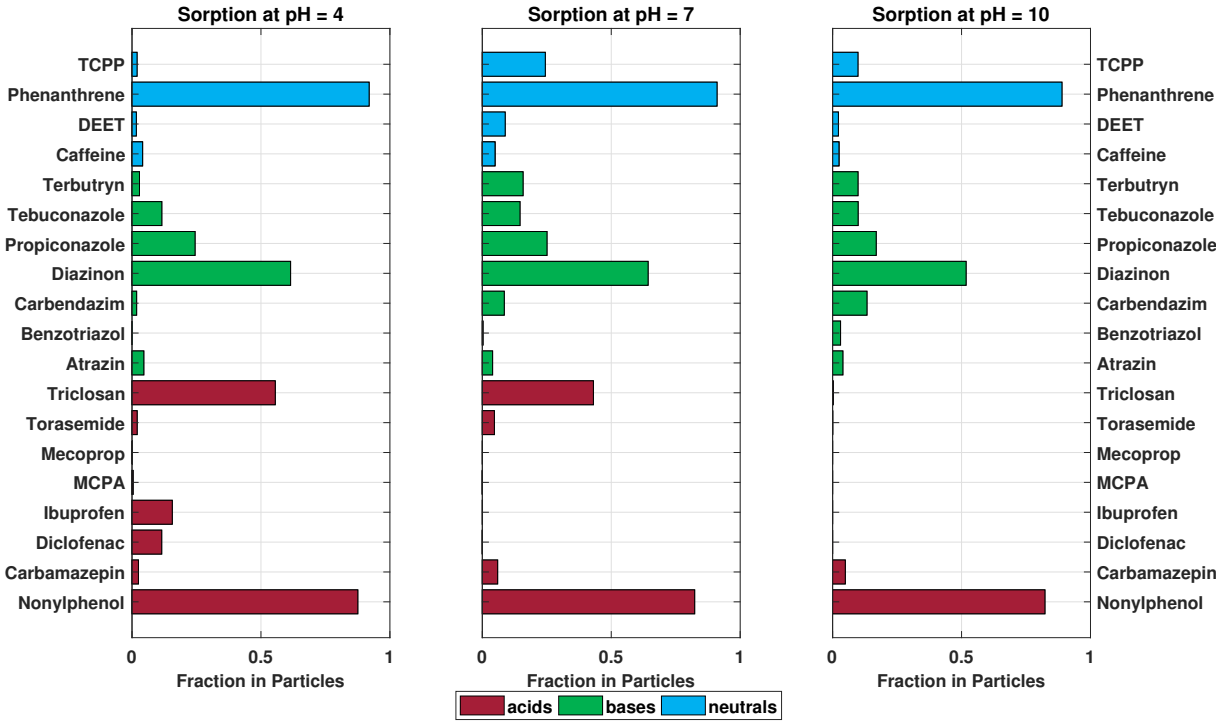

Figure 5.5: **Sorbed fractions of the investigated contaminants to polyethylene at different pH levels.** The bars are colored according to the acid/base-properties of the substances as indicated in the legend.

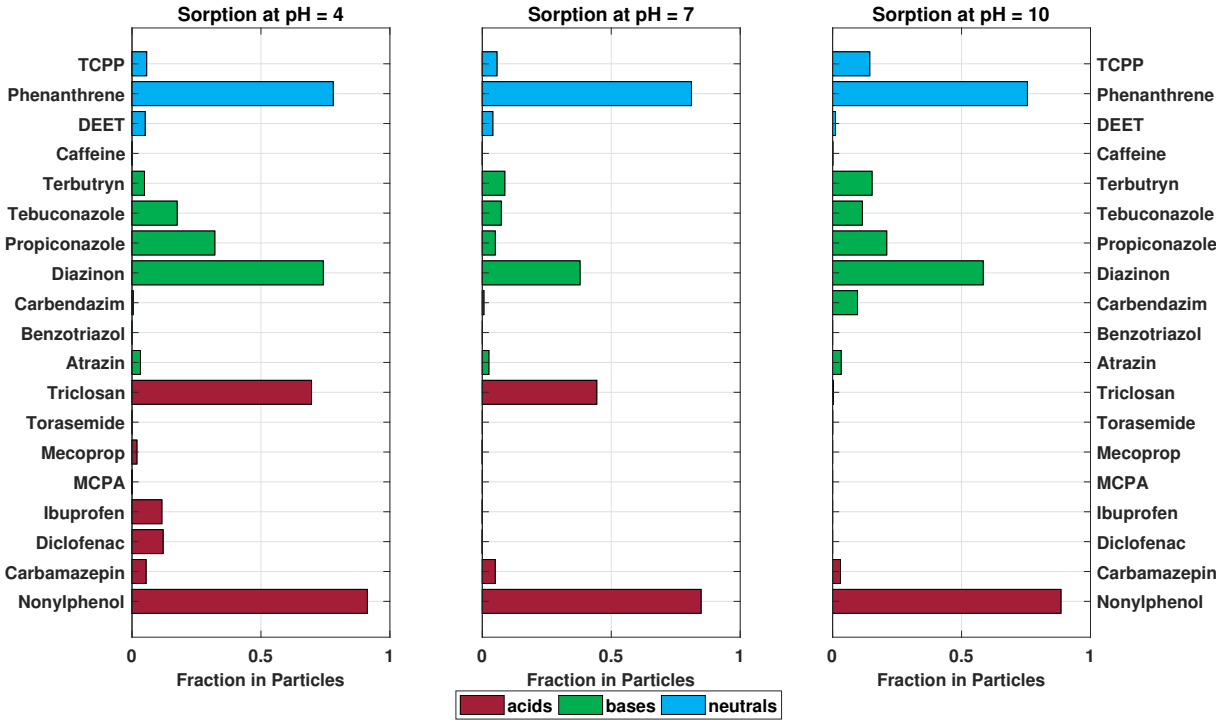

Figure 5.6: **Sorbed fractions of the investigated contaminants to polystyrene at different pH levels.** The bars are colored according to the acid/base-properties of the substances as indicated in the legend.

The detailed partitioning plots for every substance including the measured and modeled P_{pH} are reported in the corresponding supplementary information of **paper III** in Appendix III 3.5. I calculated variation coefficients for P_{pH} which revealed an increasing variation with an increasing share of ionic species. Thus, for the weakly sorbing ionic species the error escalates. However, for some of the selected substances the results indicate that although to a very minor degree, their ionic species contributed to sorption as well. This was in particular observed for substances whose neutral species sorb strongly as well (such as nonylphenol and triclosan). However, as I chose a liquid-to-solid ratio of 10^3 L kg^{-1} for my batch experiments, only slightly smaller partition coefficients (>500 L kg^{-1}) could be determined with a reasonable uncertainty. The partition coefficients determined for polar and weakly sorbing compounds were subject to greater uncertainty and the deviation between the calculated and the measured values increased with decreasing sorption independent of the pH. Therefore, the partition coefficients determined for polar and weakly sorbing compounds are subject to greater uncertainty which is reflected in the variation coefficients. Furthermore, batch setups as applied in my study focus on elucidating a specific process detail, like the species-specific sorption coefficients and do not reflect environmental relevant conditions (Lenz et al., 2016). In addition, for most of the investigated substances, the determined P_{pH}s were in the order of 10^1 to 10^2 L kg^{-1}, i.e. the mass flux from the aqueous phase into the solid is small which leads to highly uncertain measurements of K_P. Thus, sorption efficiencies reported in literature, e.g. 60% and 70% for polyfluorinated compound sorption to polyethylene and polystyrene (Llorca et al., 2018), are only possible under very low and hence unrealistic liquid-to-solid ratios. Finally, it needs to be stated that such small partition coefficients are not environmentally relevant as accumulation of such compounds in microplastics is neglectable and thus their transport is not facilitated by particles.

5.5.2 Influence of Dissolved Organic Matter

Experiments and modeling discussed in **paper IV** aimed to reveal the effects of the presence of natural dissolved organic matter (DOM) on desorption of contaminants from microplastic particles. More specific, I analyzed the shifts of mass transfer in batch systems as a function of partition coefficients which were manipulated with dissolved humic acids. In these experiments I used polyethylene particles and assessed the influence of humic acids for which previous studies already concluded a significant impact on desorption from organic phases (Smith et al., 2011; ter Laak et al., 2009). The impact, however, depends on whether mass transfer is controlled by film diffusion or intraparticle diffusion. Thus, I carried out experiments with three different substances that represent a range of hydrophobicities (water solubilities) and used six different concentrations of humic acids while the solid-to-liquid ratio (10^{-3} kg L^{-1}) was kept constant. The respective contaminant loads of microplastic particles and the experimental conditions are described in detail in **paper IV**. For all substances equilibration occurred latest after 8 h. As expected, the overall aqueous concentrations increased and, thus, the overall partition coefficients K^*_{PE-W} decreased with the DOM concentration (Figure

5.7). The experimental results match very well with the predicted values according to Equations 3.5 & 3.6. Additionally, the determined K^*_{PE-W} values correlate well with the hydrophobicity and increase with the K_{OW} as it would be expected. Measured and calculated partition coefficients into humic acid K_{DOM} for phenanthrene and tonalide show good agreement whereas they show relatively large deviations for benzophenone what I attribute to the insignificant influence of DOM. The detailed results are reported in **paper IV**. Under equilibrium conditions, increasing the DOM concentration caused the fraction of pollutants remaining in the microplastics to decrease.

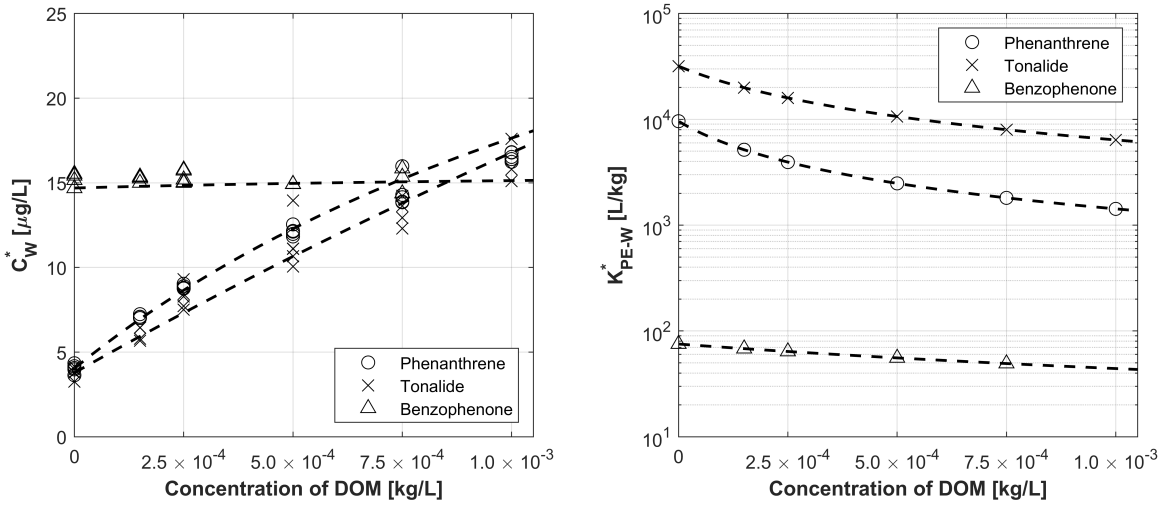

Figure 5.7: **Measured equilibrium concentrations in the aqueous phase against the concentration of DOM in the batch (top) and relationships between partition coefficients K^*_{PE-W} and the concentration of DOM in the solution (bottom).** Dashed lines are calculated by Equation 3.6 (top) and Equation 3.5 (bottom).

I analyzed the desorption kinetics by fitting the semi-analytical coupled mass transfer model which I outlined above. Within Figure 5.8, the measured concentration time series for the batches with zero and the highest DOM concentrations are shown. The model results for external and internal mass transfer only (red and green dashed lines, respectively) and for coupled mass transfer (blue solid line) are included. Detailed results regarding the results and parameter estimations are reported in **paper IV**.

Kinetics for phenanthrene (Figure 5.8, row A) show an excellent agreement between the experimental and simulation results. At early times external mass transfer controlled the kinetics while at later times internal mass transfer prevailed. With increasing DOM concentrations, the decreasing K^*_{PE-W} shifted the mass transfer from film diffusion to intraparticle diffusion control and slowed down the kinetics in the batch system. For tonalide, however, the compound with the highest hydrophobicity, such a shift could not be determined (Figure 5.8, row B). Over the whole range of DOM concentrations the kinetics were strongly controlled by external mass transfer and only at the highest DOM concentration curves for the coupled and the only external mass transfer start to deviate slightly (Figure 5.8, row B). Compared to phenanthrene and benzophenone, the aqueous equilibrium concentration was the lowest. Contradicting behavior was revealed for benzophenone (Figure 5.8, row C) as the compound with the highest water

solubility. Thus, it had the highest equilibrium concentration in the aqueous phase. The fraction of benzophenone remaining in the microplastics after equilibration ranged from only 6% (without any DOM) to less than 3% (for the three highest DOM concentrations) and the desorption kinetics were always controlled by intraparticle diffusion.

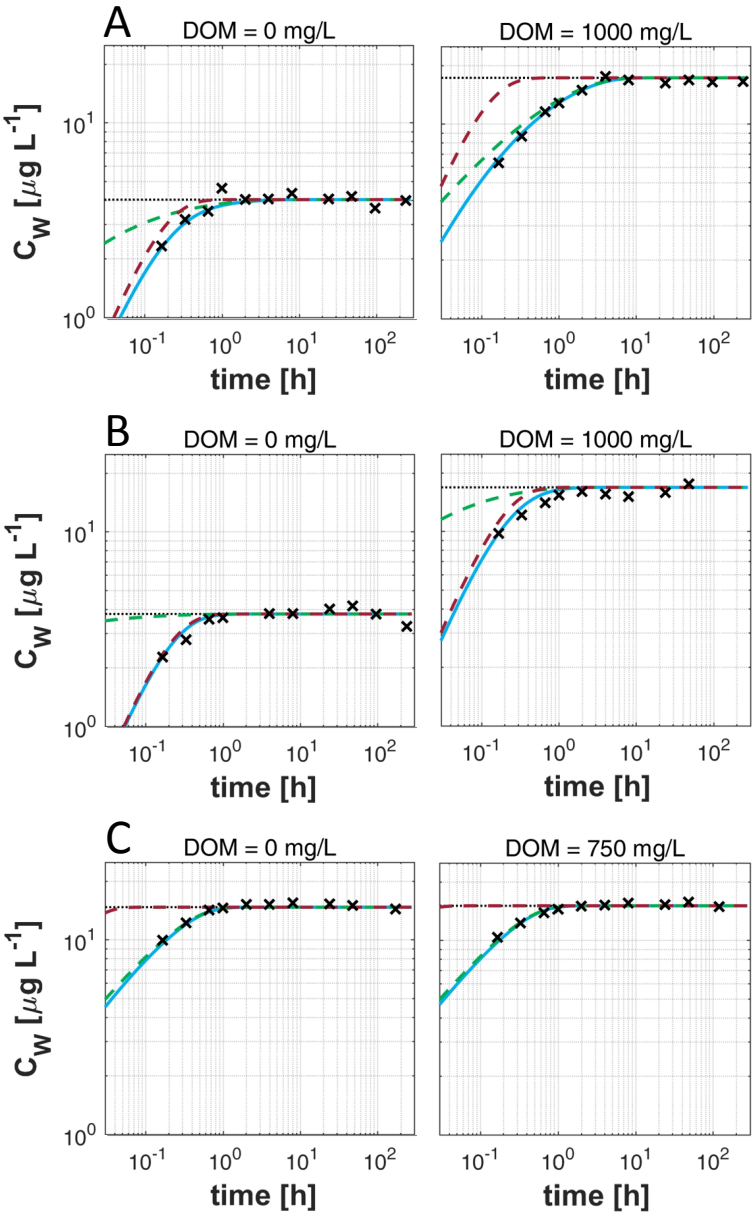

Figure 5.8: **Desorption kinetics of phenanthrene (A), tonalide (B), and benzophenone (C) from microplastics without and with the highest applied DOM concentration.** Aqueous concentrations are plotted against time and models for film diffusion, intraparticle diffusion, and coupling both diffusion processes are shown with the red dashed, the green dashed, and the solid blue line, respectively. The horizontal black dotted line shows the equilibrium concentration.

While comparable studies indicated that increasing the DOM concentration generally accelerates mass-transfer kinetics, I found the opposite in my experiments. This apparent contradiction is explained by different boundary conditions, e.g. different liquid-to-solid

ratios and finite bath *vs.* infinite bath conditions (Smith et al., 2011; ter Laak et al., 2009). Note, that increasing DOM concentrations and thus decreasing K^*_{PE-W} accelerate the external mass transfer for low solid-to-liquid ratios (infinite bath) but slow it down for high solid-to-liquid ratios (finite bath, Equations 3.14 & 3.15). As the diffusion coefficients of DOM are a factor of two to three lower than for the used compounds, mass transfer changes would be less pronounced if a large fraction partitioned into DOM (Cornel et al., 1986). For my experimental setup this would, if at all, affect tonalide at high DOM concentrations. However, the data and model do not show any significant influence of DOM. Thus, I did not specifically account for aqueous diffusion of DOM which would shift the mass transfer towards the particle interior and would result in a lower importance of film diffusion.

Regarding mass transfer under field conditions, studies on passive sampling indicated that it is usually clearly limited by external mass transfer, for compounds with K^*_{PE-W} values similar to or higher than for phenanthrene (Lampert et al., 2015). Although such passive samplers are frequently made of polyethylene, they are far thinner than the microplastic particles applied in my experiments (Lohmann, 2011) and hence internal mass transfer is less restrictive because of shorter diffusion distances. Only a limited number of studies indicated that intraparticle diffusion might be important for assessing the vector function of microplastics (Fries & Zarfl, 2012). Koelmans et al. (2013) investigated the role of organic matter on desorption kinetics and concluded that internal mass transfer might typically be the rate limiting process. While the latter authors modeled the kinetics by two first-order mass-exchange processes in series, I considered a more realistic intraparticle diffusion. Eventually, our model results and the experimental findings suggest that intraparticle diffusion is not permanently controlling the kinetics. However, Koelmans et al. (2013) applied their model to larger particles with diameters of 0.4 and 1.3 mm which might explain this contrast since internal mass transfer times become more relevant with increasing particle size (Figure 5.4).

Finally, DOM concentrations used in my batch experiments are higher than concentrations usually found in aqueous environments. Such high DOM-concentrations are more likely for (urban) wastewaters which frequently contain both organic contaminants and microplastics (Murphy et al., 2016; Rule et al., 2006). Based on thermodynamic considerations, sorption and desorption kinetics are equal and thus the mass transfer under the applied high DOM conditions can be used to estimate the particle loading in wastewater. On the other hand, experiments without or with low DOM concentrations can be applied to assess the microplastic-facilitated transport of pollutants in aquatic ecosystems. The equilibration times would increase under field conditions where the Liquid-to-solid ratio approaches infinity. Thus, mass transfer becomes independent of K^*_{PE-W} for intraparticle diffusion, but increases with increasing K^*_{PE-W} for external mass transfer control.

5.6 Environmental Implications

One major argument in microplastic research is on the concentrations applied in experiments as they are orders of magnitude above particle loadings detected in the field (Lenz et al., 2016). However, quite recently, based on new technical developments, researchers were able to detect particles down to a size of 11 μm and suggested that the numbers reported so far may underestimate the true concentrations which are nevertheless still orders of magnitude below experimental concentrations (Mintenig et al., 2017; Peeken et al., 2018). Accordingly, the question arises on how to transfer findings from the laboratory to the environment. Thus, a major achievement of the present thesis is the mechanistic mass transfer model derived from the experimental results and based on thermodynamic fundamentals. The coupled model allows a comprehensive investigation of the sorption interactions and due to the mechanistic character it is furthermore possible to extrapolate to environmental settings without uncertain assumptions being necessary.

5.6.1 The Effect of the Particle Concentration and Organic Carbon

Based on my experimental findings and well-known empirical relationships, I am able to estimate kinetic interactions under field conditions and to assess *ab initio* the potential of long-distance transfer of pollutants. As the internal mass transfer is an intrinsic property based on the polymer-dependent intraparticle diffusion coefficient, the external mass transfer is obviously the greatest uncertainty if my experimental findings are extrapolated to the field. However, based on the *Sherwood*-relationship given in Equation 5.1 it is possible to estimate the mass transfer coefficients in environmental settings based on the known energy dissipation rates. Even though the hydrodynamic conditions are highly variable, the energy dissipation rate is stable within a certain range and takes mean values of $10^{-5.5}$ and 10^{-7} m^2 s^{-3} for rivers and oceans, respectively (Chickadel et al., 2011; MacDonald et al., 2007; Moum et al., 1995). Furthermore, it goes into Equation 5.1 with a power of about 1/6 and is, thus, not very decisive. However, two more intricate determinable parameters are the particle concentration and the presence of other sorbents which both have an enormous impact on the kinetics as shown for the latter in **paper IV**.

In literature highly variable plastic particle numbers are reported, thus I used example values to illustrate the effect of the solid-to-liquid ratio. Values for the rivers were measured in a wastewater treatment plant effluent by Mintenig et al. (2017) whereas the oceanic concentrations were derived based on the estimated total weight of the small microplastic fraction in the ocean ($\sim 10^7$ kg, Worm et al. (2017)) and the total volume of water in the ocean (1.3×10^{21} L, according to the USGS). Assuming for each a polyethylene fraction of 0.25, I ended up with concentrations of 1.7×10^{-8} and 1.9×10^{-15} kg L^{-1} as representative polyethylene amounts in rivers and oceans, respectively.

It is well known that besides microplastics other sorbents, mainly natural dissolved organic carbon (DOC), are present in aquatic ecosystems and may interact with organic contaminants. Therefore, I carried out a thorough literature research and found representative dissolved organic carbon (DOC) loads of 3×10^{-5} and 1.9×10^{-6} kg L^{-1}

for rivers and oceans, respectively (Hansell et al., 2012; Ouyang, 2003; Stramska, 2009). Additionally, I assumed partition coefficients as assembled for various organic pollutants and polyethylene (Lohmann, 2011). All values are indicated in Figure 5.9 by the red and brown dashed lines for rivers and oceans, respectively.

With these values it was possible, to model virtual kinetics for both environmental settings (Figure 5.9). According to Figure 5.9 (top left), I manipulated the effective partition coefficient K^*_{PE-W} in my experiments by adding DOC, thus covering a wide range of kinetics limited by both internal and external mass transfer (Figure 5.8). Subsequently, I calculated the total characteristic time of mass transfer, computed by Equations 3.13-3.15 (Figure, 5.9 top right). At high m_P/V_W ratios, overall mass-transfer kinetics are accelerated with increasing K^*_{PE-W}, whereas they are slowed down at very low ratios, approaching infinite bath conditions. Under finite bath conditions, a decreasing effective partition coefficient increases the characteristic time $\tau_{ch}^{internal}$ of internal mass transfer while that of external mass transfer $\tau_{ch}^{external}$ is hardly affected when considering strongly sorbing compounds (Figure 5.9, top right). Nevertheless, both the microplastic and the DOC concentration used in **paper IV** as represented by the black dashed lines were considerably higher than values measured in rivers and oceans, illustrated by the red and brown dashed lines, respectively. Under infinite bath boundary conditions characteristic times of mass transfer may range between hours (for compounds with low partition coefficients intraparticle diffusion limits) and weeks (for those with high partition coefficients external mass transfer limits). As stated earlier, the relative importance of internal and external mass transfer does not depend on the solid-to-liquid ratio, improving the transferability from experimental conditions to the field. However, as discussed above it depends to some extent on particle sizes which, however, can easily be measured and accounted for (Equation 5.1). Regarding the two virtual experiments shown in the bottom row of Figure 5.9, I chose physico-chemical parameters similar to phenanthrene which is representative for HOCs. Eventually, the particle and the DOC concentration determine the kinetic behavior. As illustrated, the kinetics in oceans is almost exclusively limited by film diffusion whereas the kinetics in rivers is controlled by external mass transfer at early and by intraparticle diffusion at later times. This is mainly a result of the higher K^*_{PE-W} and the higher *Sh* in rivers. Additionally, desorption time scales in river settings are approximately by a factor of 14 faster as in ocean settings which predominantly follows from the higher particle concentrations. Moreover, follow-up simulations showed that the kinetics with solid-to-liquid ratios four orders of magnitude above the estimated mean ocean concentrations show the same pattern and are thus also expectable in plastic waste accumulation zones.

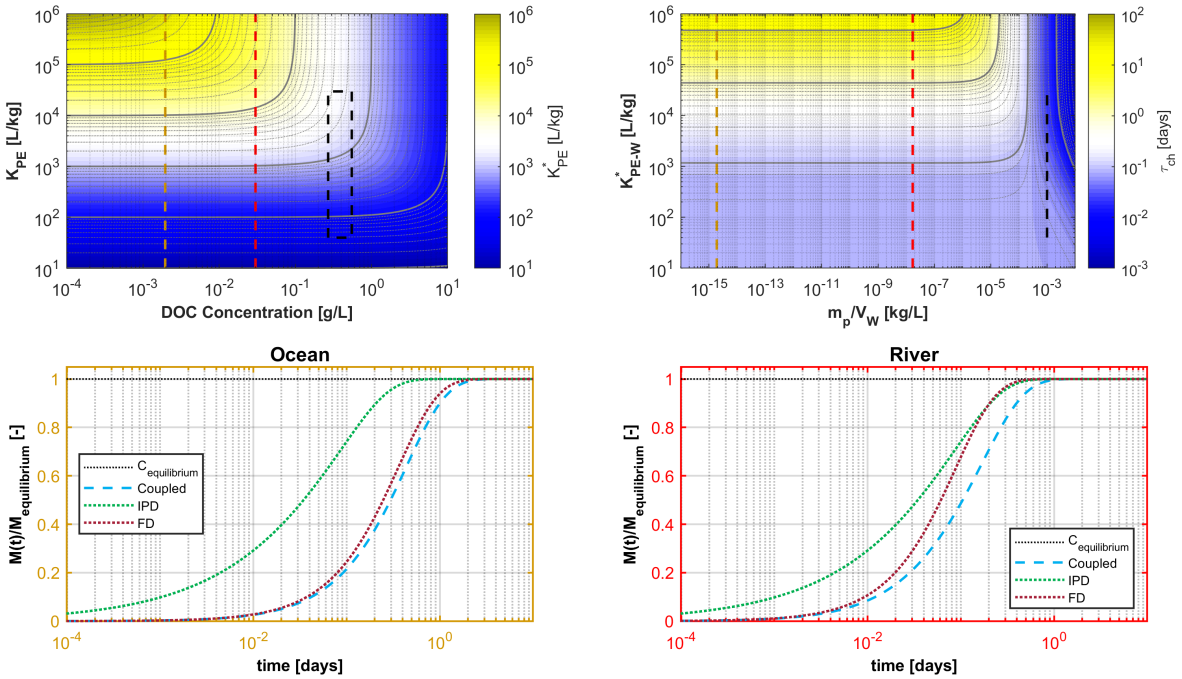

Figure 5.9: **Influence of DOC on sorption kinetics under experimental and environmental conditions.** Top row: The overall partition coefficient K^*_{PE-W} as a function of the DOC concentration and K_{PE-W} (left), and total characteristic times of mass transfer as a function of the solid-to-liquid ratio and this overall partition coefficient (right). Black, red, and brown dashed lines represent experimental, river, and ocean DOC concentrations, respectively. Bottom row: Sorption/desorption kinetics at ocean (left) and at river conditions (right). Intraparticle diffusion (IPD), film diffusion (FD), and the coupled mass transfer model are shown as the dotted green, red, and the dashed blue line, respectively. Modelling parameters are reported in the supporting information to **paper I** in Appendix I 5.2.

5.6.2 The Role of Microplastics in the Environment

A key question in microplastic-contaminant research is whether a particle sampled in rivers or oceans reflects the ambient concentrations, i.e. it acts as a passive sampler, or if it rather behaves a transport vector releasing pollutants into the environment (Gouin et al., 2011; Karapanagioti et al., 2011; Zarfl & Matthies, 2010). The models presented here can be used to address this question. According to Van Sebille et al. (2012), a considerable fraction of particles released at the coast reaches the open ocean after approximately one year, and after ten years the majority of them has arrived at one of the five subtropical maxima, better known as gyre accumulation zones (Maximenko et al., 2012; Van Sebille et al., 2012). As already outlined, using my models and the corresponding characteristic times, I can calculate the residual fraction of an organic pollutant in different types of particles as a function of their size. It is illustrated above, that mainly particle-dependent rather than substance properties are decisive for the kinetic behavior. Furthermore, with known physico-chemical properties, the models apply to a wide range of neutral HOCs. According to the general concept, larger particles take considerably longer to release a sorbed compound as diffusion distances

within the particles get longer. In Figure 5.10, I illustrate the time scales needed to reach desorption of 90%, distinguished into intraparticle and film diffusion and calculated separately for each of the three polymer types I applied within my experiments as well as with and without the presence of the representative DOC amounts. The detailed calculations are explained in **paper II**. Again, these characteristic times depend on three parameters, (i) the particle diameter, (ii) the material-specific intraparticle diffusion coefficient, and (iii) the compound-specific partition coefficient in which the latter only influences external mass transfer. The characteristic times increase with increasing particle diameter and with decreasing intraparticle diffusion coefficients (Figure 5.10). Additionally, characteristic times increase with increasing partition coefficient due to a shift to external mass transfer. Thus, film diffusion becomes slower as the presence of DOC in the settings decreases the plastic-water partition coefficient. However, the changes in the material-dependent parameters, i.e. size and intraparticle diffusion, affect the time scales much more than variations in the partition coefficient in particular when DOC concentrations are such low as in the sea (Figure 5.10). Consequently, plastic particles can act as a vector for contaminants mainly depending on material and size. Small particles equilibrate fast and thus presumably reflect the ambient concentration in water, i.e. they act as a passive sampler (Figure 5.10). The potential for long-range transport increases with the particle size squared and decreases with the intraparticle diffusion coefficient. I explicitly do not conclude that microplastics significantly enhance the aqueous contaminant concentration which has been already intensively discussed (Koelmans et al., 2016). Nevertheless, the long range transport potential is given and needs to be considered. In particular in the risk assessment of plastic associated additives and urban contaminants whose input paths differ from those of the common legacy POPs (Kwon et al., 2017).

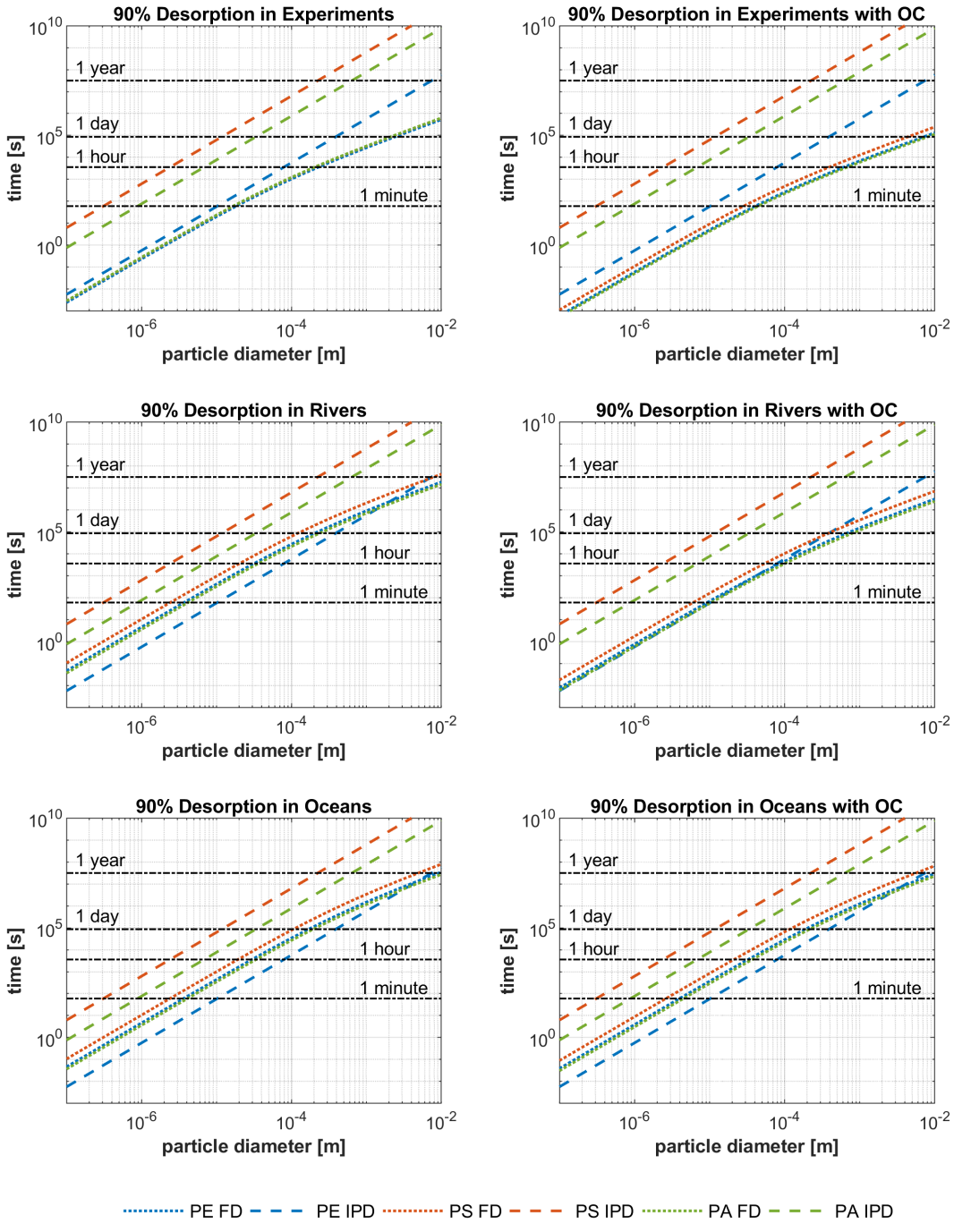

Figure 5.10: **Characteristic times for 90% of initial mass desorption under experimental conditions, in rivers and oceans, respectively, as a function of particle diameter and polymer material (polyethylene (PE), polystyrene (PS), and polyamide (PA).** The left and right panel display the times with microplastic being the sole sorbent and with river and ocean DOC loads included, respectively. Calculations are outlined above and in **papers I and II**. IPD = intraparticle diffusion, FD = film diffusion. The total characteristic time for a particular polymer is the sum of the two given curves. FD in experimental settings is always fast due to stirring and thus, IPD dominates. In rivers and oceans, *Sh* is lower and FD is slower than IPD for polyethylene. If DOC is considered, FD is slowed down in rivers but hardly affected in the ocean. Thus, for polyethylene, in rivers IPD may dominate in some cases whereas in oceans FD prevails. Kinetics for polyamide and polystyrene are always limited by IPD.

6 Conclusions & Outlook

The overall aim of this thesis was to utilize both experimental work and sophisticated modelling approaches to create a comprehensive understanding on how microplastic particles interact with organic contaminants. Furthermore, I aimed to clarify the role of microplastics in the environment, in particular whether they can be seen as sink or source of pollutants. Understanding the role of microplastics in the environment leads to an enhanced characterization of its hazard potential and thus this thesis eventually allows an improved risk assessment of microplastics and associated contaminants.

In **paper I** a newly developed semi-analytical coupled mass transfer model clearly reveals the governing mass transfer processes which are involved if sorption and desorption-interactions between microplastic particles and hydrophobic organic contaminants are considered. I could show that both external and internal mass transfer mechanisms contribute decisively to the entire kinetics. It is not possible to reveal such contributions or mass transfer shifts if simple first-order or pseudo second-order approaches are applied as they rely on bulk rate constants which are only valid for the particular conditions and cannot be transferred to e.g. other particle concentrations and flow conditions. Eventually, I gained evidence that a detailed mass transfer model is necessary to extrapolate experimental results to the environment and this thesis makes a vital contribution by developing and validating such a model.

Based on the experimental findings in **paper II** a mechanistic numerical scheme was established and successfully applied. It allows not only a detailed evaluation of the mass transfer processes involved in the kinetics but can be combined with linear and non-linear sorption isotherms. Consequently, the model can be implemented to evaluate and predict sorption kinetics to other types of suspended matter such as carbonaceous particles. I revealed that the role of microplastics is mainly dependent on the particle-dependent properties themselves, in particular on the particle size and the polymer type whereas the physico-chemical properties of the contaminants and the shape of the isotherm just play a minor role.

Attempting to perform experiments and quantify sorption interactions for more environmentally relevant settings, namely a variety of compounds with different properties, in **paper III** I studied the influence of a changing pH on the sorption of neutral and ionizable chemicals. However, at least for pristine plastic particles I could show, that partitioning is still the main sorption mechanism and sorption of charged species is irrelevant for environmental microplastic concentrations. Notwithstanding, since microplastics concentrations currently observed in the environment are very low, my results show that they are only a relevant sorbent for strongly hydrophobic compounds.

Taking an important step further, within **paper IV** the effect of the presence of dissolved natural substances as additional sorbent was evaluated and quantified. Under environmental conditions the occurrence of such competing sorbents is highly relevant and influences the redistribution of contaminants. I could show, that the partitioning is significantly influenced by the addition of dissolved organic matter. The coupled model was successfully extended to integrate such effects. Furthermore and contrary to common believe, I demonstrated that for high partition coefficients desorption kinetics is fast in batch experiments and controlled by external mass transfer. Conversely, for low partition coefficients, caused e.g. by high dissolved organic matter concentrations kinetics was slow and limited by intraparticle diffusion. Data and model again evidenced, that desorption of contaminants from microplastics depends on boundary conditions and transfer of observations from batch experiments to field conditions requires an appropriate model accounting for the relevant mass transfer mechanisms.

As a result of UV-light exposure, mechanical stress and abrasion, and other weathering processes particles undergo several changes once they have entered the environment (Andrady, 2017; Jahnke et al., 2017). This may cause the fragmentation of particles into smaller pieces which accelerates the contaminant release but may as well induce pore formation whereby retarded pore diffusion would come into play (Wu & Gschwend, 1986). Thus, future experiments should focus on such weathered particles to elucidate the effect of weathering and quantify the contribution of further processes going beyond pure film and intraparticle diffusion. Another main feature of environmental settings is the formation of biofilms on the particles. According to the extended two-film theory (Booij et al., 2007; Lewis & Whitman, 1924) they may act as an additional external resistance and thus slow down the contaminant release as the diffusion within biofilms is lower than in water. First attempts are reported in **paper I** and include biofilm-influenced mass transfer analysis based on virtual experiments. Confirming that a biofilm acts as an additional external mass transfer compartment, the kinetics is slowed down with respect to the biofilm thickness and mainly limited by external mass transfer. However, the equilibration times for scenarios with no, growing, and static biofilms just differ by a factor 3 indicating again that material dependent characteristics such as very low intraparticle diffusion coefficients may play a more important role. Obviously, this effect only comes into account if the kinetics is at least partially limited by film diffusion. Even though the calculations are based on findings of scientific articles, the assumptions are highly speculative as long as no experimental data are present. Accordingly, upcoming experimental work ought to focus as well on the influence of biofilms on the mass transfer and may be extended to reactive transport considerations once the biofilm interacts with the passing pollutants beyond its mass transfer resistance role.

Moreover, commercial plastics usually contain additives such as antioxidants, flame retardants, and plasticizers in amounts from ranging from <0.1 up to 70 mass-% (Hermabessiere et al., 2017). It has been shown that during degradation processes and after plastic particles enter the environment, such additives may be released (Gewert et al., 2018). Furthermore, a large share of such additives are hydrophobic and not readily biodegradable (Kwon et al., 2017). Since additives can change the polymer

properties, sorption experiments need to emphasize whether their release potentially influences the role of the different mass transfer mechanisms. As plasticizers change the viscosity and hence influence the mobility of the polymer segments and the free volume in the polymer, a concentration change may directly influence the intraparticle diffusion coefficients (Pascall et al., 2005; Shah & Shertukde, 2003). Thus, the internal mass transfer of both contained contaminants and additives may be a function of the additive concentration and the developed numerical model can be expanded to include time-dependent intraparticle diffusion coefficients. Once the behavior of additives is better understood, determined residual concentrations in particles found in the field may serve further as a starting point for an age estimation provided initial concentrations are known.

Since I could show that microplastics are able to take up contaminants and to transport them over long distances and out of wastewater treatment plants, the question arises what happens once they arrive in systems with large concentrations of competing sorbents. First insights can be deduced from the results presented in **paper IV** which are, however, limited to dissolved substances. As soon as other particulate sorbents are present, this leads to a redistribution of initially sorbed contaminants which significantly decrease the freely dissolved concentration in the aqueous phase. To study such redistributions, clean particles can be added to microplastic sorption experiments which are equilibrated. The subsequent decrease of the aqueous concentration can be monitored via temporally high-resolved samplings. This would hypothetically disclose a peak in the freely dissolved concentration during the contaminants exchange between the particles. Such redistributions will also mimic bioaccumulation of sorbed pollutants to small organisms. Eventually, as the redistribution should follow the same mass transfer mechanisms as the uptake, such experiments can represent a proof-of-concept approach and are furthermore applicable to assess redistribution scenarios under field conditions.

Finally, this thesis could distinctly evidence that sorption and desorption can be modeled best by using a coupled mass transfer approach. Such models are highly appropriate to extrapolate experimental findings to field settings and can serve as a solid base for risk assessment. Furthermore, one major achievement is that the theoretical mass transfer considerations also apply to other suspended particles such as suspended sediments. The utilized and well-defined microplastic particles are ideally suited to perform in-depth mass transfer studies under controlled conditions. However, ultimately they are as well surrogates for particles occurring in the environment, including microplastics in urban runoff and contaminated sediment particles in which the latter are very likely much more frequent than microplastics but undergo the same mass transfer mechanisms. Eventually, the outcome of this thesis is a valuable contribution to the improved understanding and assessment of particle facilitated transport in water bodies.

Bibliography

Akaike, H. (1974). A new look at the statistical model identification. *IEEE Transactions on Automatic Control*, 19(6):716–723.

Alexander, M. (2000). Aging, bioavailability, and overestimation of risk from environmental pollutants. *Environmental Science & Technology*, 34(20):4259–4265.

Alimi, O. S.; Farner Budarz, J.; Hernandez, L. M.; Tufenkji, N. (2018). Microplastics and nanoplastics in aquatic environments: aggregation, deposition, and enhanced contaminant transport. *Environmental Science & Technology*, 52(4):1704–1724.

Allan, I. J.; Booij, K.; Paschke, A.; Vrana, B.; Mills, G. A.; Greenwood, R. (2009). Field performance of seven passive sampling devices for monitoring of hydrophobic substances. *Environmental Science & Technology*, 43(14):5383–5390.

Allan, I. J.; Ruus, A.; Schaanning, M. T.; Macrae, K. J.; Næs, K. (2012). Measuring nonpolar organic contaminant partitioning in three Norwegian sediments using polyethylene passive samplers. *Science of the Total Environment*, 423:125–131.

Allen-King, R. M.; Grathwohl, P.; Ball, W. P. (2002). New modeling paradigms for the sorption of hydrophobic organic chemicals to heterogeneous carbonaceous matter in soils, sediments, and rocks. *Advances in Water Resources*, 25(8-12):985–1016.

Andrady, A. L. (2011). Microplastics in the marine environment. *Marine Pollution Bulletin*, 62(8):1596–1605.

Andrady, A. L. (2017). The plastic in microplastics: A review. *Marine Pollution Bulletin*, 119(1):12–22.

Auta, H. S.; Emenike, C. U.; Fauziah, S. H. (2017). Distribution and importance of microplastics in the marine environment: A review of the sources, fate, effects, and potential solutions. *Environment International*, 102:165–176.

Balk, F.; Ford, R. A. (1999). Environmental risk assessment for the polycyclic musks, AHTN and HHCB: II. Effect assessment and risk characterisation. *Toxicology Letters*, 111(1-2):81–94.

Ball, W. P.; Roberts, P. V. (1991). Long-term sorption of halogenated organic chemicals by aquifer material. 2. Intraparticle diffusion. *Environmental Science & Technology*, 25(7):1237–1249.

Barber, L. B.; Murphy, S. F.; Verplanck, P. L.; Sandstrom, M. W.; Taylor, H. E.; Furlong, E. T. (2006). Chemical loading into surface water along a hydrological, biogeochemical, and land use gradient: A holistic watershed approach. *Environmental Science & Technology*, 40(2):475–486.

Barnes, D. K.; Galgani, F.; Thompson, R. C.; Barlaz, M. (2009). Accumulation and fragmentation of plastic debris in global environments. *Philosophical Transactions of the Royal Society of London B: Biological Sciences*, 364(1526):1985–1998.

Beckingham, B.; Ghosh, U. (2017). Differential bioavailability of polychlorinated biphenyls associated with environmental particles: Microplastic in comparison to wood, coal and biochar. *Environmental Pollution*, 220:150–158.

Bernard, O.; Rémond, B. (2012). Validation of a simple model accounting for light and temperature effect on microalgal growth. *Bioresource Technology*, 123:520–527.

Besseling, E.; Foekema, E. M.; van Den Heuvel-Greve, M. J.; Koelmans, A. A. (2017). The effect of microplastic on the uptake of chemicals by the lugworm *Arenicola marina* (L.) under environmentally relevant exposure conditions. *Environmental Science & Technology*, 51(15):8795–8804.

Booij, K.; Vrana, B.; Huckins, J. N. (2007). Chapter 7: Theory, modelling and calibration of passive samplers used in water monitoring. *Comprehensive Analytical Chemistry*, Volume 48:141–169.

Brandon, J.; Goldstein, M.; Ohman, M. D. (2016). Long-term aging and degradation of microplastic particles: comparing in situ oceanic and experimental weathering patterns. *Marine Pollution Bulletin*, 110(1):299–308.

Browne, M. A.; Crump, P.; Niven, S. J.; Teuten, E.; Tonkin, A.; Galloway, T.; Thompson, R. (2011). Accumulation of microplastic on shorelines woldwide: sources and sinks. *Environmental Science & Technology*, 45(21):9175–9179.

Browne, M. A.; Galloway, T.; Thompson, R. (2007). Microplastic-an emerging contaminant of potential concern? *Integrated Environmental Assessment and Management*, 3(4):559–561.

Browne, M. A.; Niven, S. J.; Galloway, T. S.; Rowland, S. J.; Thompson, R. C. (2013). Microplastic moves pollutants and additives to worms, reducing functions linked to health and biodiversity. *Current Biology*, 23(23):2388–2392.

Bundschuh, M.; Weyers, A.; Ebeling, M.; Elsaesser, D.; Schulz, R. (2016). Narrow pH range of surface water bodies receiving pesticide input in Europe. *Bulletin of Environmental Contamination and Toxicology*, 96(1):3–8.

Burnham, K. P.; Anderson, D. R.; Huyvaert, K. P. (2011). AIC model selection and multimodel inference in behavioral ecology: Some background, observations, and comparisons. *Behavioral Ecology and Sociobiology*, 65(1):23–35.

Burns, E. E.; Boxall, A. B. (2018). Microplastics in the aquatic environment: Evidence for or against adverse impacts and major knowledge gaps. *Environmental Toxicology and Chemistry*, 37(11):2776–2796.

Careghini, A.; Mastorgio, A. F.; Saponaro, S.; Sezenna, E. (2015). Bisphenol A, nonylphenols, benzophenones, and benzotriazoles in soils, groundwater, surface water, sediments, and food: A review. *Environmental Science and Pollution Research*, 22(8):5711–5741.

Carpenter, E. J.; Anderson, S. J.; Harvey, G. R.; Miklas, H. P.; Peck, B. B. (1972). Polystyrene spherules in coastal waters. *Science*, 178(4062):749–750.

Chen, Q.; Reisser, J.; Cunsolo, S.; Kwadijk, C.; Kotterman, M.; Proietti, M.; Slat, B.; Ferrari, F. F.; Schwarz, A.; Levivier, A.; et al. (2017). Pollutants in plastics within the north Pacific subtropical gyre. *Environmental Science & Technology*, 52(2):446–456.

Chen, X.; Xiong, X.; Jiang, X.; Shi, H.; Wu, C. (2019). Sinking of floating plastic debris caused by biofilm development in a freshwater lake. *Chemosphere*, 222:856–864.

Chickadel, C. C.; Talke, S. A.; Horner-Devine, A. R.; Jessup, A. T. (2011). Infrared-based measurements of velocity, turbulent kinetic energy, and dissipation at the water surface in a tidal river. *IEEE Geoscience and Remote Sensing Letters*, 8(5):849–853.

Cornel, P. K.; Summers, R. S.; Roberts, P. V. (1986). Diffusion of humic acid in dilute aqueous solution. *Journal of Colloid and Interface Science*, 110(1):149–164.

Cornelissen, G.; Gustafsson, Ö.; Bucheli, T. D.; Jonker, M. T.; Koelmans, A. A.; van Noort, P. C. (2005). Extensive sorption of organic compounds to black carbon, coal, and kerogen in sediments and soils: Mechanisms and consequences for distribution, bioaccumulation, and biodegradation. *Environmental Science & Technology*, 39(18):6881–6895.

Cowie, J.; McEwen, I. (1977). Molecular relaxations in partially hydrogenated cis-1, 4-polybutadienes. A guide to the glass transition temperature of amorphous polyethylene. *Macromolecules*, 10(5):1124–1128.

Crank, J. (1979). The Mathematics of Diffusion. *Oxford University Press*.

Diamond, M. L.; de Wit, C. A.; Molander, S.; Scheringer, M.; Backhaus, T.; Lohmann, R.; Arvidsson, R.; Bergman, Å.; Hauschild, M.; Holoubek, I.; et al. (2015). Exploring the planetary boundary for chemical pollution. *Environment International*, 78:8–15.

Diepens, N. J.; Koelmans, A. A. (2018). Accumulation of plastic debris and associated contaminants in aquatic food webs. *Environmental Science & Technology*, 52(15):8510–8520.

Doig, S. D.; Pickering, S. C.; Lye, G. J.; Baganz, F. (2005). Modelling surface aeration rates in shaken microtitre plates using dimensionless groups. *Chemical Engineering Science*, 60(10):2741–2750.

Dołżonek, J.; Cho, C.-W.; Stepnowski, P.; Markiewicz, M.; Thöming, J.; Stolte, S. (2017). Membrane partitioning of ionic liquid cations, anions and ion pairs–estimating the bioconcentration potential of organic ions. *Environmental Pollution*, 228:378–389.

Elovich, S. Y.; Larinov, O. (1962). Theory of adsorption from solutions of non electrolytes on solid (I) equation adsorption from solutions and the analysis of its simplest form,(II) verification of the equation of adsorption isotherm from solutions. *Izvestiia Akademii Nauk SSSR, Otdelenij Chimitschesskich Nauk*, 2(2):209–216.

Endo, S.; Takizawa, R.; Okuda, K.; Takada, H.; Chiba, K.; Kanehiro, H.; Ogi, H.; Yamashita, R.; Date, T. (2005). Concentration of polychlorinated biphenyls (PCBs) in beached resin pellets: Variability among individual particles and regional differences. *Marine Pollution Bulletin*, 50(10):1103–114.

Endo, S.; Yuyama, M.; Takada, H. (2013). Desorption kinetics of hydrophobic organic contaminants from marine plastic pellets. *Marine Pollution Bulletin*, 74(1):125–131.

Eriksen, M.; Lebreton, L. C.; Carson, H. S.; Thiel, M.; Moore, C. J.; Borerro, J. C.; Galgani, F.; Ryan, P. G.; Reisser, J. (2014). Plastic pollution in the world's oceans: More than 5 trillion plastic pieces weighing over 250,000 tons afloat at sea. *PloS One*, 9(12):e111913.

Eriksen, M.; Mason, S.; Wilson, S.; Box, C.; Zellers, A.; Edwards, W.; Farley, H.; Amato, S. (2013). Microplastic pollution in the surface waters of the Laurentian Great Lakes. *Marine Pollution Bulletin*, 77(1-2):177–182.

Escher, B. I.; Schwarzenbach, R. P.; Westall, J. C. (2000). Evaluation of liposome- water partitioning of organic acids and bases. 2. Comparison of experimental determination methods. *Environmental Science & Technology*, 34(18):3962–3968.

Faure, F.; Demars, C.; Wieser, O.; Kunz, M.; De Alencastro, L. F. (2015). Plastic pollution in Swiss surface waters: Nature and concentrations, interaction with pollutants. *Environmental Chemistry*, 12(5):582–591.

Fernandez, L. A.; Harvey, C. F.; Gschwend, P. M. (2009). Using performance reference compounds in polyethylene passive samplers to deduce sediment porewater concentrations for numerous target chemicals. *Environmental Science & Technology*, 43(23):8888–8894.

Fick, A. (1855). Ueber Diffusion. *Annalen der Physik*, 170(1):59–86.

Finkel, M.; Grathwohl, P.; Cirpka, O. A. (2016). A travel time-based approach to model kinetic sorption in highly heterogeneous porous media via reactive hydrofacies. *Water Resources Research*, 52(12):9390–9411.

Fischer, F. C.; Cirpka, O. A.; Goss, K. U.; Henneberger, L.; Escher, B. I. (2018). Application of experimental polystyrene partition constants and diffusion coefficients to predict the sorption of neutral organic chemicals to multiwell plates in *in vivo* and *in vitro* bioassays. *Environmental Science & Technology*, 52(22):13511–13522.

Fisher, N.; Simpson, J.; Howarth, M. (2002). Turbulent dissipation in the Rhine ROFI forced by tidal flow and wind stress. *Journal of Sea Research*, 48(4):249–258.

Forbes, T. L.; Forbes, V. E.; Giessing, A.; Hansen, R.; Kure, L. K. (1998). Relative role of pore water versus ingested sediment in bioavailability of organic contaminants in marine sediments. *Environmental Toxicology and Chemistry*, 17(12):2453–2462.

Fries, E.; Zarfl, C. (2012). Sorption of polycyclic aromatic hydrocarbons (PAHs) to low and high density polyethylene (PE). *Environmental Science and Pollution Research*, 19(4):1296–1304.

Fu, W.; Franco, A.; Trapp, S. (2009). Methods for estimating the bioconcentration factor of ionizable organic chemicals. *Environmental Toxicology and Chemistry*, 28(7):1372–1379.

Galloway, T. S.; Lewis, C. N. (2016). Marine microplastics spell big problems for future generations. *Proceedings of the National Academy of Sciences*, 113(9):2331–2333.

Garner, F. H.; Suckling, R. D. (1958). Mass transfer from a soluble solid sphere. *AIChE Journal*, 4(1):114–124.

Gasperi, J.; Garnaud, S.; Rocher, V.; Moilleron, R. (2008). Priority pollutants in wastewater and combined sewer overflow. *Science of the Total Environment*, 407(1):263–272.

Gavrilescu, M.; Demnerová, K.; Aamand, J.; Agathos, S.; Fava, F. (2015). Emerging pollutants in the environment: Present and future challenges in biomonitoring, ecological risks and bioremediation. *New Biotechnology*, 32(1):147–156.

George, S. C.; Thomas, S. (2001). Transport phenomena through polymeric systems. *Progress in Polymer Science*, 26(6):985–1017.

Gewert, B.; Plassmann, M.; Sandblom, O.; MacLeod, M. (2018). Identification of chain scission products released to water by plastic exposed to ultraviolet light. *Environmental Science & Technology Letters*, 5(5):272–276.

Geyer, R.; Jambeck, J. R.; Law, K. L. (2017). Production, use, and fate of all plastics ever made. *Science Advances*, 3(7):e1700782.

Ghosh, U.; Talley, J. W.; Luthy, R. G. (2001). Particle-scale investigation of PAH desorption kinetics and thermodynamics from sediment. *Environmental Science & Technology*, 35(17):3468–3475.

Ghosh, U.; Zimmerman, J. R.; Luthy, R. G. (2003). PCB and PAH speciation among particle types in contaminated harbor sediments and effects on PAH bioavailability. *Environmental Science & Technology*, 37(10):2209–2217.

Goss, K.-U.; Bittermann, K.; Henneberger, L.; Linden, L. (2018). Equilibrium biopartitioning of organic anions–A case study for humans and fish. *Chemosphere*, 199:174–181.

Gouin, T.; Roche, N.; Lohmann, R.; Hodges, G. (2011). A thermodynamic approach for assessing the environmental exposure of chemicals absorbed to microplastic. *Environmental Science & Technology*, 45(4):1466–1472.

Gouliarmou, V.; Smith, K. E.; de Jonge, L. W.; Mayer, P. (2012). Measuring binding and speciation of hydrophobic organic chemicals at controlled freely dissolved concentrations and without phase separation. *Analytical Chemistry*, 84(3):1601–1608.

Grathwohl, P. (2012). Diffusion in natural porous media: Contaminant transport, sorption/desorption and dissolution kinetics. *Springer Science & Business Media*.

Grathwohl, P. (2014). On equilibration of pore water in column leaching tests. *Waste Management*, 34(5):908–918.

Grathwohl, P.; Reinhard, M. (1993). Desorption of trichloroethylene in aquifer material: Rate limitation at the grain scale. *Environmental Science & Technology*, 27(12):2360–2366.

Gregory, M. R.; Andrady, A. L. (2003). Plastics in the marine environment. *Plastics and the Environment*, 379:389–390.

Gschwend, P. M.; Wu, S. (1985). On the constancy of sediment-water partition coefficients of hydrophobic organic pollutants. *Environmental Science & Technology*, 19(1):90–96.

Guo, X.; Wang, X.; Zhou, X.; Kong, X.; Tao, S.; Xing, B. (2012). Sorption of four hydrophobic organic compounds by three chemically distinct polymers: Role of chemical and physical composition. *Environmental Science & Technology*, 46(13):7252–7259.

Hale, S. E.; Martin, T. J.; Goss, K.-U.; Arp, H. P. H.; Werner, D. (2010). Partitioning of organochlorine pesticides from water to polyethylene passive samplers. *Environmental Pollution*, 158(7):2511–2517.

Hansell, D. A.; Carlson, C. A.; Schlitzer, R. (2012). Net removal of major marine dissolved organic carbon fractions in the subsurface ocean. *Global Biogeochemical Cycles*, 26(1).

Harriott, P. (1962). Mass transfer to particles: Part I. Suspended in agitated tanks. *AIChE Journal*, 8(1):93–101.

Hartmann, N. B.; Hüffer, T.; Thompson, R. C.; Hassellöv, M.; Verschoor, A.; Daugaard, A. E.; Rist, S.; Karlsson, T.; Brennholt, N.; Cole, M.; Herrling, M. P.; Hess, M. C.; Ivleva, N. P.; Lusher, A. L.; Wagner, M. (2019). Are We Speaking the Same Language? Recommendations for a Definition and Categorization Framework for Plastic Debris. *Environmental Science & Technology*, 53(3):1039–1047.

Hartmann, N. B.; Rist, S.; Bodin, J.; Jensen, L. H.; Schmidt, S. N.; Mayer, P.; Meibom, A.; Baun, A. (2017). Microplastics as vectors for environmental contaminants: Exploring sorption, desorption, and transfer to biota. *Integrated Environmental Assessment and Management*, 13(3):488–493.

Hermabessiere, L.; Dehaut, A.; Paul-Pont, I.; Lacroix, C.; Jezequel, R.; Soudant, P.; Duflos, G. (2017). Occurrence and effects of plastic additives on marine environments and organisms: A review. *Chemosphere*, 182:781–793.

Hidalgo-Ruz, V.; Gutow, L.; Thompson, R. C.; Thiel, M. (2012). Microplastics in the marine environment: A review of the methods used for identification and quantification. *Environmental Science & Technology*, 46(6):3060–3075.

Ho, Y.-S.; McKay, G. (1999). Pseudo-second order model for sorption processes. *Process Biochemistry*, 34(5):451–465.

de Hoog, F. R.; Knight, J. H.; Stokes, A. N. (1982). An improved method for numerical inversion of Laplace transforms. *SIAM Journal on Scientific and Statistical Computing*, 3:357–366.

Horn, H.; Reiff, H.; Morgenroth, E. (2003). Simulation of growth and detachment in biofilm systems under defined hydrodynamic conditions. *Biotechnology and Bioengineering*, 81(5):607–617.

Horton, A. A.; Walton, A.; Spurgeon, D. J.; Lahive, E.; Svendsen, C. (2017). Microplastics in freshwater and terrestrial environments: Evaluating the current understanding to identify the knowledge gaps and future research priorities. *Science of the Total Environment*, 586:127–141.

Hüffer, T.; Hofmann, T. (2016). Sorption of non-polar organic compounds by micro-sized plastic particles in aqueous solution. *Environmental Pollution*, 214:194–201.

Hüffer, T.; Weniger, A.; Hofmann, T. (2018). Sorption of organic compounds by aged polystyrene microplastic particles. *Environmental Pollution*, 236:218–225.

Jahnke, A.; Arp, H. P. H.; Escher, B. I.; Gewert, B.; Gorokhova, E.; Kühnel, D.; Ogonowski, M.; Potthoff, A.; Rummel, C.; Schmitt-Jansen, M.; et al. (2017). Reducing uncertainty and confronting ignorance about the possible impacts of weathering plastic in the marine environment. *Environmental Science & Technology Letters*, 4(3):85–90.

Jambeck, J. R.; Geyer, R.; Wilcox, C.; Siegler, T. R.; Perryman, M.; Andrady, A.; Narayan, R.; Law, K. L. (2015). Plastic waste inputs from land into the ocean. *Science*, 347(6223):768–771.

Jeannot, M. A.; Cantwell, F. F. (1997). Mass transfer characteristics of solvent extraction into a single drop at the tip of a syringe needle. *Analytical Chemistry*, 69(2):235–239.

Jones, K. C.; De Voogt, P. (1999). Persistent organic pollutants (POPs): State of the science. *Environmental Pollution*, 100(1-3):209–221.

Kaiser, K.; Zech, W. (1998). Soil dissolved organic matter sorption as influenced by organic and sesquioxide coatings and sorbed sulfate. *Soil Science Society of America Journal*, 62(1):129–136.

Kan, A.; Tomson, M. (1996). UNIFAC prediction of aqueous and nonaqueous solubilities of chemicals with environmental interest. *Environmental Science & Technology*, 30(4):1369–1376.

Karapanagioti, H. K.; Endo, S.; Ogata, Y.; Takada, H. (2011). Diffuse pollution by persistent organic pollutants as measured in plastic pellets sampled from various beaches in Greece. *Marine Pollution Bulletin*, 62(2):312–317.

Karapanagioti, H. K.; Gossard, C. M.; Strevett, K. A.; Kolar, R. L.; Sabatini, D. A. (2001). Model coupling intraparticle diffusion/sorption, nonlinear sorption, and biodegradation processes. *Journal of Contaminant Hydrology*, 48(1-2):1–21.

Karapanagioti, H. K.; Klontza, I. (2008). Testing phenanthrene distribution properties of virgin plastic pellets and plastic eroded pellets found on Lesvos island beaches (Greece). *Marine Environmental Research*, 65(4):283–290.

Karickhoff, S. W.; Brown, D. S.; Scott, T. A. (1979). Sorption of hydrophobic pollutants on natural sediments. *Water Research*, 13(3):241–248.

Karlsson, M. V.; Carter, L. J.; Agatz, A.; Boxall, A. B. (2017). Novel approach for characterizing pH-dependent uptake of ionizable chemicals in aquatic organisms. *Environmental Science & Technology*, 51(12):6965–6971.

Katsnelson, A. (2015). News Feature: Microplastics present pollution puzzle. *Proceedings of the National Academy of Sciences*, 112(18):5547–5549.

Kawase, Y.; Moo-Young, M. (1987). Solid-turbulent fluid heat and mass transfer: A unified model based on the energy dissipation rate concept. *The Chemical Engineering Journal*, 36(1):31–40.

Kleineidam, S.; Schüth, C.; Grathwohl, P. (2002). Solubility-normalized combined adsorption-partitioning sorption isotherms for organic pollutants. *Environmental Science & Technology*, 36(21):4689–4697.

Ko, F.-C.; Baker, J. E. (2004). Seasonal and annual loads of hydrophobic organic contaminants from the Susquehanna River basin to the Chesapeake Bay. *Marine Pollution Bulletin*, 48(9-10):840–851.

Koelmans, A. A.; Bakir, A.; Burton, G. A.; Janssen, C. R. (2016). Microplastic as a vector for chemicals in the aquatic environment: Critical review and model-supported reinterpretation of empirical studies. *Environmental Science & Technology*, 50(7):3315–3326.

Koelmans, A. A.; Besseling, E.; Wegner, A.; Foekema, E. M. (2013). Plastic as a carrier of POPs to aquatic organisms: A model analysis. *Environmental Science & Technology*, 47(14):7812–7820.

Koelmans, A. A.; Kooi, M.; Law, K. L.; van Sebille, E. (2017). All is not lost: Deriving a top-down mass budget of plastic at sea. *Environmental Research Letters*, 12(11):114028.

König, M.; Escher, B. I.; Neale, P. A.; Krauss, M.; Hilscherová, K.; Novák, J.; Teodorović, I.; Schulze, T.; Seidensticker, S.; Hashmi, M. A. K.; Ahlheim, J.; Brack, W. (2017). Impact of untreated wastewater on a major European river evaluated with a combination of in vitro bioassays and chemical analysis. *Environmental Pollution*, 220:1220–1230.

Kwon, J. H.; Chang, S.; Hong, S. H.; Shim, W. J. (2017). Microplastics as a vector of hydrophobic contaminants: Importance of hydrophobic additives. *Integrated Environmental Assessment and Management*, 13(3):494–499.

ter Laak, T. L.; van Eijkeren, J. C.; Busser, F. J.; van Leeuwen, H. P.; Hermens, J. L. (2009). Facilitated transport of polychlorinated biphenyls and polybrominated diphenyl ethers by dissolved organic matter. *Environmental Science & Technology*, 43(5):1379–1385.

Lallas, P. L. (2001). The Stockholm Convention on persistent organic pollutants. *American Journal of International Law*, 95(3):692–708.

Laloy, E.; Vrugt, J. A. (2012). High-dimensional posterior exploration of hydrologic models using multiple-try DREAM(ZS) and high-performance computing. *Water Resources Research*, 48(1):W01526.

Lampert, D.; Thomas, C.; Reible, D. (2015). Internal and external transport significance for predicting contaminant uptake rates in passive samplers. *Chemosphere*, 119:910–916.

Largitte, L.; Pasquier, R. (2016). A review of the kinetics adsorption models and their application to the adsorption of lead by an activated carbon. *Chemical Engineering Research and Design*, 109:495–504.

Law, K. L. (2017). Plastics in the marine environment. *Annual Review of Marine Science*, 9:205–229.

Law, K. L.; Thompson, R. C. (2014). Microplastics in the seas. *Science*, 345(6193):144–145.

Lee, H.; Byun, D.-E.; Kim, J. M.; Kwon, J.-H. (2018). Desorption of hydrophobic organic chemicals from fragment-type microplastics. *Ocean Science Journal*, 53(4):631–639.

Lee, H.; Shim, W. J.; Kwon, J.-H. (2014). Sorption capacity of plastic debris for hydrophobic organic chemicals. *Science of the Total Environment*, 470:1545–1552.

Lenz, R.; Enders, K.; Nielsen, T. G. (2016). Microplastic exposure studies should be environmentally realistic. *Proceedings of the National Academy of Sciences*, 113(29):E4121–E4122.

Lewis, W.; Whitman, W. (1924). Principles of gas absorption. *Industrial & Engineering Chemistry*, 16(12):1215–1220.

Li, S.; Liu, H.; Gao, R.; Abdurahman, A.; Dai, J.; Zeng, F. (2018). Aggregation kinetics of microplastics in aquatic environment: Complex roles of electrolytes, pH, and natural organic matter. *Environmental Pollution*, 237:126–132.

Li, S.-Q.; Ni, H.-G.; Zeng, H. (2017). PAHs in polystyrene food contact materials: An unintended consequence. *Science of the Total Environment*, 609:1126–1131.

Li, Z.; Sobek, A.; Radke, M. (2016). Fate of pharmaceuticals and their transformation products in four small European rivers receiving treated wastewater. *Environmental Science & Technology*, 50(11):5614–5621.

Liu, L.; Wu, F.; Haderlein, S.; Grathwohl, P. (2013). Determination of the subcooled liquid solubilities of PAHs in partitioning batch experiments. *Geoscience Frontiers*, 4(1):123–126.

Llorca, M.; Schirinzi, G.; Martínez, M.; Barceló, D.; Farré, M. (2018). Adsorption of perfluoroalkyl substances on microplastics under environmental conditions. *Environmental Pollution*, 235:680–691.

Lohmann, R. (2011). Critical review of low-density polyethylene's partitioning and diffusion coefficients for trace organic contaminants and implications for its use as a passive sampler. *Environmental Science & Technology*, 46(2):606–618.

Lohmann, R. (2017). Microplastics are not important for the cycling and bioaccumulation of organic pollutants in the oceans-but should microplastics be considered POPs themselves? *Integrated Environmental Assessment and Management*, 13(3):460–465.

Luthy, R. G.; Aiken, G. R.; Brusseau, M. L.; Cunningham, S. D.; Gschwend, P. M.; Pignatello, J. J.; Reinhard, M.; Traina, S. J.; Weber, W. J.; Westall, J. C. (1997). Sequestration of hydrophobic organic contaminants by geosorbents. *Environmental Science & Technology*, 31(12):3341–3347.

MacDonald, D. G.; Goodman, L.; Hetland, R. D. (2007). Turbulent dissipation in a near-field river plume: A comparison of control volume and microstructure observations with a numerical model. *Journal of Geophysical Research: Oceans*, 112(C7).

Mackay, D.; Fraser, A. (2000). Bioaccumulation of persistent organic chemicals: Mechanisms and models. *Environmental Pollution*, 110(3):375–391.

Mackay, D.; McCarty, L. S.; MacLeod, M. (2001). On the validity of classifying chemicals for persistence, bioaccumulation, toxicity, and potential for long-range transport. *Environmental Toxicology and Chemistry*, 20(7):1491–1498.

MacLeod, M.; Breitholtz, M.; Cousins, I. T.; Wit, C. A. d.; Persson, L. M.; Rudén, C.; McLachlan, M. S. (2014). Identifying chemicals that are planetary boundary threats. *Environmental Science & Technology*, 48(19):11057–11063.

Mani, T.; Hauk, A.; Walter, U.; Burkhardt-Holm, P. (2015). Microplastics profile along the Rhine River. *Scientific Reports*, 5:17988.

Mato, Y.; Isobe, T.; Takada, H.; Kanehiro, H.; Ohtake, C.; Kaminuma, T. (2001). Plastic resin pellets as a transport medium for toxic chemicals in the marine environment. *Environmental Science & Technology*, 35(2):318–324.

Maximenko, N.; Hafner, J.; Niiler, P. (2012). Pathways of marine debris derived from trajectories of Lagrangian drifters. *Marine Pollution Bulletin*, 65(1-3):51–62.

McKay, G.; Bino, M. J.; Altememi, A. (1986). External mass transfer during the adsorption of various pollutants onto activated carbon. *Water Research*, 20(4):435–442.

Mendoza, L. M. R.; Jones, P. R. (2015). Characterisation of microplastics and toxic chemicals extracted from microplastic samples from the North Pacific Gyre. *Environmental Chemistry*, 12(5):611–617.

Mintenig, S.; Int-Veen, I.; Löder, M. G.; Primpke, S.; Gerdts, G. (2017). Identification of microplastic in effluents of waste water treatment plants using focal plane array-based micro-Fourier-transform infrared imaging. *Water Research*, 108:365–372.

Moum, J.; Gregg, M.; Lien, R.; Carr, M. (1995). Comparison of turbulence kinetic energy dissipation rate estimates from two ocean microstructure profilers. *Journal of Atmospheric and Oceanic Technology*, 12(2):346–366.

Murga, R.; Stewart, P. S.; Daly, D. (1995). Quantitative analysis of biofilm thickness variability. *Biotechnology and Bioengineering*, 45(6):503–510.

Murphy, F.; Ewins, C.; Carbonnier, F.; Quinn, B. (2016). Wastewater treatment works (WwTW) as a source of microplastics in the aquatic environment. *Environmental Science & Technology*, 50(11):5800–5808.

Neale, P. A.; Antony, A.; Gernjak, W.; Leslie, G.; Escher, B. I. (2011). Natural versus wastewater derived dissolved organic carbon: Implications for the environmental fate of organic micropollutants. *Water Research*, 45(14):4227–4237.

Niederer, C.; Schwarzenbach, R. P.; Goss, K.-U. (2007). Elucidating differences in the sorption properties of 10 humic and fulvic acids for polar and nonpolar organic chemicals. *Environmental Science & Technology*, 41(19):6711–6717.

O'Connor, I. A.; Golsteijn, L.; Hendriks, A. J. (2016). Review of the partitioning of chemicals into different plastics: consequences for the risk assessment of marine plastic debris. *Marine Pollution Bulletin*, 113(1-2):17–24.

Ohashi, H.; Sugawara, T.; Kikuchi, K.-I.; Konno, H. (1981). Correlation of liquid-side mass transfer coefficient for single particles and fixed beds. *Journal of Chemical Engineering of Japan*, 14(6):433–438.

Ouyang, Y. (2003). Simulating dynamic load of naturally occurring TOC from watershed into a river. *Water Research*, 37(4):823–832.

Paasivirta, J.; Sinkkonen, S.; Rantalainen, A.-L.; Broman, D.; Zebühr, Y. (2002). Temperature dependent properties of environmentally important synthetic musks. *Environmental Science and Pollution Research*, 9(5):345–355.

Pan, B.; Ghosh, S.; Xing, B. (2007). Nonideal binding between dissolved humic acids and polyaromatic hydrocarbons. *Environmental Science & Technology*, 41(18):6472–6478.

Pascall, M. A.; Zabik, M. E.; Zabik, M. J.; Hernandez, R. J. (2005). Uptake of polychlorinated biphenyls (PCBs) from an aqueous medium by polyethylene, polyvinyl chloride, and polystyrene films. *Journal of Agricultural and Food Chemistry*, 53(1):164–169.

Paul, E.; Ochoa, J. C.; Pechaud, Y.; Liu, Y.; Liné, A. (2012). Effect of shear stress and growth conditions on detachment and physical properties of biofilms. *Water Research*, 46(17):5499–5508.

Peeken, I.; Primpke, S.; Beyer, B.; Gütermann, J.; Katlein, C.; Krumpen, T.; Bergmann, M.; Hehemann, L.; Gerdts, G. (2018). Arctic sea ice is an important temporal sink and means of transport for microplastic. *Nature Communications*, 9(1):1505.

Pignatello, J. J.; Xing, B. (1996). Mechanisms of slow sorption of organic chemicals to natural particles. *Environmental Science & Technology*, 30(1):1–11.

Poulain, M.; Mercier, M. J.; Brach, L.; Martignac, M.; Routaboul, C.; Perez, E.; Desjean, M. C.; ter Halle, A. (2019). Small microplastics as a main contributor to plastic mass balance in the North Atlantic subtropical gyre. *Environmental Science & Technology*, 53(3):1157–1164.

Ranz, W.; Marshall, W. R.; et al. (1952). Evaporation from drops. *Chemical Engineering Progress*, 48(3):141–146.

Ritchie, A. (1977). Alternative to the Elovich equation for the kinetics of adsorption of gases on solids. *Journal of the Chemical Society, Faraday Transactions 1: Physical Chemistry in Condensed Phases*, 73:1650–1653.

Rittmann, B. E.; McCarty, P. L. (1980a). Evaluation of steady-state-biofilm kinetics. *Biotechnology and Bioengineering*, 22(11):2359–2373.

Rittmann, B. E.; McCarty, P. L. (1980b). Model of steady-state-biofilm kinetics. *Biotechnology and Bioengineering*, 22(11):2343–2357.

Rochman, C. M.; Hoh, E.; Hentschel, B. T.; Kaye, S. (2013). Long-term field measurement of sorption of organic contaminants to five types of plastic pellets: Implications for plastic marine debris. *Environmental Science & Technology*, 47(3):1646–1654.

Rochman, C. M.; Kurobe, T.; Flores, I.; Teh, S. J. (2014). Early warning signs of endocrine disruption in adult fish from the ingestion of polyethylene with and without sorbed chemical pollutants from the marine environment. *Science of the Total Environment*, 493:656–661.

Rockström, J.; Steffen, W.; Noone, K.; Persson, Å.; Chapin III, F. S.; Lambin, E. F.; Lenton, T. M.; Scheffer, M.; Folke, C.; Schellnhuber, H. J.; et al. (2009). A safe operating space for humanity. *Nature*, 461(7263):472.

Rügner, H.; Schwientek, M.; Beckingham, B.; Kuch, B.; Grathwohl, P. (2013). Turbidity as a proxy for total suspended solids (TSS) and particle facilitated pollutant transport in catchments. *Environmental Earth Sciences*, 69(2):373–380.

Rule, K.; Comber, S.; Ross, D.; Thornton, A.; Makropoulos, C.; Rautiu, R. (2006). Sources of priority substances entering an urban wastewater catchment-trace organic chemicals. *Chemosphere*, 63(4):581–591.

Rummel, C. D.; Jahnke, A.; Gorokhova, E.; Kühnel, D.; Schmitt-Jansen, M. (2017). Impacts of biofilm formation on the fate and potential effects of microplastic in the aquatic environment. *Environmental Science & Technology Letters*, 4(7):258–267.

Rusina, T. P.; Smedes, F.; Klanova, J. (2010). Diffusion coefficients of polychlorinated biphenyls and polycyclic aromatic hydrocarbons in polydimethylsiloxane and low-density polyethylene polymers. *Journal of Applied Polymer Science*, 116(3):1803–1810.

Ryan, P. G.; Moloney, C. L. (1993). Marine litter keeps increasing. *Nature*, 361(6407):23.

Schmidt, C.; Krauth, T.; Wagner, S. (2017). Export of plastic debris by rivers into the sea. *Environmental Science & Technology*, 51(21):12246–12253.

Schwarz, G.; et al. (1978). Estimating the dimension of a model. *The Annals of Statistics*, 6(2):461–464.

Schwarzenbach, R. P.; Escher, B. I.; Fenner, K.; Hofstetter, T. B.; Johnson, C. A.; Von Gunten, U.; Wehrli, B. (2006). The challenge of micropollutants in aquatic systems. *Science*, 313(5790):1072–1077.

Schwarzenbach, R. P.; Gschwend, P. M.; Imboden, D. M. (2005). Environmental Organic Chemistry. *John Wiley & Sons*.

Schwientek, M.; Rügner, H.; Beckingham, B.; Kuch, B.; Grathwohl, P. (2013). Integrated monitoring of particle associated transport of PAHs in contrasting catchments. *Environmental Pollution*, 172:155–162.

Seidensticker, S.; Grathwohl, P.; Lamprecht, J.; Zarfl, C. (2018). A combined experimental and modeling study to evaluate pH-dependent sorption of polar and non-polar compounds to polyethylene and polystyrene microplastics. *Environmental Sciences Europe*, 30(1):30.

Seidensticker, S.; Zarfl, C.; Cirpka, O. A.; Fellenberg, G.; Grathwohl, P. (2017). Shift in mass transfer of wastewater contaminants from microplastics in the presence of dissolved substances. *Environmental Science & Technology*, 51(21):12254–12263.

Shah, B. L.; Shertukde, V. V. (2003). Effect of plasticizers on mechanical, electrical, permanence, and thermal properties of poly(vinyl chloride). *Journal of Applied Polymer Science*, 90(12):3278–3284.

Sherwood, T.; Ryan, J. (1959). Mass transfer to a turbulent fluid with and without chemical reaction. *Chemical Engineering Science*, 11(2):81–91.

Smith, K. E.; Thullner, M.; Wick, L. Y.; Harms, H. (2011). Dissolved organic carbon enhances the mass transfer of hydrophobic organic compounds from nonaqueous phase liquids (NAPLs) into the aqueous phase. *Environmental Science & Technology*, 45(20):8741–8747.

Stramska, M. (2009). Particulate organic carbon in the global ocean derived from SeaWiFS ocean color. *Deep Sea Research Part I: Oceanographic Research Papers*, 56(9):1459–1470.

Sumbekova, S.; Cartellier, A.; Aliseda, A.; Bourgoin, M. (2017). Preferential concentration of inertial sub-Kolmogorov particles: The roles of mass loading of particles, Stokes numbers, and Reynolds numbers. *Physical Review Fluids*, 2(2):024302.

Sun, Z.; Mao, L.; XIAN, Q.; YU, Y.; LI, H.; YU, H. (2008). Effects of dissolved organic matter from sewage sludge on sorption of tetrabromobisphenol A by soils. *Journal of Environmental Sciences*, 20(9):1075–1081.

Syberg, K.; Khan, F. R.; Selck, H.; Palmqvist, A.; Banta, G. T.; Daley, J.; Sano, L.; Duhaime, M. B. (2015). Microplastics: addressing ecological risk through lessons learned. *Environmental Toxicology and Chemistry*, 34(5):945–953.

Tan, K.; Hameed, B. (2017). Insight into the adsorption kinetics models for the removal of contaminants from aqueous solutions. *Journal of the Taiwan Institute of Chemical Engineers*, 74:25–48.

Tanaka, K.; Takada, H.; Yamashita, R.; Mizukawa, K.; Fukuwaka, M.-a.; Watanuki, Y. (2013). Accumulation of plastic-derived chemicals in tissues of seabirds ingesting marine plastics. *Marine Pollution Bulletin*, 69(1-2):219–222.

Tcaciuc, A. P.; Apell, J. N.; Gschwend, P. M. (2015). Modeling the transport of organic chemicals between polyethylene passive samplers and water in finite and infinite bath conditions. *Environmental Toxicology and Chemistry*, 34(12):2739–2749.

Ternes, T. A.; Herrmann, N.; Bonerz, M.; Knacker, T.; Siegrist, H.; Joss, A. (2004). A rapid method to measure the solid–water distribution coefficient (Kd) for pharmaceuticals and musk fragrances in sewage sludge. *Water Research*, 38(19):4075–4084.

Teuten, E. L.; Rowland, S. J.; Galloway, T. S.; Thompson, R. C. (2007). Potential for plastics to transport hydrophobic contaminants. *Environmental Science & Technology*, 41(22):7759–7764.

Teuten, E. L.; Saquing, J. M.; Knappe, D. R. U.; Barlaz, M. A.; Jonsson, S.; Björn, A.; Rowland, S. J.; Thompson, R. C.; Galloway, T. S.; Yamashita, R.; Ochi, D.; Watanuki, Y.; Moore, C.; Viet, P. H.; Tana, T. S.; Prudente, M.; Boonyatumanond, R.; Zakaria, M. P.; Akkhavong, K.; Ogata, Y.; Hirai, H.; Iwasa, S.; Mizukawa, K.; Hagino, Y.; Imamura, A.; Saha, M.; Takada, H. (2009). Transport and release of chemicals from plastics to the environment and to wildlife. *Philosophical Transactions of the Royal Society B: Biological Sciences*, 364(1526):2027–2045.

Thompson, J. M.; Hsieh, C.-H.; Luthy, R. G. (2015). Modeling uptake of hydrophobic organic contaminants into polyethylene passive samplers. *Environmental Science & Technology*, 49(4):2270–2277.

Thompson, R. C.; Olsen, Y.; Mitchell, R. P.; Davis, A.; Rowland, S. J.; John, A. W.; McGonigle, D.; Russell, A. E. (2004). Lost at sea: Where is all the plastic? *Science*, 304(5672):838–838.

Van Sebille, E.; England, M. H.; Froyland, G. (2012). Origin, dynamics and evolution of ocean garbage patches from observed surface drifters. *Environmental Research Letters*, 7(4):044040.

Vrugt, J. A. (2016). Markov chain Monte Carlo simulation using the DREAM software package: Theory, concepts, and MATLAB implementation. *Environmental Modelling & Software*, 75(SI):273–316.

Wang, F.; Shih, K. M.; Li, X. Y. (2015). The partition behavior of perfluorooctanesulfonate (PFOS) and perfluorooctanesulfonamide (FOSA) on microplastics. *Chemosphere*, 119:841–847.

Wang, F.; Wong, C. S.; Chen, D.; Lu, X.; Wang, F.; Zeng, E. Y. (2018). Interaction of toxic chemicals with microplastics: A critical review. *Water Research*, 139:208–219.

Wang, J.; Tan, Z.; Peng, J.; Qiu, Q.; Li, M. (2016). The behaviors of microplastics in the marine environment. *Marine Environmental Research*, 113:7–17.

Wang, W.; Wang, J. (2018a). Comparative evaluation of sorption kinetics and isotherms of pyrene onto microplastics. *Chemosphere*, 193:567–573.

Wang, W.; Wang, J. (2018b). Different partition of polycyclic aromatic hydrocarbon on environmental particulates in freshwater: Microplastics in comparison to natural sediment. *Ecotoxicology and Environmental Safety*, 147:648–655.

Weber, W. J.; Morris, J. C. (1963). Kinetics of adsorption on carbon from solution. *Journal of the Sanitary Engineering Division*, 89(2):31–60.

Wojsławski, J.; Białk-Bielinska, A.; Paszkiewicz, M.; Tonski, M.; Stepnowski, P.; Dołzonek, J. (2018). Evaluation of the sorption mechanism of ionic liquids onto multi-walled carbon nanotubes. *Chemosphere*, 190:280–286.

Worch, E. (1993). Eine neue Gleichung zur Berechnung von Diffusionskoeffizienten gelöster Stoffe. *Vom Wasser*, 81:289–297.

Worm, B.; Lotze, H. K.; Jubinville, I.; Wilcox, C.; Jambeck, J. (2017). Plastic as a persistent marine pollutant. *Annual Review of Environment and Resources*, 42:1–26.

Wright, S. L.; Thompson, R. C.; Galloway, T. S. (2013). The physical impacts of microplastics on marine organisms: a review. *Environmental Pollution*, 178:483–492.

Wu, C.; Zhang, K.; Huang, X.; Liu, J. (2016). Sorption of pharmaceuticals and personal care products to polyethylene debris. *Environmental Science and Pollution Research*, 23(9):8819–8826.

Wu, C.-C.; Bao, L.-J.; Liu, L.-Y.; Shi, L.; Tao, S.; Zeng, E. Y. (2017). Impact of polymer colonization on the fate of organic contaminants in sediment. *Environmental Science & Technology*, 51(18):10555–10561.

Wu, S. C.; Gschwend, P. M. (1986). Sorption kinetics of hydrophobic organic compounds to natural sediments and soils. *Environmental Science & Technology*, 20(7):717–725.

Xia, G.; Ball, W. P. (1999). Adsorption-partitioning uptake of nine low-polarity organic chemicals on a natural sorbent. *Environmental Science & Technology*, 33(2):262–269.

Xu, B.; Liu, F.; Brookes, P. C.; Xu, J. (2018). The sorption kinetics and isotherms of sulfamethoxazole with polyethylene microplastics. *Marine Pollution Bulletin*, 131:191–196.

Yokota, K.; Waterfield, H.; Hastings, C.; Davidson, E.; Kwietniewski, E.; Wells, B. (2017). Finding the missing piece of the aquatic plastic pollution puzzle: Interaction between primary producers and microplastics. *Limnology and Oceanography Letters*, 2(4):91–104.

Zarfl, C.; Matthies, M. (2010). Are marine plastic particles transport vectors for organic pollutants to the Arctic? *Marine Pollution Bulletin*, 60(10):1810–1814.

Zhang, T. C.; Bishop, P. L. (1994a). Density, porosity, and pore structure of biofilms. *Water Research*, 28(11):2267–2277.

Zhang, T. C.; Bishop, P. L. (1994b). Evaluation of tortuosity factors and effective diffusivities in biofilms. *Water Research*, 28(11):2279–2287.

Zhang, X.; Zheng, M.; Wang, L.; Lou, Y.; Shi, L.; Jiang, S. (2018). Sorption of three synthetic musks by microplastics. *Marine Pollution Bulletin*, 126:606–609.

Ziccardi, L. M.; Edgington, A.; Hentz, K.; Kulacki, K. J.; Driscoll, S. K. (2016). Microplastics as vectors for bioaccumulation of hydrophobic organic chemicals in the marine environment: A state-of-the-science review. *Environmental Toxicology and Chemistry*, 35(7):1667–1676.

Part II

Appendix

Preamble

List of Papers

This thesis is an accumulation of publications. The findings are described in four papers:

Paper I

Seidensticker, Sven; Zarfl, Christiane; Grathwohl, Peter: Microplastic-Contaminant interactions: modelling of sorption kinetics to polyethylene and environmental implications. *In preparation*

Paper II

Seidensticker, Sven; Zarfl, Christiane; Cirpka, Olaf Arie; Grathwohl, Peter (2019): Microplastic-Contaminant interactions: influence of non-linearity and coupled mass transfer. *Submitted to Environmental Toxicology & Chemistry*

Paper III

Seidensticker, Sven; Lamprecht, Jonas; Grathwohl, Peter; Zarfl, Christiane (2018): A combined experimental and modeling study to evaluate pH-dependent sorption of polar and non-polar compounds to polyethylene and polystyrene microplastics. *Environmental Sciences Europe*, 30, 30

Paper IV

Seidensticker, Sven; Zarfl, Christiane; Cirpka, Olaf Arie; Fellenberg, Greta; Grathwohl, Peter (2017): Shift in mass transfer of wastewater contaminants from microplastics in the presence of dissolved substances. *Environmental Science & Technology*, 51(21), 12254-12263.

Paper not included in the thesis

Kleinteich, Julia; **Seidensticker, Sven**; Marggrander, Nicolaj; Zarfl, Christiane (2018): Microplastics reduce short-term effects of environmental contaminants. Part II: Polyethylene particles decrease the effect of polycyclic aromatic hydrocarbons on microorganisms. *International Journal of Environmental Research and Public Health*, 15(2).

I made the following contributions to the papers included in this thesis:

Paper	Contributions to [%]			
	Scientific ideas	Data generation	Analysis and interpretation	Paper writing
I	60	100	60	80
II	70	100	70	80
III	70	70	70	80
IV	60	80	60	80

Supporting Information

SI 1 Estimation and Prediction of Plastic Amounts

The estimations and predictions on the present and the future amount of marine plastic debris, respectively, base on the articles published by Geyer et al. (2017) and Jambeck et al. (2015). The data on the annual global polymer resin and fiber production from 1950-2015 compiled by Geyer et al. (2017) and amended by the data from 2016, served as the initial basis of my estimations. First, a second-degree polynomial function was fitted to these data applying a *Gauß-Newton* type least-square fitting routine implemented in Matlab (`polyfit`). The obtained polynomial coefficients were used to predict the future plastic production following the same function type. A standard prediction error Δ of ~ 7.3 was determined. My estimated cumulative plastic production of 8.2×10^9 kg in 2016 fits closely to the estimated 8.3×10^9 kg by Geyer et al. (2017) but are a factor of ~ 1.7 higher than the 4.8×10^9 kg estimated by Koelmans et al. (2017) for the same year as the latter authors only considered polymer resin production and do not include fiber production.

According to Jambeck et al. (2015) approximately 3% of the annual plastic production end up in the ocean. Note, that my predictions base on a *business-as-usual* scenario, i.e. the plastic production continuously increases as predicted by the polynomial relationship and no substantial changes are made to the waste management infrastructure and the consumer behavior. If such a scenario is assumed, the cumulative amount of plastic debris in the sea will increase from $\sim 250 \times 10^9$ kg in 2016 to $\sim 910 \times 10^9$ kg in 2050 as illustrated in Figure SI 1. Within this prediction no distinction between floating and sinking plastic is made. It additionally does not account for polymer degradation through weathering processes which happens, however, on much larger time scales and may just slightly reduce the cumulative amount of marine plastic debris (Jahnke et al., 2017).

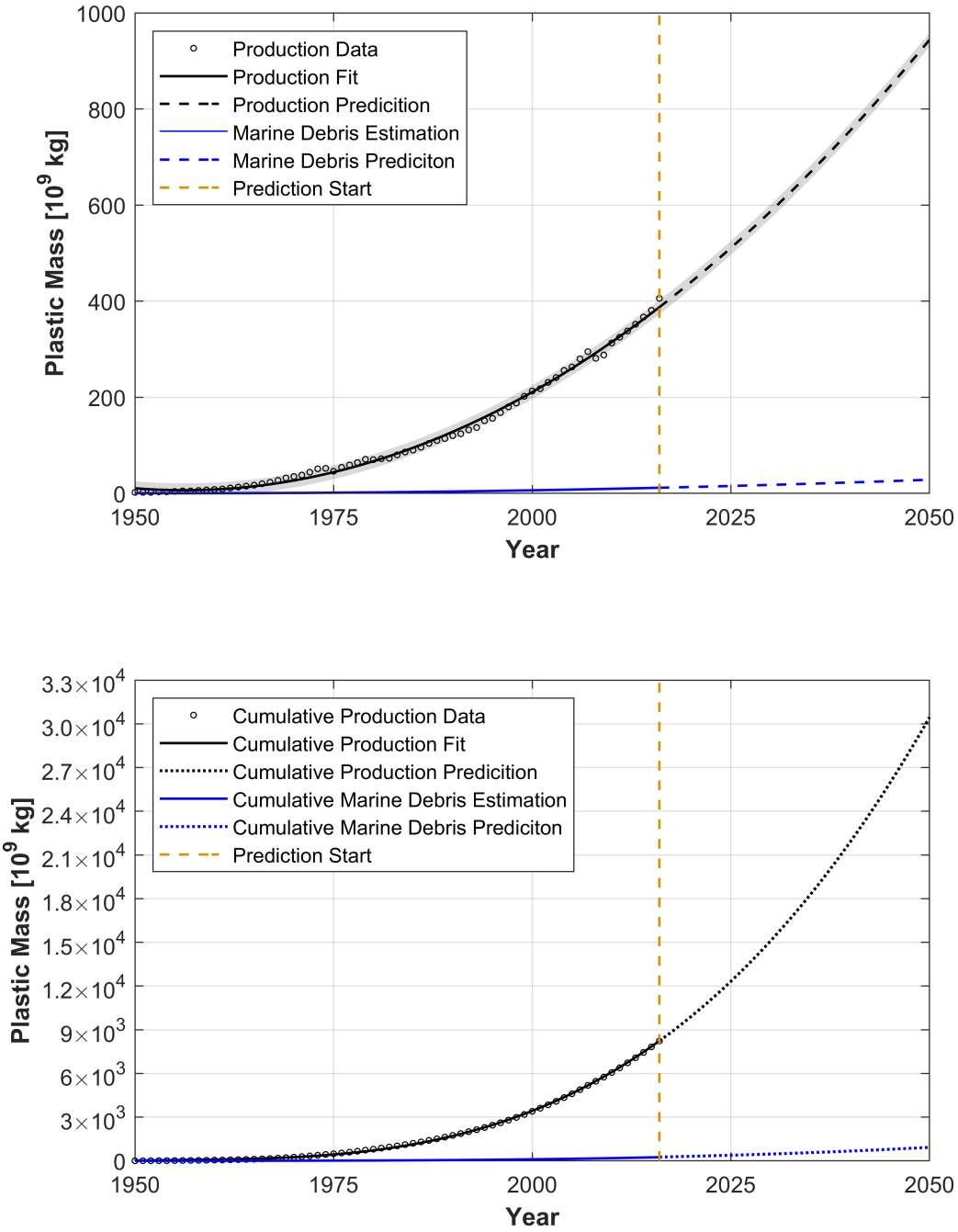

Figure SI 1: **Data and prediction of annual global plastic production including the amount of annually introduced marine plastic debris (top) and the respective cumulative curves on total polymer production and total marine plastic debris (bottom).** As outlined in the text, a second-degree polynomial function ($P_t = 40.5t^2 + 111.3t + 82.95$) was applied to fit (1950-2016) and to predict (2017-2050) the annual global polymer production P_t in year t. The amount of added marine plastic debris is assumed to be 3% of the annual production. They gray shaded area shows the 2Δ deviation with Δ as the standard error of estimation.

Paper I
Modelling of Sorption Kinetics to Polyethylene and Environmental Implications

Abstract

The ubiquitous detection of macro- and microplastics has raised global concern and sorption of organic compounds to such plastic particles is increasingly studied. As one of the most produced and environmentally abundant polymers, polyethylene is well known for its ability to take up hydrophobic organic contaminants. Usually, rate-constant based first-order or pseudo second-order approaches are applied to describe the sorption kinetics. Here, an in-depth investigation of sorption kinetics to various sized polyethylene particles were performed and the role of the different involved mass transfer processes was revealed. The kinetics were determined in closed system batch experiments. It was evidenced that both internal and external mass transfer mechanisms may contribute decisively to the entire kinetics. Thus, we applied a semi-analytical coupled mass transfer model to describe the sorption process and successfully validated the model with our experimental findings. This model does not rely on lumped rate constants and is able to simulate mass transfer shifts. Due to the mechanistic nature of the model, it was furthermore possible to extrapolate our experimental findings to different environmental conditions. Decisive parameters regarding sorption kinetics are particle diameter, intraparticle diffusion coefficient, and the polyethylene-water partition coefficients, but also particle concentrations which are usually much higher in laboratory tests compared to field conditions. In this paper, we show how a change in one or more of these parameters influences the kinetics under both experimental and environmental conditions in which the latter accounted for the presence of other sorbents and biofilm-growing as well. Material- and compound specific parameters may affect the sorption/desorption kinetic depending on boundary conditions. The results evidence that polyethylene microplastic particles play an ambiguous role under environmental conditions. Small particles dominated by external mass transfer presumably reflect the ambient concentration whereas larger particles with high sorption capacity have the potential to transport associated contaminants over longer distances. This environmental behavior is not always reflected in experimental settings and diffusion-based coupled mass transfer models are necessary to accurately transfer experimental findings to field conditions and to perform an improved risk assessment.

I 1 Introduction

The ubiquitous detection of both macroplastics and microplastics shows that anthropogenic litter particles can now be found in all environmental compartments (Alimi et al., 2018; Horton et al., 2017; Law, 2017). As the primary plastic production reaches volumes of more than 400 million tons in 2016 and is believed to increase even further, science and public have to deal with the problem (Geyer et al., 2017). One of the most produced polymers is polyethylene and in a wide variety of studies this is also the type of plastic which is most frequently detected in environmental samples (Auta et al., 2017; Hidalgo-Ruz et al., 2012; Mintenig et al., 2017). However, there is only a limited number of studies published which focus on polyethylene and in particular on its feature to sorb contaminants as it is long been known from passive sampling (Allan et al., 2009; Lohmann, 2011; Tcaciuc et al., 2015; Thompson et al., 2015). If sorption is studied, the investigations usually concentrate on equilibrium partitioning, i.e. sorption isotherms and steady-state distributions of contaminants between different sorbing phases. Only a minor percentage pay particular attention on the sorption kinetics. There is how-ever, an ongoing discussion whether microplastics contribute to the transport of contaminants (Koelmans et al., 2016) or whether they act just as passive sampler reflecting the local environmental concentration. This requires a comprehensive understanding of sorption/desorption kinetics. Within this study we will discuss and compare different kinetic sorption models and evaluate them based on highly resolved experimental data from batch experiments. Furthermore, we will demonstrate how process-based models can help to transfer experimental findings to environmental settings which is finally necessary to achieve an improved risk assessment of microplastic-associated contaminants. In particular microplastic concentrations typically used in laboratory test differ largely from those detected in the environment and only a mechanistic model allows to draw appropriate conclusions from experiments regarding the role of microplastics and associated contaminants in the environment.

I 2 Theory

I 2.1 Plastic-Pollutant Interactions

Generally two different approaches of kinetic modelling of sorptive uptake in batch experiments can be distinguished. Reaction-based models which rely on rate constants, and diffusional models which are derived from Fick's laws (Tan & Hameed, 2017). Various models from both categories have been used in microplastic research and beyond to study the sorption kinetics between particles and various (mostly organic) compounds. Within both approaches the concentration in water which is achieved under equilibrium conditions $C_{W,eq}$ can be calculated from the mass balance as:

$$C_{W,eq} = \frac{C_{W,ini} + C_{P,ini}\frac{m_P}{V_W}}{1 + K_P\frac{m_P}{V_W}} \tag{I 1}$$

with $C_{W,ini}$ and $C_{P,ini}$ as the initial concentrations in the aqueous or particulate phase, respectively and m_P,V_W, and K_P denoting the mass of particles, the volume of water, and the plastic-water partition coefficient defined as the ratio of the equilibrium concentrations in particles and water. Kinetic models usually assume a constant equilibrium partition coefficient as boundary condition. The most applied and easiest model is certainly the *first-order kinetics* (FOK) in which the governing equation for sorptive uptake reads as (Tan & Hameed, 2017):

$$C_W(t) = C_{W,eq} * K_P * \frac{m_P}{V_W}(exp[-k_1 t] - 1) + C_{W,ini} \tag{I 2}$$

where k_1 and $C_W(t)$ are the first-order rate constant for sorption and the aqueous concentration at time t, respectively. Usually k_1 is the fitting parameter and given in s-1. The second commonly applied model is the *pseudo second-order model* (PSO) developed by Ho & McKay (1999) and written as:

$$\frac{dC_P(t)}{dt} = k_2(C_{P,eq} - C_P(t))^2 \tag{I 3}$$

with k_2 as the sorption rate constant and $C_{P,eq}$ and $C_P(t)$ as the amount sorbed at equilibrium and at time t which can be rewritten as:

$$C_{P,eq} = C_{W,eq} K_P \tag{I 4}$$

and thus

$$C_P(t) = \frac{\left(C_{W,ini} - C_W(t)\right) V_W}{m_P} \tag{I 5}$$

by integrating equation I 3 with the applied boundary conditions $C_P(t) = 0$ at $t = 0$ and $C_P(t) = C_P(t)$ at $t = t$ this can be modified to:

$$C_P(t) = \frac{t}{\frac{1}{k_2 C_{P,eq}^2} + \frac{t}{C_{P,eq}}} \tag{I 6}$$

which is known as the integrated rate law for a *pseudo second-order* reaction. Analogous the concentration in the water phase is computed as:

$$C_W(t) = \frac{1 - \left(\frac{\frac{m_P}{V_W} C_{W,eq} K_P}{C_{W,ini}}\right) C_{W,eq} K_P k_2 t}{\left(1 + C_{W,eq} K_P k_2 t\right) C_{W,ini}} \tag{I 7}$$

Within these model types all relevant physical, chemical and thermodynamic pro-

cesses are condensed in rate constants which makes them not very helpful to deduce mechanistic knowledge (Tan & Hameed, 2017). Such models can be expanded, for instance to the *pseudo n-order model for n different from zero* and the *Elovich model* proposed by Ritchie (1977) and Elovich & Larinov (1962) Such an increase in complexity is usually accompanied by an increase in degrees of freedom. Concerning evaluation of data from contaminant sorption to microplastics, FOK and PSO are most frequently applied, e.g. in Llorca et al. (2018); Rochman et al. (2013); Teuten et al. (2007); Wang & Wang (2018a); Xu et al. (2018); Zhang et al. (2018).

Mechanistic models are based on Fick's diffusion laws. Diffusion of a solute between a particle and a liquid phase can be subdivided into two mass transfer processes (Karapanagioti et al., 2001; Seidensticker et al., 2017): Transport from the bulk solution to the particle surface (external mass transfer) on the one hand and subsequent diffusion within the particle (internal mass transfer) on the other hand. Such diffusion-controlled kinetic models are mechanistic and represent the physical processes involved. External mass transfer can be described as the diffusion through an aqueous boundary layer (ABL) which surrounds the particle. Whereas this can be well described by first-order approaches (I 2), addressing internal mass transfer, i.e. intraparticle diffusion (IPD), needs a solution for Fick's second law:

$$\frac{\partial C_P}{\partial t} - D_P \left[\frac{\partial^2 C_P}{\partial r^2} + \frac{2}{r} \frac{\partial C_P}{\partial r} \right] = 0 \tag{I 8}$$

in which D_P and r are the material-dependent intraparticle diffusion coefficient and the radial coordinate, respectively. Commonly, external and internal mass transfer are studied with separate models. For instance, Weber & Morris (1963) proposed a modeling approach to describe kinetics which are limited by IPD and regarding microplastics was e.g. used by Wang & Wang (2018a):

$$C_P(t) = C_{W,ini} - \left(\frac{m_P}{V_W} k_p t^{1/2} + x_i \right) \tag{I 9}$$

where k_p denotes the IPD rate constant and x_i an additional term that is needed to consider diffusion through an ABL which would literally mean that at $t = 0$ already some instantaneous sorption occurred (Largitte & Pasquier, 2016). The square root of time part of equation I 9 denotes an early time approximation of analytical solutions of equation I 8. As shown in previous studies such simple approaches can have severe limitations and thus coupled models are needed (Seidensticker et al., 2017). Such models describe both mass transfer mechanisms which is necessary to fully analyze and understand sorption kinetics. The model assumes as initial condition a homogeneous distribution of the compound either in the particle or the water phase (whether sorption or desorption cases are observed) and the concentration at the particle surface is in local equilibrium to the aqueous concentration at the particle/water interface as described by K_P. Mass transfer from a surrounding bulk solution of defined volume V_W is controlled by the ABL and driven by the concentration gradient between the bulk

solution and the concentration at the water/particle interface $C_{W/P}$. Continuity of mass fluxes requires:

$$J(t) = -\left(C_W(t) - C_{W/P}(t)\right) k_W = -D_P \rho_P \left.\frac{\partial C_P}{\partial r}\right|_{r_P} \tag{I 10}$$

In which J is the mass-flux density and k_W is the external mass transfer coefficient of the pollutant from the bulk into the particulate phase. Multiplication by the plastic's mass density ρ_P on the right-hand side of the equation is necessary as the concentration needs to be expressed as mass of compound per mass of particle material. As the experiments are typically performed in closed systems (batch experiments with finite bath boundary conditions), the concentration in the water phase changes according to the total mass flux across the area of all particles which leads to the following mass balance equation:

$$\frac{dC_W}{dt} = \left(C_{W/P}(r_P, t) - C_W(t)\right) k_W \frac{3}{r_P} \frac{m_P}{V_W \rho_P} \tag{I 11}$$

An analytical solution of equations I 8 and I 10 was derived after Laplace transformation in time whose complete and detailed derivation is described in the supporting information to Seidensticker et al. (2017). Three cases of mass transfer controls are considered: (i) by external mass transfer only, that is, in the limit of $D_P \to \infty$, (ii) by intraparticle diffusion only, that is, in the limit $k_W \to \infty$ and (iii) by both processes in parallel. The analytical Laplace-transform solution of the bulk-phase concentration is back-transformed into the time domain by the numerical method of de Hoog et al. (1982) implemented in Matlab. Furthermore, characteristic times τ_{ch} may be calculated for the two aforementioned mass transfer processes and sensitivity of particle size and intraparticle diffusion coefficients can be evaluated. Characteristic times were derived from the Laplace transformed analytical solution of the coupled mass transfer. Briefly, the overall characteristic time is defined as:

$$\tau_{ch} = \frac{\int_0^\infty \left(C_W(t) - C_{W,eq}\right) dt}{C_W(0) - C_{W,eq}} \tag{I 12}$$

and summarizes the equilibration time between the particulate and aqueous phase and can be split into the two characteristic times $\tau_{ch}^{internal}$ and $\tau_{ch}^{external}$ for internal and external mass transfer, respectively. They read as:

$$\tau_{ch}^{internal} = \frac{r_P^2}{\left(1 + K_P \frac{m_P}{V_W}\right) 15 D_P} \tag{I 13}$$

and

$$\tau_{ch}^{external} = \frac{K_P \rho_P r_P}{\left(1 + K_P \frac{m_P}{V_W}\right) 3 k_W} \quad \text{(I 14)}$$

Since these characteristic times are additive, the overall mass transfer is slower than either of the single processes. The inverse of the characteristic times may be considered as rate constants [s^{-1}]. Sorption kinetics in the finite bath accelerates with increasing solid to liquid ratio (and increasing K_P in equation I 13) which is not reflected in frequently used simple first order (equation) or pseudo second order models (equations I 2 & I 3).

I 3 Materials & Methods

I 3.1 Batch Experiments

Batch experiments, i.e. measurements under finite bath boundary conditions, were performed to study sorption kinetics of phenanthrene to two different types of polyethylene particles which are listed in Table 1.

Table I 1: **Properties of microplastic particles used in this study**

Parameter	**Small Polyethylene (PE)**	**Large Polyethylene (PE)**
Supplier	Azelis, Gotalene 120	German Federal Institute for Materials Research and Testing
Mean diameter [μm]	260	4.2×10^3
Density [kg L^{-1}]	0.92	0.92
BET surface area [m^2 g^{-1}]	0.23	0.18

The experiments were performed in 0.5 L amber glass bottles (Duran, Borosilicate glass, Wertheim, Germany) in the dark and under a constant temperature of 20° C. Phenanthrene (CAS# 85-01-8) was chosen as representative contaminant and purchased from Sigma-Aldrich Supelco (Bellefonte, PA, USA) with a purity ≥99.5%. For the initial solution, ultrapure water was prepared with a Milli-Q water purification system. Phenanthrene was spiked into the initial solution with concentrations of 106 μg L^{-1} and 116 μg L^{-1} for the experiments with small (d_P = 0.26 mm) and large PE (d_P = 4.2 mm), respectively. To avoid biodegradation, 0.05 g L^{-1} NaN_3 were added. The experiments were performed with 500 mL solution and 500 mg of plastic particles which led to a solid-to-liquid ratio of 10-3 kg L^{-1}. The bottles were placed on a stirrer and constantly stirred with 840 rpm. Glass stir bars (25×6 mm) were used to avoid sorbate loss to the system. Samples were taken every 2 min in the first 10 min, after 15, 20, 30, and 40 min, 1, 2, 4, 8, 24, and 48 hours, and continued until equilibrium was reached,

i.e. that no significant concentration change was determined anymore. Experimental duration for large particles was at least 10 days and samples were taken every 5 to 10 days once 120 h of duration was reached. Exact sampling times and measured aqueous concentrations are reported in the supporting information. The sorption to glass walls, stir bars etc. of the batch system was determined in triplicate using a 260 μg L^{-1} solution of phenanthrene and found to be negligible (less than 2% loss in concentration and thus smaller than the uncertainty of the GC measurements, data shown in Appendix I 5.2). As organic solvents cyclohexane, acetone, and acetonitrile were used, all purchased from Merck Millipore (Darmstadt, Germany) in a GC gradient grade purity. As the large PE particles were non-spherical, rather flat cylindrically shaped, sphere equivalent radii based on the volume to surface ratio were calculated from the diameter and height of the PE particles.

I 3.2 Chemical Analysis

Aqueous phenanthrene concentrations were analyzed by GC-MS. Sampling of 1 mL solution were carried out at the described times using a glass pipette. To avoid plastic particles in the samples, a filtration step was performed for both plastic types, using inorganic membrane filters (Whatman Anodisc, pore size 0.2 μm, diameter 13 mm) mounted to a stainless steel membrane holder which was attached to a glass syringe via a Luer lock connection. For quantification 10 μL of deuterated internal standard (20 μg mL^{-1} of phenanthrene D_{10} in acetonitrile) were added to the sample post filtration. Subsequently a liquid/liquid extraction with 300 μL of cyclohexane was executed. Measurements were performed using an Agilent 6890 N GC equipped with an Agilent 7683 B Autosampler and coupled to an Agilent 5973 inert MS. For separation, a J&W Scientific DB-5MS column (dimethylsiloxane 30 m × 0.025 mm ID, 0.25 μm film thickness) and helium as carrier gas were used. The flow rate was 0.7 mL min^{-1} and the device was operated in a pulsed splitless injection mode. Mass-to-charge ratios used for quantification of phenanthrene and phenanthrene D_{10} were 178 and 188 for, respectively.

I 3.3 Parameter Estimation

For all kinetic models except the coupled model, parameters were fitted using the `LSQ-Curvefit` routine implemented in Matlab, a Gauß-Newton type least-square method. To avoid local minima in the fitting procedure, a wide range of initial arbitrary values for the parameters to be fitted that cover several log orders were tried. As the coupled model has two fitting parameters, namely the intraparticle diffusion coefficient D_P and the mass-transfer coefficient k_W of the aqueous boundary layer, a Markov-Chain Monte Carlo method, $DREAM_{ZS}$, was applied. It estimates the parameter distributions conditioned on the measurements (Laloy & Vrugt, 2012; Vrugt, 2016). A uniform prior distribution was considered. As objective function, the sum of the absolute differences between the measurements and the simulated values was calculated. The computed mean absolute errors (MAE) and root mean square errors

(RMSE) are reported in Table 2. Additionally, the 5-95% quantiles are reported to cover the uncertainty of the fitting procedure in the resulting parameter values.

To assess which of the kinetic models fits best to the purpose, an estimator which evaluates the model selection needs to be calculated. As such model selection criteria, the *Akaike Information Criterion* (AIC) and the *Bayesian Information Criterion* (BIC) were chosen. Both do not just appraise the *goodness-of-fit* but as well consider the complexity of the models by contemplating the number of fitted parameters (Akaike, 1974; Schwarz et al., 1978):

$$AIC = -2ln(\hat{\theta}) + 2k \tag{I 15}$$

$$BIC = -2ln(\hat{\theta}) + ln(n)k \tag{I 16}$$

where $ln(\hat{\theta})$, k, and n determine the *log-likelihood*, the number of fitting parameters, and the sample size, respectively. Commonly the maximized *log-likelihood* $ln(\hat{\theta})$) is used to assess the *goodness-of-fit*. However, we applied the relationship between $ln(\hat{\theta})$) and the *residual sum of squares* (*RSS*), which reads as (Burnham et al., 2011):

$$ln(\hat{\theta}) = -\frac{n}{2} ln\left(\frac{RSS}{n}\right) \tag{I 17}$$

Thus, the *RSS* as a standard fitting procedure output can be used to calculate the information criteria. For both approaches, a smaller value indicates a better suitability of the model.

Finally, mass transfer in the aqueous boundary layer is a well-known process and may be characterized by utilizing *Sherwood* relationships, which are scaled by the particle diameter and are transferable to different hydrodynamic setups through the *Reynolds* and the *Schmidt* number, *Re* and *Sc*. The *Sherwood* number *Sh* here was calculated as (Ohashi et al., 1981):

$$Sh = 2 + cRe^{1/2}\, Sc^{1/3} = 2 + 0.59\left(\frac{d_P^{4/3}\varepsilon^{1/3}}{\nu}\right)^{0.57}\left(\frac{\nu}{D_{aq}}\right)^{1/3} \tag{I 18}$$

with the particle diameter d_P [L] and with the kinematic viscosity of water ν [L^2 T^{-1}], the substance specific aqueous diffusion coefficient D_{aq} [L^2 T^{-1} and the unknown energy dissipation rate ε [L^2 T^{-3}]. If mass transfer is limited by film diffusion, k_W may be sensitively fitted and Sh ($Sh = k_W d_P D_{aq}^{-1}$) can be calculated from the experimental results.

I 4 Results & Discussion

I 4.1 Kinetics-Experimental Determination

The results of the kinetic experiments are shown in Figure I 1 and reported in Table I 2. It is obvious from the comparison of measured data and different model approaches, that mass transfer to the small PE particles (Figure I 1, left panel) is largely limited by film diffusion whereas mass transfer to the large particles is mainly dominated by intraparticle diffusion (Figure I 1, right panel). The larger the particles the more mass transfer is limited by intraparticle diffusion and fitted coefficients for film diffusion are not sensitive for large PE. Thus, the film diffusion parameters fitted for small PE can be used to calculate the mass transfer coefficient k_W for large PE adapted to the particle size and the hydrodynamic conditions. Eventually, Sh for small PE was estimated as 7.1 and based on equation I 18, ε for our experimental setup could now be estimated as $10^{4.2}$ m^2 s^{-3} which is reasonable for stirred systems and can be used to calculate a theoretical Sh for the large particles of 45 and thus k_W for the large particles which was estimated as $\sim 8\times10^{-6}$ m s^{-1} (Kawase & Moo-Young, 1987). The numerical results of the kinetic experiments including the outcome for the fitted rate constants are summarized in Table I 2.

Table I 2: **Results of the kinetic experiments.**

Parameter	Small Polyethylene (PE)	Large Polyethylene (PE)
Coupled Model		
mean absolute error [μg L^{-1}]	2.7	0.9
root mean square error [μg L^{-1}]	4.3	1.2
Log K_{PE}	4.18	4.20
k_W [m s^{-1}]	2.1×10^{-5}	2.5×10^{-5}
range, 5-95% quantile	$1.9-2.2\times10^{-5}$	$2.4-2.5\times10^{-5}$
D_P [m^2 s^{-1}]	7.2×10^{-14}	6.4×10^{-14}
range, 5-95% quantile	$4.8-12.3\times10^{-14}$	$5.9-6.8\times10^{-14}$
Sherwood number **calculated/measured**	-/7.1	45/130
Other Models		
First-Order **rate constant** [s^{-1}]	$4.7\pm0.3\times10^{-4}$	$1.7\pm0.2\times10^{-5}$
Pseudo Second-Order **rate constant** [kg g^{-1} s^{-1}]	$1.1\pm0.2\times10^{-8}$	$2.3\pm1.7\times10^{-10}$

For the large particles the theoretically expected and fitted *Sherwood* number differ only slightly. Furthermore, if the waterfilm thickness is expressed as percentage of the particle diameter, it is ~1% and ~10% for the large and small particles, respectively. Film diffusion seems to be slightly more relevant than expected for large particles maybe due to the shape of the particles (cylinders and not spheres) or it can be still a result from the non-sensitive fitting. Nonetheless, the fitted intraparticle diffusion coefficients are very similar as it would be expected for the same material and are furthermore in good agreement to literature values (Lohmann, 2011; Seidensticker et al., 2017). Additionally, the partition coefficients compare very well to earlier measurements (Lohmann, 2011; Rusina et al., 2010; Seidensticker et al., 2017). As expected larger particles take considerably longer to reach equilibrium, around $10^{3.9}$ h compared to approximately $10^{1.5}$ h for the small particles (Figure I 1, left panel) which is a factor of ~ 250 and reflect difference between the diameters squared which is a factor of ~ 260. Furthermore, the model evaluation metrics *AIC* and *BIC* are the smallest for the coupled model in both cases, confirming it performed best in simulating the kinetics compared to the *FOK* and *PSO* models. However, the differences between these selection criteria were greater for the large particles. This is attributed to the fact, that mass transfer to the small particles is mostly limited by film diffusion which can be estimated with an *first-order* exponential function. On the other hand, the shift from film to intraparticle diffusion is much more pronounced for the large particles and thus the coupled model has a greater advantage as both processes need to be considered.

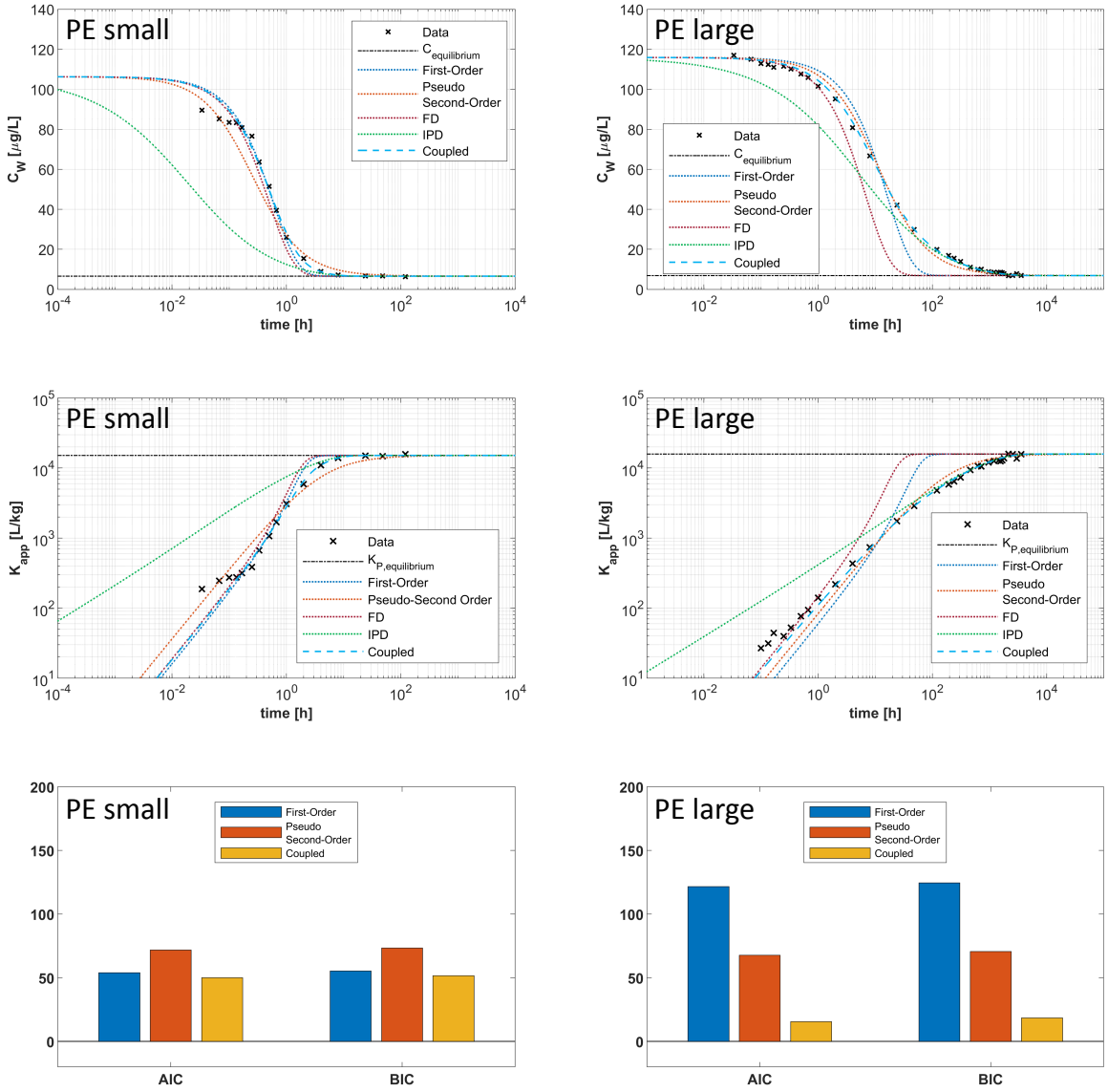

Figure I 1: **Experimental results of phenanthrene sorption to small PE (left panel) and to large PE (right panel).** First and second row show semi-logarithmic plots of the measured aqueous concentrations and double-logarithmic plots of apparent partition coefficients over time, respectively. In the third row the results of the calculated model information criteria *AIC* and *BIC* are illustrated. Note, that smaller values for the ICs indicate a better model performance. FD = film diffusion, IPD = intraparticle diffusion.

I 4.2 Kinetics - Influence of Particle Size, Sorption and Intraparticle Diffusion Coefficients

With increasing particle size *Sh* increases (equation I 18) and external mass transfer resistance becomes less important compared to intraparticle diffusion. At early times, however, film diffusion is relevant since intraparticle diffusion distances are very short and concentration gradients are steep. The effect of the particle size, i.e. the radius, can be elucidated by calculating the characteristic times as a function of radii as illustrated in Figure I 2 for both experimental (left, finite bath) and environmental (right, infinite bath) settings.

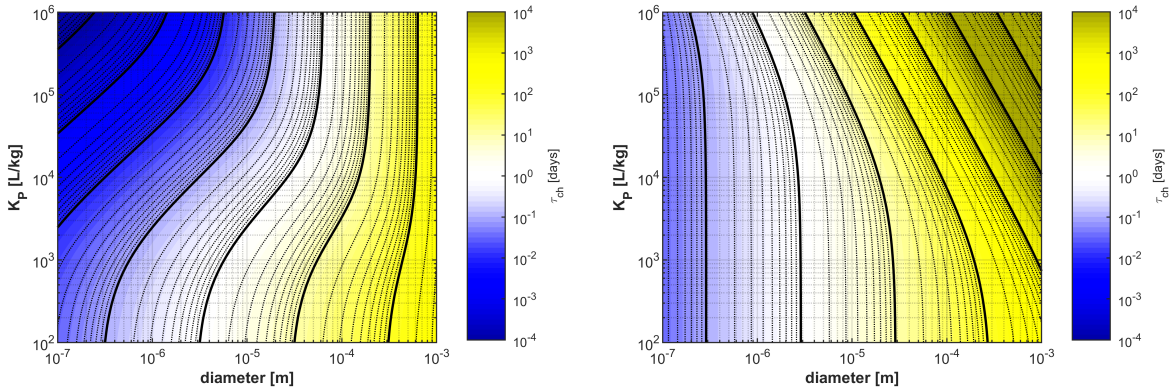

Figure I 2: **Effect of particle radius and partition coefficient on the total characteristic time τ_{ch}**: left experimental conditions, i.e. a solid-to-liquid ratio and a *Sherwood* number of 10^{-3} kg L^{-1} and 7.1; right infinite bath conditions ("oceans") with a solid to liquid ratio of 10^{-10} kg L^{-1} and a *Sherwood* number of 2. In both cases the intraparticle diffusion coefficient was set to 1×10^{-13} m^2 s^{-1}.

In both cases mass transfer is slower for larger particles suggesting slow accumulation of ambient contaminants ("passive samplers") and slow release of e.g. pre-contained additives ("pollutant vectors"). Under environmental conditions (infinite bath) increasing partition coefficient for large particles (intraparticle diffusion dominated) cause longer times scales e.g. for desorption while for small particles film diffusion dominates and the influence of K_P becomes less pronounced. Under finite bath boundary conditions (laboratory tests in batch experiments) time scales are much shorter which is not reflected by first order or second order models. For large particles not only the size has a huge influence on mass transfer time scales but also intraparticle diffusivities which may vary orders of magnitude depending on the material (Pascall et al., 2005). The lower the intraparticle diffusion coefficients are, the slower is the internal mass transfer and hence the whole kinetics. D_P is strongly related to the glass transition temperature T_g of the plastic material (Pascall et al., 2005). Is the ambient temperature $>T_g$, the segmental and thus the free intraparticle volume is increased which results in higher diffusion. The effect of D_P on the total τ_{ch} is shown in Figure I 3. Obviously, a smaller D_P results in a slower mass transfer. Again, the time scales expected in experimental settings are faster due to the higher solid-to-liquid ratio and the subsequently accelerated external mass transfer. The itemized characteristic times for

sole external and internal mass transfer are reported in the Appendix I 5.2.

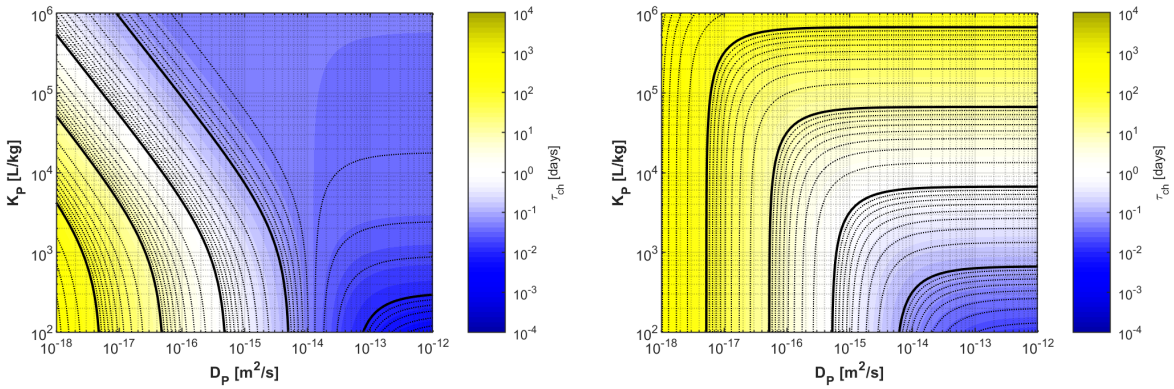

Figure I 3: **Effect of intraparticle diffusion coefficients and partition coefficient on the total characteristic time τ_{ch}.** The left figure shows experimental conditions, i.e. a solid-to-liquid ratio of 10^{-3} kg L^{-1} and a *Sherwood* number of 7.1. The right figure shows environmental settings, i.e. a solid-to-liquid ratio of 10^{-10} kg L^{-1} and a *Sherwood* number of 2. For both cases the particle diameter was 250 μm.

Depending on contaminants (and not so much on plastic types), the partition coefficient can spread over several orders magnitude as well. They are not only important for determination of sorbed amounts but also influence the kinetics, but which also depends on the boundary conditions, i.e. finite vs. infinite bath. Under experimental conditions (finite bath) increasing KP leads to an acceleration of kinetics. Since microplastic concentrations used in experimental setups are considerably higher than those observed in the environment (Lenz et al., 2016) kinetics under laboratory and field conditions are hardly comparable. In experiments, i.e. under finite bath boundary conditions with large particle concentrations, kinetics is fast (equilibration is achieved within hours, Figure I 4).

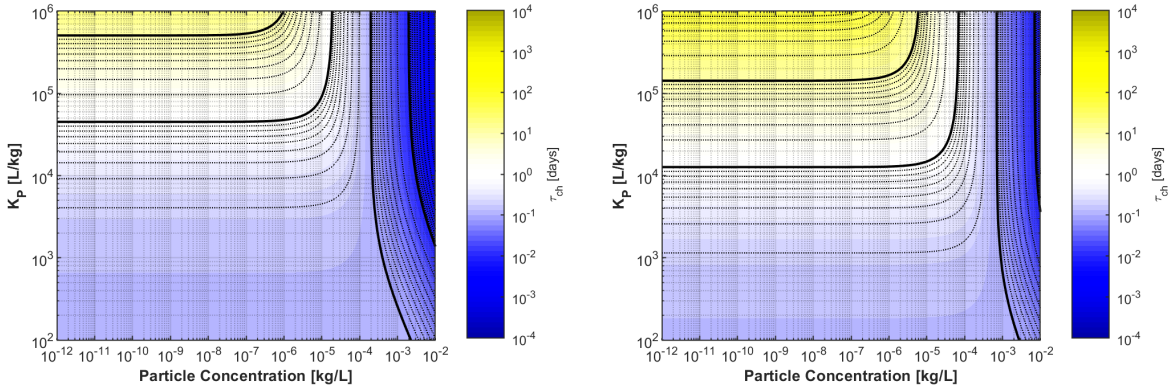

Figure I 4: **Effect of particle concentration and partition coefficient on the total characteristic time τ_{ch}.** The left figure shows experimental conditions, i.e. Sherwood number of 7.1 whereas the right figure shows environmental settings, i.e. a minimum Sherwood number of 2. For both cases the particle diameter was 250 μm and cases the intraparticle diffusion coefficient was 1×10^{-13} m^2 s^{-1}.

External mass transfer is independent of K_P whereas internal mass transfer is accelerated with increasing K_P. Under environmental conditions, i.e. $V_W \rightarrow \infty$, the kinetics are generally slower (Figure I 4). Here, internal mass transfer is independent of K_P while external mass transfer is slowed down with increasing sorption. The changes between environmental and experimental conditions in Figure I 4 are solely due to the different energy dissipation rates reflected in the different *Sherwood* numbers and a faster external mass transfer in experiments.

It is not possible to reveal such shifts if kinetics are modelled using simple *FOK* and *PSO* approaches as they do not take separate mass transfer processes into account and the determined rate constants are only valid for the particular conditions and cannot be transferred to e.g. other particle concentration or flow conditions. Therefore, it is clear that models considering both film and intraparticle diffusion processes need to be considered in modelling of sorption/desorption kinetics and only this allows proper risk assessment; simple first order or second order curve fitting models will misjudge pollutant sorption/desorption timescales if findings from the lab are extrapolated to field settings.

I 5 Implications & Outlook

I 5.1 Influence of Organic Carbon and Similar Sorbents

It is well known that besides microplastics other sorbents are present in rivers and oceans e.g. particulate organic carbon which as well takes up organic contaminants. Utilizing our mechanistic models and based on our previous experimental findings (Seidensticker et al., 2017) for example regarding the influence of dissolved organic matter on partition coefficients and sorption/desorption kinetic we can extrapolate experimental results to field conditions. As energy dissipation rates for rivers and oceans are known, external mass transfer in the environment can be estimated based on the Sherwood relationship shown in equation I 18. Representative data regarding both the microplastic concentration and the dissolved organic carbon (DOC) loads in rivers and oceans were collected within the literature and described in detail in the supporting information. In Figure I 5 we illustrate the influence of organic carbon on the overall partition coefficient (top left) and its influence on the total characteristic time (top right). Again, overall mass transfer is accelerated at high solid-to-liquid ratios and high partition coefficients where-as kinetics is slower under field conditions. Note, that the river and ocean DOC loads are only representative concentrations which can enormously vary in the environment. The two graphs in the bottom row show the kinetics under ocean (left) and river (right) conditions, which differ only slightly. Due to the lower organic carbon load, i.e. lower partition coefficients, the kinetics in the ocean are almost only limited by film diffusion. In rivers, external mass transfer controls the kinetics and at later times internal mass transfer comes into account. Eventually, the results of this virtual experiment show the necessity for mechanistic models since the transferability between lab and field conditions is still given if conditions, i.e. the concentration of further sorbing phases, change.

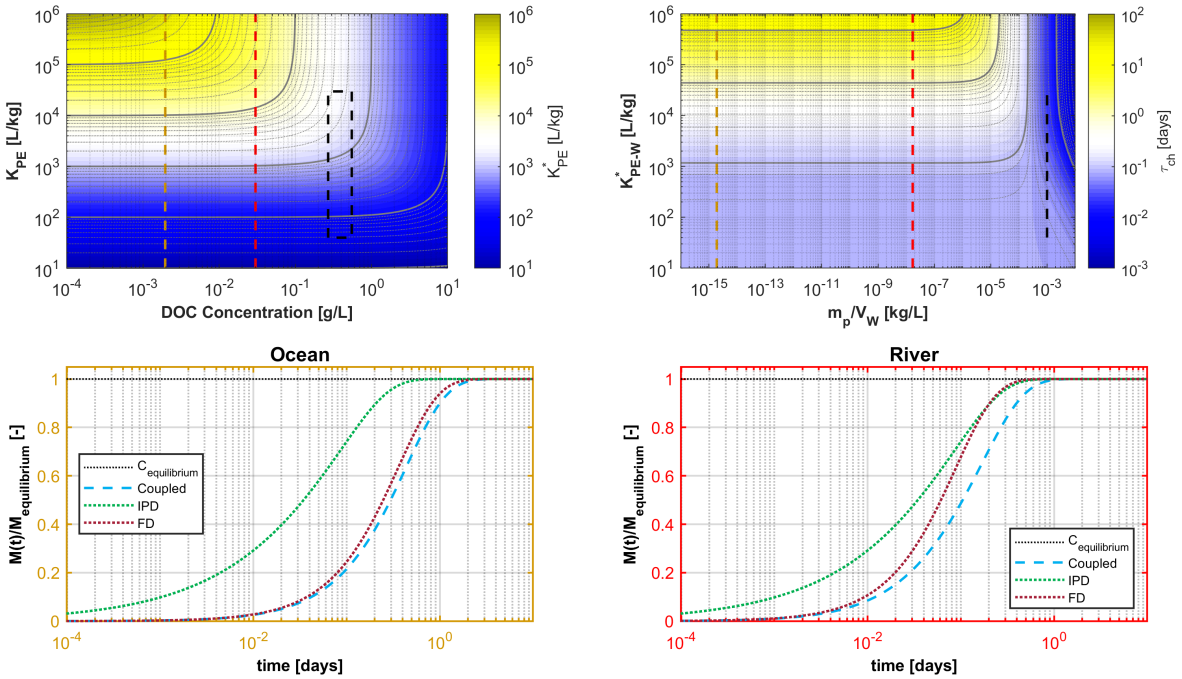

Figure I 5: **Influence of DOC on sorption kinetics under experimental and environmental conditions.** Top row: The overall partition coefficient K^*_{PE-W} as a function of the DOC concentration and K_{PE-W} (left), and total characteristic times of mass transfer as a function of the solid-to-liquid ratio and this overall partition coefficient (right). Black, red, and brown dashed lines represent experimental, river, and ocean DOC concentrations, respectively. Bottom row: Sorption/desorption kinetics at ocean (left) and at river conditions (right). Intraparticle diffusion (IPD), film diffusion (FD), and the coupled model are shown as the dotted green, red, and the dashed blue line, respectively. Modelling parameters are reported in Appendix I 5.2.

I 5.2 Influence of Biofilms on Kinetics

It is widely assumed that biofilms attach to floating microplastics and there is a discussion how this may impact mass transfer (Rummel et al., 2017). Mechanistic models easily allow to elucidate this in more detail. Given, that in a steady-state flux between the aqueous phase and the particles, the effective diffusion coefficient can be estimated as the harmonic average of mass transfer in the two interfaces as explained in the supporting information. Since biofilms consist of >90% water, diffusion coefficients in biofilms are close to aqueous diffusion coefficients (Rittmann & McCarty, 1980a). The maximum biofilm thickness is strongly connected to the flow conditions and depends on hydrodynamic conditions (Horn et al., 2003; Paul et al., 2012). The maximum thickness was derived from a study performed by Chen et al. (2019) in which the thickness for the maximum grown biofilm was ≈ 25% of the plastic thickness. For a virtual experiment two scenarios were considered which are explained in detail in the Appendix I 5.2. Briefly, the coupled model was amended by a two-film diffusion model following Lewis & Whitman (1924) to model effective diffusion (diffusion in the ABL plus diffusion in biofilm) and mass transfer through the ABL, the biofilm, and the particle in series. Within the first scenario the biofilm was directly set to its maximum

value (Figure I 6, static). In the second scenario an exponential growth function was utilized to model the biofilm growth (Bernard & Rémond, 2012; Rittmann & McCarty, 1980b). Thus, for this scenario both the biofilm thickness and the effective diffusion are a function of time and hence the external mass transfer changes with time as well (Figure I 6, growing).

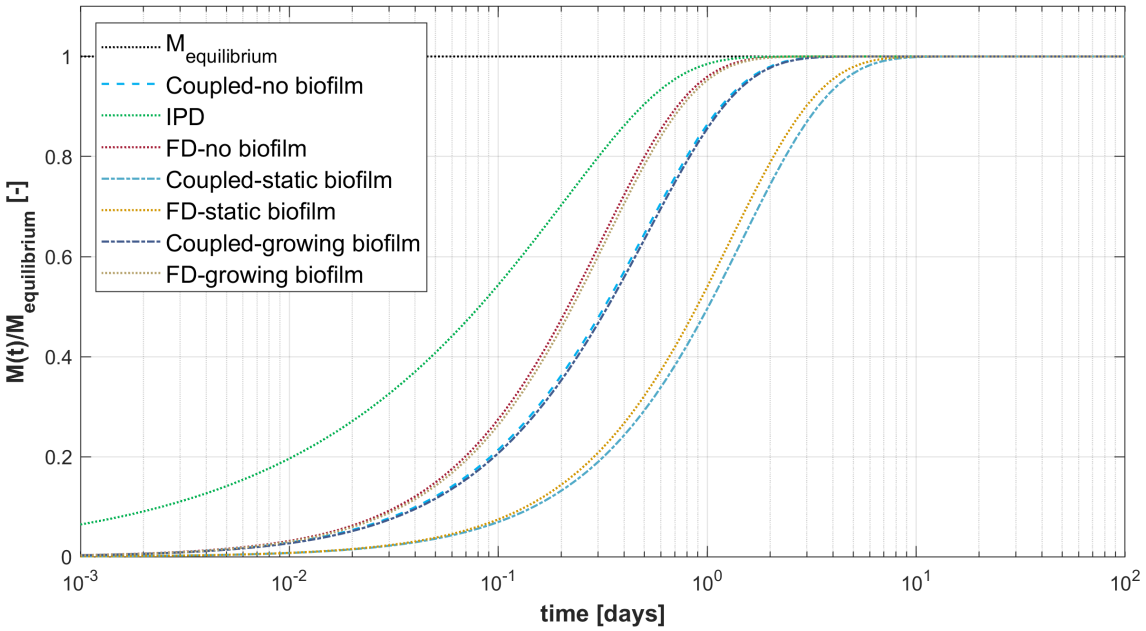

Figure I 6: **Modelling of sorption/desorption from PE under three different biofilm scenarios (no biofilm, growing biofilm, static biofilm).** The thickness of PE particles was set to 250 μm, i.e. the maximum biofilm thickness was 62.5 μm. Growth of biofilm was simulated with a growth rate of 1.6 d^{-1}, a cell thickness of 10 μm, and an initial thickness of 1 μm utilized in an exponential growth function. Initial concentration in the spheres was 50 mg kg^{-1} with a log K_P of 4.0. D_P and D_{bio} were 6.8×10^{-14} and 2.99×10^{-10} m^2 s^{-1}, respectively. For external mass transfer, a Sh of 5 calculated according to equation I 18 was chosen.

As PE was used for the modelling, the kinetics is mainly limited by film diffusion. The biofilm acts as an additional external mass transfer resistance and slows down kinetics. The scenario with the static biofilm shows the longest time until equilibration whereas the dynamic scenario is in between these two but just slightly faster than kinetics without a biofilm at all. However, it could be shown that within both biofilm scenarios, the kinetics are clearly limited by external mass transfer. This, however, can be different if intraparticle diffusion coefficients are lower which would be expected for other polymeric materials (Pascall et al., 2005). The presented modeling results however, have to be supported by experimental work.

Regarding the heavily discussed vector function of microplastic particles (Koelmans et al., 2016; Lohmann, 2017) this study could distinctly reveal that sorption and desorption can be modeled best by using a coupled model based on a diffusional approach. Furthermore, such mechanistic models are a prerequisite to transfer experimental findings to environmental conditions. This may be applied to analyze the vector potential

and to perform an improved risk assessment. Furthermore, the growth of a biofilm on the plastic surface, which is likely to happen under environmental conditions, causes external mass transfer resistance to dominate and depending on the film thickness significantly slows down desorption kinetics and would thus enhance the probability of particles acting as a pollutant vector.

A I
Supporting Information to Paper I

System Sorption

The loss of phenanthrene to the batch system, i.e. the sorption by the system, was estimated by using a batch setup with the materials (e.g. glass bottle, glass stir bar, etc.) but without plastic particles. The initial concentration of phenanthrene in that setup was 266 μ g L^{-1}, measured by GC-MS as described in the main manuscript. Samples were taken after various time points with the latest after 264 h. As it can be seen from Figure I A1, the loss of phenanthrene to the system does not show any trend over time but varies around $C_{W,ini}$ with a maximum deviation of 1.7%.

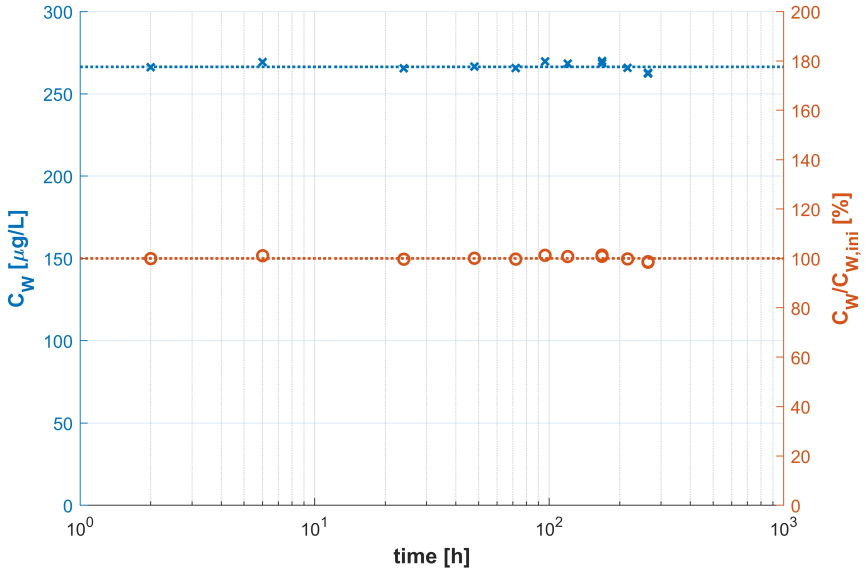

Figure I A1: **Concentration-time series of the system sorption batch.** Concentrations of phenanthrene are plotted on the left y-axis with $C_{W,ini}$ as dashed blue line. Values of the percentage deviation of $C_W(t)$ from $C_{W,ini}$ at the respective times are plotted to the right y-axis.

Experimental Data

Table I A1: **Sampling time points and aqueous phenanthrene concentrations from the kinetic batch experiments for the small and large PE particles.**

time	measured concentration	
	small PE	large PE
[min]	[μg L^{-1}]	
initial	106.3	115.9
2	89.5	117.0
4	85.3	115.0
6	83.4	112.9
8	83.4	112.4
10	80.9	111.0
15	76.6	111.5
20	63.7	110.1
30	51.5	107.6
40	39.6	105.9
60	26.0	101.6
120	15.4	95.1
240	8.9	80.9
480	7.1	66.8
[days]		
1	6.7	42.1
2	6.7	29.9
5	6.4	20.0
8		16.9
10		15.6
13		13.9
19		11.1
26		9.9
30		10.0
40		8.9
50		8.5
60		8.4
70		8.3
75		7.8
90		6.9
105		6.9
125		7.8
150		6.9

Modelling Parameters

Table I A2: **Parameters considered for the different modelling setups and the respective references.**

Parameter	Value [unit]	Reference
Microplastic concentration river	1.7×10^{-8} [kg L^{-1}]	Mintenig et al. (2017)
Microplastic concentration ocean	1.9×10^{-15} [kg L^{-1}]	calculated according to Worm et al. (2017)
Diffusion coefficient water D_{aq}	7.6×10^{-10} [m^2 s^{-1}]	calculated according to Worch (1993)
Diffusion coefficient PE D_{PE}	1.6×10^{-13} [m^2 s^{-1}]	Seidensticker et al. (2017)
turbulence kinetic energy dissipation rate river	$10^{-5.5}$ [m^2 s^{-3}]	Chickadel et al. (2011); MacDonald et al. (2007)
turbulence kinetic energy dissipation rate ocean	$10^{-7.0}$ [m^2 s^{-3}]	Moum et al. (1995)
Total organic carbon river	5×10^{-5} [kg L^{-1}]	Ouyang (2003)
Total organic carbon ocean	1.9×10^{-6} [kg L^{-1}]	DOC: Hansell et al. (2012), POC: Stramska (2009)
Biofilm porosity ε	0.72 [-]	Zhang & Bishop (1994a)
Biofilm tortuosity factor	1.31 [-]	Zhang & Bishop (1994b)
Biofilm density	1002.2 [kg m^{-3}]	Zhang & Bishop (1994a)
Diffusion coefficient biofilm	$D_{aq} \times \varepsilon^3$ [m^2 s^{-1}]	Zhang & Bishop (1994b)
Biofilm growth rate	1.6 [s^{-1}]	Bernard & Rémond (2012)
Biofilm single cell thickness	10^{-5} [m]	Murga et al. (1995)

Total Characteristic Times

Influence of Intraparticle Diffusion Coefficients

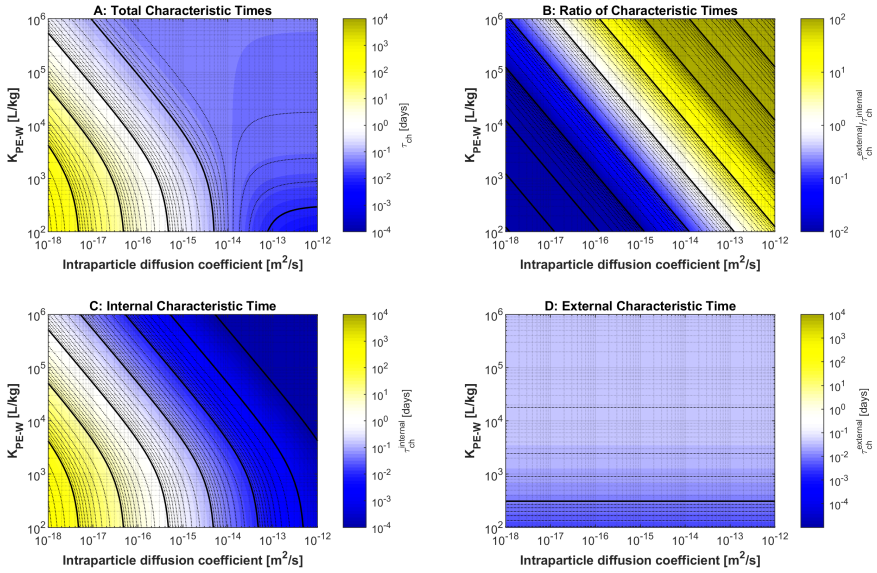

Figure I A2: **Effect of intraparticle diffusion coefficient on τ_{ch} in an experimental setting.** Top left: Total τ_{ch}, top right: Ratio of characteristic times, bottom left: $\tau_{ch}^{internal}$, bottom right: $\tau_{ch}^{external}$. Calculations base on a plastic concentration of 10^{-3} kg L^{-1}, particle diameter of 250 μm, and a Sherwood number of 7.1.

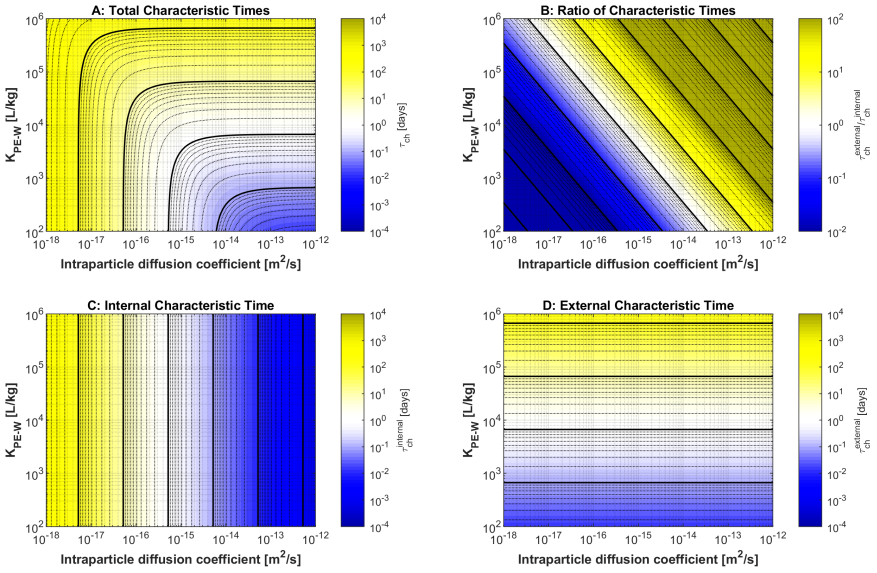

Figure I A3: **Effect of intraparticle diffusion coefficient on τ_{ch} under infinite bath boundary conditions.** Top left: Total τ_{ch}, top right: Ratio of characteristic times, bottom left: $\tau_{ch}^{internal}$, bottom right: $\tau_{ch}^{external}$. Calculations base on a plastic concentration of 10^{-10} kg L^{-1}, particle diameter of 250 μm, and a Sherwood number of 2.

Influence of Particle Size

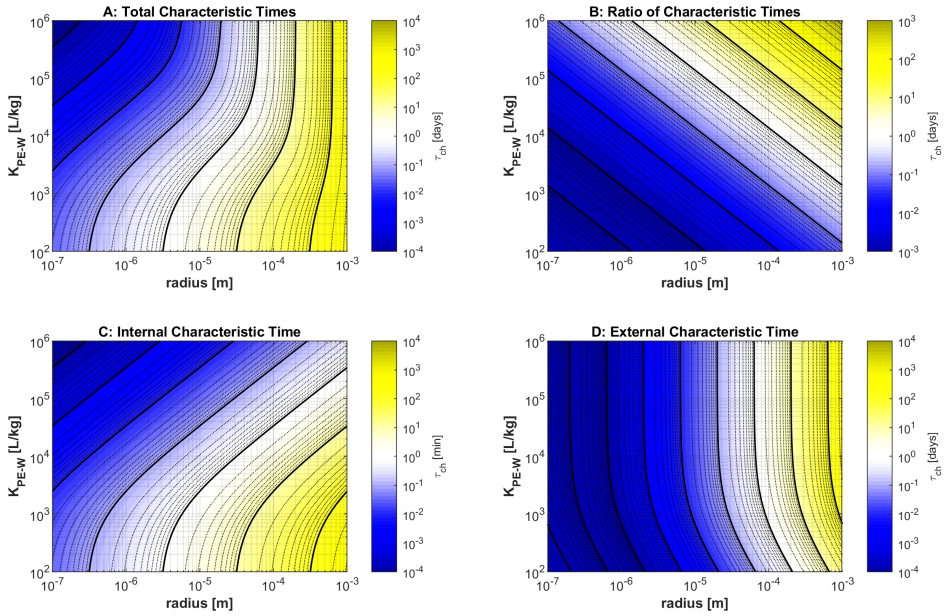

Figure I A4: **Effect of the particle diameter on τ_{ch} in an experimental setting.** Top left: Total τ_{ch}, top right: Ratio of characteristic times, bottom left: $\tau_{ch}^{internal}$, bottom right: $\tau_{ch}^{external}$. Calculations base on a plastic concentration of 10^{-3} kg L^{-1}, $D_{PE} = 1.6 \times 10^{-13}$ m^2 s^{-1}, and a Sherwood number of 7.1.

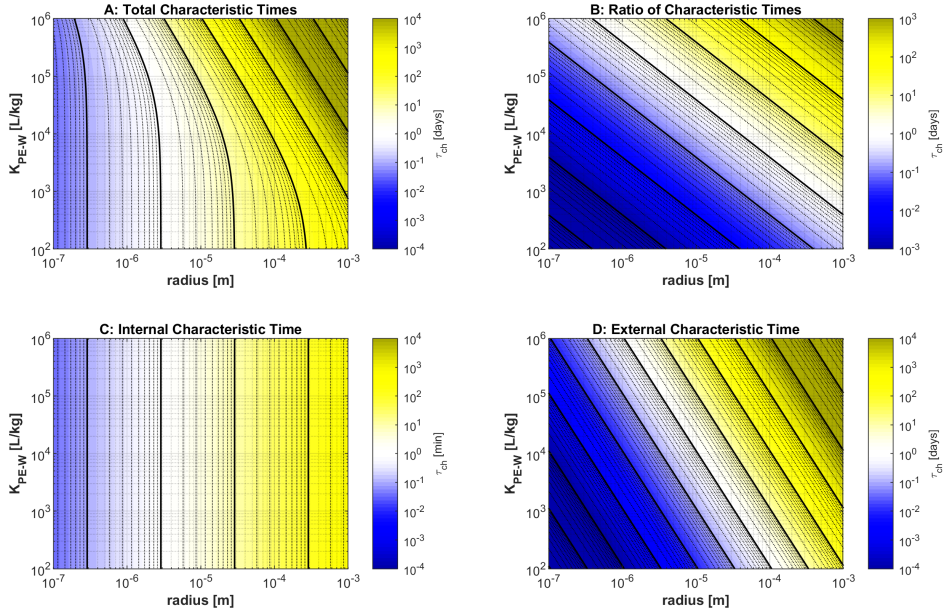

Figure I A5: **Effect of the particle diameter on τ_{ch} under infinite bath boundary conditions.** Top left: Total τ_{ch}, top right: Ratio of characteristic times, bottom left: $\tau_{ch}^{internal}$, bottom right: $\tau_{ch}^{external}$. Calculations base on a plastic concentration of 10^{-10} kg L^{-1}, $D_{PE} = 1.6 \times 10^{-13}$ m^2 s^{-1}, and a Sherwood number of 2.

Influence of Particle Concentration

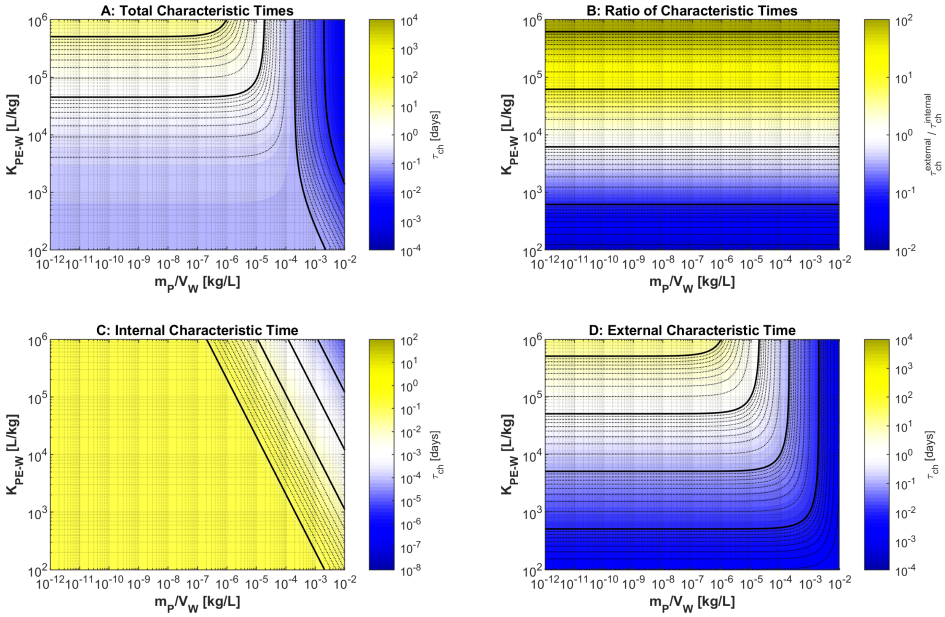

Figure I A6: **Effect of the particle concentration on τ_{ch} in an experimental setting.** Top left: Total τ_{ch}, top right: Ratio of characteristic times, bottom left: $\tau_{ch}^{internal}$, bottom right: $\tau_{ch}^{external}$. Calculations base on a particle diameter of 250 μm, $D_{PE} = 1.6 \times 10^{-13}$ m^2 s^{-1}, and a Sherwood number of 7.1.

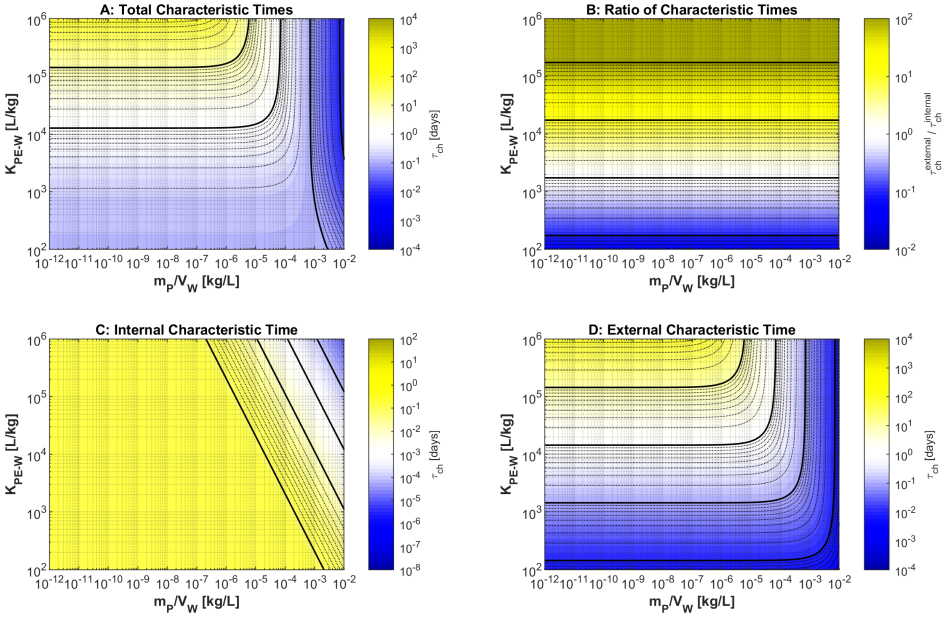

Figure I A7: **Effect of the particle concentration on τ_{ch} under infinite bath boundary conditions.** Top left: Total τ_{ch}, top right: Ratio of characteristic times, bottom left: $\tau_{ch}^{internal}$, bottom right: $\tau_{ch}^{external}$. Calculations base on a particle diameter of 250 μm, $D_{PE} = 1.6 \times 10^{-13}$ m^2 s^{-1}, and a Sherwood number of 2.

Modelling of Biofilm Kinetics

The mass transfer through the biofilm was modelled following a two-film approach after Lewis & Whitman (1924). Thus, mass transfer through the aqueous boundary layer and mass transfer through the biofilm were integrated in an overall external mass transfer k_{all} which represents the two different diffusional processes in series. Given, that in a *steady-state* flux between the aqueous phase and the particles, the effective diffusion coefficient can be estimated as the harmonic average of mass transfer in the two interfaces, the overall external mass transfer through an aqueous boundary layer and a biofilm can be calculated as:

$$k_{all} = \frac{D_{eff}}{\delta_{bio} + \delta_W} \tag{I A1}$$

with

$$D_{eff} = \frac{\delta_{bio} + \delta_W}{\frac{\delta_{bio}}{D_{bio}} + \frac{\delta_W}{D_W}} = \frac{\delta_{bio} + \delta_W}{k_{bio}^{-1} + k_W^{-1}} \tag{I A2}$$

where δ_W and $delta_{bio}$ denote the thickness of the aqueous boundary layer and the biofilm, respectively, whereas D_W, D_{bio}, and D_{eff} are the diffusion coefficients in water, the biofilm, and the effective diffusion coefficient, respectively. Since biofilms consist of >90% water (Rittmann & McCarty, 1980a), D_{bio} is close to D_W. As specified in the main manuscript, the maximum biofilm thickness of $\delta_{bio,max} = d_P \times 0.25$ was derived from Chen et al. (2019). Within two scenarios, $delta_{bio}$ was once set directly to its maximum value (static) and once grown (dynamic) over time based on a first-order growth (Rittmann & McCarty, 1980b) which is the easiest approach but sufficient to give first insights. For that purpose a growth rate constant of 1.6 d^{-1} (valid for microalgal growth (Bernard & Rémond, 2012)) was modeled utilizing an exponential growth, limited to the maximum thickness $\delta_{bio,max}$ (Rittmann & McCarty, 1980b). All relevant biofilm parameters are reported in I A2. Diffusion coefficients within biofilms can be estimated form their porosity ε. Within the present simulation, Dbio was estimated based on the relationship obtained by Zhang & Bishop (1994b) which calculates D_{bio} as $D_W \times \varepsilon^3$.

Paper II
Microplastic–Contaminant Interactions: Influence of Non-Linearity and Coupled Mass Transfer

Abstract

Microplastic particles are ubiquitously detected in the environment. Despite intensive public and scientific discussions, their potential of transporting contaminants in rivers and oceans under environmental conditions is still under assessment. In this study, we measured sorption isotherms and kinetics in batch experiments using phenanthrene as typical hydrophobic wastewater contaminant and microplastic particles, differing in size and material. We observed a linear sorption isotherm for polyethylene, contrasted by nonlinear sorption of polyamide and polystyrene which could be described best by the *Freundlich* and *Polanyi-Dubinin-Manes* isotherms, respectively. We model sorption kinetics as a combination of external mass transfer governed by diffusion through an aqueous boundary layer and intraparticle diffusion within the plastic. Which of these processes controls the kinetics depends on the sorption strength, particle size, diffusion coefficients, and time. We used semi-analytical and numerical methods to simulate the coupled mass transfer for both linear and non-linear sorption. We successfully applied the semi-analytical model to polyethylene and the numerical code to polyamide and polystyrene, reproducing the measured kinetics and obtaining reasonable values for mass transfer and intraparticle diffusion coefficients. Subsequently, we used these coefficients to estimate the transport potential and relevant time scales for microplastic-bound contaminants under environmental conditions.

II 1 Introduction

Plastic debris in general and microplastics, i.e. items <5 mm, in particular have raised many concerns and attracted attention in both science and public (Horton et al., 2017; Law, 2017; Syberg et al., 2015). Most published studies focus on the detection and quantification of plastic particles in different environmental matrices, the fate of particles, or ecotoxicological effects of microplastics on organisms. Even though there is an ongoing discussion how microplastics contribute to the transport of contaminants in aquatic systems (Burns & Boxall, 2018; Koelmans et al., 2016), only a limited number of studies addresses the kinetics of sorption and desorption of contaminants to and from plastics, the underlying mechanisms, and the corresponding role of plastics as potential pollutant vector (Hartmann et al., 2017; Zarfl & Matthies, 2010). Recent modelling studies could show that under certain conditions and time scales, plastic particles may contribute to the accumulation of PAHs in aquatic food webs (Diepens & Koelmans, 2018). Nevertheless, for a more realistic assessment of their accumulation and transport-vector potential it is necessary to adequately describe sorption/desorption of pollutants over time accounting for both particle and chemical properties. Recently, a growing number of studies reported sampling of plastics from the ocean and extraction of the associated pollutants (Chen et al., 2017). Whether such sorbed pollutants represent ambient concentrations (in which plastic acts as passive sampler) or traveled long distance with the plastic (in which plastic acts as transport vector) is unclear. In order to address this question, the aim of this study was to develop mechanistic models that consider the sorption/desorption kinetics, to validate these models by experimental data from the laboratory, and to extrapolate the obtained knowledge to environmentally relevant time scales and settings.

II 1.1 Plastic-Pollutant Interactions

Equilibrium sorption of organic contaminants into plastic has been described by different types of sorption isotherms such as the linear, *Freundlich*, and *Langmuir* models (Hüffer & Hofmann, 2016). Quite recently more refined models such as the poly-parameter linear free energy relationship were applied to predict partitioning more accurately (Hüffer et al., 2018). However, because sorption involves the incorporation of the compounds into the interior of the solid plastic particles, assuming local equilibrium between the surrounding water and the microplastics may be misleading. A variety of models have been developed to describe the kinetics of sorption onto/into particles (Endo et al., 2013; Teuten et al., 2009). Typically, Fickian diffusion is considered to be the rate limiting step. Diffusion between a particle and a liquid phase usually is subdivided into transport from the bulk solution to the particle surface (external mass transfer) and subsequent diffusion within the particle (internal mass transfer) (Pignatello & Xing, 1996; Tcaciuc et al., 2015). In this framework, external mass transfer can be described as the diffusion through an aqueous boundary layer surrounding the particle. While external mass transfer can be well described by a first-order approach, in which the mass flux is proportional to the concentration difference across the aqueous boundary layer, the internal mass transfer, i.e. intraparticle diffusion, requires a description accounting

for the temporal change of the concentration profile within the particle (Grathwohl, 2012). Seidensticker et al. (2017) presented a semi-analytical model to describe the kinetic mass transfer between aqueous solutions of organic contaminants and spherical particles of polyethylene (PE). This model required sorption to be linear (partitioning). In the present study, we consider sorption of phenanthrene onto/into different types of plastic particles such as polyamide (PA) and polystyrene (PS). The kinetics will be linked to the respective sorption isotherms to achieve a comprehensive explanation of the sorptive interactions. In case of linear sorption isotherms, the semi-analytical model is applicable, In the case of non-linear sorption isotherms, however, we need to apply a numerical model of diffusive mass transfer within the particles and across the aqueous boundary layer because closed-form expressions are not available.

II 2 Theory

II 2.1 Mass Conservation Laws

Within the microplastic particles, the diffusion equation in spherical coordinates applies:

$$\frac{\partial C_P}{\partial t} - D_P \left[\frac{\partial^2 C_P}{\partial r^2} + \frac{2}{r} \frac{\partial C_P}{\partial r} \right] = 0 \tag{II 1}$$

in which C_P [M M^{-1}] is the mass-related concentration of the organic compound in the plastic, t [T] is time, and D_P [L^2 T^{-1}] and r [L] are the material-dependent intraparticle diffusion coefficient and the radial coordinate, respectively. Sorption equilibrium between the plastic and water at the surface of the plastic particle, and a concentration gradient of zero in the center of the sphere are assumed as boundary conditions. As initial condition, we assume the concentration in the particle to be uniform. The particle exchanges mass with a surrounding bulk solution of a defined volume V_W [L^3] via the aqueous boundary layer. Mass transfer through the boundary layer is driven by the concentration gradient between the bulk solution and the aqueous concentration at the surface of the particles. Then, the mass balance at the surface requires:

$$\frac{dC_{surf}}{dt} = \left(C_W(t) - C_{W/P}(t) \right) k_W - D_P \rho_P \left. \frac{\partial C_P}{\partial r} \right|_{r_P} \tag{II 2}$$

in which C_P [M L^{-3}] is the bulk phase concentration $C_{W/P}$ [M L^{-3}] is the aqueous concentration at the particle surface C_{surf} [M L^{-2}] as the mass of sorbate per surface area, K_P [L^3 M^{-1}] is the plastic-water partition coefficient, r_P [L] denotes the particle radius, and k_W [L T^{-1}]] is the mass-transfer velocity. Multiplication by the mass density ρ_P [M L^{-3}] of the particles in the intraparticle-diffusion term of the equation is needed because the concentration in the particles is expressed as mass of the compound per mass of the particle material, whereas the concentration in the aqueous phase is volumetric.

As the experiments are performed in a closed system, the concentration in the water phase changes according to the total mass flux across the area of all particles, leading to the following mass balance equation:

$$\frac{dC_W}{dt} = \left(C_{W/P}(r_P, t) - C_W(t)\right) k_W \frac{3}{r_P} \frac{m_P}{V_W \varrho_P} \tag{II 3}$$

in which m_P [M] is the mass of all particles, the factor $3/r_P$ is the area-to-volume ratio of a single particle, and m_P/ρ_P is the total volume of all particles. Equations II 2 & II 3 must be amended by initial conditions of C_W and $C_{W/P}$. In addition to absorption within the particles, we assume instantaneous adsorption onto the surface obeying the same sorption isotherm of the plastic material:

$$C_{surf}(t) = K_{surf} \rho_P C_{P,eq}\left(C_{W/P}(t)\right) \tag{II 4}$$

with C_{surf} [M L^{-2}] denoting the mass of the sorbate per surface area,$C_{P,eq}\left(C_{W/P}(t)\right)$ [M M^{-1}] as the equilibrium concentration in the plastic material for a given aqueous concentration $C_{W/P}(t)$ at the plastic-water interface, and K_{surf} [L] as the thickness of a virtual plastic layer instantaneously sorbing the contaminant. The latter parameterizes the effects of surface roughness. As we show in the SI (SEM images of the particles) and in Table II 1, the particles have rough surfaces and the true surface areas are different from those calculated for perfect spheres. We account for these effects by considering effective surface adsorption.

II 2.2 Sorption Isotherm

For the evaluation of equilibrium sorption, we tested three different sorption isotherms. The simplest isotherm is linear one with a constant distribution constant K_d [L^3 M^{-1}]. We also considered the *Freundlich* and the *Polanyi-Dubinin-Manes* non-linear sorption isotherm (Allen-King et al., 2002; Kleineidam et al., 2002):

$$\textit{linear} \qquad C_{P,eq} = K_d C_{W,eq} \tag{II 5}$$

$$\textit{Freundlich} \qquad C_{P,eq} = K_{Fr} C_{W,eq}^{n_{Fr}} \tag{II 6}$$

$$\textit{Polanyi} \qquad C_{P,eq} = V_o \rho_o \exp\left[\left(\frac{-RT\left(ln\frac{S_W}{C_{W,eq}}\right)}{E}\right)^b\right] \tag{II 7}$$

with K_{Fr} [M^{1-n} L^{3n} M^{-1}] and n_{Fr} being the *Freundlich* partition coefficient and the *Freundlich* exponentrespectively, V_o denoting the maximum volume of sorbate per unit of sorbent [L^3 M^{-1}], ρ_o [ML^{-3}] sorbate's density, $R = 8.314$ J mol^{-1} K^{-1} the ideal gas constant, T [temp] absolute temperature, and S_W the subcooled liquid solubility of the organic compound in water [ML^{-3}]. E [ML^{2}T^{-2}] is the characteristic free energy of

absorption (Allen-King et al., 2002). The exponent b [-] is usually an integer ranging between 1 and 5. Chossing $b = 2$ results in the *Dubinin-Radushkevich* model (Allen-King et al., 2002).

For the the specific case of linear sorption without instantaneous adsorption (i.e. $K_{surf} = 0$), Seidensticker et al. (2017) presented an analytical solution after Laplace transformation in time and analyzed three cases of mass-transfer control: (i) by external mass transfer only, that is, in the limit of $D_P \rightarrow \infty$, (ii) by intraparticle diffusion only, that is, in the limit $k_W \rightarrow \infty$, and (iii) by both processes in sequence. The analytical Laplace-transform solution of the bulk-phase concentration is back-transformed into the time domain by the numerical method of de Hoog et al. (1982) implemented in Matlab. For the case of a non-linear sorption isotherm with $C_{P,eq}(C_W)$, a closed-form solution in the Laplace-domain cannot be derived, requiring thus a numerical scheme. For this purpose, we discretized equation II 1 by the Finite Volume method subdividing the particles into n [-] shells of identical thickness,coupled it to equations II 2 & and II 3 and integrated the resulting non-linear system of ordinary differential equations by the Gear solver `ode15s` implemented in Matlab (see the supplementary information for details).

II 3 Materials & Methods

II 3.1 Batch Experiments

Batch experiments were performed to study both sorption kinetics and isotherms. Three different types of microplastics were compared, some properties of which are listed in Table II 1. Further characteristics of the used particles, e.g. SEM pictures, are provided in the supplementary information. The three chosen polymer materials are among the most common plastics detected in the environment (Burns & Boxall, 2018; Mintenig et al., 2017).

The kinetic experiments were performed in 0.5 L amber glass bottles (Duran, Borosilicate glass, Wertheim, Germany) under a constant temperature of 20 $°C$ and in the dark. As representative contaminant and sorbate, phenanthrene (CAS# 85-01-8) was chosen and purchased from Sigma-Aldrich Supelco (Bellefonte, PA, USA) with a purity >99.5%. The experiments were performed with 500 mL solution (containing ultrapure water and phenanthrene) and 500 mg of plastic particles which led to a solid-to-liquid ratio of 10^{-3} kg L^{-1}. Initial concentrations of phenanthrene in the batches were between 110-125 μg L^{-1} (the exact concentration was measured in each case). To avoid biodegradation, 0.05 g L^{-1} NaN_3 were added. The bottles were placed on a stirrer and constantly stirred with 840 rpm. Glass stir bars (25 × 6 mm) were used to avoid sorbate loss to the system. We took samples every 2 min in the first 10 min, after 15, 20, 30, and 40 min, 1, 2, 4, 8, 24, 48, hours and continued sampling until equilibrium was reached, i.e. when no significant difference was determined anymore. Exact sampling times for every sorbent are reported in the supporting information. The sorption to glass walls, stir bars etc. of the batch was determined in triplicate using a 260 μg L^{-1} solution of phenanthrene and found to be negligible (less than 2% loss in concentration and thus smaller than the

Table II 1: **Properties of microplastic particles used in this study. PE = polyethylene, PS = polystyrene, PA = polyamide.**

Parameter	Polyethylene (PE)	Polystyrene (PS)	Polyamide (PA)
Supplier	Azelis, Gotalene 120	Goodfellow	Goodfellow
Mean diameter [μm][a]	260	250	25
Density [kg L^{-1}]	0.92	1.05	1.14
Calculated surface area [m^2 g^{-1}]	0.03	0.023	0.30
BET surface area [m^2 g^{-1}]	0.23	0.65	0.86
BJH pore volume [cm^3 g^{-1}]	*no pores*	0.003	0.000013
Porosity [%]		0.32	0.01
Average pore width [Å]	*no pores*	195.3	18.8
Glass transition temperature[b] [°C]	-120	100	50

a nominal diameters, normally distributed with σ^2=0.05

b literature values from Hüffer & Hofmann (2016)

uncertainty of the GC measurements, data shown in the supplementary information). We used cyclohexane, acetone, and acetonitrile, all purchased from Merck Millipore (Darmstadt, Germany) in a GC gradient grade purity, as organic solvents.

Additional batch experiments were performed in triplicates to measure the sorption isotherms. The solid-to-liquid ratio was the same as in the other experiments. At the end of the experiment the whole aqueous phase was extracted and analyzed with GC-MS as described below. To cover a wide range, we chose eight different initial phenanthrene concentrations of 320, 160, 80, 40, 20, 10, 1, and 0.1 μg L^{-1}. The aqueous concentrations were measured in the initial state and after six weeks (42 d) of shaking, assuming that, at this time, sorption had reached equilibrium.

II 3.2 Chemical Analysis

The aqueous concentration of phenanthrene in the batch system, was determined with GC-MS. Samples of 1 mL solution were taken at the described time points using a glass pipette. To avoid plastic particles in the samples, a filtration step was performed, using inorganic membrane filters (Whatman Anodisc, pore size 0.2 μm, diameter 13 mm) mounted to a stainless steel membrane holder which was attached to a glass syringe via a Luer lock connection. Preliminary experiments revealed that no phenanthrene loss to the filter occurred. For quantification 10 μL of a deuterated internal standard (20 μg mL^{-1} of phenanthrene D_{10} in acetonitrile) were added to

the sample after filtration. Subsequently the samples were extracted with 300 μL of cyclohexane. Measurements were performed using an Agilent 6890 N GC equipped with an Agilent 7683 B Autosampler and coupled to an Agilent 5973 inert MS. For separation, a J&W Scientific DB-5MS column (Dimethylsiloxane 30 m × 0.025 mm ID, 0.25 μm film thickness) and helium as carrier gas were used. The flow rate was 0.7 mL min-1 and the device was operated in a pulsed splitless injection mode. The mass-to-charge ratios used for quantification were 178 and 188 for phenanthrene and phenanthrene D_{10}, respectively.

II 3.3 Parameter Estimation

We evaluated the kinetics with the model described above. Towards this end, we fitted the model to the data using DREAM$_{ZS}$, a Markov-Chain Monte Carlo method yielding parameter distributions conditioned to the measurements (Laloy & Vrugt, 2012; Vrugt, 2016).While the distribution coefficient K_d was determined from the kinetic experiments in the fits of the linear models, we took the coefficients of the sorption isotherm determined from the (presumably) equilibrium data as fixed properties when fitting the nonlinear models to the kinetic data. In both model types, we fitted the intraparticle diffusion coefficient D_P and the mass-transfer coefficient k_W of the aqueous boundary layer as kinetic parameters. For each parameter we considered a uniform prior distribution within a wide range. As the objective function of the fit, we took the sum of the absolute differences between the measurements and simulated values. The computed mean absolute errors (MAE) and root-mean-square errors (RMSE) as reported in the results are based on a conditional sample size of 3000. Furthermore, the 5-95% quantiles of the estimated parameters are reported to assess their uncertainty. The isotherm models were fitted with a Gauß-Newton type least-square method implemented in the optimization toolbox of Matlab (`lsqcurvefit`). To assess the suitability of the different isotherm models, the *Bayesian Information Criterion* (BIC) which adds the sum of weighted residuals and the sum of parameters times the logarithm of the number of observations, was calculated (for details, see the supporting information). A smaller BIC-value indicates a higher suitability of the model.

II 4 Results & Discussion

II 4.1 Isotherms

Table II 2 lists results of the isotherm measurements. Even though the *Freundlich* sorption with an exponent close to unity scored slightly better, PE showed in essence linear partitioning (Figure II 1). This is consistent with PE showing practically no porosity, as determined by the N_2-BET measurements reported in Table II 1. For both PA and PS, sorption is clearly non-linear as indicated by the highest BIC-values of the non-linear isotherms (see Table II 2) and shown in Figure II 1. While for PA, the *Freundlich* model scored best, the *Polanyi-Dubinin-Manes* isotherm described the sorption onto PS the best. This is in agreement with other findings as well as with the

measured pore volumes of PA and PS (Table II 1) as an increasing presence of pores shifts the isotherm towards non-linear sorption (Allen-King et al., 2002; Kleineidam et al., 2002).

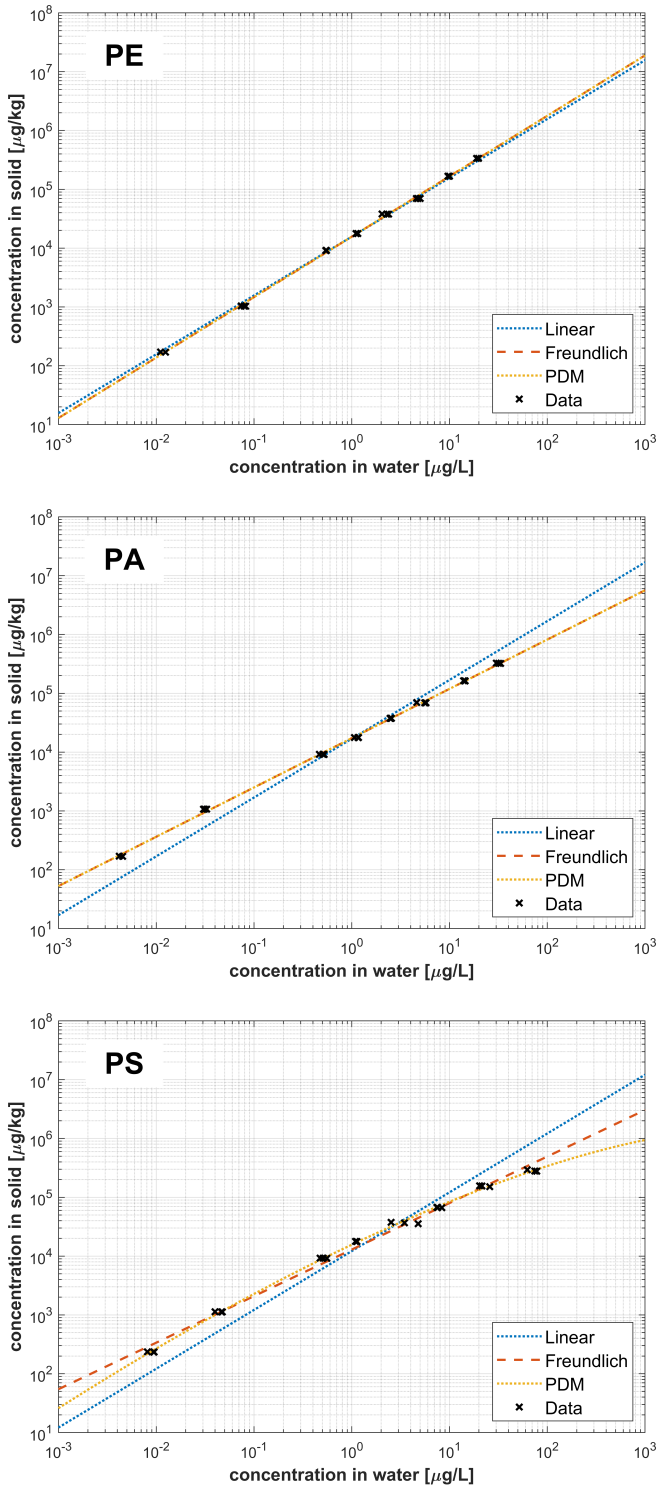

Figure II 1: **Double logarithmic plot of data and models (linear, *Freundlich*, and *PDM*) for sorption isotherms of phenanthrene to polyethylene (PE), polyamide (PA), and polystyrene (PS).**

II 4.2 Kinetics

Table II 2 compares model fits assuming linear sorption (using the semi-analytical solution) with those assuming non-linear sorption (fully relying on numerical simulations). For PE, we considered only linear sorption as the isotherm experiments indicated negligible non-linearity. For PA and PS, we considered *Freundlich* and *Polanyi-Dubinin-Manes* sorption, respectively, in the non-linear fits. Mass transfer of phenanthrene onto/into PE shifts from film diffusion at early times to intraparticle diffusion at later times (Figure II 2, left panel). The fitted intraparticle diffusion coefficient are within the range of other findings (Lohmann, 2011; Rusina et al., 2010). By contrast, the kinetics of PS (Figure 3) and PA (Figure II 2, right panel) are limited by intraparticle diffusion almost all the time because the diffusion coefficients in these materials are several orders of magnitude lower than that in PE. Thus, fitted mass transfer coefficients for film diffusion are not sensitive and, hence, the k_W-value determined for PE was used to compute k_W-values for PS and PA adapted to hydrodynamic conditions and particle size, because the k_W-value depends on the hydrodynamic conditions in the respective experiment (Jeannot & Cantwell, 1997).

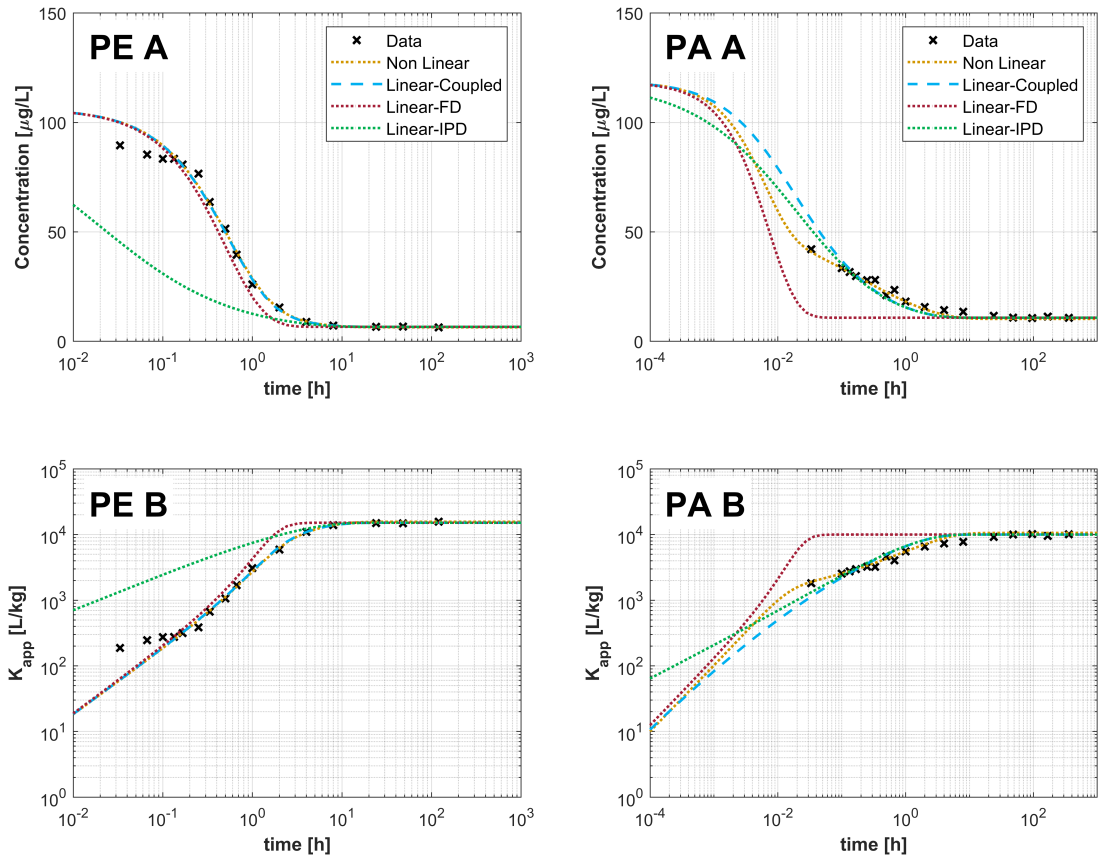

Figure II 2: **Results of the sorption of phenanthrene to polyethylene (PE, left panel) and polyamide (PA, right panel).** Row A shows semi-logarithmic plots of water concentrations over time. Row B shows double-logarithmic plots of apparent partition coefficients over time. The respective denotations are indicated in the legends. FD=film diffusion, IPD=intraparticle diffusion.

As all kinetic experiments were performed with the same experimental procedure, empirical relationships can be applied to consistently estimate the value of k_W for PA and PS. From the Reynolds and Schmidt numbers, *Re* and *Sc*, in the system the Sherwood number *Sh* can be estimated as (Ohashi et al., 1981):

$$Sh = 2 + cRe^{1/2}\,Sc^{1/3} = 2 + 0.59\left(\frac{d_P^{4/3}\varepsilon^{1/3}}{\nu}\right)^{0.57}\left(\frac{\nu}{D_{aq}}\right)^{1/3} \qquad \text{(II 8)}$$

Because the experimental setup is the same for all materials, *Sh* can be calculated from the particle diameter d_P [L] and the kinematic viscosity of water ν [$L^2\ T^{-1}$], the substance specific aqueous diffusion coefficient D_{aq} [$L^2\ T^{-1}$] and the unknown energy dissipation rate ε [$L^2\ T^{-3}$]. Since PE is clearly limited by film diffusion, the k_W-value was sensitively fitted and *Sh* ($Sh = k_W d_P D_{aq}^{-1}$) could be calculated from the experiment. Eventually, *Sh* for PE was estimated as 7.1 and based on Equation II 8, ε for our experimental setup could now be estimated as $10^{-4.2}$ $m^2\ s^{-3}$ which is reasonable for stirred systems (more detailed descriptions in the SI, Kawase & Moo-Young (1987); Ohashi et al. (1981). As ε is identical for all types of plastics and independent of the particles, it was utilized in Equation II 8, where only d_P varies among the different plastic types, to approximate Sherwood numbers and corresponding scaling factors to compute the value of k_W in the PS and PA experiments. We subsequently used these scaling factors (± 5%) as initial guess in the fitting of the models. Finally, the k_W-values listed in Table 2 and Sh of 7.0 and 2.7 were obtained for PS and PA, respectively.

II 4.3 Influence of Non-Linearity and Surface Heterogeneity

At early times, the observed concentrations in water were lower than predicted by the model, in which early concentration changes are dominated by the external mass transfer. The observed difference indicates an unknown rapid sorption process. A potential mechanism could be quick sorption of phenanthrene onto the heterogeneous external surface of the plastic particles, implying that the amount of phenanthrene removed from the aqueous phase by this process would be proportional to the true surface area. As reported in Table II 1, significant errors are expectable if the surface area is calculated rather than measured since the surface roughness of the particles (compare SEM pictures in the SI) has to be considered. Such a rough surface may lead to fast surface adsorption and thus apparent instantaneous sorption was consequently included in the non-linear model, utilized by a fit of the surface absorption coefficient K_{surf}, which quantifies the thickness of a virtual plastic shell undergoing instantaneous sorption. Accounting for K_{surf} results in a better reproduction of the data in comparison to the linear semi-analytical model where instantaneous sorption was not considered. However, the estimated K_{surf} were on the order of 0.1, 0.58, and 0.62 μm for PE, PA, and PS, respectively, indicating that this process although observable in laboratory experiments is most likely negligible under environmental conditions where time scales of interest are much larger than observed in the experiment. Values of the root mean square error (RMSE) [$\mu g\ L^{-1}$] for PE, PA, and PS were 4.3, 4.2, and 1.5 versus 10.7 and

7.9 for the linear and the non-linear model, respectively.

Table II 2: **Results from isotherm and kinetic batch experiments.** For all particles, results from the semi-analytical and the numerical approach are reported. *Freundlich* values for polystyrene (PS) and polyamide (PA) fitted by the kinetic model are written in parentheses. PE = polyethylene, BIC = *Bayesian Information Criterion*, MAE = mean absolute error, RMSE = root mean square error. Reported kinetic data for PS are from simulations with fitted K_{Fr} and n_{Fr}.

Parameter	Polyethylene (PE)	Polystyrene (PS)	Polyamide (PA)
Isotherm experiments			
Partition coefficient (linear) K_D [L kg^{-1}]	15670	12200	16900
Freundlich coefficient K_{Fr} [mg^{1-n} L^n kg^{-1}]	15640	13000 (46000)	17300 (13000)
Freundlich exponent [-]	1.0	0.79 (0.72)	0.84 (0.84)
Affinity coefficient E [kJ mol^{-1}]	*n.a.*	7.5	*n.a.*
PDM exponent [-]	*n.a.*	1.5	*n.a.*
max. sorbed volume V_o [cm^3 kg^{-1}]	*n.a.*	1.3	*n.a.*
BIC linear model	-94.6	-15.7	-31.7
BIC *Freundlich* model	-101.1	-65.9	-110.1
BIC *PDM* model	-97.9	-93.2	-107.0
Kinetic experiments			
MAE linear/non-linear [μg L^{-1}]	2.7/*n.a.*	8.5/5.6	2.7/1.1
RMSE linear/non-linear [μg L^{-1}]	4.3/*n.a.*	10.7/7.9	4.2/1.5
K_{surf} [m]	1.3×10^{-7}	6.2×10^{-7}	5.8×10^{-7}
k_W linear [m s^{-1}]	2.1×10^{-5}	2.1×10^{-5}	1.15×10^{-4}
range, 5-95% quantile	$1.9-2.2\times10^{-5}$	$2.0-2.2\times10^{-5}$	$1.1-1.2\times10^{-4}$
k_W non-linear [m s^{-1}]	*n.a.*	4.3×10^{-5}	1.02×10^{-4}
range, 5-95% quantile		$3.5-5.0\times10^{-5}$	$0.7-1.9\times10^{-4}$
D_P linear [m^2 s^{-1}]	7.5×10^{-14}	4.4×10^{-17}	7.5×10^{-16}
range, 5-95% quantile	$5.0-13.3\times10^{-14}$	$3.9-5.1\times10^{-17}$	$6.3-8.6\times10^{-16}$
D_P non-linear [m^2 s^{-1}]	*n.a.*	7.3×10^{-17}	4.4×10^{-16}
range, 5-95% quantile		$6.0-8.5\times10^{-17}$	$3.2-5.9\times10^{-16}$

Since they are scaled according to the hydrodynamic conditions, the mass transfer coefficients show a high similarity. While film diffusion limits sorption kinetics of PE, intraparticle diffusion coefficients differ significantly among the different plastic materials (see Table II 2). Intraparticle diffusion coefficients estimated for PS and PA with the non-linear model are slightly different from the estimations of the linear model and if instantaneous sorption is not considered. For PS, Li et al. (2017) determined D_P to be 1.4×10^{-17} m^2 s^{-1}, which is still a factor of 5 smaller than our estimated coefficients. However, ranges of one order of magnitude are expected for diffusion coefficients in such diverse materials as PA and PS.

Figures II 2 & II 3 additionally show the apparent distribution coefficients $K_{P,app}(t)$ for both cases (instantaneous *vs.* usual kinetics) as function of time and compared to the data. Such $K_{P,app}$ values are more sensitive than concentration measurements because the latter get very small at late times. The curve of the data points confirms that PE kinetics is limited by film diffusion (linear increase of apparent distribution coefficient with time) whereas PA and PS are controlled by intraparticle diffusion already at early times (increase with the square root of time). For PS, however, Figure 3 indicates that at early times pure film diffusion matches the data best whereas the non-linear model without consideration of instantaneous surface diffusion takes over when approximately 30% equilibration is reached. As illustrated in Figures II 2 & II 3, we needed a combination of film and intraparticle diffusion to explain the PE data, whereas the PS and PA data could only be explained when considering non-linear sorption, film and intraparticle diffusion, and quick adsorption onto the particles. Among all contributions to the kinetics, the slow intraparticle diffusion depends the strongest on the particle material.

To illustrate the effect and importance of the non-linearity of sorption, we simulated the pollutant uptake by PS under infinite bath boundary conditions (where $V_W \rightarrow \infty$) with varying initial concentrations (Figure II 3 C). To be consistent, we used the parameters estimated from the isotherm experiments. We chose particles with a diameter of 250 μm and two initial aqueous concentrations. The non-linearity of the isotherm leads to a strong increase of the apparent partition coefficients at very low concentrations (Figure II 1, PS) which increases the concentration difference between the linear and the non-linear isotherm by a factor of ~ 4.3 and also causes a shift towards film diffusion due to a more accentuated role of external mass transfer. As shown in Figure II 3 C, the non-linear model predicts higher equilibrium uptake at low concentrations and less uptake at high concentrations in comparison to the linear model, and both models deviate in their kinetics prediction. Eventually, the non-linear model predicts a slower uptake at lower concentrations and a faster uptake at higher concentrations. The impact of non-linearity is the highest at the lowest concentrations, which are more frequent in environmental settings than in most laboratory studies. It is also of high relevance for very hydrophobic compounds with very low water solubility, such as PCBs or PBDEs (Diepens & Koelmans, 2018; Lohmann, 2011).

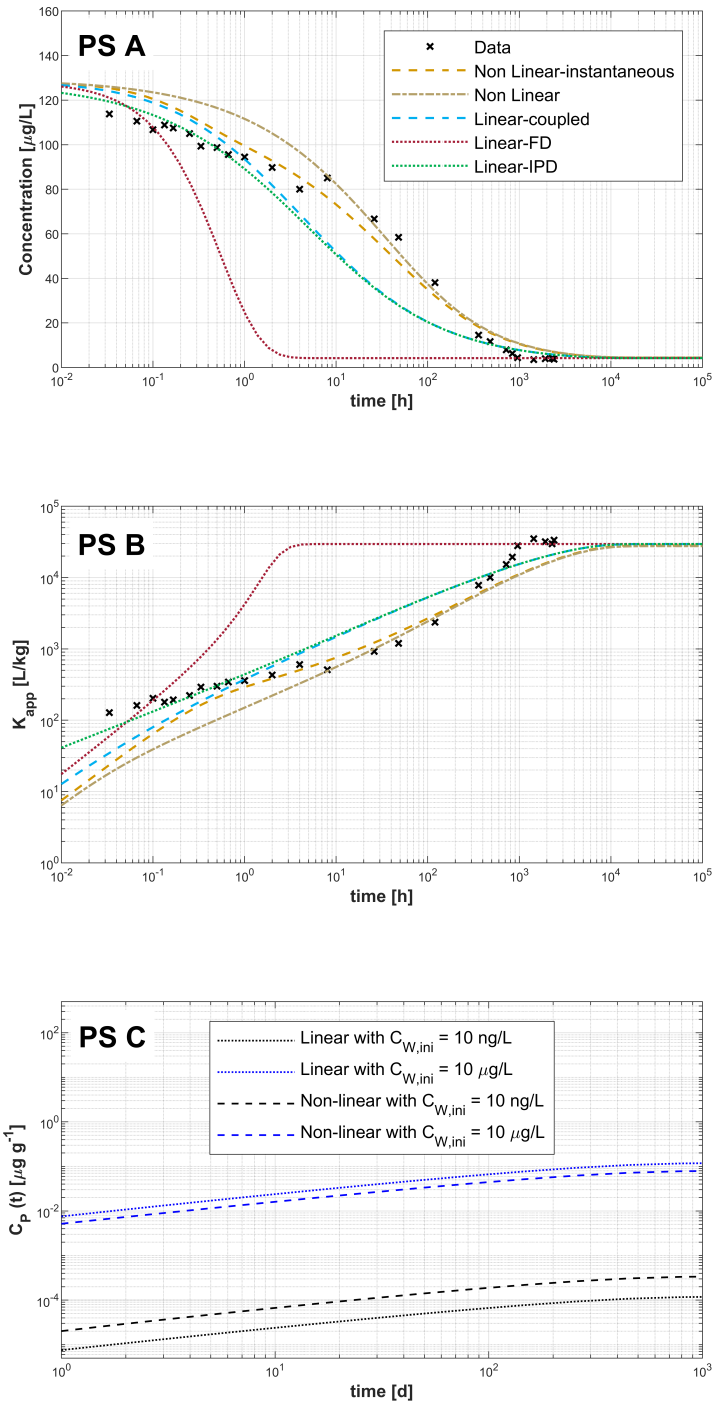

Figure II 3: **Results of the sorption of phenanthrene to polystyrene (PS).** Plot A shows semi-logarithmic plots of water concentrations over time. Plot B shows double-logarithmic plots of apparent partition coefficients over time. The respective denotations are indicated in the legends. FD=film diffusion, IPD=intraparticle diffusion. In plot C the uptake into PS predicted based on linear (dotted lines) and non-linear (*Freundlich*, dashed lines) sorption isotherms at different initial aqueous concentrations under infinite bath boundary conditions with: d_P=250 μm, log $K_D = 4.08$, log $K_{Fr} = 4.11$, $n_{Fr} = 0.79$, $D_P = 7.3 \times 10^{-17}$ m^2 s^{-1}, and $k_W = 6.1 \times 10^{-6}$ m s^{-1} based on the experimental findings and on an empirical *Sherwood* number of 2.

II 4.4 The Role of Microplastics in the Environment

A major question in microplastic-pollutant research is whether a sampled particle in rivers or the ocean reflects the ambient concentration, i.e. it acts as a passive sampler, or whether it acts as a transport vector that releases pollutants into the environment (Gouin et al., 2011; Karapanagioti et al., 2011; Zarfl & Matthies, 2010). The models presented here can be used to address this question. According to Van Sebille et al. (2012), a considerable fraction of particles released at the coast reaches the open ocean after approximately one year, and after ten years the majority has made it to one of the five subtropical maxima, the so-called gyre accumulation zones (Maximenko et al., 2012; Van Sebille et al., 2012). Using our models and corresponding characteristic times, we can calculate the residual fraction of an organic pollutant in the particles as a function of their size and time. We performed our experiments with phenanthrene, but with known physico-chemical properties, the models apply to a wide range of neutral hydrophobic contaminants. According to the general concept, large particle sizes imply large times to release a sorbed compound. Figure II 4 illustrates the time scales needed to reach 20% (A) and 90% (B) of the equilibrium value. These times depend on three parameters: the particle diameter, the material-specific intraparticle diffusion coefficient, and the compound-specific partition coefficient.

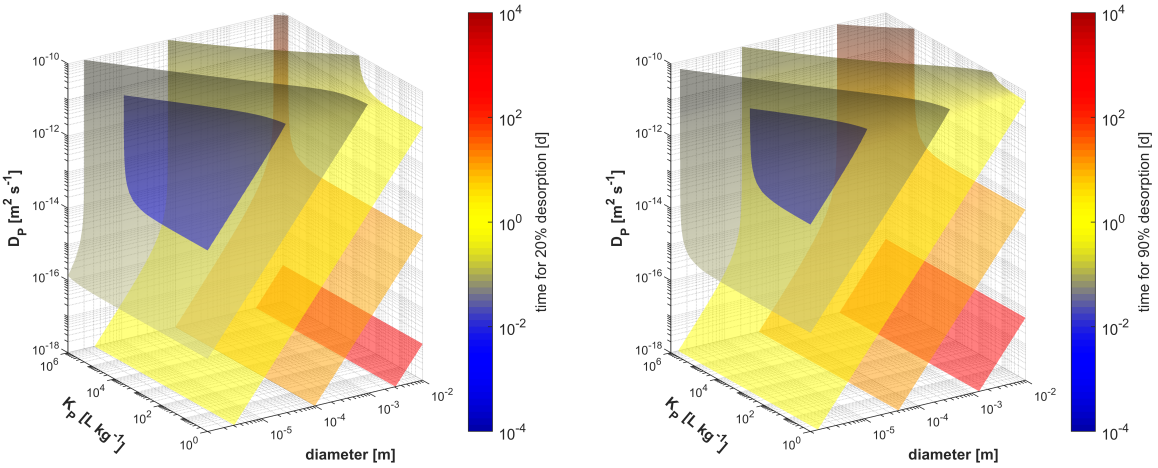

Figure II 4: **Characteristic times to achieve 20% (left) and 90% (right) of equilibration as a function of particle diameter, partition coefficient K_P, and intraparticle diffusion coefficient D_P.** The time is illustrated through coloring and plotted in iso-surfaces, i.e. colored areas which connect identical times. Equilibration is fast for small particles and high intraparticle diffusion coefficients and slow for large particles and small intraparticle diffusion coefficients. The surfaces show the sum of characteristic times for film diffusion and intraparticle diffusion.

To transfer our findings from our experimental to environmental conditions, we calculated the Sherwood number and the external mass transfer according to Ohashi et al. (1981) for single particles in suspension (for details see the SI). In brief, we estimated the mass transfer coefficient by the Sh-relationship of equation II 8. The energy dissipation rates ε in rivers and oceans may differ by one order of magnitude. Here, we used an

intermediate mean value. The characteristic times increase with increasing particle diameter squared and with decreasing intraparticle diffusion coefficients (Figure II 4). Additionally, characteristic times increase with increasing partition coefficient due to an increase of the boundary layer size and thus a deceleration of external mass transfer. However, the changes in the material parameters, i.e. size and intraparticle diffusion, affect the time scales much more than variations in the partition coefficient (Figure II 4). Consequently, plastic particles can act as a vector for contaminants mainly depending on material and size. Small particles equilibrate fast and thus presumably reflect the ambient concentration in water, i.e. they act as a passive sampler (Figure II 4). The potential for long-range transport increases with the particle size squared and decreases with increasing intraparticle diffusion coefficient. Microplastics do not significantly enhance the contaminant concentration which has been already intensively discussed (Koelmans et al., 2016). Nevertheless, the long range transport potential is given and may be important in the risk assessment of plastic associated additives whose input paths differ from those of the common legacy POPs (Kwon et al., 2017). As illustrated in the graphical abstract, we presume, according to estimated time scales, that times which are necessary to achieve 50% equilibration can serve as a tool to distinguish whether particles may act as vector or sampler.

II 5 Implications

Knowledge about sorption mechanisms and desorption kinetics allow properly assessing *ab initio* the potential of long-distance transfer of pollutants by plastic material. If pollutant concentrations get very low non-linearity has to be considered, like in the case of PA or PS. The numerical model developed here allows a detailed evaluation of sorption kinetics under laboratory conditions and can be utilized to predict sorption behavior in the environment. The model can easily be modified to address simple particle shapes differing from spheres (in particular fibers and discs), whereas more complex geometries may require multi-dimensional intraparticle diffusion descriptions. Furthermore, the model offers the opportunity to separately account for external and internal mass transfer in combination with linear and non-linear sorption isotherms and can thus be applied to other types of suspended matter such as carbonaceous particles.

Particles undergo several changes once they have entered the environment, because of UV-light exposure, mechanical stress, and abrasion, among other weathering processes (Andrady, 2017; Brandon et al., 2016). This may cause the fragmentation of particles into smaller pieces which accelerates contaminant release. Our model can be applied to different particle sizes and could thus also be expanded to include the size as a function of time. Nevertheless, breakdown of microplastics under environmental conditions in rivers and oceans is very slow, most likely much slower than the analyzed kinetic mass transfer.

Biofilms may form on the particle which act as an additional resistance and thus slow down the contaminant release (Zhang & Bishop, 1994b). To account for the salt contents of water bodies, the *Setschenow* equation can be used to account for the salting-out effect on partitioning (Schwarzenbach et al., 2005). Additionally, our model

can be extended to consider the presence of other sorbents such as natural organic substances adjusting the partition coefficients, which was done by Seidensticker et al. (2017). Thus, our model can provide an improved and comprehensive understanding of the basic plastic-pollutant-interactions and can be expanded with the respective environmental factors to further assess the function of microplastics as a pollutant transporter under different environmental conditions.

A II
Supporting Information to Paper II

Particle Properties

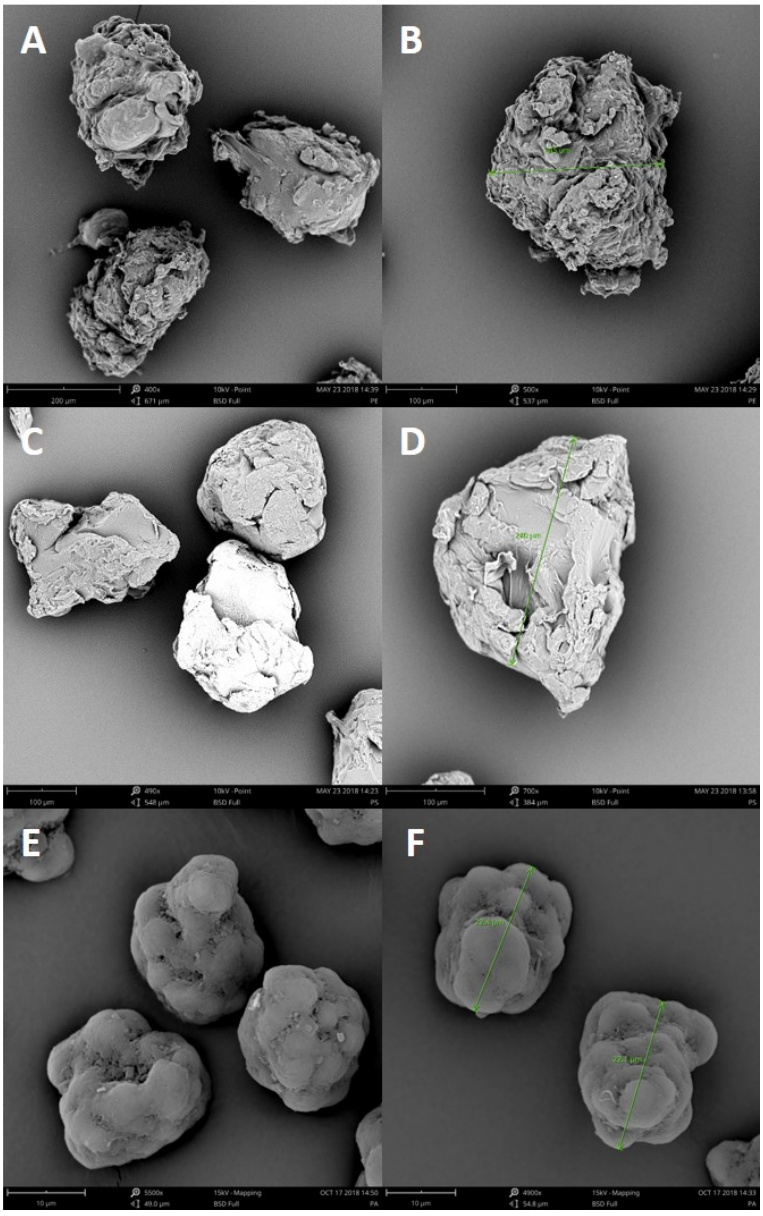

Figure II A1: **SEM images of PE (first row, A and B), PS (second row, C and D), and PA (third row, E and F) particles.** Scales are shown in the images. Labels at the dimension measures are 245 μm (B), 240 μm (D), and 22.4 and 22.1 μm, respectively.

Isotherms

To assess which sorption isotherm model fits best to describe our data, an estimator evaluating the model selection needs to be calculated. As model selection criterion we chose the Bayesian Information Criterion (BIC). This criterion do not just appraise the *goodness-of-fit* but also consider the complexity of the models by contemplating the number of fitted parameters (Schwarz et al., 1978).

$$BIC = -2ln(\hat{\theta}) + ln(n)k \tag{II A1}$$

where $ln(\hat{\theta})$, k, and n as the *log-likelihood*, the number of fitting parameters, and the sample size, respectively. Commonly the maximized *log-likelihood* $ln(\hat{\theta})$ is used to assess the *goodness-of-fit*. Since a $least-square$ fitting routine (implemented as `LSQ-Curvefit` in Matlab) was performed, we applied the relationship between the $ln(\hat{\theta})$ and the *residual sum of squares (RSS)* which reads as:

$$ln(\hat{\theta}) = -\frac{n}{2} ln\left(\frac{RSS}{n}\right) \tag{II A2}$$

with n denoting the sample size (Burnham et al., 2011). Therefore, the *RSS* as a standard fitting procedure output can be used as well to calculate the selection criterion. It holds for the BIC approach (eq. II A1) that a smaller value indicates a preferred model. BICs were calculated for the linear, the *Freundlich*, and the *Polanyi-Dubinin-Manes* (*PDM*) isotherms and are shown in Figures II A2-II A4.

Polyethylene

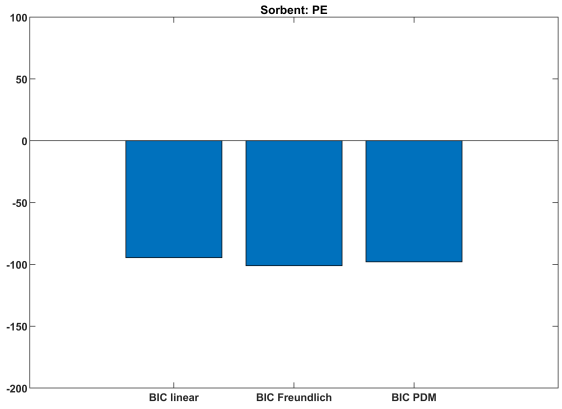

Figure II A2: **BICs of the different isotherms models for sorption of phenanthrene to PE.**

Polyamide

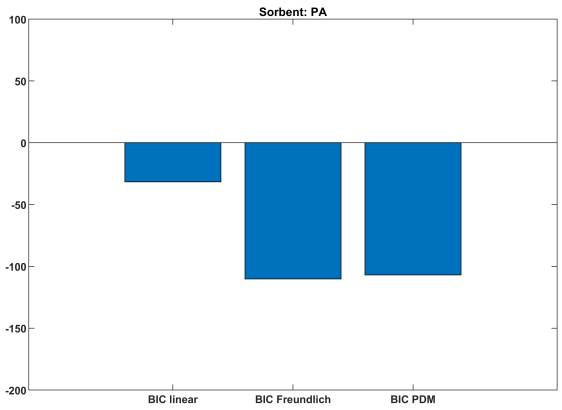

Figure II A3: **BICs of the different isotherms models for sorption of Phenanthrene to PA.**

Polystyrene

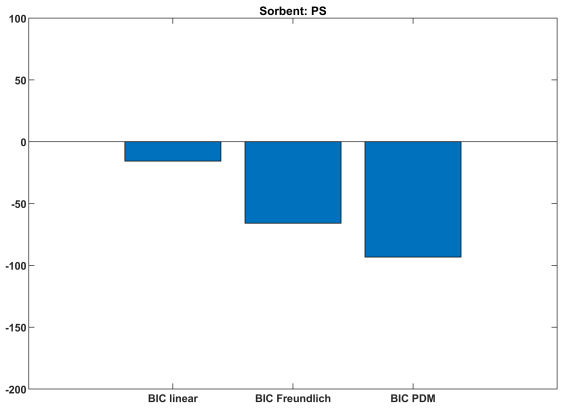

Figure II A4: **BICs of the different isotherms models for sorption of Phenanthrene to PS.**

Linear Model

As specified in the main manuscript, the diffusion equation in spherical coordinates, i.e. Fick's second law, applies to describe diffusive fluxes between a bulk water and plastic particles. Sorption equilibrium between the plastic and water at the surface of the plastic particle, and a concentration gradient of zero in the midpoint of the sphere are assumed as boundary conditions. As initial condition, the concentration in the particle is assumed to be uniform:

$$C_P(r_P,t) = C_{P,eq}\left(C_{W/P}(t)\right)\forall t \quad \text{(II A3)}$$

$$\left.\frac{\partial C_P}{\partial r}\right|_{r=0} = 0\forall t \quad \text{(II A4)}$$

$$C_P(r,t=0) = C_P(0)\forall r \quad \text{(II A5)}$$

in which $C_{P,eq}(C_W)$ [$\mathrm{MM^{-1}}$] is the equilibrium concentration in the plastic for a given aqueous-phase concentration C_W [$\mathrm{ML^{-3}}$], $C_{W/P}(t)$ [$\mathrm{ML^{-3}}$] is the aqueous concentration at the particle surface, r_P [L] denotes the particle radius, and $C_P(0)$ [$\mathrm{MM^{-1}}$] is the initial concentration in the plastic particle. The detailed derivation is reported in the supporting information to Seidensticker et al. (2017).

Numerical Model

The detailed derivation and explanation of the semi-analytical model can be found in the supplementary material to Seidensticker et al. (2017). However, as explained in the main manuscript, the semi-analytical model requires that the governing equations are linear, implying a linear sorption isotherm In case of a non-linear sorption isotherm, a numerical model is necessary. Diffusion within the particles follows the linear diffusion equation in spherical coordinates:

$$\frac{\partial C_P}{\partial t} - D_P\left[\frac{\partial^2 C_P}{\partial r^2} + \frac{2}{r}\frac{\partial C_P}{\partial r}\right] = 0 \quad \text{(II A6)}$$

subject to a uniform initial condition, a zero-gradient condition at the cell center, and a yet to define concentration at the surface of the sphere:

$$C_P(t=0,r) = C_{P,0}\forall r \quad \text{(II A7)}$$

$$\left.\frac{\partial C_P}{\partial r}\right|_{r=0} = 0\forall t \quad \text{(II A8)}$$

$$C_P(t,R) = f_{eq}\left(C_{W,surf}\right)\forall t \quad \text{(II A9)}$$

in which $C_P(t,r)$ [mol/kg] is the mass-related concentration of the compound in the particle, t [s] is time, r [m] denotes the radial coordinate, D_P [$\mathrm{m^2/s}$] is the diffusion

coefficient in the particle, $C_{P,0}$ [mol/kg] is the initial value of C_P, $C_{W,surf}$ [mol/m^3] is the aqueous-phase concentration directly at the surface of the particle, R [m] is the radius of the particles, and $f_{eq}\left(C_{W,surf}\right)$ [mol/kg] is the sorption isotherm.

Assuming that (i) the bulk water is perfectly mixed, (ii) a non-storing water film causing an external mass trans-fer resistance exists around the plastic particles, (iii) the surface of the spheres exhibits sorption sites undergoing instantaneous sorption in the same matter as the respective plastic material, i.e. in linear or non-linear equilibrium with the aqueous concentration, and (iv) the concentration in the plastic and in the water are in nonlinear equilibrium directly at the interface, we can formulate the following additional mass balance equations:

$$\frac{dC_W}{dt} = \left(C_{W/P}(r_P,t) - C_W(t)\right) k_W A_P n_P \quad \text{(II A10)}$$

$$C_W(t=0) = C_{W/P}(t=0) = C_{W,0} \quad \text{(II A11)}$$

$$C_{surf}(t) = K_{surf}\varrho_P C_{P,eq}\left(C_{W/P}(t)\right) \quad \text{(II A12)}$$

in which V_W [m^3] is the volume of water, $k_W = D_W/\delta_W$ [m/s] is the mass-transfer velocity through the aqueous boundary layer with the aqueous diffusion coefficient D_W [m^2/s] and the thickness δ_W [m] of the aqueous boundary layer, $A_P = 4\pi R^2$ [m^2] is the surface area of a single particle, n_P [-] is the total number of particles, K_{surf} [m] is the thickness of a virtual plastic layer instantaneously sorbing the contaminant, and ϱ_P [kg/m^3] is the mass density of the particles. The aqueous concentration at the plastic-water interface is given as $C_{W/P}$ [mol/m^3], the amount of sorbate per surface area as $C_{surf}(t)$ [mol m^{-2}] and the equilibrium concentration in the plastic phase as $C_{P,eq}$ [mol/ kg]. The volume of water and the number of particles can be computed from the bulk volume V_{bulk} [m^3], the total mass of particles m_p [kg], and the mass densityϱ_P and radius R of the particles by:

$$V_W = V_{bulk} - \frac{m_p}{\varrho_P} \quad \text{(II A13)}$$

$$n_P = \frac{m_p}{\varrho_P} \cdot \frac{3}{4\pi R^3} \quad \text{(II A14)}$$

For the intraparticle diffusion, we subdivide the particles into n [−] shells of identical thickness $\Delta r = R/n$as illustrated in Figure II A5 and apply the Finite Volume method.

Numbering the shells from the inside to the outside with cell index i, the discretized total diffusive mass-flux $F_{i\rightarrow i+1}$ [mol/s] at the interface from cell i to cell $i+1$ in a single particle is:

$$F_{i\rightarrow i+1} = 4\pi(i\Delta r)^2 \frac{D_P}{\Delta r}\left(C_{p_i} - C_{p_{i+1}}\right) \quad \text{(II A15)}$$

in which C_{p_i} [mol/kg] is the concentration in shell i, and we have considered the surface area of shell i.

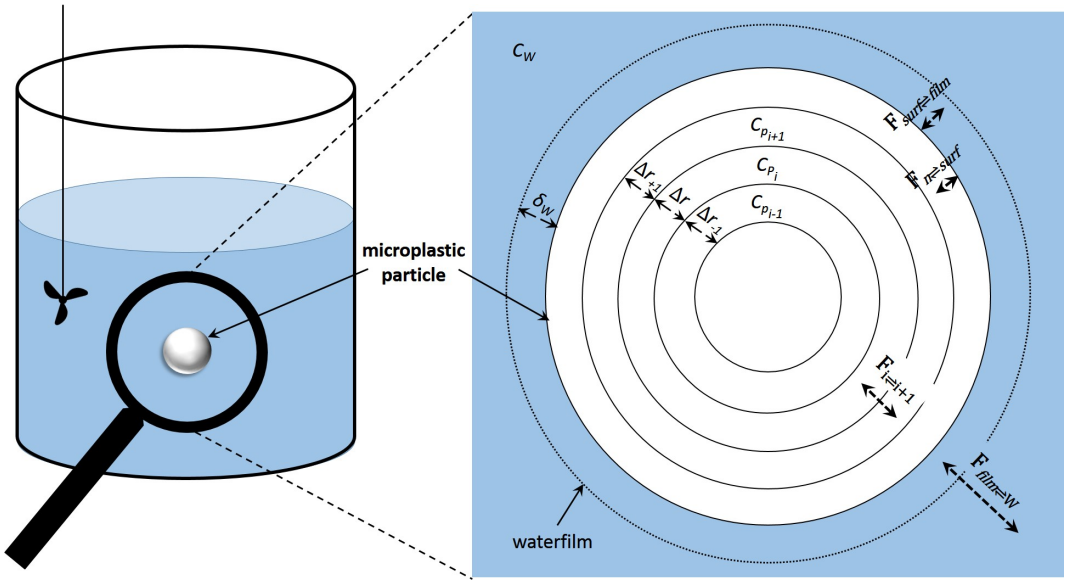

Figure II A5: **Scheme of the conceptual framework of the numerical model.** Not to scale.

For the outermost shell, the diffusive distance is half as big, and the outside concentration is the surface concentration on the plastic side of the particle, resulting in:

$$F_{n\to n+1} = F_{n\to surf} = 4\pi R^2 \left.\frac{\partial C_P}{\partial r}\right|_{r=R} D_P = 4\pi R^2 \frac{2D_P}{\Delta r}\left(C_{p_n} - f_{eq}\left(C_{W,surf}\right)\right) \quad \text{(II A16)}$$

whereas the total flux at the inside of the inner-most shell is zero:

$$F_{0\to 1} = 0 \quad \text{(II A17)}$$

Finally, we have to consider the volume of shell i in a single particle:

$$V_{P.i} = \frac{4}{3}\pi \Delta r^3 \left(i^3 - (i-1)^3\right) = \frac{4}{3}\pi \Delta r^3 \left(3i^2 - 3i + 1\right) \quad \text{(II A18)}$$

Then, the mass balance for shell i reads as:

$$\frac{dC_{p_i}}{dt} = \frac{1}{V_{P.i}}\left(F_{n-1\to n} - F_{n\to n+1}\right) \quad \text{(II A19)}$$

Equations II A10, II A12 & II A19 (together with the other equations defining the terms) form the system of $n+2$ nonlinear ordinary equations solved with backward-differentiation formulas implemented in the matlab function `ode15s`.

System Sorption

The loss of phenanthrene to the batch system, i.e. the sorption by the system, was estimated by using a batch setup with the materials (e.g. glass bottle, glass stir bar, etc.) but without plastic particles. The initial concentration of phenanthrene in that setup was 266 μg L^{-1}, measured by GC-MS as described in the main manuscript. Samples were taken after various time points with the latest after 264 h. As it can be seen from Figure II A6, the loss of phenanthrene to the system does not show any trend over time but varies around $C_{W,ini}$ with a maximum deviation of 1.7%.

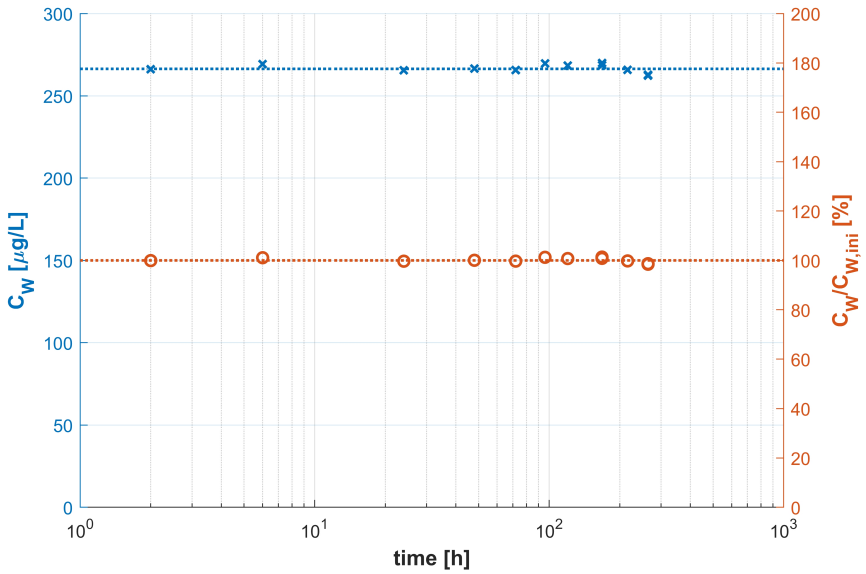

Figure II A6: **Concentration-time series of the system sorption batch.** Concentrations of phenanthrene are plotted on the left y-axis with $C_{W,ini}$ as dashed blue line. Values of the percentage deviation of $C_W(t)$ from $C_{W,ini}$ at the respective times are plotted to the right y-axis.

Experimental Data

Table II A1: **Sampling time points and aqueous phenanthrene concentrations from the kinetic batch experiments for the three tested plastic types.**

time	measured concentration		
	PE	PA	PS
[min]	[μg L^{-1}]		
initial	106.3	118.5	128.3
2	89.5	42.1	113.8
4	85.3		110.6
6	83.4	33.4	106.7
8	83.4	31.6	108.8
10	80.9	29.8	107.5
15	76.6	28.0	105.0
20	63.7	28.0	99.4
30	51.5	21.1	98.7
40	39.6	23.4	95.6
60	26.0	18.2	94.4
120	15.4	15.6	89.7
240	8.9	14.2	80.0
480	7.1	13.5	85.0
[days]			
1	6.7	11.6	66.7
2	6.7	10.8	58.5
4		10.6	
5	6.4		38.1
7		11.2	
15		10.7	14.6
20			11.6
30			7.9
35			6.3
40			4.4
80			3.9
95			4.2

Parameter Estimation

For the numerical model the mass transfer coefficient k_W and the intraparticle diffusion coefficient D_P were fitting parameters. Fitting for both models was performed as described in the main manuscript with DREAM(ZS) (Laloy & Vrugt, 2012; Vrugt, 2016), which is a Markov chain Monte Carlo method, resulting in a posterior distribution of the log-parameters. We used three chains with 10,000 generations. The initial distribution of the log-parameters was uniform within given bounds (see Table II A2) chosen lay outside of the range of the posterior distribution. The $\hat{R}^d$-statistics of all three chains reached the critical value ≤ 1.2 within 3,000 generations. The first 9,000 generations were considered as burn-in, and only the last 1,000 accepted log-parameter combinations were further analyzed.

Table II A2: **Prior parameter ranges for the linear and the non-linear model.**

parameter	unit of non-logarithmic parameter	material	minimum	maximum
linear model				
$\ln\left(k_W/D_{aq}^{2/3}\right)$	$(s\ m)^{-1/3}$	PE	-5	10
		PA	4.9	5.0
		PS	3.1	3.3
$\ln(D_P)$	$m^2\ s^{-1}$	PE	-40	0
		PA	-40	0
		PS	-40	0
non-linear model				
$\log(k_W)$	$m\ s^{-1}$	PE	-7	-3
		PA	-4.2	-3.7
		PS	-5.0	-4.3
$\log(D_P)$	$m^2\ s^{-1}$	PE	-20	-10
		PA	-20	-10
		PS	-20	-10
$\log\left(K_{surf}\right)$	m	PE	-9	-3
		PA	-9	-3
		PS	-9	-3
$\log(n_{Fr})$	-	PA	-0.08	-0.07
		PS	-0.3	0

Posterior log-Distributions of Fitting Parameters with Instantaneous Sorption

Polyethylene

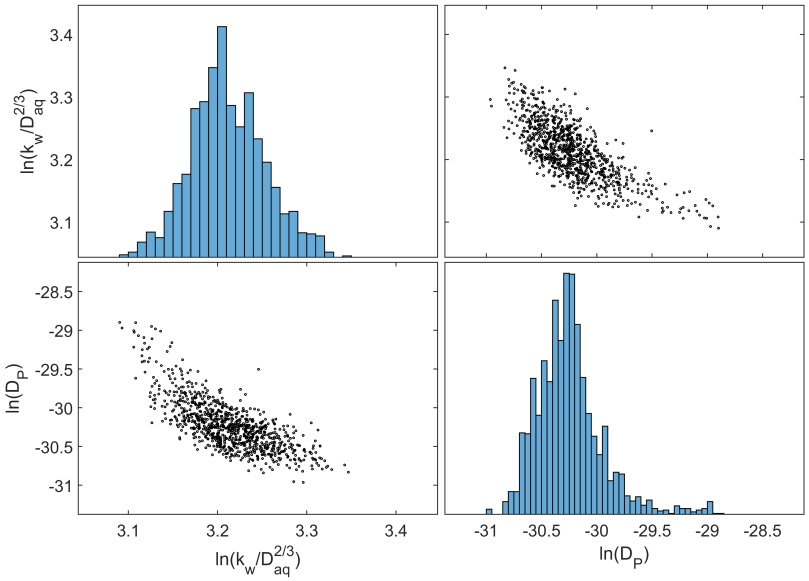

Figure II A7: **Scatter plot and histograms of the posterior log-parameter distribution (3,000 ensemble members) for the fit of the linear model.**

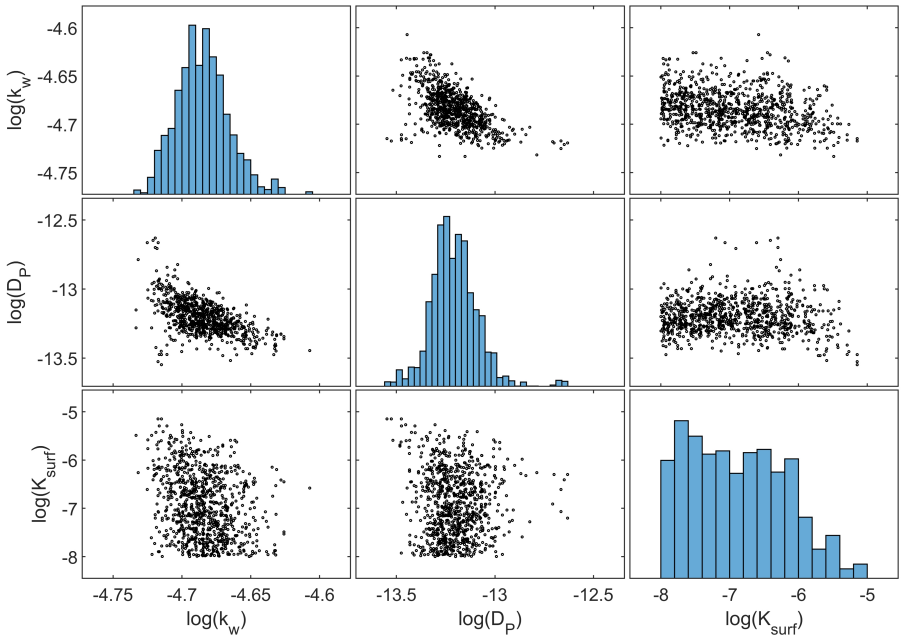

Figure II A8: **Scatter plot and histograms of the posterior log-parameter distribution (3,000 ensemble members) for the fit of the non-linear model.**

Polyamide

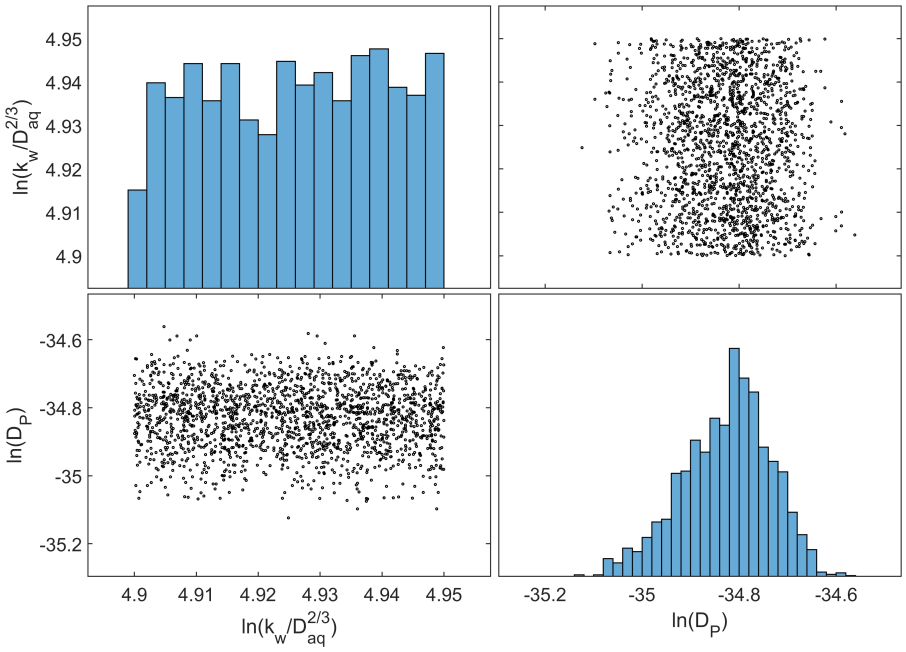

Figure II A9: **Scatter plot and histograms of the posterior log-parameter distribution (3,000 ensemble members) for the fit of the linear model.**

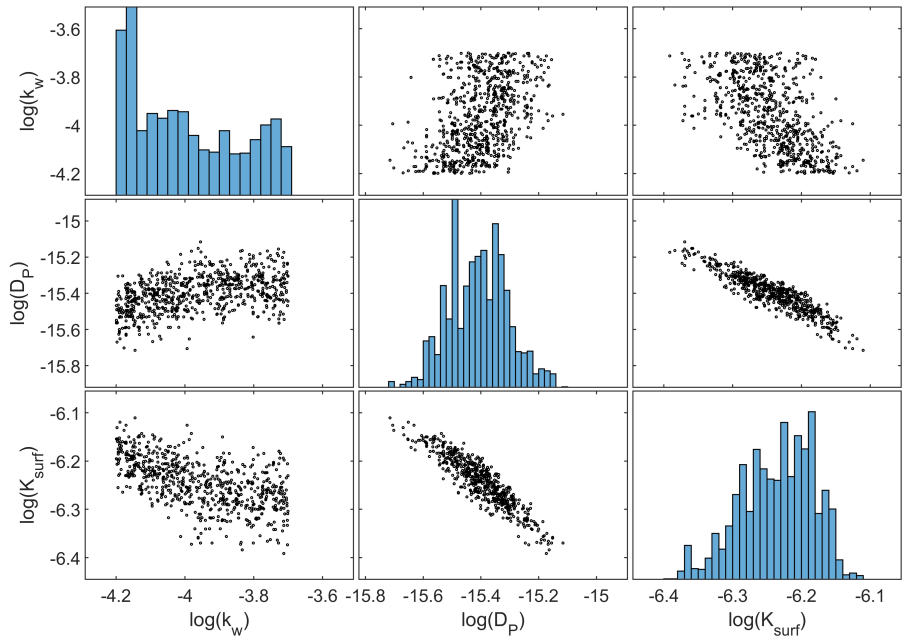

Figure II A10: **Scatter plot and histograms of the posterior log-parameter distribution (3,000 ensemble members) for the fit of the non-linear model.**

Results of the posterior log-parameter distribution for the case that the *Freundlich* exponent n is included in the fit.

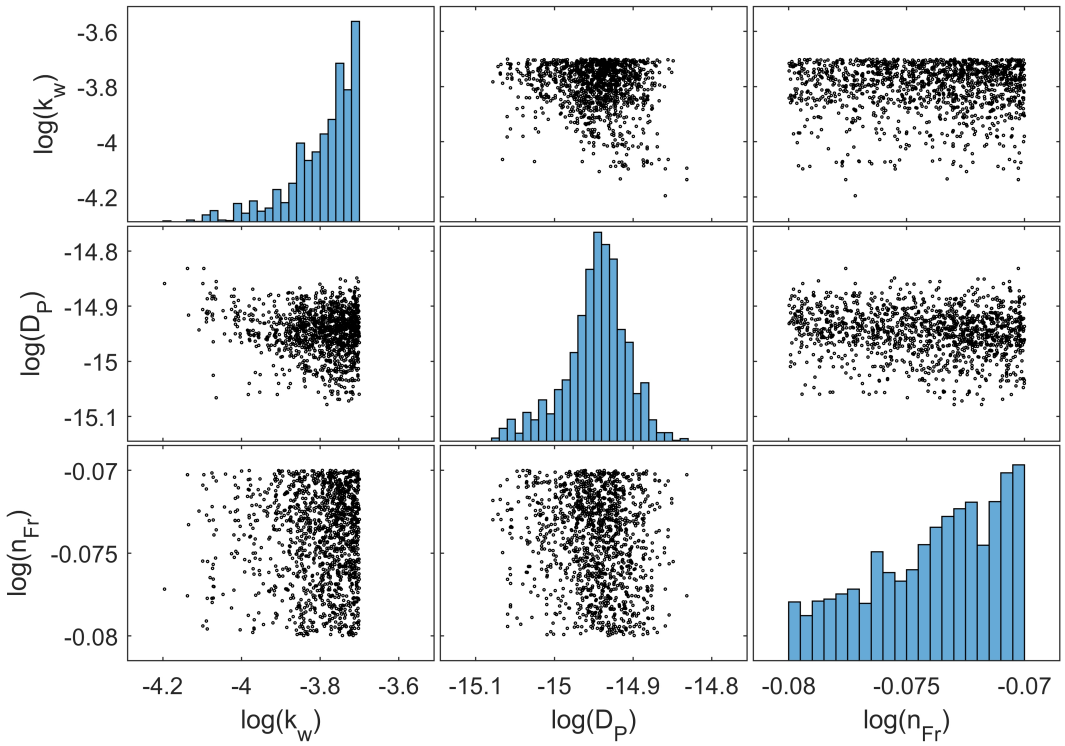

Figure II A11: **Scatter plot and histograms of the posterior log-parameter distribution (3,000 ensemble members) for the fit of the non-linear model with the *Freundlich* exponent included in the fit.**

Polystyrene

Results of the posterior log-parameter distribution for the case that the *Freundlich* exponent is not included in the fit.

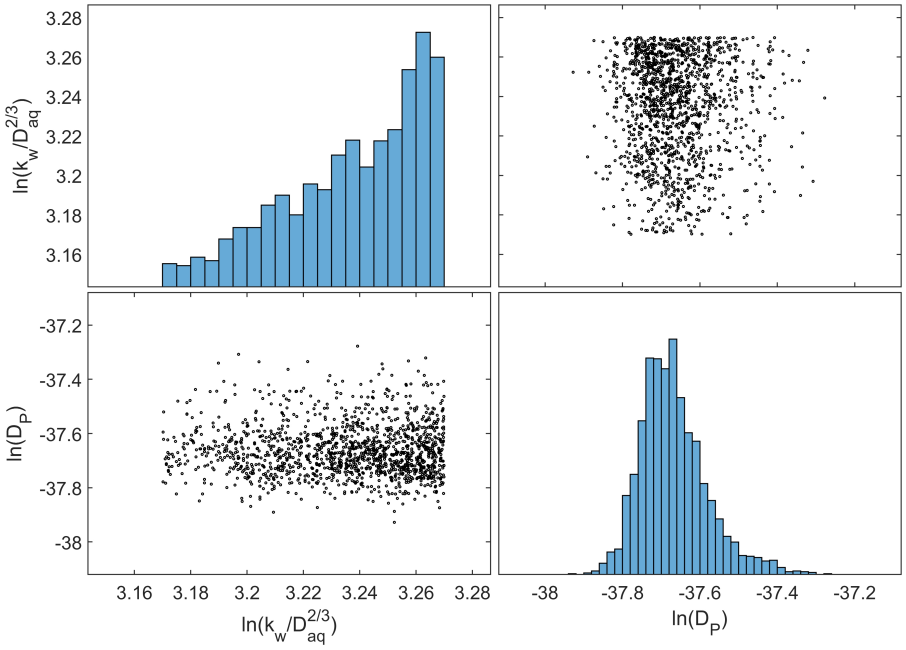

Figure II A12: **Scatter plot and histograms of the posterior log-parameter distribution (3,000 ensemble members) for the fit of the linear model.**

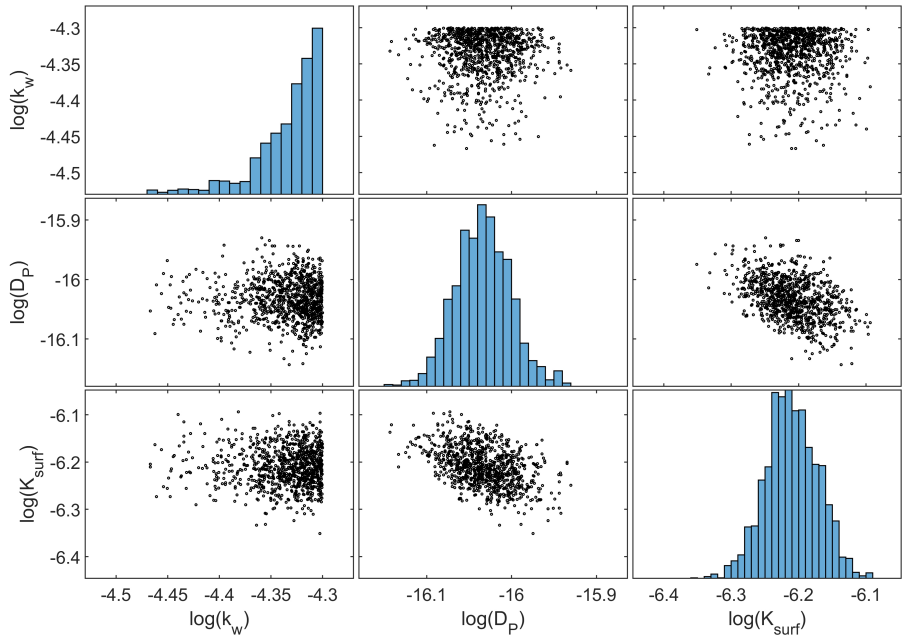

Figure II A13: **Scatter plot and histograms of the posterior log-parameter distribution (3,000 ensemble members) for the fit of the non-linear model.**

Results of the posterior log-parameter distribution for the case that the *Freundlich* exponent n is included in the fit.

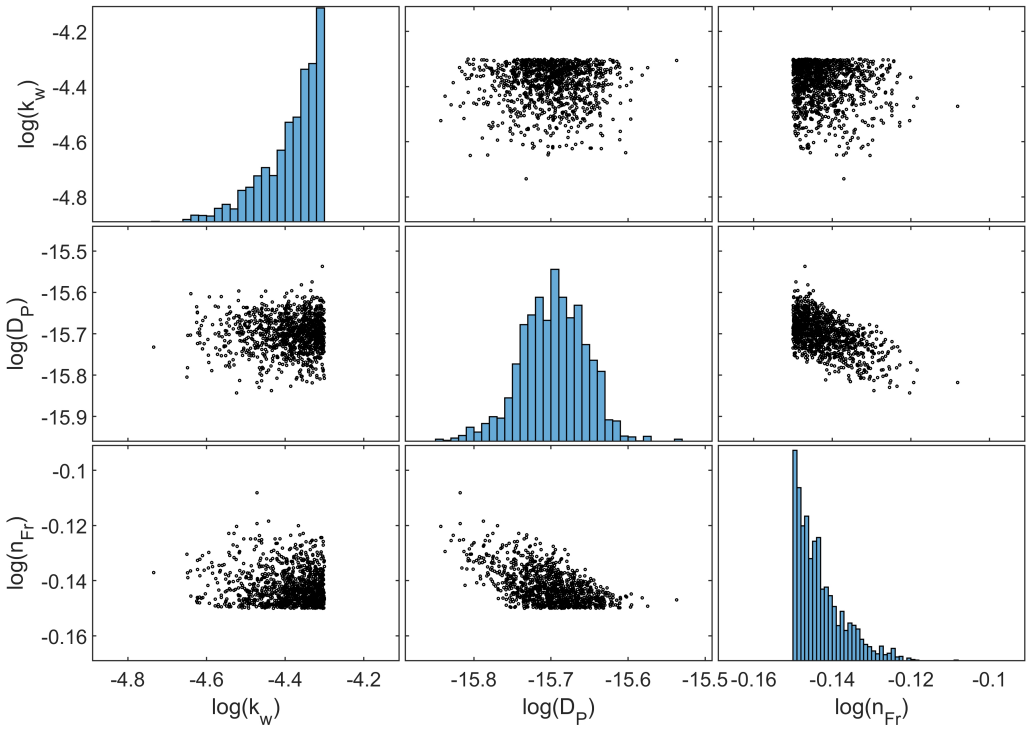

Figure II A14: **Scatter plot and histograms of the posterior log-parameter distribution (3,000 ensemble members) for the fit of the non-linear model with the *Freundlich* exponent included in the fit.**

Hydrodynamics

Certain Sherwood relationships can be used to transfer our lab findings to field settings where, due to its dependence on hydrodynamic conditions, the film diffusion may be different from our experimental settings. One important parameter is the turbulent kinetic energy dissipation rate ϵ which is between $10^{-5} - 10^{-6} m^2 s^{-3}$ for rivers (Chickadel et al. (2011), Fisher et al. (2002), MacDonald et al. (2007)) and approximately one order of magnitude lower for near surface water in the ocean (Moum et al., 1995). With known particle properties and energy dissipation rates, the particles Stokes number St which characterizes their behaviour in a carrier fluid can be calculated as:

$$St = \frac{\tau_P}{\tau_f} = \frac{\frac{1}{18}\frac{\rho_P}{\rho_W}\frac{d_P^2}{\nu}}{\sqrt{\nu\epsilon^{-1}}} \tag{II A20}$$

where τ_P and τ_f are the relaxation times of the particles with ρ_P and d_P as the particles density and diameter, and the dissipation time of the carrier fluid turbulence dissipation with ν as the kinematic viscosity of water, respectively (Sumbekova et al., 2017). With ϵ set to $10^{-5.5}$and 10^{-7} for river and ocean settings, respectively, St for all types of our particles were $\ll 1$ indicating a slip velocity close to unity and thus the particles may follow the current as it would be expected from their density.

For our experimental setup we fitted ϵ based on the specific power group, which is $\epsilon^{1/3} d_P^{4/3} \nu^{-1}$ where d_P is the particle diameter and ν is the kinematic viscosity of water (Ohashi et al., 1981). The specific power group is strongly related with the particles Reynolds number Re_P. For particles which follow the Stokes regime, the correlation is:

$$\epsilon^{1/3} d_P^{4/3} \nu^{-1} = 1.36 Re_P^{2/3} \tag{II A21}$$

As outlined in the main manuscript, PE is sensitive to film diffusion and therefore we can calculate our experimental ϵ based on the Sherwood number calculated for PE, i.e. 7.05, and the empirical relationship obtained by Ohashi et al. (1981):

$$Sh = 2 + 0.59 \left(\frac{\epsilon^{1/3} d_P^{4/3}}{\nu} \right)^{0.57} Sc^{1/3} \tag{II A22}$$

For our experimental setup we obtain an ϵ of $10^{-4.2}$ which is in the lower range of typical energy dissipation rates (Ohashi et al., 1981). The Schmidt number Sc is 1318. Finally one can calculate the particles Sherwood number for the two aforementioned environmental settings using the same empirical relationship.

Characteristic Times

As explained in the main manuscript, characteristic times can be used to estimate sorption-desorption time scales in dependence of the plastic material and the particle size.

Film Diffusion

Due to the similar experimental conditions, the same relationship applies for all particles and sorption kinetics. Transfer to environmental settings can be made via ϵ. As Sh is now known for the experimental setup and the two different model scenarios, the mass transfer coefficient k_w can be calculated as described in the main manuscript based on the relationship, that $Sh = (k_w d_P) D_{aq}^{-1}$. With known k_w the characteristic times for 20% and 90% desorption due to external mass transfer for our experiment and under infinite bath boundary conditions can be estimated from:

$$finitebath \quad ln(1-x) = \frac{y}{\frac{d_P K_P \rho_P}{6k_w}\left(1 + K_P \frac{m_P}{V_W}\right)} \tag{II A23}$$

$$infinitebath \quad ln(1-x) = y\frac{d_P K_P \rho_P}{6k_w} \tag{II A24}$$

where x denotes the released fraction and y denotes a mass release-dependent constant which is 0.223 and 2.3 for 20% and 90% desorption, respectively. K_P, ρ_P, and d_P are the partition coefficient, density, and diameter of the plastic, respectively. In Figure II A15 the relationships between Sh, k_w, and the particle diameter for the two model scenarios is shown. Note, that the minimum possible Sh is two (Ranz et al., 1952) due to mass balance. Since Sh and k_w are solely dependent on the hydrodynamic conditions (represented by Re_P or the specific power group) and Sc, theses parameters are equal for the three tested plastic particle types and independent on their properties and partitioning characteristics (Sherwood & Ryan (1959), Harriott (1962)).

Intraparticle Diffusion

The characteristic time required to remove 20% and 90% of the initial contaminant load can be calculated based on the approximations of intraparticle diffusion that are described in detail in Grathwohl (2012). Intraparticle diffusion in general can be expressed as:

$$\frac{M}{M_{eq}} = 1 - exp\left[-ln\left(\frac{6}{\pi^2}\sum_{n=1}^{\infty}\frac{1}{n^2}exp\left[-n^2\pi^2 t\frac{D_P}{r^2}\right]\right)t\right] \tag{II A25}$$

However, for short and long terms, certain approximations can be utilized. For long terms equation II A25 yields:

$$\frac{M}{M_{eq}} = 1 - exp\left[\left[-\frac{ln\left(\frac{6}{\pi^2}\right)}{t} + \pi^2\frac{D_P}{r^2}\right]t\right] \tag{II A26}$$

Now, this can be solved for certain M/M_{eq} ratios for long terms, i.e. if equilibrium is approached. For instance, if $M/M_{eq} = 0.9$ we yield:

$$t_{90} = \frac{r^2}{5.5D_P} \tag{II A27}$$

For short terms, however, another approximation has to be applied where M/M_{eq} becomes:

$$\frac{M}{M_{eq}} = 1 - exp\left[\left[\frac{-ln\left(1 - 6\sqrt{\frac{D_P t}{r^2\pi}}\right)}{t}\right]t\right] \tag{II A28}$$

Solving this for an unknown t where $M/M_{eq} = 0.2$, we end up with

$$t_{20} = \frac{r^2}{286D_P} \tag{II A29}$$

Such considerations and approximations are extensively discussed, e.g. in Ball & Roberts (1991) and Grathwohl (2012). These characteristic times can be used to analyze whether the kinetics at the certain time and for a particle with a particular size, is limited by film diffusion or intraparticle diffusion. Examples with characteristic times for 20% and 90% equilibration as a function of material properties, i.e. intraparticle diffusion coefficients, and particle diameter are shown in Figure II A16. The experimentally determined partition coefficients for the three different polymers were used as reported in Table 2 in the main manuscript.

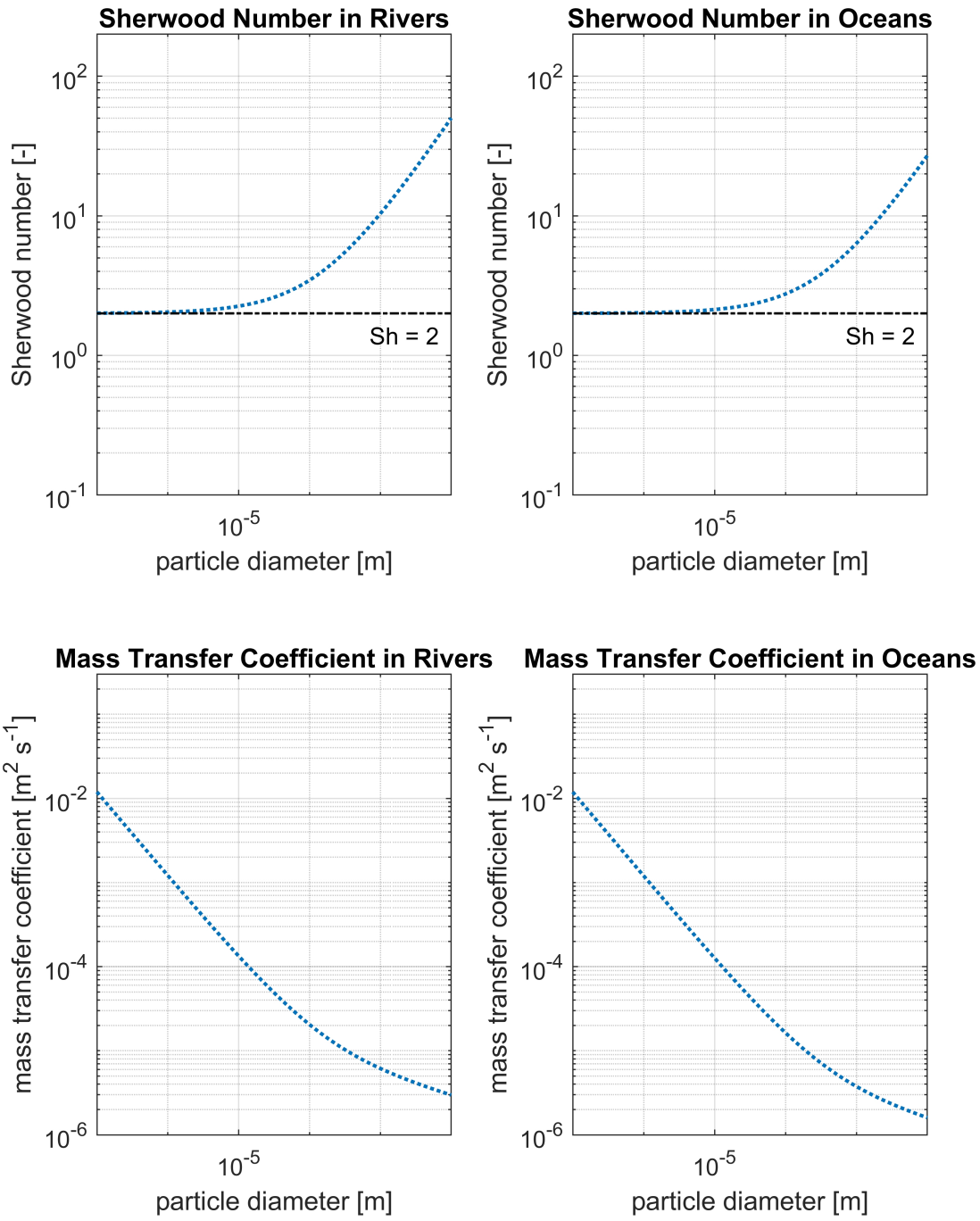

Figure II A15: **Sherwood numbers and mass transfer coefficients in rivers and oceans as a function of the particle diameter.** Both are equal for the three tested types of plastics as they are independent on the particle properties and partition coefficients.

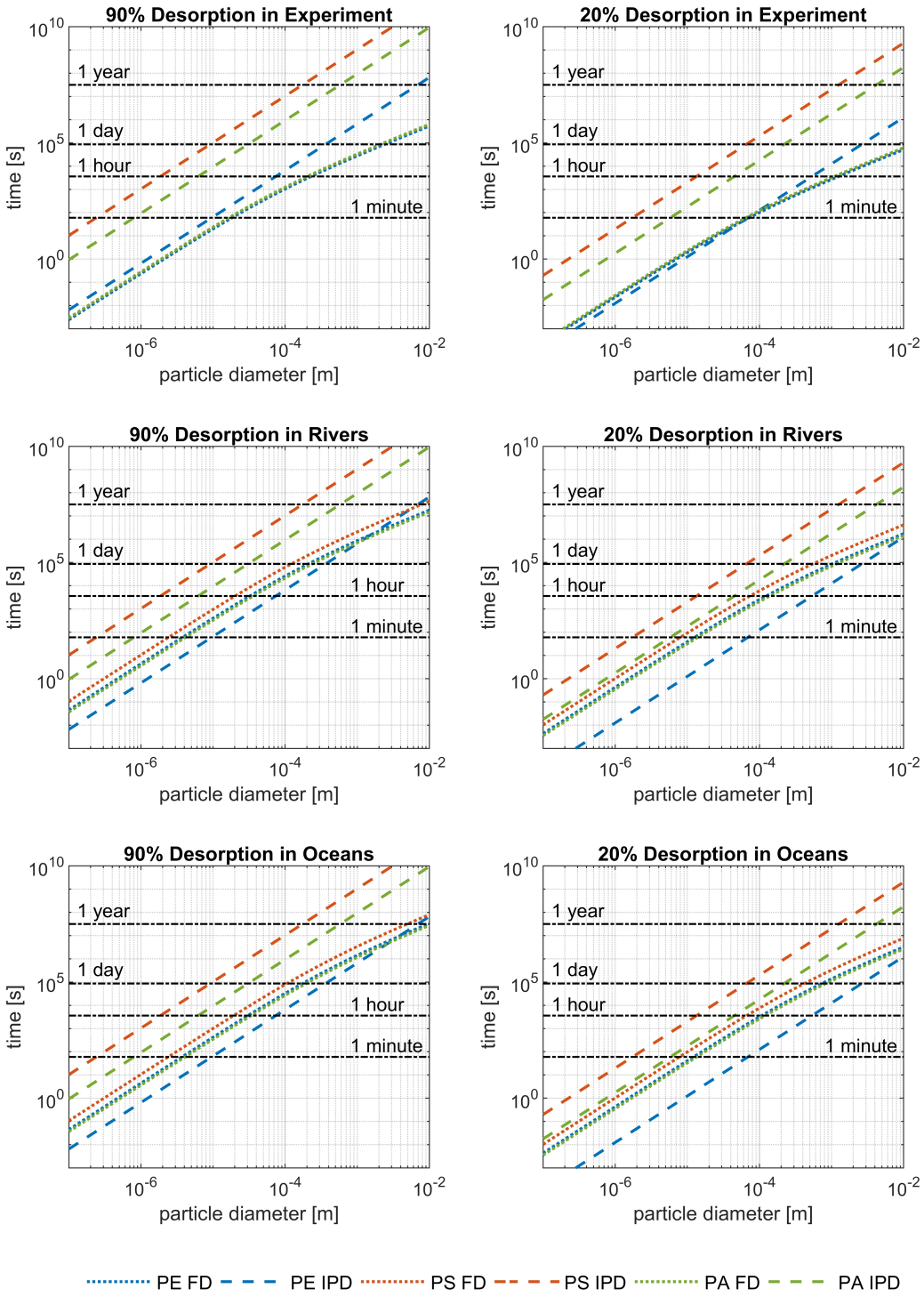

Figure II A16: **Characteristic times for 90% (left panel) and 20% (right panel) of initial mass desorption under experimental conditions, and in rivers and oceans, respectively, as a function of particle diameter and material (PE, PA, PS).** Calculations are outlined above. The total characteristic time for a particular polymer would be the sum of the two displayed curves. Equilibrium partition coefficients are reported in Table II 2 in the main manuscript. FD = film diffusion, IPD = intraparticle diffusion.

Paper III
A Combined Experimental and Modeling Study to Evaluate pH-dependent Sorption of Polar and Non-Polar Compounds to Polyethylene and Polystyrene Microplastics

Abstract

The contamination of aquatic ecosystems with both anthropogenic pollutants and particles in particular (microscopic) plastic debris items is of emerging concern. Since plastic particles can accumulate contaminants and potentially facilitate their transport it is important to properly investigate sorption mechanisms. This is especially required for a large variety of chemicals that can be charged under environmental conditions and for which interactions with particles may hence go beyond mere partitioning. In this study sorption experiments with two types of microplastic particles (polyethylene and polystyrene) and 19 different contaminants (pesticides, pharmaceuticals, and personal care products) were performed at three different pH values. We could show that sorption to plastic particles is stronger for hydrophobic compounds and that neutral species usually contribute more to the overall sorption. Bulk partitioning coefficients were in the same order of magnitude for both types of plastics. Furthermore, our results confirm that partition coefficients for polar compounds can only be accurately determined if the solid-to-liquid ratio in batch experiments is more than six to seven orders of magnitude higher than any plastic concentration detected in the environment. Consequently only a minor fractions of pollutants in water bodies is associated with microplastics. Although neutral species primarily dominate the overall sorption, contribution of ionic species cannot be neglected for some compounds. Whereas for the major fraction of contaminants sorption was driven by partitioning, further mechanisms such as e.g. electrostatic interactions may play a role under environmental settings. Notwithstanding, our results show that since microplastics concentrations as currently observed in the environment plastic particles are very low they are only a relevant sorbent for strongly hydrophobic compounds.

III 1 Introduction & Background

Chemical pollution is of emerging concern and has even been considered to be a planetary boundary threat (Diamond et al., 2015; Rockström et al., 2009). In addition, contamination with anthropogenic litter such as microplastics raises public concern (Barnes et al., 2009; Horton et al., 2017; Mani et al., 2015). Since in freshwaters pollutants distribute between the freely dissolved water phase and natural but also anthropogenic particles, microplastics may be an additional vector for spreading pollutants (Koelmans et al., 2016). Therefore, one important aspect is to assess the impact of particle-bound contaminants. Since transport of particles and associated contaminants, i.e. for particle-facilitated transport, is different compared to purely dissolved chemicals (Barber et al., 2006), sorption/desorption kinetics and thus particle properties such as density, shape, material, and size are decisive. Sorbed contaminants are less available for biodegradation and may therefore be transported further than chemicals freely available in the aqueous phase that are more easily prone to transformation processes (Alexander, 2000; Forbes et al., 1998). Furthermore, determined partition coefficients can serve for an improved understanding of sorption processes and hence a deepened risk assessment of sorbed contaminants. For compounds with slow desorption kinetics, i.e. with high partition coefficients (Seidensticker et al., 2017), microplastics may act as transport vectors, whereas they act as passive samplers and reflect the ambient concentration of the organic pollutants in the environment as soon as sorption equilibrium is reached. In both cases, partition coefficients are crucial to calculate i) characteristic times for contaminant release and ii) the ambient concentration (e.g. in the water) at the sampling location. Kinetics and impact of partition coefficients are thoroughly discussed in Seidensticker et al. (2017). In freshwater systems, one major path for microplastics to enter rivers is via the effluent of wastewater treatment plants where large numbers of particles have been observed (Mintenig et al., 2017; Murphy et al., 2016). In such effluents however, also high concentrations of micropollutants such as pharmaceuticals and pesticides occur (Gasperi et al., 2008; Gavrilescu et al., 2015; Li et al., 2016; Schwarzenbach et al., 2006). Therefore, plastic particles might especially act as a sorbent and potential transporter for frequently occurring wastewater contaminants and are hence a factor that needs to be considered if the environmental fate of micropollutants is examined.

Depending on their physico-chemical properties, many pollutants dissociate under certain pH conditions and hence their fate and behavior in the environment is strongly influenced by changes in the pH (Bundschuh et al., 2016; Karlsson et al., 2017). Among these ionizing chemicals are pesticides, flame-retardants, but also pharmaceuticals and further household chemicals like detergents. From studies with natural particles and sediments it is known that sorption interaction mostly takes place between sorbents and neutral species and that charged compounds sorb only little or not at all (Fu et al., 2009; Karlsson et al., 2017). Unlike many natural particles, microplastics can be charged electrostatically (Wang et al., 2015; Yokota et al., 2017). Therefore, the uptake of ionizable substances theoretically might not only determined by mere partitioning between microplastic particles and the neutral species but also by possible ionic bounds.

Sorption interactions between charged species and different types of microplastics have not been extensively studied so far. Thus, the aim of our study was to clarify the sorption behavior to microplastics in freshwater under varying pH of five neutral substances (as control) and a set of 14 selected ionizable compounds including pesticides and insecticides, but also pharmaceuticals, detergents and flame retardants that represent trace pollutants emitted via the wastewater treatment plant. Pristine polyethylene and polystyrene particles were used since in the wastewater canalization system "young" particles occur and enter the WWTP where they get in contact with various (emerging) contaminants such as pharmaceuticals and personal care products which we used in this study. Both plastic types are among the most abundant in WWTP (as reported e.g. Mintenig et al. (2017) and Murphy et al. (2016).

III 2 Materials & Methods

In total, 19 different chemicals were tested for their sorption interactions with different microplastics. These chemicals include seven bases with dissociation constants (pK_a) ranging from 1.09 to 8.37, eight acids covering pK_a values of 3.13 to 13.9 and four neutral substances. Details on the physico-chemical properties of these compounds are listed in Table III 1.

All chemicals except phenanthrene were purchased from LGC standards (Wesel, Germany). The latter was purchased from Sigma-Aldrich Supelco (Bellefonte, PA, USA).

Polyethylene (PE) and polystyrene (PS) were used as representative types of microplastics and were purchased from Azelis (trade name Gotalene 120, Moers, Germany) and Goodfellow Cambridge Ltd. (Huntingdon, UK), respectively. Sizes of polyethylene and polystyrene microparticles were given by the supplier (uniform size distribution with mean sizes of 260 μm and 250 μm, respectively) and confirmed by visual inspection under SEM (see images in the supporting information). Particles with comparable sizes were chosen to better compare sorption mechanisms and to exclude huge differences due to size effects. Further, N_2-BET surface areas were measured and revealed that PE is non-porous while PS is mesoporous with an average pore size of 195 Å. According to Pascall et al. (2005) glass transition temperatures T_g of polyethylene and polystyrene are in the range of -120 $°C$ and 100 $°C$, respectively.

III 2.1 Batch Experiments

To study equilibrium partitioning of charged and non-charged compounds, we performed batch experiments with ultrapure water (electric conductance of 0.057 $\mu S cm^{-1}$ and microplastic particles at three different pH levels (4, 7, and 10) and the mix of selected substances. For all compounds, initial concentrations in the water phase were around 5 $\mu g L^{-1}$ except for phenanthrene and 4*n*-nonylphenol. Due their high hydrophobicity, these two substances were expected to sorb very strongly. Therefore, initial concentrations were 50 $\mu g L^{-1}$ and 30 $\mu g L^{-1}$, respectively, to avoid aqueous concentrations below the detection limit. Initial concentrations of all substances were below 1 % of their water solubility to avoid competitive sorption. The batches were spiked from an

aqueous contaminant solution to avoid co-solvent effects of organic solvents. Either formic acid or ammoniac were used to adjust the pH in the batches. For preparing the neutral solution, 0.02 M Na_2PO_4 (Rotifair, Carl Roth) was used. For each pH, the solutions were prepared in one glass vessel before they were distributed into the single batches. During the experiments, frequent pH measurements were performed to control the stability. All experiments were prepared in ultrapure water and performed in amber glass bottles to avoid biodegradation and photo-oxidation. Blanks were included to confirm that neither biodegradation nor sorption to glass walls or seals etc. take place. The liquid-to-solid ratio in the batches was 0.001 kgL^{-1}, namely 100 mg of microplastics in 100 mL of solution. Batch experiments for each pH were performed in triplicates and samples of 2×1 mL were taken at the beginning (t=0) to quantify the actual initial concentration. Further samples were taken after two, four, seven, and eleven (only for PS) days to measure the overall partitioning of the substances and to ensure that equilibrium was reached within the batches. Samples were taken from completely independent batches, and all samples were considered to take outliers into account as well. For detailed studies on kinetics and conformation of fast equilibration see Seidensticker et al. (2017). The bottles were constantly shaken on a horizontal shaker with a rotational speed of 150 rpm and kept in a dark room tempered to 20 $°C$. The sampling procedure ensured that the liquid-to-solid ratio changed less than 10 %. Thus, this minor change was neglected in the subsequent data analysis since it is in the range of the analytical error. As discussed below, only partition coefficients larger than 50 Lkg^{-1} can be reliably determined since at larger liquid to solid ratios the measurement errors escalate. Therefore, all data resulting in smaller partition coefficients are not reported. Furthermore, the coefficients of variation (CV) have been calculated as the standard deviation normalized to the mean values of the replicates and given in %. CV values >100 % were as well a criterion for exclusion.

III 2.2 Chemical Analysis

Phenanthrene, 4*n*-nonylphenol, and TCPP were quantified via GC-MS. For analysis, an Agilent 6890 N GC coupled to an Agilent 7973 inert MS was used. For separation, a J+W Scientific DB-5MS (30 m length, 0.025 mm ID, 0.25 μm film thickness) capillary column was used. The device was operated in a pulsed splitless mode with a Helium flow of 0.7 $mLmin^{-1}$. Samples were taken as described above and internal standards (phenanthrene-D_{10} and 4*n*-nonylphenol-D_8) were added. Subsequently, the samples were extracted with 400 μL of cyclohexane, shaken overnight, and measured.

The other 16 substances were quantified with LC-MS/MS and samples were directly injected after gravitational phase separation. Since the LC-System is equipped with a pre-column filter, remaining particles would not be able to enter the column and to produce false-positive results. For quantification, a calibration curve with nine different concentration levels from 0.025 μgL^{-1} to 10 μgL^{-1} was generated. For analysis, an Agilent 1290 infinity LC coupled to an Agilent 6490 Triple Quadrupole was used. Separation was performed with an Agilent InfinityLab C18 poroshell column (length 100 mm, 2.1 μm ID). For elution, water (with 0.1 % acetic acid and 0.01 mM ammonium

acetate) and acetonitrile (ACN, with 0.1 % acetic acid) were used. The gradient elution looks as follows (with percentage of ACN): start with 2 %, stepwise increase to 80 % until 17 min, 100 % until 23 min, then again 2 % until 32 min. For the quantification of the samples from the batch experiments with either Triclosan or Diclofenac, two isocratic methods with 57% ACN or 70 % ACN were used, respectively. For these measurements, specific calibration curves were generated as well (concentration range from 0.5 $\mu g L^{-1}$ to 250 $\mu g L^{-1}$ with seven calibration levels). Substances were ionized with an ESI source operated either in positive or negative mode. Details on the ionization mode, mass transitions, and other analytical characteristics are reported in the appendix.

Table III 1: **Physico-chemical properties of the investigated substances.** Properties are either taken from EPISuite (molecular weight and log K_{OW} of neutral species) or the PubChem database (pK_a). Subcooled liquid solubilities (WS) were estimated based on melting points according to Kan & Tomson (1996) and Liu et al. (2013).

compound	**CAS#**	**molecular weight** $[gmol^{-1}]$	**WS**$_{sub}$ $[molL^{-1}]$	**log** K_{OW}	pK_a	**Acid-base reaction**
Atrazine	1912-24-9	215.69	5.43×10^{-3}	2.61	1.60	Base
Benzotriazole	95-14-7	119.13	1.05	1.44	8.37	Base
Caffeine	58-08-2	194.19	1.65×10^{1}	0.07		Neutral
Carbamazepine	298-46-4	236.28	3.10×10^{-3}	2.45	13.9	Acid
Carbendazim	10605-21-7	191.19	9.27×10^{-2}	1.52	4.29	Base
DEET	134-62-3	191.28	Liquid	2.18		Neutral
Diazinon	333-41-5	304.35	1.31×10^{-3}	3.81	2.60	Base
Diclofenac	15307-86-5	296.15	1.87×10^{-4}	4.51	3.99	Acid
Ibuprofen	15687-27-1	206.29	3.69×10^{-4}	3.97	4.45	Acid
MCPA	94-74-6	200.62	3.13×10^{-2}	3.25	3.13	Acid
Mecoprop	7085-19-0	214.65	1.62×10^{-2}	3.20	3.78	Acid
4*n*-Nonylphenol	104-40-5	220.36	4.78×10^{-5}	5.76	10.7	Acid
Phenanthrene	85-01-8	178.24	3.95×10^{-5}	4.46		Neutral
Propiconazole	60207-90-1	342.22	Liquid	3.72	1.09	Base
TCPP	13674-84-5	327.57	Liquid	2.59		Neutral
Tebuconazole	107534-96-3	307.83	7.78×10^{-4}	3.70	1.76	Base
Terbutryn	886-50-0	241.36	7.15×10^{-4}	3.74	4.30	Base
Torasemide	56211-40-6	348.42	2.10×10^{-2}	3.37	6.68	Acid
Triclosan	3380-34-5	289.55	7.55×10^{-5}	4.76	7.90	Acid

III 2.3 Model-Based Data Analysis

Linear partitioning of a substance between two phases, here water and a type of microplastics, is given as the equilibrium partition coefficient K_P $[Lkg^{-1}]$, i.e. the concentration ratio of the sorbed (C_P in $[\mu g kg^{-1}]$) and dissolved (C_W in $[\mu g L^{-1}]$) fraction.

$$K_P = \frac{C_{PE}}{C_W} \text{ in equilibrium} \tag{III 1}$$

For ionizable compounds, the pH-dependent partition coefficient D_P can be calculated.

$$D_P = K_{P,n} f_n + K_{P,i} f_i \tag{III 2}$$

where f_n and f_i are the fractions of the neutral and ionized species and $K_{P,n}$ and $K_{P,i}$ are the species-specific partition coefficients for the neutral and the ionized species, respectively. f_n and f_i were calculated from the known pK_a and pH values according to the rearranged *Henderson-Hasselbalch* equation while the species-specific partition coefficients were deduced from fitting the calculated DP value to the experimentally determined D_P values. At each pH and for each substance, D_P was calculated from nine or twelve measured aqueous concentrations for PE and PS, respectively. No measurement results were excluded. For the fitting procedure a MATLAB Code (Version R2017b) was used. Within this code, a nonlinear least-squares solver was used to calculate $K_{P,n}$ and $K_{P,i}$ from fitting equation III 2 to measured D_P values. This procedure allows to calculate a theoretical D_P for each substance over the full pH range. To assess the uncertainty of the determination of partition coefficients a simple error evaluation was considered:

$$\frac{K_{P,c} - K_{P,m}}{K_{P,c}} = \frac{\epsilon + \frac{V_W}{m_P K_{P,c}} \epsilon}{1 + \epsilon} = \frac{\epsilon}{1 + \epsilon} \left(1 + \frac{V_W}{m_P K_{P,c}} \right) \tag{III 3}$$

with $K_{P,c}$ and $K_{P,m}$ as the calculated and measured partition coefficients, respectively and V_W, m_P, and ϵ denote the volume of water, the mass of particles and the uncertainty of the measurement (e.g. a standard deviation).

III 2.4 Aqueous Pollutant Concentrations in Two Scenarios

Experimental results on the overall sorption coefficients of the investigated substances at three pH values were used to calculate two scenarios with different microplastic concentrations. In both scenarios organic carbon (values for K_{OC} were taken from US EPA EPISuite 4.1 and apply for so-called "normal" soil organic matter) was present as a natural sorbent which can compete for the sorbates and is able to act as a vector as well. In order to compare the results from our experiments with an environmental relevant setting, two different liquid-to-solid ratios (LSR) concerning the amount of plastics were chosen. To match our experimental conditions, in Scenario I, a LSR of 10^3 Lkg^{-1}

and to reflect particle concentrations closer to current environmental conditions and in Scenario II a LSR of $10^10\,Lkg^{-1}$ (comparable to conditions at the effluent of WWTPs, according to particle concentrations recorded by Mintenig et al. (2017) were chosen. The mass of organic carbon was set to 10 mg, i.e. a concentration of $10^{-5}\,kgL^{-1}$. The dissolved fraction f_{diss} in the water, i.e. the ratio between the equilibrium and the initial concentration, may be easily calculated:

$$f_{diss} = \frac{1}{1 + K_{OC}\, m_{OC}/V_W + K_P\, m_P/V_W} \tag{III 4}$$

V_W, m_{OC}, and m_P denote the volume of water, the mass of organic carbon and the mass of plastic particles, respectively. Each scenario was calculated over a range of K_{OC}- and K_P-values and for the three different pH values used in the experiments. For the investigated substances, K_P was quantified with the particle-water partition coefficient that was experimentally determined.

III 3 Results & Discussion

III 3.1 Equilibrium Sorption to PE

Sorption to PE is in general strongly dependent on the substance properties and is mostly driven by partitioning. Polymer properties as e.g. density (O'Connor et al., 2016), branching of polymer chains and crystallinity (Endo et al., 2005) may as well influence sorptive interactions. Sorption of non-polar compounds is stronger than sorption of polar compounds and sorption of charged species is weaker than sorption of neutral species (Figure III 1). Fluctuations of sorbed percentages will be discussed below. Detailed sorption plots of every substance and the respective agreement with the model can be found in the SI. In general, the model could be fitted to the measured overall partition coefficients quite well. The derived $K_{PE,n}$ and $K_{PE,i}$ are listed in Table III 2, to secure reliability, exactly values were only reported if K_{PE} were <50 Lkg^{-1} and/or CV were >100 %.

Table III 2: **$K_{PE,n}$ and $K_{PE,i}$ values derived from the model fit (Eq. III 2) to measured D_P values and compared to the log K_{OW}.** K values below 50 Lkg^{-1} are not reported due to too large uncertainties.

compound	log K_{OW}	$K_{PE,n}$	$K_{PE,i}$	%-variation coefficients of D_P		
				pH 4	pH 7	pH 10
Atrazine	2.61	$<5.0\times10^1$	5.0×10^1	49.3	60.1	54.7
Benzotriazole	1.44	$<5.0\times10^1$	$<5.0\times10^1$	185.3	69.2	38.8
Caffeine	0.07	$<5.0\times10^1$	n.a.	69.4	63.1	157.0
Carbamazepine	2.45	6.7×10^1	$<5.0\times10^1$	129.2	59.3	60.6
Carbendazim	1.52	$<5.0\times10^1$	$<5.0\times10^1$	161.8	54.2	57.3
DEET	2.18	5.2×10^1	n.a.	122.0	44.3	100.8
Diazinon	3.81	1.75×10^3	$<5.0\times10^1$	39.0	75.8	14.7
Diclofenac	4.51	1.5×10^2	$<5.0\times10^1$	57.9	61.6	133.6
Ibuprofen	3.97	2.6×10^2	1.9×10^2	35.5	59.4	81.0
MCPA	3.25	8.8×10^3	$<5.0\times10^1$	74.2	163.3	13130.3
Mecoprop	3.20	$<5.0\times10^1$	$<5.0\times10^1$	146.7	522.4	139.9
4*n*-Nonylphenol	5.76	6.0×10^3	7.2×10^2	13.5	13.6	12.4
Phenanthrene	4.46	9.9×10^3	n.a.	8.7	12.4	28.3
Propiconazole	3.72	3.4×10^2	$<5.0\times10^1$	45.0	52.0	26.2
TCPP	2.59	2.2×10^2	n.a.	77.5	84.8	24.6
Tebuconazole	3.70	1.4×10^2	$<5.0\times10^1$	48.0	75.0	35.4
Terbutryn	3.74	6.2×10^1	6.3×10^1	31.8	53.8	18.1
Torasemide	3.37	1.3×10^2	$<5.0\times10^1$	210.6	34.1	34.0
Triclosan	4.76	1.1×10^3	$<5.0\times10^1$	27.8	38.2	203.1

Even though it is expected, that the species-specific partition coefficient of the ions is zero or close to zero, for some compounds the species-specific partition coefficients indicate that the charged species contribute to sorption as well. For these cases, the $K_{PE,i}$'s difference from zero is greater for weakly sorbing compounds. These results will be discussed in more detail below. For some substances, sorption did not significantly decrease with increasing share of ionized species indicating that structural features as e.g. the hydrophobic neutral tail of the surfactant-like nonylphenol are responsible for sorptive interactions.

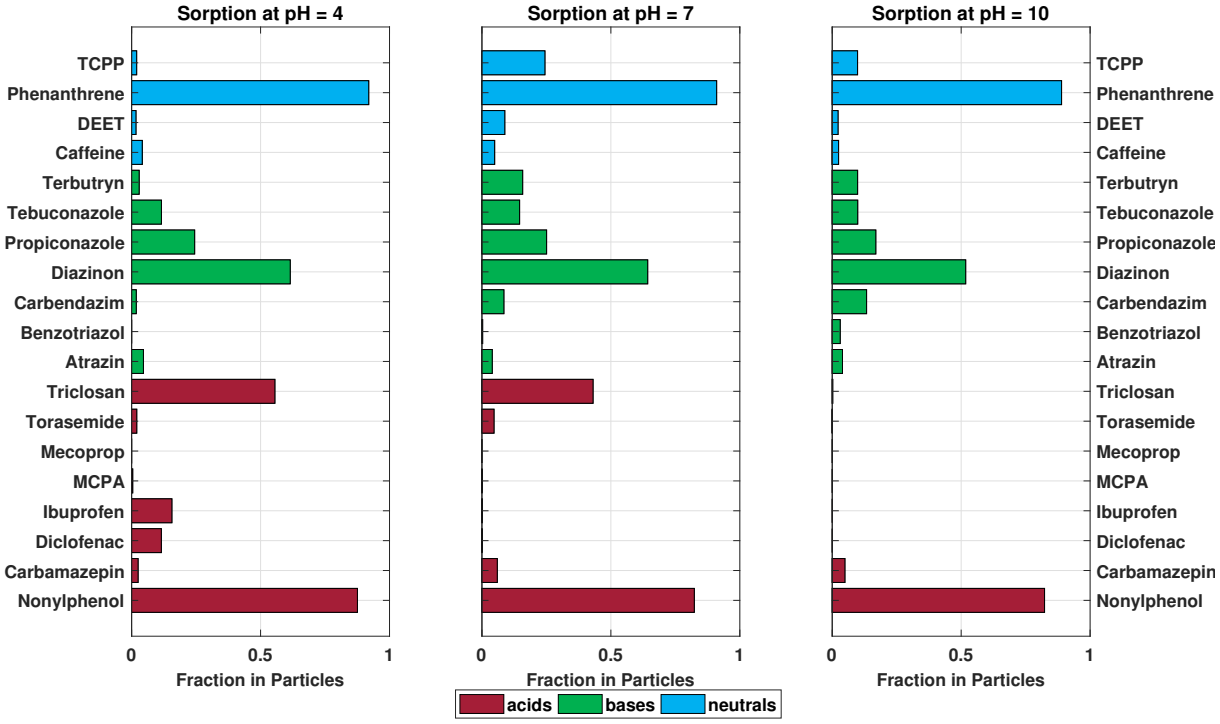

Figure III 1: **Sorbed fractions of the investigated contaminants to polyethylene at different pH levels.** The bars are colored according to the acid/base-properties of the substances as indicated in the legend. For substances for which a negative D_P has been determined, the sorbed percentage was set to zero.

III 3.2 Equilibrium Sorption to PS

Sorption to PS was stronger than sorption to PE for most of the investigated substances and driven by both partitioning and adsorption (e.g., a pore-filling mechanisms confirmed by the non-linear sorption isotherms (as provided in the SI) which is in agreement with findings of other authors (Wang & Wang, 2018a; Hüffer & Hofmann, 2016). Nevertheless, sorption coefficients for both plastic types are within the same order of magnitude. Furthermore, in analogy to the case for PE, sorption to PS was driven by hydrophobicity as well and substances that sorbed strongly to PE also sorbed strongly to PS (Figure III 2). Detailed plots of measured and modeled DP for all substances can be found in the SI. Again, the model could be fitted to measured overall partition coefficients well and, again, the model fits were better for stronger sorbing compounds. Based on the deduced $K_{PS,n}$ and $K_{PS,i}$, sorption of neutral species to PS is stronger than to PE

whereas sorption of the ionic species is weaker for most of the substances (Tables III 2 and III 3). Coefficients of variation increase with increasing share of ionic species, thus decreasing sorption what leads to the conclusion that for weakly sorbing ionic species the error escalates. Differences between sorption to PE and PS can most likely be explained due to the non-linearity of sorption to PS. Consideration of the differences between ambient concentrations and water solubility are crucial if nonlinear sorption mechanisms are investigated. Studies performed e.g. by Hüffer & Hofmann (2016) and Lee et al. (2014) determined higher partition coefficients for PS whereas other studies by Pascall et al. (2005) indicate stronger sorption to PE.

Table III 3: **$K_{PS,n}$ and $K_{PS,i}$ values derived from the model fit (Eq. III 2) to measured D_P values and compared to the log K_{OW}.** K values below 50 Lkg^{-1} are not reported due to too large uncertainties.

compound	log K_{OW}	$K_{PS,n}$	$K_{PS,i}$	%-variation coefficients of D_P		
				pH 4	pH 7	pH 10
Atrazine	2.61	$<5.0\times10^{1}$	5.0×10^{1}	244.2	335.9	257.3
Benzotriazole	1.44	$<5.0\times10^{1}$	$<5.0\times10^{1}$	444.7	88.4	213.7
Caffeine	0.07	$<5.0\times10^{1}$	n.a.	1785.7	428.3	1199.7
Carbamazepine	2.45	$<5.0\times10^{1}$	$<5.0\times10^{1}$	172.2	175.6	283.2
Carbendazim	1.52	$<5.0\times10^{1}$	$<5.0\times10^{1}$	471.1	598.5	117.5
DEET	2.18	$<5.0\times10^{1}$	n.a.	177.1	240.7	500.2
Diazinon	3.81	2.15×10^{3}	2.09×10^{3}	93.6	82.5	53.5
Diclofenac	4.51	2.70×10^{2}	$<5.0\times10^{1}$	93.0	214.2	6101.7
Ibuprofen	3.97	2.05×10^{2}	$<5.0\times10^{1}$	45.9	184.0	161.0
MCPA	3.25	$<5.0\times10^{1}$	$<5.0\times10^{1}$	699.7	1564.9	196.7
Mecoprop	3.20	$<5.0\times10^{1}$	$<5.0\times10^{1}$	138.6	609.1	2206.8
4*n*-Nonylphenol	5.76	7.21×10^{3}	3.74×10^{3}	18.7	49.8	31.2
Phenanthrene	4.46	7.21×10^{3}	n.a.	29.8	21.5	40.4
Propiconazole	3.72	1.17×10^{2}	$<5.0\times10^{1}$	44.5	169.0	48.9
TCPP	2.59	1.06×10^{2}	n.a.	42.5	61.5	30.6
Tebuconazole	3.70	9.89×10^{1}	$<5.0\times10^{1}$	57.3	97.0	85.7
Terbutryn	3.74	$<5.0\times10^{1}$	$<5.0\times10^{1}$	158.7	166.8	90.2
Torasemide	3.37	$<5.0\times10^{1}$	$<5.0\times10^{1}$	2502.6	95.4	70.5
Triclosan	4.76	5.12×10^{3}	$<5.0\times10^{1}$	95.6	123.4	241.9

In general, there is a lack of experiments comparing sorption to different types of microplastics. Experiments performed in our own lab showed that sorption of a polycyclic aromatic hydrocarbon (phenanthrene) and two heterocyclic compounds to PE and PS was stronger for PE and revealed a slight non-linearity of sorption isotherms to PS (reported in the SI). Therefore, we conclude that sorption to PE is driven by partitioning, i.e. absorption, whereas sorption to PS may be driven by both adsorption

and subsequent pore-filling mechanisms which are confirmed by the nonlinear sorption isotherms. According to the high glass transition temperature of PS, the fee volume within the polymeric matrix is low and hence adsorption is favored in comparison to absorption (Pascall et al., 2005). As there are many producers of plastics using different ingredients, the differences between the same types of plastics can be as manifold as the number of manufacturers. Hence, the outcome of such sorption experiments can be different depending on the material supplier and comparability is in general difficult.

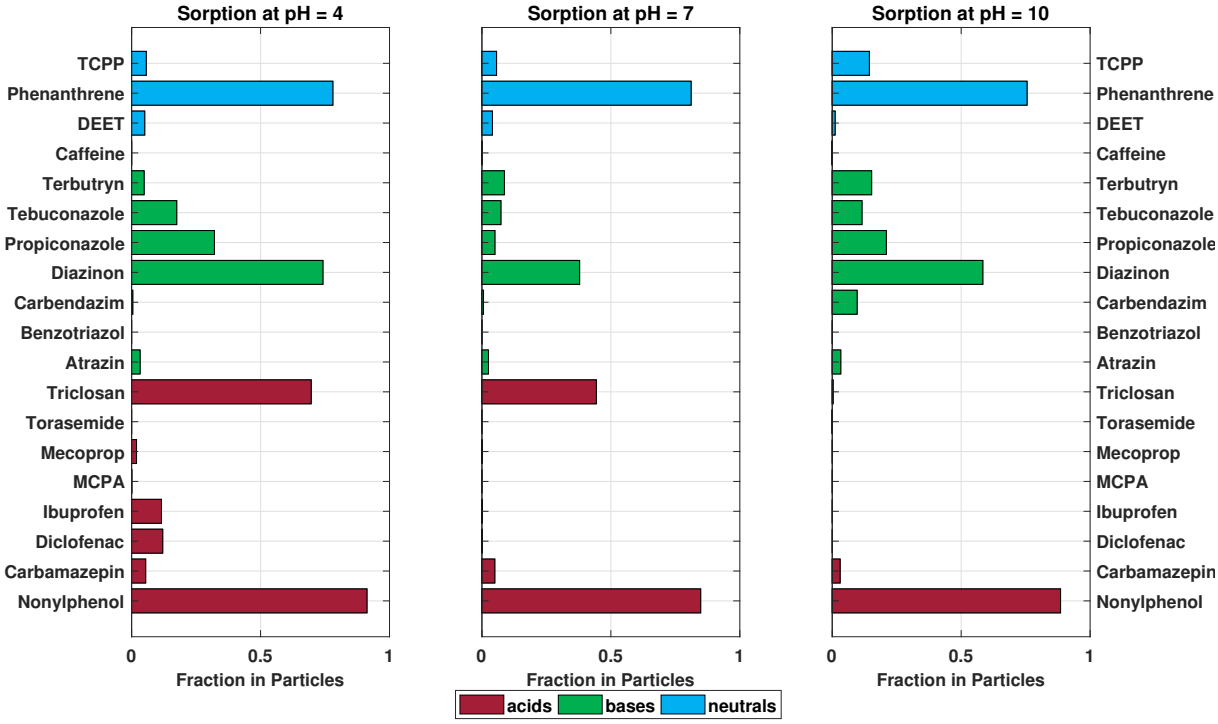

Figure III 2: **Sorbed fractions of the investigated contaminants to polystyrene at different pH levels.** The bars are colored according to the acid/base-properties of the substances as indicated in the legend. For substances for which a negative D_P has been determined, the sorbed percentage was set to zero.

III 3.3 Sorption of the Ionic Species

As expected, the species-specific partition coefficients for most substances were higher for the neutral species the ionic species of some substances showed some significant sorption as well. This occurred especially for more hydrophobic substances such as nonylphenol and triclosan whereas for weakly sorbing compounds species-specific partitioning coefficients of the ionic species where at least one order of magnitude smaller. Whereas predictions solely based on the log KOW which is the classic parameter for estimating hydrophobicity fail to predict accumulation of ionic species (Escher et al., 2000) there is some evidence that polar species can accumulate within organisms as well and play an important role in bioaccumulation in fat (Dołżonek et al., 2017; Goss et al., 2018). Also carbon nanotubes can sorb ionic liquids (Wojsławski et al., 2018).

III 3.4 Impact of Particle Concentration

The best practice to sensitively measure partition coefficients is to choose a liquid-to-solid ratio (LSR) in the same range or lower as the prospective partition coefficient that should be determined. This allows determination of the partition coefficient with a sufficiently low uncertainty. In our experiments, the LSR was $10^3\ Lkg^{-1}$, thus only partition coefficients greater than $10^3\ Lkg^{-1}$ or slightly smaller ($<50\ Lkg^{-1}$) can be determined with small errors. As it can be seen in Figure III 3, the partition coefficients determined for polar and weakly sorbing compounds are subject to greater uncertainty and the deviation between the calculated and the measured partition coefficients increase with decreasing sorption independent of the pH. Therefore, the partition coefficients determined for polar and weakly sorbing compounds are subject to greater uncertainty which is reflected in the variation coefficients.

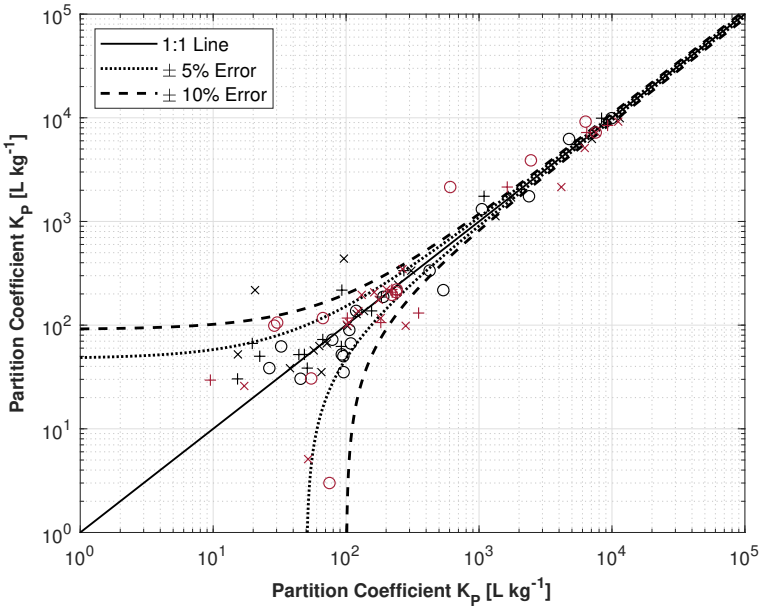

Figure III 3: **Uncertainty of partition coefficients calculated according to equation III 3.** Uncertainties were determined with standard analytical errors of $\epsilon = \pm 5\ \%$ (dotted lines) and of $\epsilon = \pm 10\ \%$ (dashed lines). The differences between the measured DP (x-axis) and the calculated DP (y-axis) are displayed by the black and red symbols for PE and PS, respectively. Crosses, circles and pluses indicate DP values determined at pH 4, pH 7, and pH 10, respectively.

A LSR of $10^3\ Lkg^{-1}$ as chosen in our batch experiments represents microplastics concentrations that are orders of magnitude larger than the ones that were detected in the environment where LSRs are usually $>10^9\ Lkg^{-1}$ (Koelmans et al., 2016; Mintenig et al., 2017; Schmidt et al., 2017). Thus, batch setups focusing on elucidating a specific process detail, like the species-specific sorption coefficients in this study, do not reflect environmental relevant conditions, in particular when considering that plastic debris is just a very minor fraction compared to all natural particles that environmental contaminants can partition to. In addition, for most of the substances investigated within this study, the determined D_Ps were below the order of 10^1 to $10^2\ Lkg^{-1}$, i.e.

the lower the particle concentration the smaller is the mass flux of the substance into the solid phase and, with this, the resulting highly uncertain measurements of K_P. Therefore, adsorption efficiencies reported in literature (e.g. 60 % and 70 % for PFC sorption to PE and PS (Llorca et al., 2018)) are only possible under very low (and thus unrealistic) LSRs. This is even more true under environmental conditions as there are more sorbing phases such as black carbon or dissolved organic matter available which take up contaminants as well and partly even much stronger than polymers (Beckingham & Ghosh, 2017). Calculations on equilibrium distribution in a freshwater system containing natural sorbents (organic carbon) and microplastic particles show that microplastics are only relevant if their concentration in water is much higher than the concentration of other organic carbon containing phases (Scenario I, Figure III 4, top). However, at environmental relevant concentrations of microplastics the effect of natural organic particles likely prevails. If K_P is smaller than the LSR, the distribution of the tested substances shifts and almost all compounds would predominantly be available in the freely aqueous phase (Scenario II, Figure III 4, bottom).

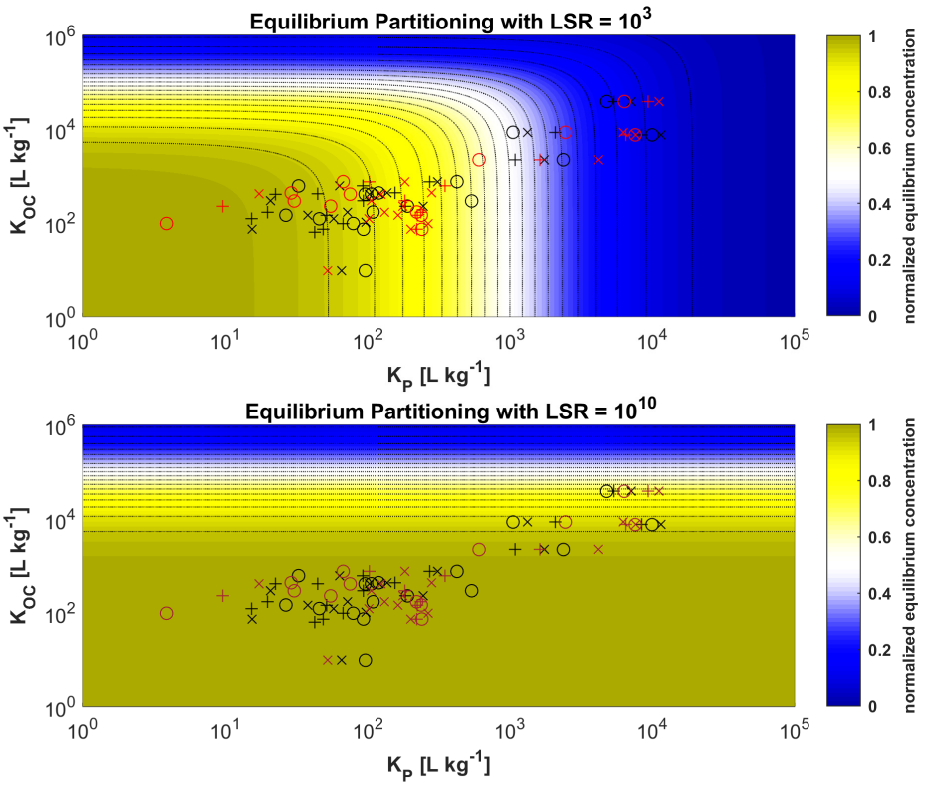

Figure III 4: **Equilibrium distribution map for a freshwater system with natural particles (organic carbon) and microplastic particles under two different concentration scenarios.** Experimental conditions (plastic LSR = $10^3\ Lkg^{-1}$, Scenario I) are shown in the top panel and environmental conditions (plastic LSR = $10^{10}\ Lkg^{-1}$, Scenario II) in the bottom panel. Crosses, circles and pluses show the aqueous equilibrium concentrations at pH 4, pH 7, and pH 10, respectively, in μgL^{-1} calculated with the experimentally determined DP for PE (black symbols) and for PS (red symbols) and the investigated substances. For both cases, a constant concentration of $10^{-5}kgL^{-1}$ OC were assumed. K_{OC} values were estimated using EPISuite 4.1.

Thus, our findings for ionizable compounds also support arguments which state that microplastic particles are not substantial vectors for contaminants in terms of substance mass transported due to their low environmental concentrations (Koelmans et al., 2016; Lohmann, 2017). In particular this is true if considered that at very low, but environmental relevant concentration, e.g. for phenanthrene, field-measured K_d-values for partitioning to suspended sediment particles lead to much larger K_{OC}-values (Rügner et al., 2013) than estimated from the EPISuite-database due to nonlinear sorption. Thus, the particles' sorption capacity may be even larger as assumed in our model calculations. Even though particle properties and sorption interactions may change under environmental conditions in particular due to aging (Jahnke et al., 2017), studying sorption to rather pristine particles is highly relevant since the alteration through aging can only be investigated if sorption processes to pristine particles are known.

III 3.5 Conclusion & Outlook

To assess the potential effects of microplastics and associated contaminants on ecosystems it is important to properly evaluate the particle-pollutant interactions especially since this determines their bioavailability which is yet not well understood. Hydro- and geochemical parameters as well as contact with biota may change particle characteristics, e.g. their surface charge and texture, and may procure aggregation (Li et al., 2018; Wang et al., 2016). Thus, it is essential to analyze whether sorption interactions occur which are going beyond mere partitioning as investigated here. At least for pristine plastic particles we could show, that partitioning is still the main sorption mechanism and sorption of charged species at least with current environmental microplastic concentrations in freshwaters is irrelevant.

A III
Supporting Information to Paper III

Calculations

To calculate the fractions of neutral and charged species equation (III A1) and equation (III A2) were used for acids and bases, respectively.

$$f_{n,a} = \frac{1}{1 + 10^{pH - pK_a}} \tag{III A1}$$

$$f_{n,b} = \frac{1}{1 + 10^{pK_a - pH}} \tag{III A2}$$

The used pK_a values are listed in Table III 1 in the main manuscript.

For all substances the pH-dependent partition coefficient D_P was calculated for each pH. As explained in the main manuscript a *MATLAB* Code using a nonlinear least-square solver was operated to estimate the partition coefficients $K_{P,n}$ and $K_{P,i}$ for the neutral and the ionic species, respectively for both types of plastic particles. Subsequently the theoretical $D_{P,calc}$ were calculated for each pH using equation (III A3).

$$D_{P,calc} = f_n K_{P,n} + (1 - f_n) K_{P,i} \tag{III A3}$$

To compare each of the measured D_Ps with the theoretical $D_{P,calc}$, for each pH, each compound, and the two different types of microplastics error calculations were performed as specified in the manuscript.

Particle Properties

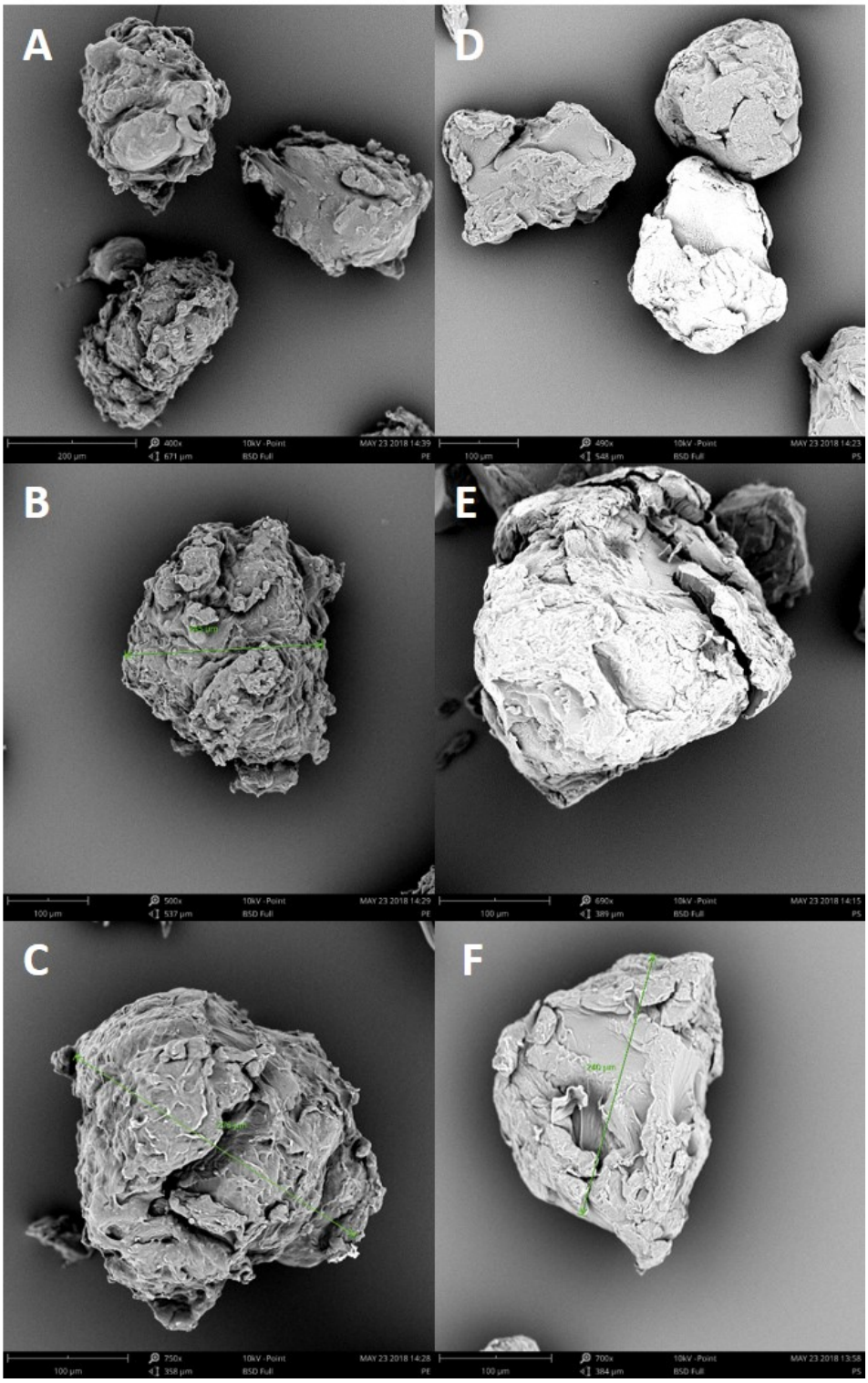

Figure III A1: **SEM images of used PE (left panel, A-C) and PS (right panel, D-F) particles.**

Results for Polyethylene Particles

The measured partition coefficients between the chosen contaminants and polyethylene are listed in Tables III A1, III A2, and III A3 for pHs of 4, 7, and 10, respectively. Comparison between estimated and measured partition coefficients are shown in Figures III A2, III A3, and III A4 for acids, bases, and neutrals, respectively.

Table III A1: **Measured D_P and calculated $D_{P,calc}$ for sorption of investigated compounds to polyethylene at pH = 4.**

Substance	Measured Partition coefficient D_P	Calculated Partition coefficient $D_{P,calc}$
Nonylphenol	7063	6248
Carbamazepin	72	67
Diclofenac	102	98
Ibuprofen	246	246
MCPA	96	438
Mecoprop	<50	-133
Torasemide	120	128
Triclosan	1330	1123
Atrazin	<50	38
Benzotriazol	<50	-9
Carbendazim	57	57
Diazinon	1741	1706
Propiconazole	309	335
Tebuconazole	137	137
Terbutryn	63	63
Caffeine	65	35
DEET	<50	52
Phenanthrene	11451	9909
TCPP	<50	218

Table III A2: **Measured D_P and calculated $D_{P,calc}$ for sorption of investigated compounds to polyethylene at pH = 7.**

Substance	Measured Partition coefficient D_P	Calculated Partition coefficient $D_{P,calc}$
Nonylphenol	4755	6246
Carbamazepin	109	67
Diclofenac	95	50
Ibuprofen	190	187
MCPA	<50	-224
Mecoprop	79	72
Torasemide	106	90
Triclosan	1051	1313
Atrazin	<50	38
Benzotriazol	<50	-5
Carbendazim	<50	30
Diazinon	2376	1750
Propiconazole	425	336
Tebuconazole	119	137
Terbutryn	<50	62
Caffeine	96	35
DEET	93	52
Phenanthrene	9921	9909
TCPP	539	218

Table III A3: **Measured D_P and calculated $D_{P,calc}$ for sorption of investigated compounds to polyethylene at pH = 10.**

Substance	Measured Partition coefficient D_P	Calculated Partition coefficient $D_{P,calc}$
Nonylphenol	5353	5514
Carbamazepin	<50	67
Diclofenac	<50	50
Ibuprofen	184	187
MCPA	<50	-225
Mecoprop	67	73
Torasemide	<50	52
Triclosan	2089	2034
Atrazin	51	38
Benzotriazol	<50	-42
Carbendazim	<50	30
Diazinon	1091	1750
Propiconazole	272	336
Tebuconazole	155	137
Terbutryn	92	62
Caffeine	<50	35
DEET	<50	52
Phenanthrene	8353	9909
TCPP	93	218

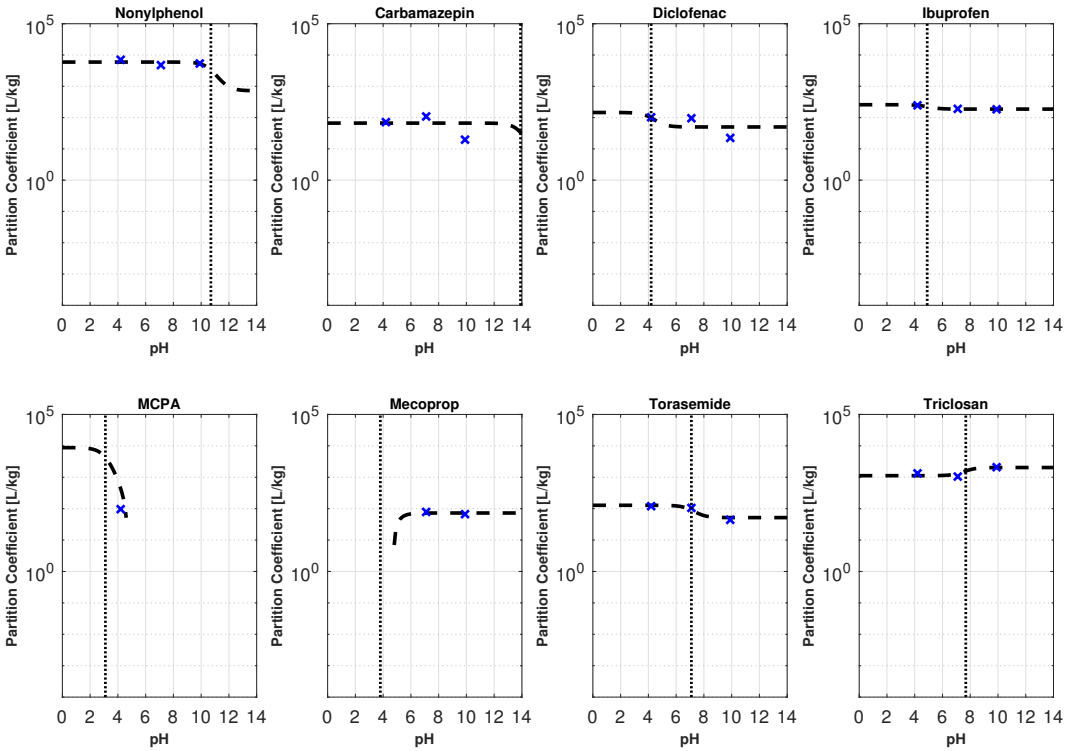

Figure III A2: **Comparison of measured D_P and theoretical partitioning for sorption of acids to polyethylene illustrated by the blue crosses and dashed lines, respectively.** The vertical dotted lines indicate the pK_a values. Due to the log-scale of the y-axis only positive values can be displayed.

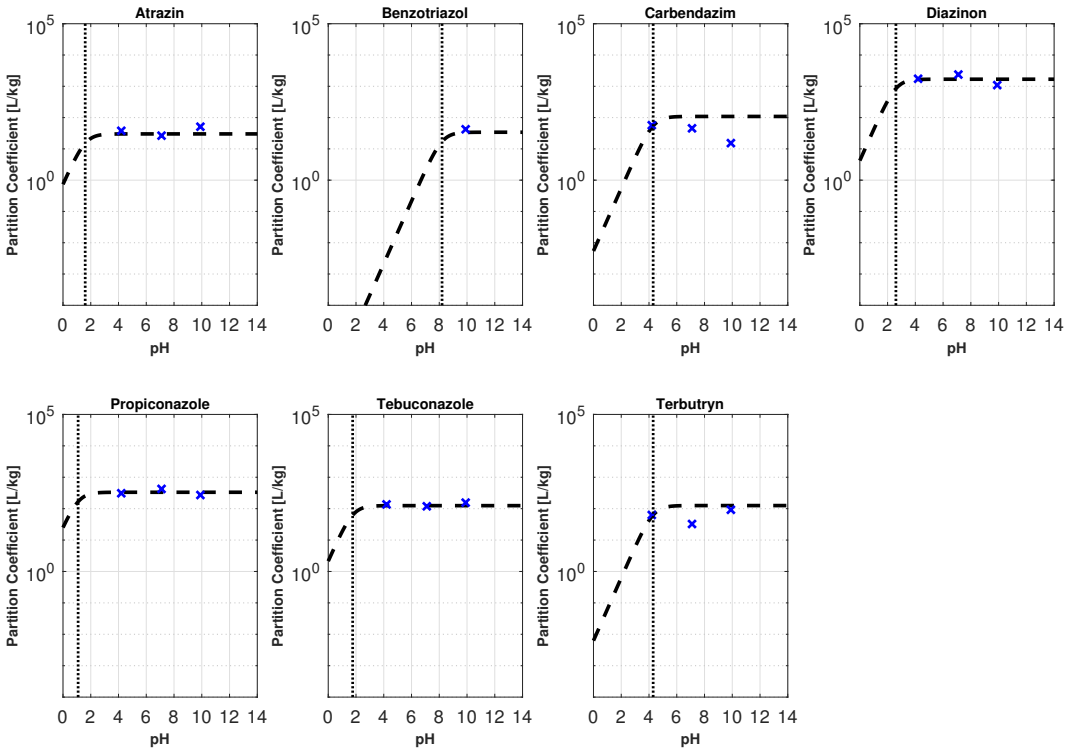

Figure III A3: **Comparison of measured D_P and theoretical partitioning for for sorption of bases to polyethylene illustrated by the blue crosses and dashed lines, respectively.** The vertical dotted lines indicate the pK_a values. Due to the log-scale of the y-axis only positive values can be displayed.

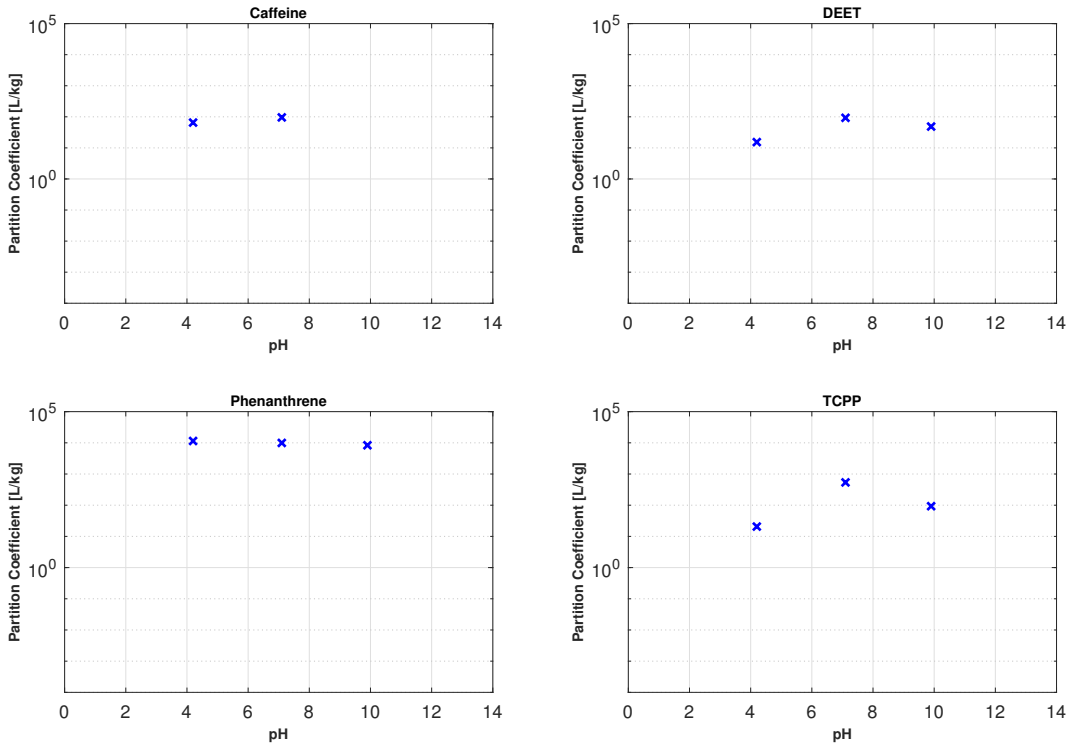

Figure III A4: **Measured D_P for sorption of neutrals to polyethylene illustrated by the blue crosses.** Due to the log-scale of the y-axis only positive values can be displayed.

Results for Polystyrene Particles

The measured partition coefficients between the chosen contaminants and polystyrene are listed in Tables III A4, III A5, and III A6 for pHs of 4, 7, and 10, respectively. Comparison between estimated and measured partition coefficients are shown in Figures III A5, III A6, and III A7 for acids, bases, and neutrals, respectively

Table III A4: **Measured D_P and calculated $D_{P,calc}$ for sorption of investigated compounds to polystyrene at pH = 4.**

Substance	Measured Partition coefficient D_P	Calculated Partition coefficient $D_{P,calc}$
Nonylphenol	11149	9182
Carbamazepin	131	196
Diclofenac	124	137
Ibuprofen	176	176
MCPA	<50	4193
Mecoprop	266	348
Torasemide	<50	26
Triclosan	6243	5114
Atrazin	163	207
Benzotriazol	<50	-19
Carbendazim	101	101
Diazinon	4162	2147
Propiconazole	182	117
Tebuconazole	281	99
Terbutryn	<50	1
Caffeine	52	5
DEET	201	221
Phenanthrene	7623	7212
TCPP	105	106

Table III A5: **Measured D_P and calculated $D_{P,calc}$ for sorption of investigated compounds to polystyrene at pH = 7.**

Substance	Measured Partition coefficient D_P	Calculated Partition coefficient $D_{P,calc}$
Nonylphenol	6330	9180
Carbamazepin	221	196
Diclofenac	75	3
Ibuprofen	55	31
MCPA	<50	-2217
Mecoprop	<50	-26
Torasemide	<50	-24
Triclosan	2456	3885
Atrazin	238	208
Benzotriazol	<50	-23
Carbendazim	<50	-16
Diazinon	607	2148
Propiconazole	67	117
Tebuconazole	<50	99
Terbutryn	<50	130
Caffeine	<50	5
DEET	240	221
Phenanthrene	7549	7212
TCPP	<50	106

Table III A6: **Measured D_P and calculated $D_{P,calc}$ for sorption of investigated compounds to polystyrene at pH = 10.**

Substance	Measured Partition coefficient D_P	Calculated Partition coefficient $D_{P,calc}$
Nonylphenol	9273	8438
Carbamazepin	236	196
Diclofenac	<50	3
Ibuprofen	<50	30
MCPA	<50	-2226
Mecoprop	<50	-26
Torasemide	<50	-73
Triclosan	<50	-766
Atrazin	222	208
Benzotriazol	<50	-82
Carbendazim	<50	-16
Diazinon	1631	2148
Propiconazole	102	117
Tebuconazole	<50	99
Terbutryn	351	131
Caffeine	<50	5
DEET	221	221
Phenanthrene	6465	7212
TCPP	182	106

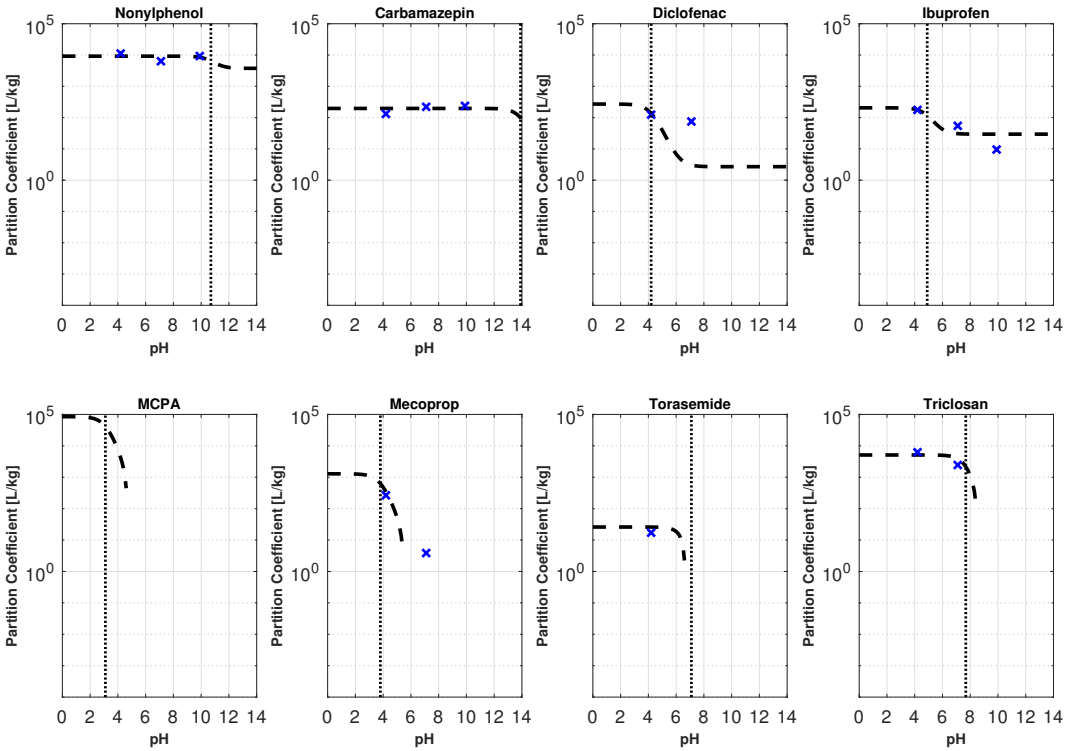

Figure III A5: **Comparison of measured D_P and theoretical partitioning for sorption of acids to polystyrene illustrated by the blue crosses and dashed lines, respectively.** The vertical dotted lines indicate the pK_a values. Due to the log-scale of the y-axis only positive values can be displayed.

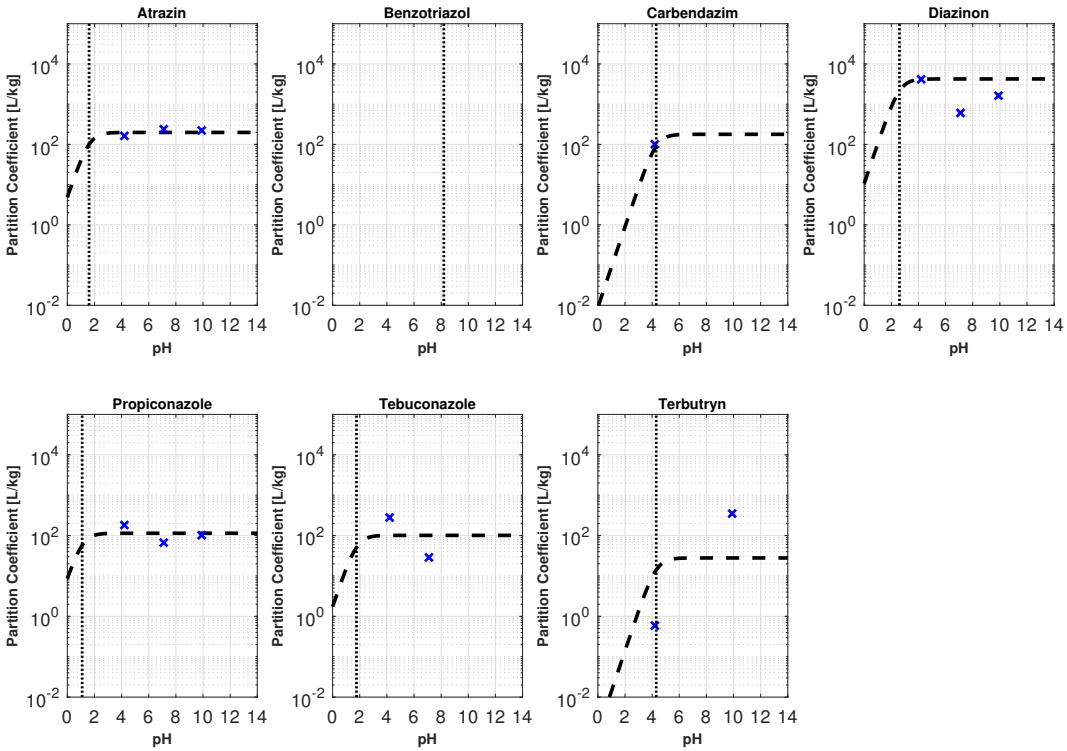

Figure III A6: **Comparison of measured D_P and theoretical partitioning for sorption of bases to polystyrene illustrated by the blue crosses and dashed lines, respectively.** The vertical dotted lines indicate the pK_a values. Due to the log-scale of the y-axis only positive values can be displayed.

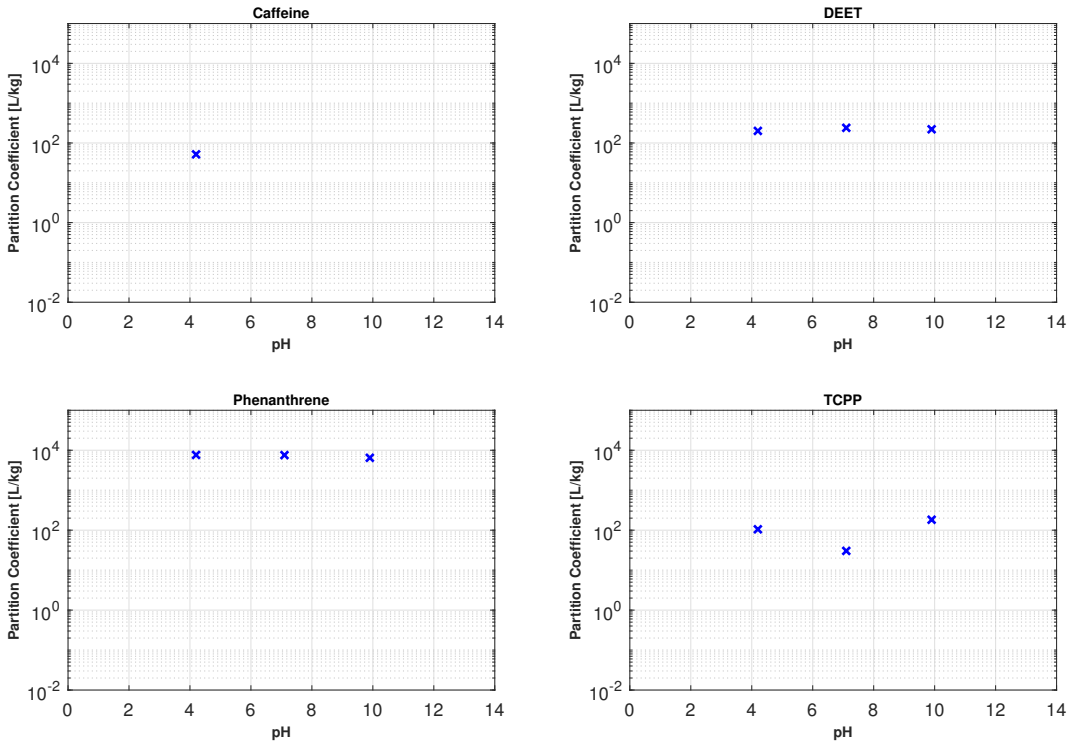

Figure III A7: **Measured D_P for sorption of neutrals to polystyrene illustrated by the blue crosses.** Due to the log-scale of the y-axis only positive values can be displayed.

Isotherms

To evaluate sorption mechanisms for pollutants on PE and PS, we measured sorption isotherms. As sorbates phenanthrene (PAH), dibenzofuran (O-Heteroclylic), and dibenzothiophene (S-Heteroclylic) were used. The best fit for sorption on PE resulted in a linear isotherm whereas sorption on PS could best be described by a power function indicating nonlinear sorption mechanisms (Figure III A8). R-squared values for all six isotherms were >0.98. The exponents of the fitted power functions were in the range of $0.75-0.78$. N_2-BET measurements were used to determine surface area and pore volumes of the different plastic particles. While PE is non-porous and had a surface area of 0.098 m^2g^{-1} (the applied method was not able to determine a pore volume), PS can be characterized as a porous material with a surface area of 0.6518 m^2g^{-1} and a pore volume of 0.0032 cm^3g^{-1}. Thus, different sorption isotherms can be explained by different involved mechanisms since pore-filling mechanisms may play a role in partitioning to PS.

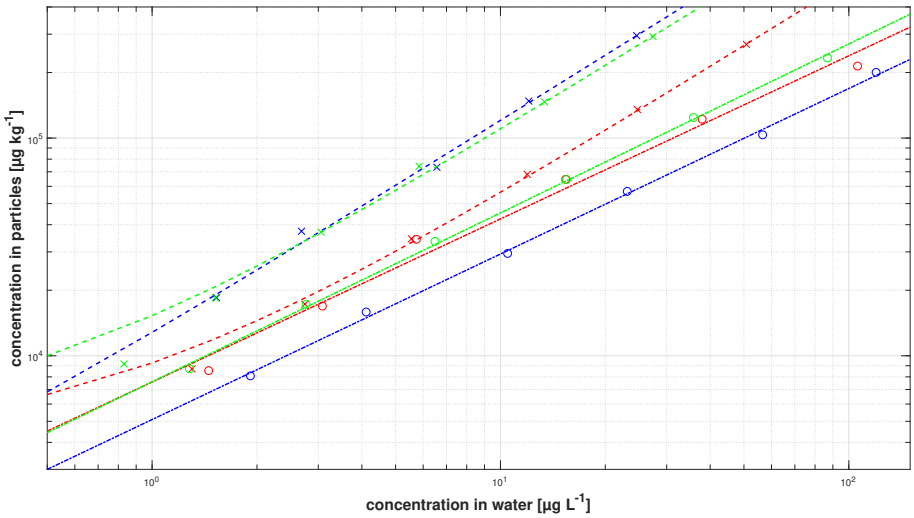

Figure III A8: **Sorption isotherms for phenanthrene (blue), dibenzofuran (red), and dibenzothiophene (green).** Both axes scaled logarithmic. Crosses and circles show sorption to PE and PS, respectively.

Paper IV
Shift in Mass Transfer of Wastewater Contaminants from Polyethylene in the Presence of Dissolved Substances

Abstract

In aqueous environments, hydrophobic organic contaminants are often associated with particles. Besides natural particles, microplastics have raised public concern. The release of pollutants from such particles depends on mass transfer, either in an aqueous boundary layer or by intraparticle diffusion. Which of these mechanism controls mass-transfer kinetics, depends on partition coefficients, particle size, boundary conditions, and time. We have developed a semi-analytical model accounting for both processes, and performed batch experiments on desorption kinetics of typical wastewater pollutants (phenanthrene, tonalide, benzophenone) at different dissolved-organic-matter concentrations, which change overall partitioning between microplastics and water. Initially, mass transfer is externally dominated while finally intraparticle diffusion controls release kinetics. Under boundary conditions typical for batch experiments (finite bath), desorption accelerates with increasing partition coefficients for intraparticle diffusion, while it becomes independent of partition coefficients if film diffusion prevails. Contrary, under field conditions (infinite bath), pollutant release controlled by intraparticle diffusion is not affected by partitioning of the compound while external mass transfer slows down with increasing sorption. Our results clearly demonstrate that sorption/desorption time scales observed in batch experiments may not be transferred to field conditions without an appropriate model accounting for both mass transfer mechanisms and the specific boundary conditions at hand.

IV 1 Introduction & Background

The pollution of freshwater ecosystems by an increasing number of chemicals causes adverse effects on aquatic organisms and even human health (Schwarzenbach et al., 2006). Within these systems, however, hydrophobic contaminants are often associated with various kinds of particles rather than being freely dissolved. Thus, the investigation of particle facilitated transport is important (Barber et al. (2006), Ko & Baker (2004)). The relevant particle types include colloids, such as natural organic substances, suspended sediments, different kinds of black carbon, and plastic-debris (Cornelissen et al., 2005; Luthy et al., 1997; Ghosh et al., 2003; Beckingham & Ghosh, 2017). The contamination and ubiquitous detection of plastic particles in freshwater ecosystems has attracted both public and scientific attention (Barnes et al., 2009; Eriksen et al., 2013). Microplastics are defined as particles made of any synthetic polymer with a size smaller than 5 *mm* (Thompson et al., 2004). These particles can be ingested and accumulated by organisms (Browne et al., 2013; Tanaka et al., 2013). Whether they significantly contribute to pollutant transfer is currently discussed in literature(Besseling et al., 2017). They can also influence the ecosystem by releasing plastic additives, such as plasticizers and flame retardants, and by acting as a vector for transport of hydrophobic contaminants (Rochman et al., 2014; Teuten et al., 2007). It is of relevance to which extent microplastics facilitate the transport of organic contaminants in freshwater ecosystems, particularly in light that they are often introduced in urban, polluted areas (Mani et al., 2015; Rule et al., 2006). The potential for microplastics to act as a sorbent for hydrophobic contaminants has been shown in several studies (Fries & Zarfl, 2012; Guo et al., 2012; Lee et al., 2014; Mato et al., 2001; Rochman et al., 2013; Teuten et al., 2007). Most of these studies focused on equilibrium partitioning of contaminants between microplastics and water. The aim of this study is to investigate the sorption kinetics of wastewater pollutants from microplastics. Specifically, we analyze shifts of mass transfer from external film diffusion to intraparticle diffusion in batch systems as a function of partition coefficients (Gschwend & Wu, 1985). We used frequently occurring wastewater contaminants to study their sorption properties from low-density-polyethylene (LDPE) particles, which are frequently detected in the environment (Andrady, 2011; Faure et al., 2015). In addition, we used standard humic acids (HA) which solubilizes organic contaminants in water and thus allows to cover a wide range of partition coefficients (Gouliarmou et al., 2012; Pan et al., 2007). Previous studies revealed that humic acids significantly impact desorption of hydrophobic compounds from organic phases into aqueous solutions (Smith et al., 2011; ter Laak et al., 2009). This, however, depends on whether mass transfer is controlled by intraparticle or external film diffusion. The latter may be expressed by two mass-transfer processes in series, an external and an internal one, respectively (Finkel et al., 2016; Grathwohl, 2014). In the present study, we derived a semi-analytical solution of mass transfer between particles and the bulk fluid considering both processes and experimentally validated it with compounds of different hydrophobicity at different concentrations of dissolved organic matter.

IV 2 Materials & Methods

The suppliers of all chemicals and instruments are reported in the supporting information IV 4.3.

IV 2.1 Batch Experiments

Desorption kinetics was studied in batch experiments involving polyethylene spheres pre-loaded with hydrophobic pollutants (phenanthrene, tonalide and benzophenone) with different concentrations of humic acid in aqueous solution. Humic acid solutions were prepared by adding 2 g of a raw humic-acid standard to 1 L ultrapure water containing 2 mM phosphate-buffered saline (PBS) buffer solution leading to a slightly alkaline pH of 7.7 and shaken overnight. Particles were removed by subsequently passing the solution through 1.5 μm, 0.7 μm, and 0.45 μm pore sized filters. To obtain a final concentration of 1 gL^{-1}, the solution was diluted in 2 mM PBS solution. The organic carbon fraction of the dissolved humic acids was 0.41. In the course of the experiments, frequent DOC and pH measurements were performed to control the stability. Blank measurements of DOM solutions revealed that they contained no substances which might distort the measurement of the dissolved pollutants. The polyethylene (PE) spheres were clear particles without dye (density = 0.92 kgL^{-1}) that are usually used as an ingredient of cosmetic products. The particles were approximately spherical shaped and had a diameter of 260 μm. The microplastics were loaded with pollutants by shaking 2 g of them in a 200 mL methanol/water solution (20/80 v/v) for 96 h and adding 80 μg of phenanthrene and 250 μg of tonalide or benzophenone. Chemicals were added one at a time in separate experiments to avoid mixture effects. Methanol was added to decrease the partition coefficients which accelerates loading with hydrophobic compounds. After shaking and sieving with 75 μm mesh, the microplastics were rinsed three times with ultrapure water to prevent pollutants precipitating on the surface during subsequent drying under a gentle nitrogen stream. A subsample of microplastics were extracted afterwards to determine the amount of pollutant uptake in the spheres. The extraction of microplastics was performed with cyclohexane. Analyzed concentrations (± relative standard deviation) in the plastic were 42.8 (± 2.9 %), 124 (± 1.4 %), and 15.8 (± 0.5 %) $\mu g g^{-1}$ of phenanthrene, tonalide, and benzophenone, respectively. Relevant properties of the selected compounds are shown in Table IV 1. The concentration of microplastics in batch experiments was kept constant (1 gL^{-1}) while six different concentrations of humic acids (0, 0.15, 0.25, 0.50, 0.75, 1.00 gL^{-1}) were used. We added 0.25 g microplastics, loaded with the contaminants, to 250 mL of contaminant-free aqueous solutions in 0.25 L amber glass bottles. To avoid biodegradation as well as photooxidation, we added 0.05 gL^{-1} of NaN_3 and kept the bottles in the dark. The lids were equipped with PTFE seals. The bottles were constantly shaken on a horizontal shaker with rotational speed of 150 rpm and kept in a room constantly tempered to 20 $°C$. We took samples of 1 mL solution in duplicates at 10, 20, 40 min, 1, 2, 4, 8, 24, 48, 96 h, and last sampling after 120, 170, or 240 h and processed them as described below. Due to the sampling procedure, the liquid-to-solid ratio changed less than 10 %, which was neglected in the subsequent analysis of the data since the change is in

the range of the analytical error. As shown later (Figure IV 3), equilibration occurred latest after 8 h. Sorption to glass walls, seals etc. of the batch system was determined in triplicate using a 200 $\mu g L^{-1}$ solution of the pollutants and was found to be smaller than the uncertainty of the GC measurements.

Table IV 1: **Compound-specific properties of the chosen substances.** D_{aq} and D_{PE} are the diffusion coefficients in water and polyethylene, respectively. Data were obtained as specified in the subtext.

parameter	phenanthrene	tonalide	benzophenone
molecular weight[a] $[g\ mol^{-1}]$	178.2	258.2	188.2
molecular volume[a] $[cm^3]$	157.7	280.9	167.5
D_{aq} **after Worch (1993)** $[m^2\ s^{-1}]$	7.6×10^{-10}	6.2×10^{-10}	7.4×10^{-10}
D_{PE} **after Lohmann (2011)** $[m^2\ s^{-1}]$	4.1×10^{-13}	6.7×10^{-15}	3.0×10^{-13}
D_{PE} **after Rusina et al. (2010)** $[m^2\ s^{-1}]$	3.5×10^{-13}	2.8×10^{-14}	2.6×10^{-13}
water solubility[a,b] $[mg\ L^{-1}]$	1.15	1.25	137
melting point[a,c] $[°C]$	99.2	57.0	47.8
subcooled liquid solubility[d] $[mg\ L^{-1}]$	4.2	2.9	260
$\log K_{OW}$[a,b]	4.5	5.7	3.2

a data obtained from ChemSpider database (www.chemspider.com)
b values for tonalide were taken from Balk & Ford (1999)
c values for tonalide were taken from Paasivirta et al. (2002)
d calculated according to Kan & Tomson (1996) and Liu et al. (2013)

IV 2.2 Chemical Analysis

We determined the concentrations of the selected pollutants in the bulk aqueous solution (water including dissolved organic matter) by GC-MS. Samples of 1 mL solution were taken at the described time points using a glass pipette and 10 μL of deuterated internal standard were added. Subsequently the samples were extracted with 400 μL of cyclohexane and analyzed by GC-MS. For separation, a 30 m long dimethylsiloxane-coated capillary column with 0.025 mm inner diameter and 0.25 μm film thickness and helium as carrier gas were used (flow rate 0.7 $mL\ min^{-1}$). The mass-to-charge ratios used for quantification were 105, 178, and 243 for benzophenone, phenanthrene, and tonalide, respectively.

IV 3 Theory

IV 3.1 Equilibrium Partitioning

Linear partitioning of a compound between two phases, here polyethylene (PE) and water, is given as the concentration ratio in equilibrium (i.e. the partition coefficient in Lkg^{-1}):

$$K_{PE-W} = \frac{C_{PE}}{C_W} \text{ in equilibrium} \tag{IV 1}$$

By introducing a second dissolved phase, here humic acids, the chemical has to equilibrate between the three phases in the system and the partition coefficient K^*_{PE-W} between the overall aqueous solution and the solids decreases with increasing concentration $[kgL^{-1}]$ of dissolved organic matter (DOM) is (Schwarzenbach et al., 2005):

$$K^*_{PE-W} = \frac{K_{PE-W}}{1 + K_{DOM} DOM} = \frac{C_{PE}}{C^*_{W,eq}} \tag{IV 2}$$

K_{DOM} is the partition coefficient $[Lkg^{-1}]$ between the dissolved organic matter and pure water. Only if the product $K_{DOM} \times DOM$ becomes larger than unity, a significant change in partitioning of a compound between aqueous solution and solids may be expected. Since DOM contents typically are below 0.001 kgL^{-1}, only compounds with K_{DOM} larger than 1000 are significantly affected. C^*_W represents the concentration in the bulk solution, i.e. the freely dissolved concentration plus the concentration in the DOM phase. Based on the mass balance in the three-phase system, the equilibrium concentration $C^*_{W,eq}$ $[\mu gL^{-1}]$ in the DOM-inclusive aqueous phase for given initial concentration $C_{PE}(0)$ $[\mu gkg^{-1}]$ in the PE and $C^*_W(0)$ $[\mu gL^{-1}]$ in the aqueous phase (in our experiments always zero) can be computed as a function of the liquid-to-solid ratio V_W/m_P $[Lkg^{-1}]$ and via the partition coefficients on the DOM-concentration by:

$$C^*_{W,eq} = \frac{C_{PE}(0) + C^*_W(0)\frac{V_W}{m_P}}{\frac{V_W}{m_P} + K^*_{PE-W}} \tag{IV 3}$$

IV 3.2 Mass Transfer Model

The mass transfer of organic pollutants between the particles and a surrounding bulk solution of finite volume comprises diffusion within the plastic particles and subsequent transfer from the particle surface through an aqueous boundary layer into the bulk solution (Fernandez et al., 2009; Thompson et al., 2015). The slower process controls the overall kinetics. The underlying assumptions for the analysis of our finite-volume batch experiments are: (i) the bulk solution is homogeneously mixed, (ii) the external mass transfer between the particles and the bulk solution is proportional to the difference

of the aqueous (DOM-inclusive) concentrations between the bulk solution and the particle surface, (iii) at the particle surface, local equilibrium between the two phases exists, and (iv) the mass flux within the plastic particles is by diffusion in the polymer. Additionally, we assumed equilibrium partitioning between water and DOM. This conceptual framework is illustrated in Figure IV 1, where we implicitly assume that the contaminant is restricted to the plastic particle with uniform concentration in the initial state.

To consider both internal and external mass transfer in series, we formulate a coupled transport model. Within the plastic particles, we consider the diffusion equation in spherical coordinates:

$$\frac{\partial C_{PE}}{\partial t} - D_{PE}\left[\frac{\partial^2 C_{PE}}{\partial r^2} + \frac{2}{r}\frac{\partial C_{PE}}{\partial r}\right] = 0 \tag{IV 4}$$

$$\left.\frac{\partial C_{PE}}{\partial r}\right|_{r=0} = 0 \ \forall t \tag{IV 5}$$

with a uniform initial concentration

$$C_{PE}(r, t=0) = C_{PE}(0) \ \forall r \tag{IV 6}$$

where D_{PE} $[m^2 s^{-1}]$, r $[m]$, and t $[s]$ denote the diffusion coefficient in PE, the radial coordinate, and time, respectively. C_{PE} $[\mu g\, kg^{-1}]$ is the concentration in the plastic sphere. The mass flux through the external boundary layer must be identical to the internal mass flux at the particle surface:

$$J = -\left(C_W^* - \frac{C_{PE}(r_P)}{K_{PE-W}^*}\right) k_W = -D_{PE}\varrho_{PE}\left.\frac{\partial C_{PE}}{\partial r}\right|_{r=r_P} \tag{IV 7}$$

in which J $[\mu g\ m\ L^{-1}\ s^{-1}]$ and k_W $[ms^{-1}]$ are the mass flux density and the aqueous mass transfer coefficient, respectively. C_W^* $[\mu g L^{-1}]$ denotes the concentration in the bulk solution, r_P is the radius of the spherical particle, and ρ_{PE} $[kg L^{-1}]$ denotes its mass density.

In a finite bath, the concentration in the bulk phase changes according to the total mass flux across the area of all particles, leading to the following balance equation:

$$\frac{dC_W^*}{dt} = \left(\frac{C_{PE}(r_P)}{K_{PE-W}^*} - C_W^*\right) k_W \frac{3}{r_P}\frac{m_P}{V_w \varrho_{PE}} \tag{IV 8}$$

which is subject to a known initial concentration $C_W^*(0)$, where m_P $[kg]$ and V_W $[L]$ denote the mass of particles and the volume of water, respectively. No mass is stored in the aqueous boundary layer.

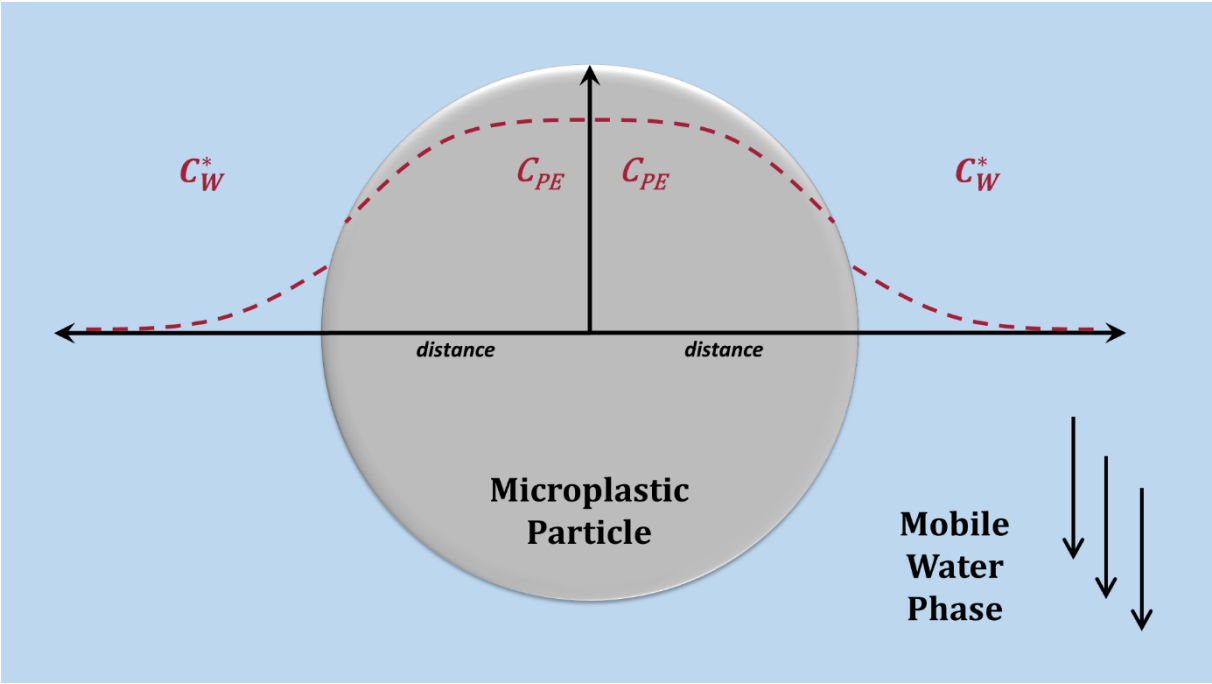

Figure IV 1: **Conceptual framework of the mass transfer model.** A hypothetical concentration profile of a substance is shown. The concentration in the particle decreases from the center to the edge whereas the concentration in water decreases with increasing distance from the particle. C_W^* and C_{PE} denote the concentration in water and particle, respectively. At the interface, local equilibrium is assumed hence the concentration at the interface is: $C_{PE} = K_{PE-W}^* C_W^*$

We derived the analytical solution of equations IV 4-IV 8 after Laplace transformation in time (see Appendix IV 4.3), and consider three cases of mass-transfer controls: (1) by external mass-transfer only, i.e. in the limit of $D_{PE} \to \infty$, (2) by intraparticle diffusion only, i.e. in the limit $k_W \to \infty$, and (3) by both processes. The analytical Laplace-transform solution of the bulk-phase concentration is back-transformed into the time domain by the numerical method of de Hoog et al. (1982), implemented in Matlab.

We fitted the model to the contaminant concentration data in water of the experiments described above. The initial concentrations $C_{PE}(0)$ in the microplastics and $C_W^*(0) = 0$ in the water are known from the experimental set-up as well as liquid-to-solid ratio V_W/m_P , the radius r_P and mass density ρ_{PE} of the spheres. The partition coefficients K_{PE-W} of the three pollutants between PE and the pure water were determined from the late-time concentrations. We assumed that the external mass-transfer coefficient k_W of different pollutants scales with the known aqueous diffusion coefficient by $D_{aq}^{2/3}$ (see Sherwood-relationship in the Appendix IV 4.3), and depends otherwise on the hydrodynamic conditions in the batch (McKay et al., 1986; Ranz et al., 1952), which did not differ among the tests. Then $k_W/D_{aq}^{2/3}$, three values of D_{PE} and three values of K_{DOM} (one for each compound) were the fitting parameters. We fitted all experiments jointly, computing the partition coefficients K_{PE-W}^* for each DOM-concentration by equation IV 2. Note, that the intensity of shaking affects the external mass transfer, but the shaking was kept constant in all experiments of the present study. Thus, the fitted coefficient $k_W/D_{aq}^{2/3}$ is identical for all compounds and needs to be identified by jointly fitting all

experiments. Fitting k_W for each compound individually, would have added more degrees of freedom, and we may not have retrieved the $D_{aq}^{2/3}$-scaling valid for turbulent boundary layers (McKay et al., 1986; Ranz et al., 1952). Log-parameters were estimated using $\mathtt{DREAM}_{ZS}$, a Markov-Chain Monte-Carlo method that estimates distributions of the log-parameters conditioned on the measurements (Laloy & Vrugt, 2012; Vrugt, 2016). A uniform prior distribution within a wide range for each log-parameter was considered. As objective function, we took the sum of the absolute differences between all measurements and simulated values. The computed mean absolute errors (MAE) and root mean square errors (RMSE) as reported in the results are based on a conditional sample size of 3000. Furthermore, we report the 5-95 % quantiles of the estimated parameters to assess their uncertainty.

IV 3.3 Analysis of Characteristic Times

As explained above, overall mass transfer is controlled by an external and an internal process in series. To evaluate the relative importance of the two mass transfer processes, we derived the characteristic time τ_{ch} $[s]$ from our Laplace-transform analytical solution. It is defined as:

$$\tau_{ch} = \frac{\int_0^\infty \left(C_W^*(t) - C_{W,eq}\right) dt}{C_W^*(0) - C_{W,eq}} \tag{IV 9}$$

and summarizes how long equilibration between the bulk solution and the spheres takes. The characteristic time can be split into a characteristic time for the case of external mass transfer:

$$\tau_{ch}^{external} = \frac{K_{PE-W}^* \varrho_{PE} r_P}{\left(1 + K_{PE-W}^* \frac{m_P}{V_W}\right) 3k_W} \tag{IV 10}$$

and a characteristic time for the case of internal mass transfer:

$$\tau_{ch}^{internal} = \frac{r_P^2}{\left(1 + K_{PE-W}^* \frac{m_P}{V_W}\right) 15 D_{PE}} \tag{IV 11}$$

The two characteristic times are additive, i.e. the overall mass transfer is slower than either of the single processes. Note, that for increasing K_{PE-W}^*, the characteristic time in the case of externally controlled mass transfer (equation IV 10) becomes independent of K_{PE-W}^* whereas the characteristic time of the internally controlled mass transfer (equation IV 11) decreases with increasing K_{PE-W}^*. In rivers or lakes, V_W tends to infinity ("infinite bath") and the term in the parentheses of equations IV 10 & IV 11 becomes 1. While in equation IV 10 the characteristic time refers to 63.2 % of the equilibrium concentration achieved, this does not hold for equation IV 10 where the

degree of equilibration depends on the liquid-to-solid ratio and K^*_{PE-W} (see Appendix IV 4.3). Hence, for $K^*_{PE-W} \times {}^{m_P}/_{V_W}$ ranging from 0.01 (infinite bath) to 30 (maximum in our experiments), $\tau_{ch}^{internal}$ corresponds to the timepoint when 67.5 - 88.9 % of the equilibrium concentration has been reached. The relative importance of the respective mass-transfer process for the overall mass transfer can be expressed as the ratio of their characteristic times:

$$\frac{\tau_{ch}^{external}}{\tau_{ch}^{internal}} = \frac{5K^*_{PE-W}\varrho_{PE}D_{PE}}{k_W r_P} \tag{IV 12}$$

For values >1 , the mass transfer in the water is limiting, whereas mass transfer in the particles controls kinetics for values <1. Equation IV 12 exemplifies that the relative importance of the two mass-transfer processes does not depend on the liquid-to-solid ratio. Mass transfer of hydrophobic substances with high partition coefficients are externally limited. Furthermore, equation IV 11 shows that for internally limited kinetics a decreasing partition coefficient slows down kinetics in a batch system despite increasing the equilibrium concentration in the water (equation IV 3).

IV 4 Results & Discussion

IV 4.1 Equilibrium Partitioning

Figure IV 2 (top) shows the measured equilibrium concentrations in the aqueous phase as function of the DOM concentration in the respective batches. The concentration in water increases with increasing DOM as expected from equation IV 3. Figure IV 2 shows the calculated partition coefficients between PE and the aqueous solution K^*_{PE-W} as function of the DOM concentration. We fixed the measured K^*_{PE-W} for zero DOM and calculated K^*_{PE-W} as a function of DOM according to equation IV 2 within the joint fit of all experiments. Figure IV 2 (bottom) shows that K^*_{PE-W} predicted with equation IV 2 matches measured values very well. The measured K^*_{PE-W}-values increase with increasing octanol-water partition coefficient K_{OW} of the compounds as expected. Measured and calculated partition coefficients into humic acid (K_{DOM}) for phenanthrene and tonalide show good agreement whereas the partition coefficients for benzophenone show relatively large deviations, which we attribute to the insignificant influence of DOM. Under equilibrium conditions, increasing the DOM concentration caused the fraction of pollutants remaining in the microplastics to decrease.

Table IV 2 lists the fitted K_{DOM}-values, together with their uncertainty range, for every substance and the associated K_{DOC}-values in which the humic acid concentrations are normalized with respect to the fraction of organic carbon (0.41). Table IV 2 also includes two metrics of the quality of the model fits for each compound: the mean absolute error (MAE), and the root mean square error (RMSE). All obtained K_{DOC}-values are in good agreement with literature values (Careghini et al., 2015; Neale et al., 2011; Niederer et al., 2007; Ternes et al., 2004). Possible sorption of DOM on/in microplastics could furthermore alter both the sorption behavior of certain compounds

and the sorption properties of the particles themselves (Kaiser & Zech, 1998; Sun et al., 2008). However, we performed fluorescence measurements with DOM and different amounts of microplastics indicating that no sorption occurred. These results are confirmed by previous findings reporting that interactions between DOM and soil particles mainly took place between DOM and the mineral phase and that interactions between humic acids and PE were found to be negligible, respectively (Kaiser & Zech, 1998; Wu et al., 2016).

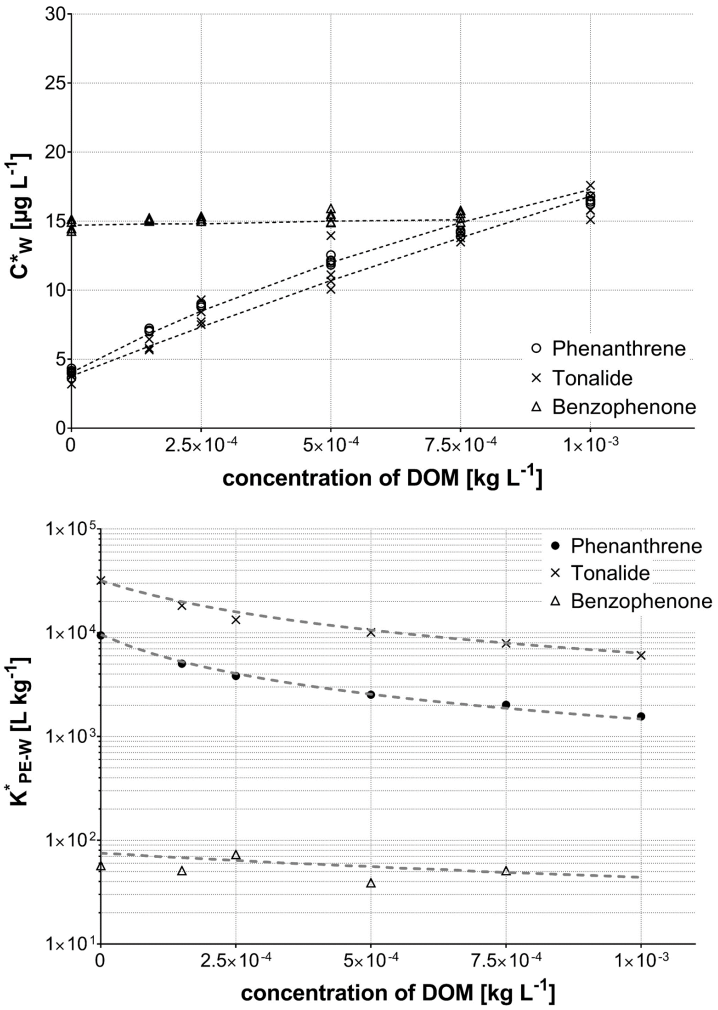

Figure IV 2: **Measured equilibrium concentrations in the aqueous phase.** Concentrations are plotted against the concentration of DOM in the batch (top) and relationships between partition coefficientsK^*_{PE-W} and the concentration of DOM in the solution (bottom). Dashed lines are calculated by equation IV 3 and equation IV 2 (bottom) based on values reported in Table IV 2.

IV 4.2 Desorption Kinetics

We analyzed desorption kinetics by fitting the complete coupled model described above. Figure IV 3 shows the measured concentration time series and model results of the fitted complete model (blue solid lines), model predictions considering only external mass

transfer using the parameters of the complete model (red dashed line), and predictions considering only intraparticle diffusion (green dashed lines). Equilibrium in the batches was usually reached at latest after 8 h. Table IV 2 contains the estimated values of the mass transfer coefficients and the intraparticle diffusion coefficient as well as the ranges of their 5-95% quantiles.

Table IV 2: **Partitioning and mass transfer parameters.** Mean absolute errors (MAE) and root mean square errors (RMSE) were calculated based on the variability of the experimental data. K_{DOM}, k_W, and D_{PE} were fitted within the model (geometric means of the posterior distribution). K_{DOC} was subsequently calculated from the 41.2% of OC in the DOM. The estimated values are reported together with their respective 5-95% quantiles (range).

parameter	phenanthrene	tonalide	benzophenone
MAE $[\mu g\ L^{-1}]$	0.47	0.81	0.34
RMSE $[\mu g\ L^{-1}]$	0.61	1.15	0.38
$\mathbf{K_{PE-W}}$ $[L\ kg^{-1}]$	9,630	31,8000	75
$\mathbf{K_{DOM}}$ $[L\ kg^{-1}]$	5,500	4,000	700
range	5,200-5,800	3,700-4,300	100-3,000
$\mathbf{K_{DOC}}$ $[L\ kg^{-1}]$	13,400	10,000	1,700
range	12,500-14,100	9,100-10,400	200-7,100
$\mathbf{k_W}$ $[m\ s^{-1}]$	7.2×10^{-5}	6.3×10^{-5}	7.0×10^{-5}
range	$5.6-9.4\times10^{-5}$	$5.0-8.3\times10^{-5}$	$5.5-9.3\times10^{-5}$
$\mathbf{D_{PE}}$ $[m^2\ s^{-1}]$	1.6×10^{-13}	5.6×10^{-13}	1.7×10^{-12}
range	$1.3-1.9\times10^{-13}$	$0.1-5.4\times10^{-12}$	$1.5-1.9\times10^{-12}$

Phenanthrene

Figure IV 3A shows an excellent agreement between experimental and simulation results for phenanthrene. At very early times, experimental data are lacking. At these times, the model shows that external mass transfer always controls the overall mass transfer. At later times, intraparticle diffusion becomes limiting. At zero or small DOM concentrations, the relative importance of external mass transfer is larger than at high DOM concentrations. With increasing DOM concentrations K^*_{PE-W} decreases and this shifts mass transfer control to intraparticle diffusion and slows down release kinetics in the batch system, which is predicted by equation IV 11. The good agreement between the model jointly fitted over all DOM concentrations and the measurements indicates that dominant mechanisms are captured well by the model.

Tonalide

Figure IV 3B shows the experimental and simulation results for the comparably hydrophobic compound tonalide. Here, the kinetics are strongly controlled by the external mass transfer for all DOM concentrations. Only at the highest DOM concentrations, the full model and the model disregarding intraparticle diffusion start to deviate slightly. Compared to phenanthrene and benzophenone, the equilibrium concentration in the aqueous phase is the lowest, which is in accordance with the higher hydrophobicity. K_{DOM} is lower than expected from hydrophobicity which may be due to less specific interactions compared to the highly aromatic phenanthrene. As explained above, the data are not sensitive to intraparticle diffusion, which results in a high uncertainty in the fitted intraparticle diffusion coefficient D_{PE} (Table IV 2).

Benzophenone

Figure IV 3C shows the experimental and simulation results for the least hydrophobic compound investigated in this study, benzophenone. In comparison to the other compounds, it has the highest equilibrium concentration in the aqueous phase. The fraction of benzophenone remaining in the microplastics after equilibration ranged from only 6 % (without any DOM) to less than 3 % (for the three highest DOM concentrations). The effects of DOM on desorption of benzophenone are negligible so that the fitted K_{DOM}-values are extremely uncertain. Desorption kinetics are always controlled by intraparticle diffusion, and the associated diffusion coefficient D_{PE} is fairly certain. However, the estimated value is about one order of magnitude larger than values calculated from empirical relationships (see Table IV 1).

While comparable studies indicated that increasing the DOM concentration generally accelerates mass-transfer kinetics, we found the opposite in the batch system. This apparent contradiction is explained by different boundary conditions (different liquid-to-solid ratios, finite bath vs. infinite bath) and the use of different polymers (Smith et al., 2011; ter Laak et al., 2009). Note, that increasing DOM accelerates the external mass transfer in the infinite bath and slows it down slightly in the finite bath (Figure IV 4). Since the diffusion coefficients of DOM are a factor of two to three lower than for our compounds mass transfer changes would be less pronounced if a large fraction partitions into DOM (Cornel et al., 1986). In our study this would, if at all, affect tonalide at high DOM concentrations. However, the data and model do not show any significant influence of DOM and hence we did not specifically account for this effect. Regarding mass transfer under field conditions, studies on passive sampling indicated that it is usually clearly limited by external mass transfer, for compounds with K_{PE-W} values similar to or higher than for phenanthrene (Lampert et al., 2015; Tcaciuc et al., 2015). Such passive samplers are frequently made of PE but are far thinner than the spheres used in our study so that intraparticle diffusion is less restrictive because of shorter diffusion distances (Lohmann, 2011). Only a limited number of studies indicated that intraparticle diffusion might be important for assessing the vector function of microplastics (Fries & Zarfl, 2012). Koelmans et al. (2013) investigated the role of

surfactants and organic matter on desorption kinetics, concluding that the internal mass transfer might typically be the rate limiting process. While the latter authors modeled the kinetics by two first-order mass-exchange processes in series, we considered true intraparticle diffusion. Both our model and the experimental findings suggest that intraparticle diffusion is not permanently controlling the kinetics. However, Koelmans et al. (2013) applied their model to larger particles with diameters of 0.4 and 1.3 mm which might explain this contrast since internal mass transfer times becomes more relevant with increasing particle size.

Other polymers such as polystyrene (PS), polyvinyl chloride (PVC), and polyamide (PA) have glass transition temperatures $>50\ °C$ which are much higher than in polyethylene (-78 $°C$) and thus smaller diffusion coefficients (George & Thomas, 2001; Cowie & McEwen, 1977). Therefore, we expect that diffusion coefficients of organic compounds are lower within PS, PVC, and PA than in PE, so that the intraparticle diffusion may be more restrictive in the overall mass-transfer process. Furthermore, for porous (as PS) or weathered particles the effective diffusion coefficient needs to be derived for each individual case. On the other hand, diffusion in polydimethylsiloxane (PDMS), which is frequently used as a passive sampler, is much faster and hence mass transfer is often controlled by external mass transfer (Rusina et al., 2010). Often thin PDMS fibers are used (i.e. diameters of 6.5 μm, (ter Laak et al., 2009)) which also favors external mass transfer control.

Finally, DOM concentrations used in the batch experiments are higher than concentrations usually found in rivers or lakes. High DOM-concentrations are more likely for (urban) wastewater which are also hotspots for organic contaminants and microplastics (Murphy et al., 2016; Rule et al., 2006). Since sorption and desorption kinetics are equal, the mass transfer under high DOM conditions can be used to estimate the loading of microplastics with contaminants in wastewater whereas the results from experiments without or with low DOM concentrations can be applied to assess the microplastics-facilitated transport of pollutants in large aquatic ecosystems (rivers and lakes). The equilibration times would increase under field conditions where the volume-to-solids ratio approaches infinity (and become independent on K^*_{PE-W} for intraparticle diffusion, but increase with increasing K^*_{PE-W} for external mass transfer control).

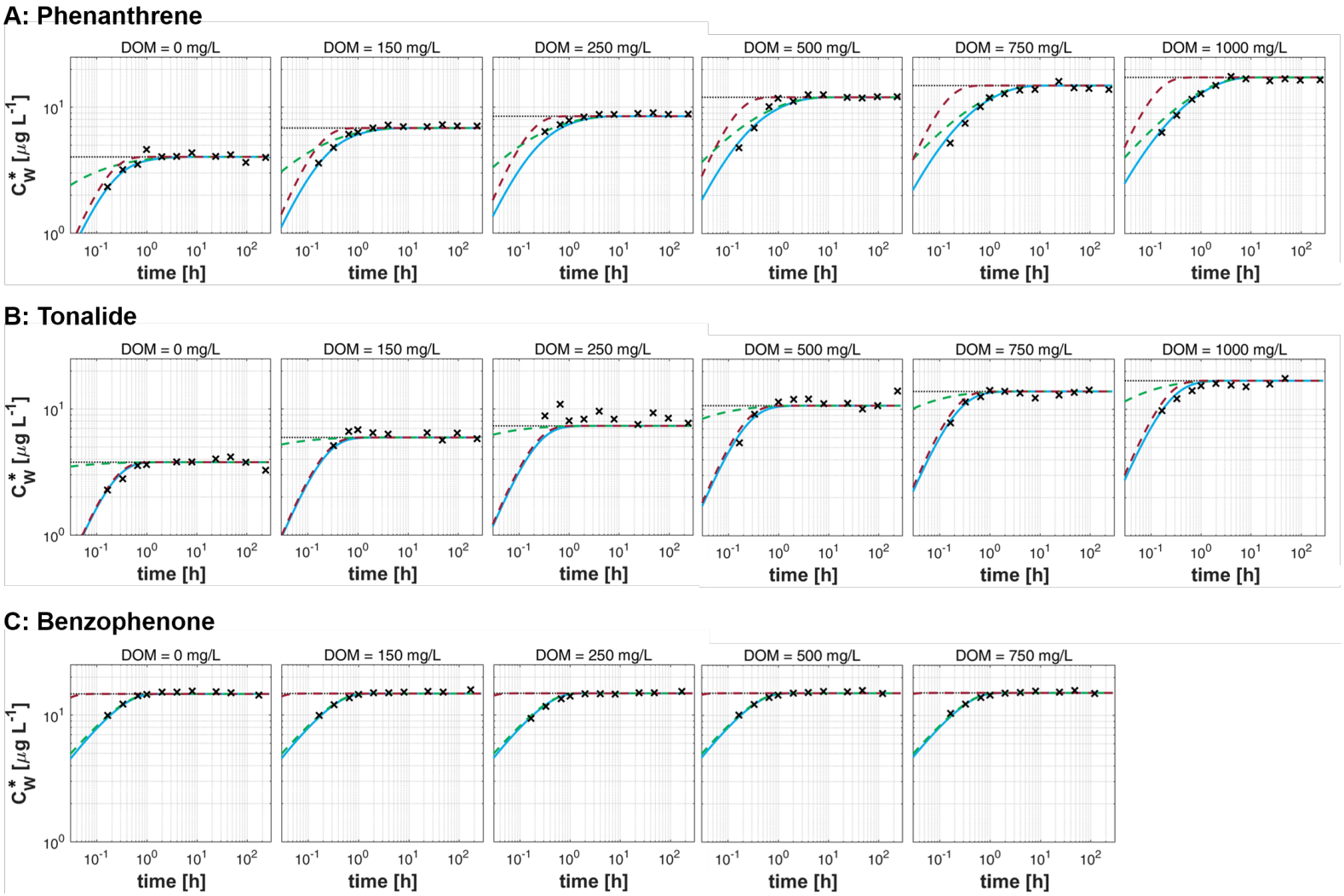

Figure IV 3: **Desorption kinetics of, phenanthrene (A), tonalide (B), and benzophenone (C) from microplastics at different DOM contents.** Models for film diffusion, intraparticle diffusion, and the coupled diffusion are shown with the red dashed, the green dashed, and the solid blue line, respectively. The horizontal black dotted line shows the equilibrium concentration.

IV 4.3 Mass Transfer Analysis and Implications

While the experimental data reflect the specific conditions of the analyzed batch system, the model can be applied to different conditions from a finite bath with high solid-to-liquid ratio to the infinite bath in which particles are strongly diluted. In the experiments, we could show how differences in effective partition coefficient alter not only sorption equilibrium but also the mass-transfer kinetics. In this section, we use the calibrated model to explore conditions which are more comparable to the field. We do this by means of the characteristic times, computed by equations IV 9-IV 11, spanning wide ranges of effective partition coefficients K^*_{PE-W} and solid-to-liquid ratios m_P/V_W. Figure 4 shows the corresponding characteristic times, keeping the diffusion coefficients constant. While Figures 4C and 4D show the individual contributions of internal and external mass transfer to the characteristic time according to equations IV 11 and IV 10, respectively, Figure IV 4A shows the total characteristic time of mass transfer (equation IV 9), and Figure IV 4B the ratio of the two times (equation IV 12). At high m_P/V_W ratios, overall mass-transfer kinetics are accelerated with increasing K^*_{PE-W}, whereas they are slowed down at very low m_P/V_W ratios, and approach infinite bath conditions. Under finite bath conditions, a decreasing effective partition coefficient increases the characteristic time $\tau_{ch}^{internal}$ of internal mass transfer while that of external mass transfer $\tau_{ch}^{external}$ is hardly affected when considering strongly sorbing compounds (Figure IV 4, C and D). We manipulated the effective partition coefficient K^*_{PE-W} in our experiments by adding DOM, thus covering a wide range of kinetics limited by both internal and external mass transfer. Nevertheless, the microplastic concentration used in our study was considerably higher than values found in the environment. Mintenig et al. (2017) sampled effluents of wastewater treatment plants and identified and quantified microplastics down to a size of 20 μm. Using a microplastics concentration of 9×10^3 particles m^{-3} as it was detected in the effluent of a wastewater treatment plant in Germany and assuming that a quarter of these particles might be PE with a radius comparable to that of the particles used in our study (Mintenig et al., 2017), we estimate environmentally relevant PE concentrations in urban areas on the order of $1.7\times10^{-8} kg L^{-1}$ and correspond to infinite bath conditions. We further assume partition coefficients as assembled for various organic pollutants in the literature (Lohmann, 2011), resulting in the parameter range indicated by the red dashed line in Figure IV 4. Applying such m_P/V_W ratio, characteristic times of mass transfer may range between hours (for compounds with low partition coefficients: intraparticle diffusion limits) and weeks (for those with high partition coefficients external mass transfer limits).

As discussed above, the relative importance of internal and external mass transfer does not depend on the solid-to-liquid ratio, improving the transferability from experimental lab conditions to the field. However, it may depend on particle size (which can easily be measured) and on the mass-transfer constant k_W, which depends on the strength of turbulence in rivers. The exact expression of mass transfer depend on the shape of the particles and can be derived for other geometric forms. The qualitative findings on the relative importance of external and internal mass transfer are not affected by the shape. Furthermore, microplastics may be covered with biofilms affecting the external mass transfer (Wu et al., 2017). Since the effective diffusion in biofilms is slower than in

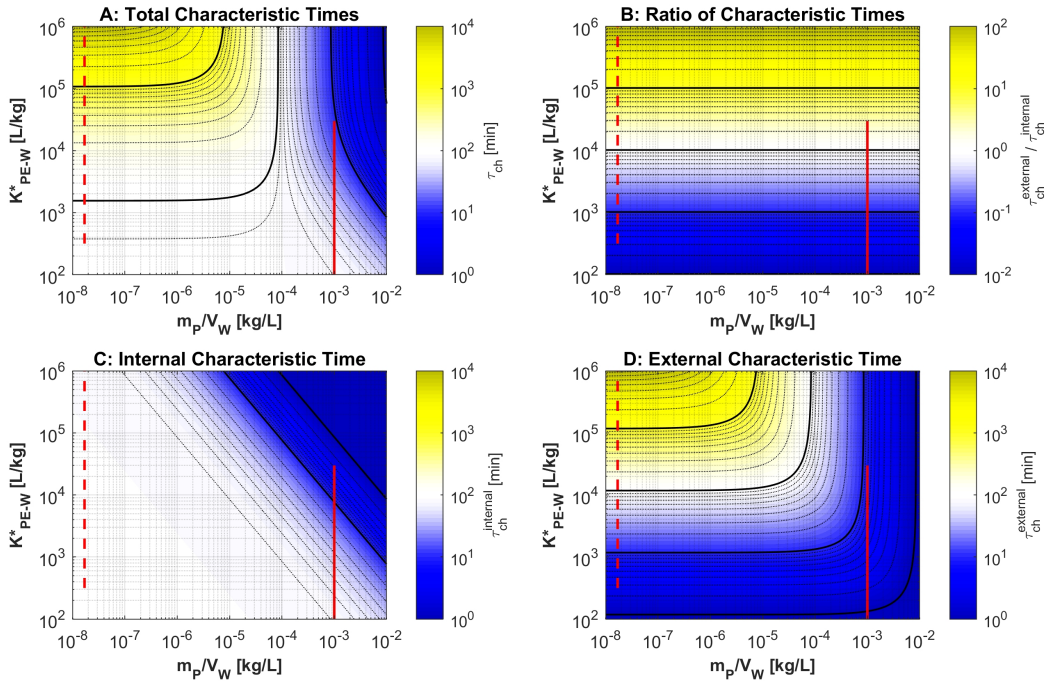

Figure IV 4: **Characteristic times of mass transfer as function of the solid-to-liquid ratio m_P/V_W and the partition coefficient K^*_{PE-W}.** A: total characteristic time; B: ratio of external to internal characteristic time; C: internal characteristic time; D: external characteristic time of mass transfer. The solid red line shows the range of experimental conditions while the dashed red line refers to microplastics concentrations found in the environment (Mintenig et al., 2017). Solid-to-liquid ratios of suspended sediments in rivers typically range from $10^{-5} - 10^{-3}\ kgL^{-1}$ (Schwientek et al., 2013).

water, the external mass transfer would be slowed down. To consider this, diffusive mass transfer through the biolayer could explicitly be modelled. The thickness of the water boundary layer in our experiments was in the range of 10 μm and hence the external mass transfer may be substantially slowed down if the biofilm cover exceeds a certain thickness or density. A reliable model on this, however, requires more experimental data, in particular on diffusion coefficients in biofilms and biofilm-plastic partitioning.

The theoretical considerations of our study also apply to other suspended particles such as suspended sediments in rivers where the solid-to-liquid ratio is typically in the range of 10^{-5} to $10^{-3}\ kgL^{-1}$ (which corresponds to our laboratory conditions) (Schwientek et al., 2013). Well-defined microplastic particles, as used here, are ideally suited for mass transfer studies under controlled conditions but ultimately are only surrogates for particles occurring in the environment, including microplastics in urban runoff and contaminated sediment particles. The latter are very likely much more frequent than microplastics but undergo the same mass transfer characteristics as discussed in this study.

A IV
Supporting Information to Paper IV

Suppliers of Chemicals and Instruments

Solvents and Standards

As organic solvents cyclohexane, acetone, methanol, and acetonitrile were used which were all purchased from Merck Millipore (Darmstadt, Germany) in a GC gradient grade purity. Ultrapure water was prepared with a Milli-Q water purification system (Merck Millipore, Darmstadt, Germany) leading to a resistivity of 18.2 $M\Omega cm$. A standard of benzophenone (CAS# 119-61-9, purity ≥ 99.5%) as well as deuterated standards of phenanthrene (D_{10}), benzophenone (D_{10}), and 4-n-nonylphenol (D_8) were purchased from LGC Standards (Wesel, Germany). Standards of phenanthrene (CAS# 85-01-8, purity ≥ 99.5%) and tonalide (CAS# 21145-77-7, purity ≥ 97%) were purchased from Sigma-Aldrich Supelco (Bellefonte, PA, USA) and Fluka (Honeywell Chemicals, Seelze, Germany), respectively. Humic acid (CAS# 1415-93-6) was purchased from Sigma-Aldrich Supelco (Bellefonte, PA, USA). For preparing a dissolved organic matter (DOM) stock solution, 2 g of the raw humic acid were dissolved in 1 L of 2 mM phosphate-buffered saline (PBS) buffer solution (containing 137 mM NaCl, 2.7 mM KCl, 8 mM Na_2HPO_4, and 2 mM KH_2PO_4) with slightly alkaline pH of 7.7 and shaken overnight. Due to the alkaline conditions almost complete dissolution of HA was achieved. To remove particulate HA, the solution was passed subsequently through 1.5 μm, 0.7 μm, and 0.45 μm pore sized filters (Whatman 934-AH, Fisherbrand MF 300, and Whatman ME 25, respectively). To obtain a final concentration of 1 g L-1, the solution was diluted in 2 mM PBS solution. Microplastics (MP) were provided by Azelis (Moers, Germany) under the trade name Gotalene 120 (clear particles without dye, density=0.92 $kg\ L^{-1}$) and are usually used as an ingredient of cosmetic products. Information provided by the supplier were confirmed by visual measurements and showed that the particle diameter is 260 μm and that they are approximately spherical shaped.

Devices and Auxiliaries

The dissolved organic carbon (DOC) content was quantified with an elemental analyzer (Elementar vario TOC cube, Elementar Analysensysteme, Langenselbold, Germany) resulting in an organic carbon fraction of 0.41. Experiments were performed in 0.25 L amber glass bottles (Duran, Borosilicate glass, Wertheim, Germany, 250 mL water and 0.25 g MP). The concentrations of selected pollutants in the solution, i.e. in aqueous solution (water including DOM) were determined with GC-MS. Samples of 1 mL solution were taken at the described time points using a glass pipette. 10 μL of deuterated internal standard (20 $\mu g\ mL^{-1}$ either in acetone or acetonitrile) were added

to the sample. Subsequently the samples were extracted with 400 μL of cyclohexane. Measurements were performed using an Agilent 6890 N GC equipped with an Agilent 7683 B Autosampler and coupled to an Agilent 5973 inert MS. For separation, a J&W Scientific DB-5MS column (dimethylsiloxane 30 m x 0.025 mm ID, 0.25 μm film thickness) and helium as carrier gas were used. The flow rate was 0.7 $mL\ min^{-1}$ and the device was operated in a pulsed splitless injection mode. The mass-to-charge ratios used for quantification were 105, 178, and 243 for benzophenone, phenanthrene, and tonalide, respectively.

DOM Fluorescence Measurements

The freely dissolved DOM concentration in the water phase can be analyzed via fluorescence measurements. The DOM solution was prepared as described above and in the main article. The absorbance was measured with an UV-Vis spectrometer at a wavelength of 254 nm using quartz cuvettes. Stepwise, the solution was diluted until an absorbance value of 0.3 was reached. Subsequently a fluorescence spectrum was taken to obtain the maximum of excitation and emission wavelengths as shown in Figure IV A1.

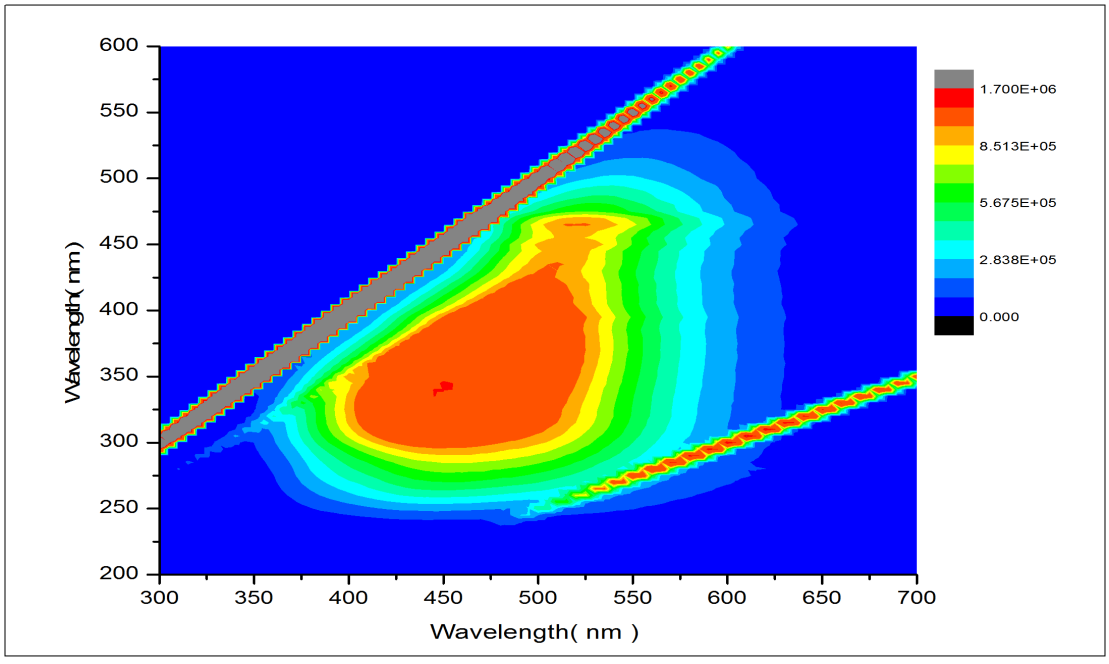

Figure IV A1: **Fluorescence spectrum of DOM solution.**

20 mL of DOM solution was added to 20 mL vials. Different amounts of microplastics (0, 5, 10, 15 mg) were mixed in 20 mL solution. Vials were shaken for 48 h and afterwards a subsample was analyzed with a single point measurement using the obtained excitation and emission wavelength. The change in intensity relative to the intensity without the influence of MP were 0.07%, 0.03%, and 0.12% for 5, 10, and 15

mg of MP, respectively. These values underline the assumption that an interaction between MP ans DOM is negligible. This is confirmed by previous findings reporting that DOM in soils mainly interacted with the mineral phase (Kaiser & Zech, 1998)) and that interactions between humic acid and PE particles were found to be negligible (Wu et al. (2016)).

Laplace-Transform Solution of Mass Transfer from a Mixed Reactor to Spheres Considering Intraparticle Diffusion and an Aqueous Boundary Layer

Governing Equations

We consider diffusion in a sphere made of polyethylene (PE). D_{PE} is the diffusion coefficient in the sphere, r denotes the radial coordinate, r_P is the radius of the sphere, t is time, and $C_{PE}(r,t)$ is the concentration in the PE-particle. In the initial state, the concentration within the sphere is uniform, $C_{PE}(0)$. The concentration at the surface of the sphere is in local equilibrium to the aqueous concentration at the sphere surface $C_{aq}(r_P,t)$. Then, the governing equations read as:

$$\frac{\partial C_{PE}}{\partial t} - D_{PE}\left(\frac{\partial^2 C_{PE}}{\partial r^2} + \frac{2}{r}\frac{\partial C_{PE}}{\partial r}\right) = 0 \tag{IV A1}$$

$$C_{PE}(r_P,t) = K_{PE-W} C_{aq}(r_P,t)\ \forall t \tag{IV A2}$$

$$\left.\frac{\partial C_{PE}}{\partial r}\right|_{r=0} = 0\ \forall t \tag{IV A3}$$

$$C_{PE}(r,t=0) = C_{PE}(0)\ \forall r \tag{IV A4}$$

in which K_{PE-W} is the dimensional partition coefficient (mass-related concentration in PE divided by volumetric concentration in water at equilibrium).

The particle exchanges solute mass with a bulk solution of finite volume V_w via an aqueous boundary layer. We assume that the boundary layer itself does not store solute mass. Mass transfer through the boundary layer is driven by the concentration difference between the bulk solution and the aqueous concentration at the surface of the spheres: Then, the continuity of mass fluxes requires:

$$J(t) = -\left(C_W^*(t) - C_{aq}(r_P,t)\right) k_W = -D_{PE}\,\varrho_{PE}\left.\frac{\partial C_{PE}}{\partial r}\right|_{r=r_P} \tag{IV A5}$$

in which J is the mass-flux density, C_W^* is the bulk phase concentration, and k_W is the mass-transfer velocity. Multiplication by the mass density ϱ_{PE} of the spheres on the right-hand side of the equation is needed if the concentration in the spheres is expressed as mass of the compound per mass of the sphere material.

Next we perform the mass balance in the bulk phase:

$$\begin{aligned}\frac{dC_W^*}{dt} &= JA_{sp}\frac{n_{sp}}{V_w} \\ &= \left(C_{aq}(r_P,t) - C_W^*(t)\right) k_W 4\pi r_P^2 \frac{n_{sp}}{V_w}\end{aligned} \tag{IV A6}$$

in which $A_{sp} = 4\pi r_P^2$ is the surface area of an individual sphere, n_{sp} denotes the number of spheres, and V_w is the volume of water. The number of spheres can be estimated from the mass m_P of all spheres, the mass density ϱ_{PE} of the sphere material, and the volume of a single sphere V_{sp}^{single}:

$$n_{sp} = \frac{m_P}{\varrho_{PE} V_{sp}^{single}} = \frac{m_P}{\varrho_{PE}\frac{4\pi}{3}r_P^3} \tag{IV A7}$$

Substitution into Eq. (IV A6) yields:

$$\frac{dC_W^*}{dt} = \left(C_{aq}(r_P,t) - C_W^*(t)\right) k_W \frac{3}{m_P}\frac{r_P}{V_W \varrho_{PE}} \tag{IV A8}$$

with the initial value $C_W^*(0)$. Eqs. (IV A1-IV A5 & IV A8) define the problem statement.

Solution in the Laplace Domain

Laplace transformation of Eqs. (IV A1-IV A3) yields:

$$s\tilde{C}_{PE} - C_{PE}(0) - D_{PE}\left(\frac{d^2\tilde{C}_{PE}}{dr^2} + \frac{2}{r}\frac{d\tilde{C}_{PE}}{dr}\right) = 0 \tag{IV A9}$$

$$\tilde{C}_{PE}(r_P) = K_{PE-W}\tilde{C}_{aq}(r_P) \tag{IV A10}$$

$$\left.\frac{\partial\tilde{C}_{PE}}{\partial r}\right|_{r=0} = 0 \tag{IV A11}$$

in which variable symbols with a tilde are Laplace transforms, and s is the complex Laplace coordinate. The solution of this second-order linear differential equation for the given boundary conditions is:

$$\tilde{C}_{PE}(r,s) = \frac{r_P}{r}\frac{\sinh\left(r\sqrt{\frac{s}{D_{PE}}}\right)}{\sinh\left(r_P\sqrt{\frac{s}{D_{PE}}}\right)}\left(K_{PE-W}\tilde{C}_{aq}(r_P) - \frac{C_{PE}(0)}{s}\right) \tag{IV A12}$$

The radial derivative of C_{PE} at the surface reads in the Laplace domain as:

$$\left.\frac{d\tilde{C}_{PE}}{dr}\right|_{r=r_P} = \left(\sqrt{\frac{s}{D_{PE}}}\coth\left(r_P\sqrt{\frac{s}{D_{PE}}}\right) - \frac{1}{r_P}\right)\left(K_{PE-W}\tilde{C}_{aq}(r_P) - \frac{C_{PE}(0)}{s}\right) \tag{IV A13}$$

Eq. (IV A5), expressing the continuity of fluxes at the sphere surface, becomes in the

Laplace domain:

$$\left(\tilde{C}_W^* - \tilde{C}_{aq}(r_P)\right) k_W = \varrho_{PE} \left(\sqrt{D_{PE} s} \coth\left(r_P \sqrt{\frac{s}{D_{PE}}}\right) - \frac{D_{PE}}{r_P}\right) \left(K_{PE-W} \tilde{C}_{aq}(r_P) - \frac{C_{PE}(0)}{s}\right) \tag{IV A14}$$

which leads to the Laplace-transformed concentration in the aqueous phase at the sphere surface as function of the initial concentration within the sphere $C_{PE}(0)$ and the Laplace-transformed bulk concentration $\tilde{C}_W^*$:

$$\tilde{C}_{aq}(r_P) = \frac{k_W \tilde{C}_W^* + \left(\sqrt{D_{PE} s} \coth\left(r_P \sqrt{\frac{s}{D_{PE}}}\right) - \frac{D_{PE}}{r_P}\right) \varrho_{PE} \frac{c_{PE}(0)}{s}}{k_W + \left(\sqrt{D_{PE} s} \coth\left(r_P \sqrt{\frac{s}{D_{PE}}}\right) - \frac{D_{PE}}{r_P}\right) \varrho_{PE} K_{PE-W}} \tag{IV A15}$$

Laplace transformation of the mass-balance equation (IV A8) in the bulk phase yields:

$$s\tilde{C}_W^* - C_W^*(0) \quad = \quad \left(\tilde{C}_{aq}(r_P) - \tilde{C}_W^*\right) k_W \frac{3}{r_P} \frac{m_P}{V_W \varrho_{PE}} \tag{IV A16}$$

Substituting Eq. (IV A15) into Eq. (IV A16) and rearranging terms finally yields:

$$\begin{aligned} \tilde{C}_W^* &= \frac{C_W^*(0) + \frac{a}{K_{PE-W}} \frac{C_{PE}(0)}{s}}{a + s} \\ \text{with } a &= \frac{\left(\sqrt{D_{PE} s} \coth\left(r_P \sqrt{\frac{s}{D_{PE}}}\right) - \frac{D_{PE}}{r_P}\right)}{k_W + \left(\sqrt{D_{PE} s} \coth\left(r_P \sqrt{\frac{s}{D_{PE}}}\right) - \frac{D_{PE}}{r_P}\right) \varrho_{PE} K_{PE-W}} k_W \frac{3}{r_P} K_{PE-W} \frac{m_P}{V_W} \end{aligned} \tag{IV A17}$$

We may consider two limiting cases:

1. $\lim k_W \to \infty$: This describes case with a negligible aqueous boundary layer. Here, the expression in the denominator of Eq. (IV A17) approaches k_W, which cancels with the k_W in the nominator, resulting in:

$$\begin{aligned} \tilde{C}_W^* &= \frac{C_W^*(0) + \frac{a_{particle}}{K_{PE-W}} \frac{C_{PE}(0)}{s}}{a_{particle} + s} \\ \text{with } a_{particle} &= \left(\sqrt{D_{PE} s} \coth\left(r_P \sqrt{\frac{s}{D_{PE}}}\right) - \frac{D_{PE}}{r_P}\right) \frac{3}{R} K_{PE-W} \frac{m_P}{V_W} \end{aligned} \tag{IV A18}$$

2. $\lim D_{PE} \to \infty$: This describes the case of a well mixed sphere, in which the aqueous boundary layer forms the only resistance to mass transfer:

$$\begin{aligned} \tilde{C}_W^* &= \frac{C_W^*(0) + \frac{a_{film}}{K_{PE_W}} \frac{C_{PE}(0)}{s}}{a_{film} + s} \\ \text{with } a_{film} &= \frac{K_{PE_W} k_W \frac{m_P}{V_W}}{k_W + \frac{1}{3} r_P s \varrho_{PE} K_{PE-W}} s \end{aligned} \tag{IV A19}$$

Back-transformation into the time-domain is non-trivial with the exception of the case controlled by the aqueous boundary layer only, where the analytical expression is an exponential function. We perform numerical back-transformation using the method of de Hoog et al. (1982), implemented in Matlab.

Characteristic Times of Mass Transfer

The concentrations in the large-time limit are:

$$C_W^{*\infty} = \frac{C_W^*(0) + \frac{m_P}{V_W} C_{PE}(0)}{1 + \frac{m_P}{V_W} K_{PE-W}} \tag{IV A20}$$

$$C_{PE}^{\infty} = K_{PE-W} C_W^{*\infty} \tag{IV A21}$$

We now consider the deviation from the large-time limit:

$$C_W'^*(t) = C_W^*(t) - C_W^{*\infty} \tag{IV A22}$$

and define the characteristic time τ_{ch} as the integral scale of the concentration signal, that is, the integral of $C_W'^*(t)$ over time divided by the initial value:

$$\tau_{ch} = \frac{\int_0^\infty C_W'^*(t)dt}{C_W'^*(0)} = \frac{\lim_{s\to 0} \tilde{C}_W'^*(s)}{C_W'^*(0)} \tag{IV A23}$$

in which the initial deviation $C_W'^*(0)$ is:

$$C_W'^*(0) = \frac{\frac{m_P}{V_W}}{1 + \frac{m_P}{V_W} K_{PE-W}} \left(K_{PE-W} C_W^*(0) - C_{PE}(0) \right) \tag{IV A24}$$

Figure IV A2 visualizes the concept of the characteristic time. The curve $C_W'^*(t)/C_W'^*(0)$ is characterized by a rectangle from zero to τ_{ch} with unit height that has the same integral as the curve $C_W'^*(t)/C_W'^*(0)$. This is neither an early-time nor a late-time approximation of mass transfer, but characterizes the entire curve.

Eq. (IV A22) reads in the Laplace domain:

$$\tilde{C}_W'^* = \tilde{C}_W^* - \frac{C_W^{*\infty}}{s} \tag{IV A25}$$

with $\tilde{C}_W$ given in Eq. (IV A17) and C_W^∞ given in Eq. (IV A20). As stated in Eq. (IV A23), we need the limit of $\tilde{C}_W'^*(s)$ at $s \to 0$. In order to perform this evaluation, we need the following series expansion of the hyperbolic cotangens:

$$\lim_{x\to 0} \coth(x) = \frac{1}{x} + \frac{x}{3} - \frac{x^3}{45} \tag{IV A26}$$

Making use of Eq. (IV A26), substituting Eqs. (IV A17 & IV A20) into Eq. (IV A23) and rearranging terms finally leads to:

$$\tau_{ch} = \frac{\varrho_{PE} K_{PE-W} \frac{r_P}{3k_W} + \frac{r_P^2}{15 D_{PE}}}{1 + K_{PE-W} \frac{m_P}{V_W}} \tag{IV A27}$$

which can be interpreted as the sum of two characteristic times $\tau_{ch}^{external}$ and $\tau_{ch}^{internal}$ for the cases with a perfectly mixed sphere and without film, respectively:

$$\tau_{ch}^{external} = \frac{\varrho_{PE} K_{PE-W}}{\left(1 + K_{PE-W} \frac{m_P}{V_W}\right)} \cdot \frac{r_P}{3k_W} \tag{IV A28}$$

$$\tau_{ch}^{internal} = \frac{1}{\left(1 + K_{PE-W} \frac{m_P}{V_W}\right)} \cdot \frac{r_P^2}{15 D_{PE}} \tag{IV A29}$$

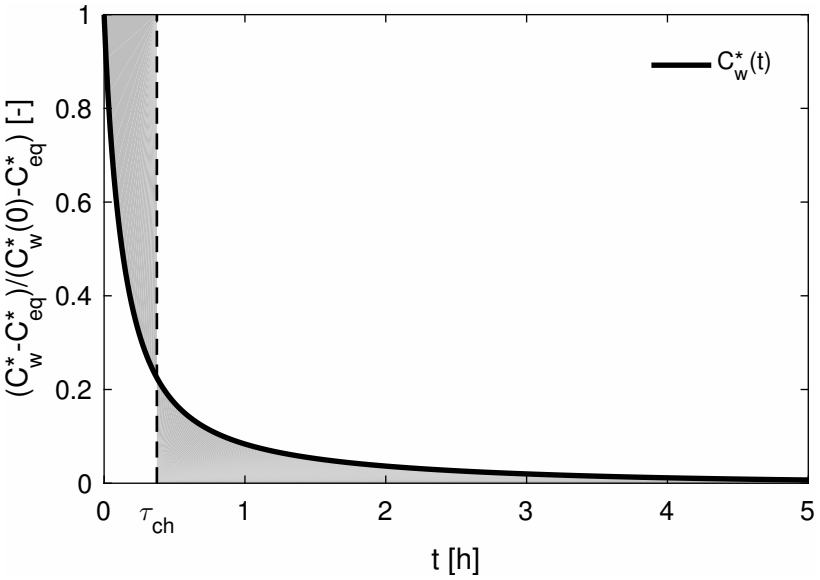

Figure IV A2: **Visualization of the characteristic time τ_{ch}.** Bold line: Deviation $C'^*_W(t)$ of the bulk-phase concentration $C^*_W(t)$ from the large-time limit $C^{*\infty}_W$, normalized by the initial deviation $C'^*_W(0)$. With $1 + K_{PE-W}\,(m_P/V_W) = 10.63$. Dashed line: characteristic time τ_{ch}. The area of the gray patch to the left of τ_{ch} equals that to the right.

Fitting the Model to the Data

We fitted the full analytical solution to the measured data of phenanthrene, tonalide, and benzophenone, assuming that the partitioning coefficients K_{PE-W} between PE and water without dissolved organic matter are known. We also assumed that the mass-transfer velocity k_W scales with the known aqueous diffusion coefficients D_{aq} according to (see Section IV 4.3):

$$k_W \propto D_{aq}^{2/3} \tag{IV A30}$$

and that the effective PE/water distribution coefficient K^*_{PE-W} for a given concentration C_{DOM} of dissolved organic matter depends on the compound-specific distribution coefficient K_{DOM} between dissolved organic matter and water by:

$$K^*_{PE-W} = \frac{K_{PE-W}}{1 + K_{DOM} C_{DOM}} \tag{IV A31}$$

Then, the parameters to be fitted were $k_W / D_{aq}^{2/3}$, the three substance-specific K_{DOM}-coefficients, and the three substance-specific diffusion coefficients D_{PE} of the respective compounds within PE. We fitted the logarithms of these seven parameters, taking the sum of absolute differences between simulated and measured concentrations as objective function.

Fitting was performed with DREAM(ZS) (Laloy & Vrugt, 2012; Vrugt, 2016), which is a Markov chain Monte Carlo method, resulting in a posterior distribution of the log-parameters. We used three chains with 10,000 generations. The initial distribution of the log-parameters was uniform within given bounds (see Table IV A1) chosen lay outside of the range of the posterior distribution. The $\hat{R}^d$-statistics of all three chains reached the critical value ≤ 1.2 within 3,000 generations. The first 9,000 generations were considered as burn-in, and only the last 1,000 accepted log-parameter combinations were further analyzed. In the standard fit, K_{PE-W} was fixed based on the measured equilibrium concentrations for zero DOM, and K^*_{PE-W} was calculated according to equation (IV A31). Figure IV A3 shows the corresponding posterior distribution of log-parameters.

We also tested a fit in which the three K_{PE-W}-values of the compounds were jointly fitted with the other parameters from all experimental data. The corresponding fitted parameter values and uncertainty ranges are listed in Table IV A2, whereas Figure IV A4 shows the posterior distribution of log-parameters. As can be seen, the uncertainties of $\ln(K_{PE-W})$ and $\ln(K_{DOM})$ are highly correlated for phenanthrene and tonalide, even though the range of uncertainty is modest. Also, the K_{PE-W}-value of phenanthrene fitted over all experiments is significantly smaller than the value obtained from the case with zero DOM only. The value used in the standard fit, however, agrees better with independent measurements in experiments not shown here.

Table IV A1: **Prior parameter ranges.** In the standard fit, values of $\ln(K_{PE-W})$ were fixed.

parameter	unit of non-logarithmic parameter	compound	minimum	maximum
$\ln\left(k_W/D_{aq}^{2/3}\right)$	$(s\ m)^{-1/3}$	-	0	10
$\ln(D_{PE})$	$m^2\ s^{-1}$	Phenanthrene	-35	-25
		Tonalide	-35	-25
		Benzophenone	-30	-20
$\ln(K_{DOM})$	$L\ kg^{-1}$	Phenanthrene	5	15
		Tonalide	5	15
		Benzophenone	0	15
$\ln(K_{PE-W})$	$L\ kg^{-1}$	Phenanthrene	8	10
		Tonalide	9.5	11.5
		Benzophenone	3.5	5.5

Table IV A2: **Metrics of the posterior parameter distributions for the case in which$\ln(K_{PE-W})$ was simultaneously estimated with the other parameters.**

parameter	unit	compound	geometric mean	5%-95% range
$k_W/D_{aq}^{2/3}$	$(s\ m)^{-1/3}$	-	72.4	59.5- 86.8
D_{PE}	$m^2\ s^{-1}$	Phenanthrene	1.8×10^{-13}	1.5×10^{-13}- 2.1×10^{-13}
		Tonalide	1.8×10^{-12}	3.0×10^{-13}- 1.1×10^{-11}
		Benzophenone	1.6×10^{-12}	1.4×10^{-12}- 1.8×10^{-12}
K_{DOM}	$L\ kg^{-1}$	Phenanthrene	4490	3940 - 5140
		Tonalide	3234	2770 - 3730
		Benzophenone	23	1.6 - 594
K_{PE-W}	$L\ kg^{-1}$	Phenanthrene	8380	7700 - 9090
		Tonalide	27620	2.5×10^4 - 3.0×10^4
		Benzophenone	47	35 - 61

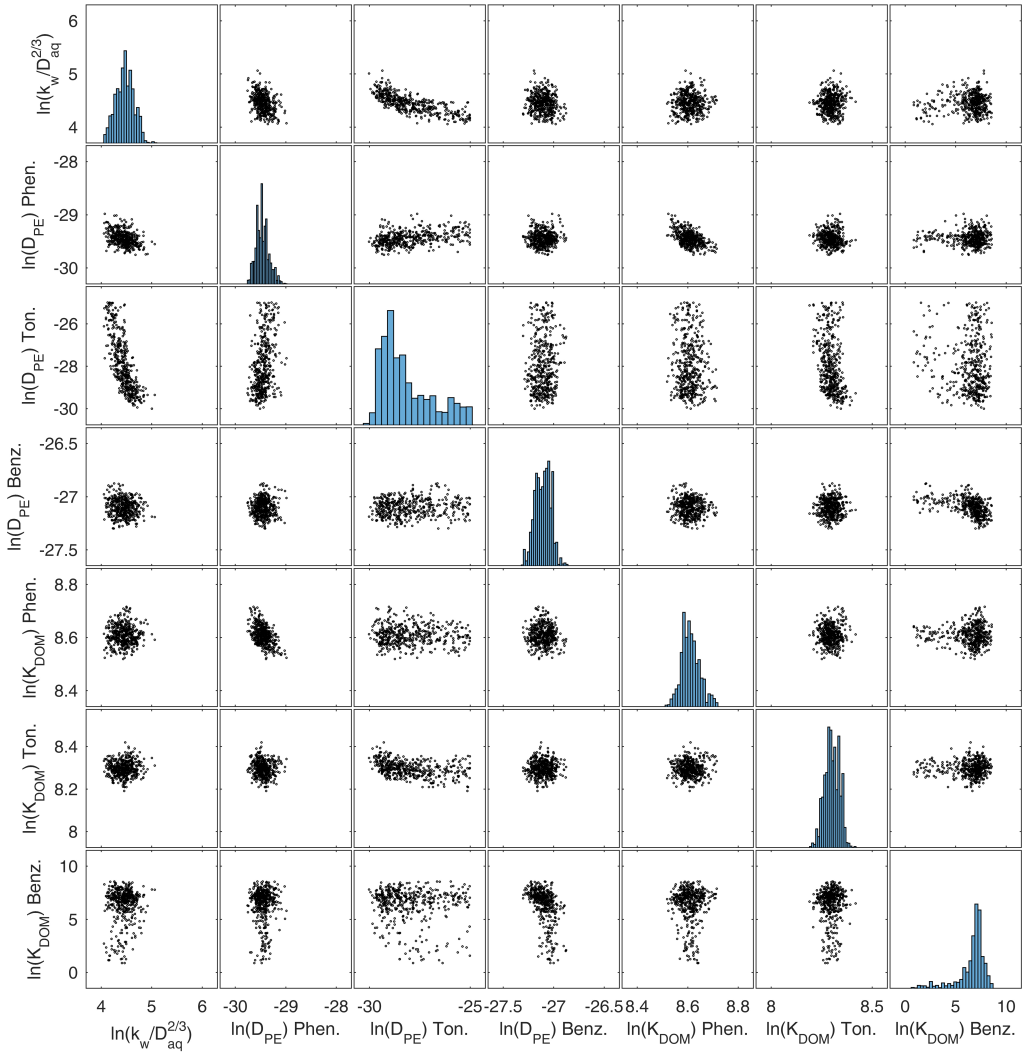

Figure IV A3: **Scatter plot and histograms of the posterior log-parameter distribution (3,000 ensemble members).** Displayed are results of the standard fit, in which K_{PE-W} is fixed for each organic pollutant.

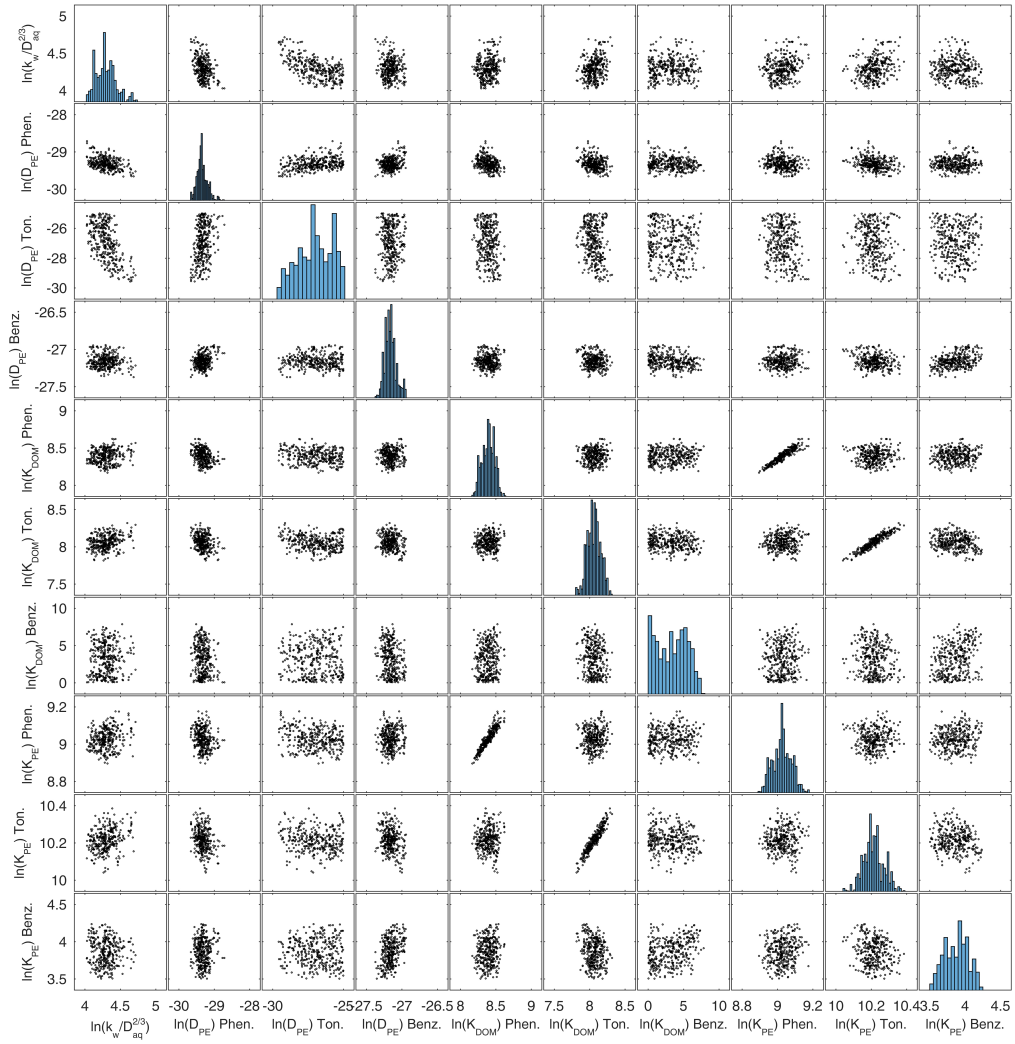

Figure IV A4: **Scatter plot and histograms of the posterior log-parameter distribution if all partition coefficients are fitted (3,000 ensemble members).** Displayed are results of the fit, in which K_{PE-W} for each organic pollutant belongs to the fitting parameters.

Empirical Relationships

Diffusion Coefficients

Substance specific coefficients as both modelling parameters and comparative values for the estimated results were calculated according to empirical relationships. D_{aq} were calculated according to Worch (1993):

$$D_{aq} = 3.595 \times 10^{-14} \frac{T}{\eta M W^{0.53}} \qquad \text{(IV A32)}$$

with T as the temperature (in K), η as the dynamic viscosity of water (in Pas), and MW as the molecular weight of the respective compound given in $gmol^{-1}$. The experiments were performed in a room constantly tempered to 20 $°C$ (≡ 293.15 K) hence η were $8.9 \times 10^{-4} Pas$. The fitted D_{PE} was compared to estimations calculated with available empirical relationships. For this, the equations obtained by Rusina et al. (2010) and Lohmann (2011) were applied. Rusina et al. (2010) obtained a correlation between the molecular weight MW and D_{PE}:

$$\log D_{PE} = -0.0137 MW - 10.01 \tag{IV A33}$$

whereas Lohmann (2011) calculated D_{PE} as a function of the molecular volume V_M:

$$\log D_{PE} = -0.0145 V_M + 10.1 \tag{IV A34}$$

As specified in the main manuscript, the D_{PE} calculated as described above were compared to the fitted D_{PE}.

Mass-Transfer Coefficients

Several studies on mass-transfer towards a spherical body in turbulent flows have been performed and analyzed by dimensional analysis. A typical finding is (Ranz et al., 1952; Garner & Suckling, 1958):

$$Sh = k \cdot Re^{1/2} \cdot Sc^{1/3} \tag{IV A35}$$

with an empirically determined coefficient k, depending on the exact experimental setup, and the Sherwood, Reynolds, and Schmidt numbers, Sh, Re, Sc, defined by:

$$Sh = \frac{k_w d_P}{D_{aq}} \tag{IV A36}$$

$$Re = \frac{v d_P}{\upsilon_{aq}} \tag{IV A37}$$

$$Sc = \frac{\upsilon_{aq}}{D_{aq}} \tag{IV A38}$$

in which υ_{aq}, v, and d_P are the kinematic viscosity, the flow velocity, and the particle diameter, respectively. Hence, the following scaling of the mass transfer coefficient with the aqueous diffusion coefficient applies:

$$k_w \propto D_{aq}^{2/3} \tag{IV A39}$$

The Sh calculated from the experimentally estimated k_W would range from 24.5 to 26.2. The aqueous diffusion coefficients D_{aq} of the used compounds are reported in Table 2 in the main article. These values are in good agreement with the Sh calculated by an empirical relationship obtained by Doig et al. (2005). We estimated the Re for

our experimental conditions to be 26. The flow velocity is the quotient of the shaker amplitude and the shaking speed which were 4 cm and 150 rpm, respectively. The kinematic viscosity υ_{aq} of water at 20 $°C$ is $1 \times 10^6 m^2 s^{-1}$. Therefore, Sc ranges from 1,316 to 1,613 for our experimental conditions.

Relative Importance of Internal and External Mass Transfer

Increasing the DOM-concentration, and hence decreasing the partitioning coefficients, increases the characteristic time $\tau_{ch}^{internal}$ of internal mass transfer (Eq. (IV A29)) while that of the external mass transfer,$\tau_{ch}^{external}$ is hardly affected for strongly hydrophobic compounds (Eq. (IV A28)) under batch boundary conditions (finite bath). Figure IV A5 shows the computed ratio of these characteristic times according to Eqs. (IV A28) and (IV A29) for all three compounds at all DOM-concentrations. As already discussed in the context of the concentration time series, the mass transfer of tonalide is uniquely controlled by the external mass transfer from the bulk solution to the surface of the spheres, whereas the mass transfer of benzophenone is governed by intraparticle diffusion at all DOM-concentrations. For phenanthrene, the ratio of characteristic times is always < 1 indicating that desorption was controlled by internal mass transfer. Nevertheless, the ratios for low DOM concentrations are close to one implying that both mass transfer processes are relevant. At higher DOM concentrations the internal mass transfer clearly dominates. Since the ratio of the characteristic times is independent of the solid to liquid ratio the same mass transfer patterns would occur in the environment.

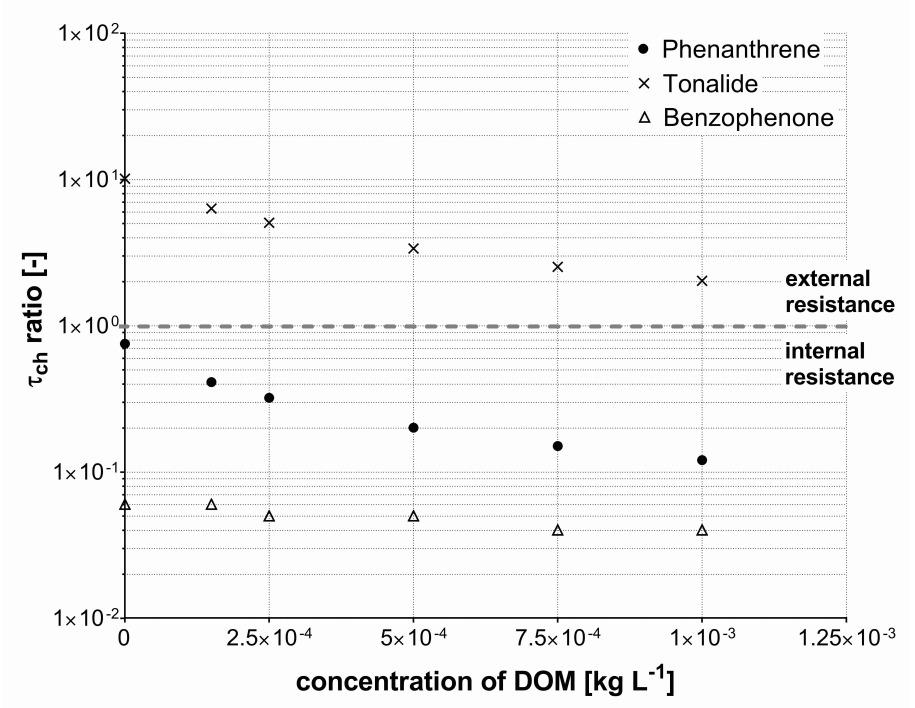

Figure IV A5: **Pattern of mass transfer resistances with increasing DOM amounts.** The ratio of the external and the internal mass transfer process ($\tau_{ch}ratio$) is plotted against the DOM concentration. The horizontal line at $\tau_{ch}ratio$=1 thus points out equality of the processes.